Department of Physics and Astronomy
University College London
University of London

The role of fluctuations near antiferromagnetic and spin-triplet nematic quantum critical points

Gregor Maximilian Hannappel

I, Gregor Maximilian Hannappel, declare that the work presented in this thesis is my own. Where information has been obtained from other sources, I declare this has been clearly indicated in the thesis.

Abstract

The formation of exotic orders in the vicinity of magnetic quantum critical points is a promising research field. Particularly motivating is the discovery of high temperature superconductors with novel ordering symmetries. In this thesis we extend the fermionic quantum order by disorder approach to analyse phase formation in the vicinity of antiferromagnetic and spin-triplet nematic quantum critical points.

We first investigate a fundamental model for itinerant antiferromagnetism. Already at mean field level this model exhibits exciting behaviour. Nesting and van-Hove physics drive incommensurate order and a discontinuous transition to the antiferromagnetic phase. These phenomena can be related to the Fulde-Ferrell-Larkin-Ovchinnikov state of superconductivity. Additional phenomena are driven by fluctuations. Applying the fermionic order by disorder approach we discover a multitude of phases. In addition to the antiferromagnetic order we consider d-wave superconductivity and d-wave bond density wave order. Finally, we analyse mode-mode coupling between all pairs of these three orders. The resulting phase diagram is in qualitative agreement with experimental findings in cuprate superconductors and offers an alternative perspective to the standard theoretical approaches.

In the absence of an antiferromagnetic quantum critical point we instead consider superconducting order driven by ferromagnetic spin fluctuations. We analyse a model for spin-triplet nematic order and investigate its susceptibility to the formation of spatially modulated nematic order, fluctuation driven p-wave superconductivity and composite pair density wave order. Here, the presence of spin-triplet nematic order enhances the superconducting transition temperature dramatically.

Dedicated to Alison Chenwen Wang

Acknowledgements

First of all, I would like to thank my supervisor Andrew Green for his continuous guidance and support during the time of this PhD.

Further, I would like to thank my collaborators and colleagues for their many useful comments and discussions. Foremost I am thankful to Chris Pedder for answering a mass of questions and his thorough advice throughout. I'd also like to thank Andrew Berridge and Frank Krüger for the numerous constructive discussions in or outside a pub.

Thanks to my fellow students and friends for baring with my rants and moods during times of slow progress. Thanks to Phil, Thuong, Oliver, Jenny, Saad, Tom, Aizhan, Elisabeth and many more.

Thanks to my parents, Karin and Chris, for their financial as well as loving psychological support.

Finally, I would like to thank Rich and the Vauxwall and Arch climbing walls for keeping me sane.

Units and conventions

Momenta and wavevectors are scaled by the lattice constant, a, so that

$$a\mathbf{k} \rightarrow \mathbf{k}.$$

We adopt Planck units, which set the reduced Planck constant and Boltzmann constant to unity:

$$\hbar = 1$$

$$k_B = 1.$$

Integrals over momentum space will often be written as sums. For example in 2 spatial dimension in the presence of a lattice we write the integral over the first Brillouin zone as:

$$\sum_{\mathbf{k}} = \frac{1}{(2\pi)^2} \int_{-\pi}^{\pi} dk_x \int_{-\pi}^{\pi} dk_y.$$

Contents

IV   Nematic quantum critical point   170

8   Fluctuation-induced instabilities of the spin-triplet nematic   171

V   Conclusion   197

9   Conclusion   198

Part I

Context and introductory material

Chapter 1

Introduction

1.1 *Motivation and background*

1.1.1 Superconductivity

In 1911 Heike Kamerlingh Onnes discovered, that upon cooling mercury below 4.2 Kelvin the electric conductivity suddenly dropped to values smaller than he was able to experimentally measure. First termed supraconductivity, Onnes and others went on to demonstrate this phenomenon in a range of materials with ever increasing transition temperatures. However, after years of search, an upper limit seemed to emerge. This was supported by the theoretical models of the time. In particular, Bardeen, Cooper and Schrieffer developed a microscopic model for superconducting pairing due to the interaction of the electrons with vibrational modes of the ion lattice [1, 2]. This electron-phonon interaction leads to an attraction between electrons, which in response form bound states. These, so called, Cooper-pairs are bosonic states, which condense into a superconducting ground state with an energy bandgap. The limited strength of the electron-phonon interaction restricts the superconducting transition temperature to about 40 Kelvin [3]. For decades, this held true. Then, in 1986 Bednorz and Müller discovered superconductivity in a new type of ceramic compound, LaBaCuO [4]. Only one year later Wu et.al. analysed YBaCuO with the remarkable transition temperature of 93 Kelvin [5].

A whole new class of superconductors had been discovered: the cuprates, characterised by thin stacks of copper-oxide planes separated by insulating layers of varying composition (see Figure 1.1). To date the record critical temperature at ambient pressure is about 135 Kelvin in an ordered superstructure of Hg-Ba-Ca-Cu-O [6].
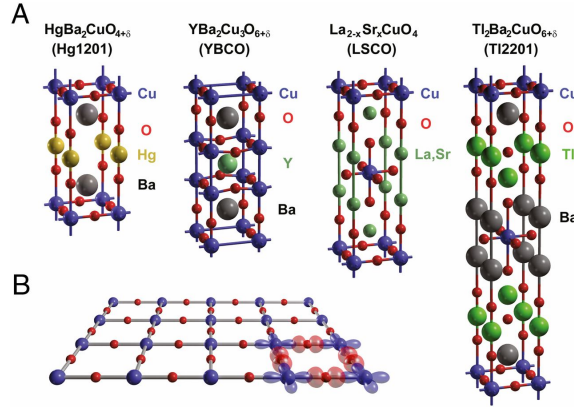
Figure 1.1: **Crystal structure of a few cuprates and the copper-oxide plane.** **A** shows the perovskite structure of a few cuprate superconductors. **B** displays the copper-oxide plane. Additionally, **B** highlights the copper $d_{x^2-y^2}$-orbital and oxygen p_x and p_y-orbital believed to be responsible for the copper oxide plain's conductivity upon doping. Figure from [7].

These remarkably high transition temperatures are well above the theoretical limit for phonon mediated pairing. A new model was needed. The task was complicated by the complexity of the generic phase diagram of the cuprates and the exotic nature of the phases involved, see Figure 1.2. In 1987 Anderson proposed, that the superconducting pairing is driven by electronic and magnetic correlations originating in the antiferromagnetic insulting state of the parent compounds [8]. This opened up a new avenue of theoretical attack; the idea that high temperature superconductivity in cuprates is a result of strong quantum fluctuations in the vicinity of a putative quantum critical point.

1.1.2 Quantum criticality

Classical phase transition are governed by the interplay of thermal fluctuations and interactions. This behaviour is usually well described in Fermi liquid theory. Here, the effect of interactions is accounted for by a renormalisation of the dynamical properties of the electrons, such as their mass. The resultant quasiparticles are then
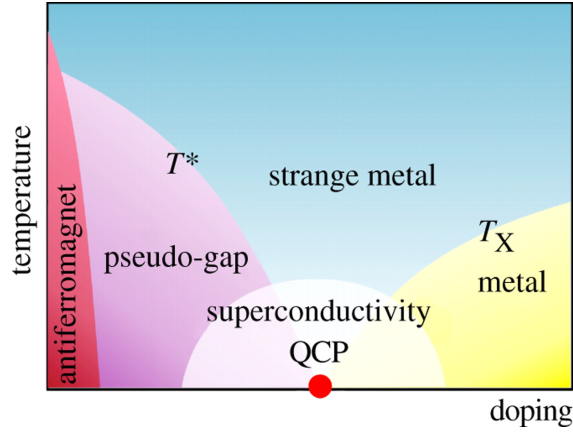
Figure 1.2: **Generic temperature-doping phase diagram of the underdoped cuprate superconductors.** At zero doping the parent compounds are antiferromagnetic Mott insulators (red) [9]. Upon doping the mysterious pseudo-gap [9,10] phase develops below T^*. A superconducting dome is centred around optimal doping, covering a putative quantum critical point (QCP). In the limit of high doping the system turns into a conventional metallic Fermi liquid (yellow). Above the superconducting dome non-Fermi liquid behaviour is observed, dubbed strange metal. Other phases present in the cuprates, such as charge order [11,12] or the spin glass phase [13], are not shown in this sketch. Figure from [14].

treated as a non-interacting gas of particles. This description fails if a continuous transition is tuned to absolute zero. Here the magnitude of thermal fluctuations vanishes and quantum fluctuations due to Heisenberg's uncertainty principle become strongest. The zero temperature transition is called a quantum critical point. The proliferation of quantum fluctuations in the vicinity of quantum critical points changes the physics dramatically and invalidates the Fermi liquid approach.

Figure 1.3 displays a typical quantum critical phase diagram. Here, the electron's behavioural change is observed in measurements of the electric conductivity as a function of temperature. While Fermi liquid theory predicts a quadratic temperature dependence, the quantum critical regime often displays a linear relationship [15].

The first attempt at a description of magnetic quantum critical points was presented by Hertz [17] and extended by Millis [18]. Their work applies to systems, where the continuous magnetic transition extends all the way to zero temperature. This theory explains the universal scaling behaviour in the vicinity of naked quantum critical points. However, even in seemingly ideal candidates of naked quantum criticality, for example $CeCu_{5.9}Au_{0.1}$ [19,20] or $YbRh_2Si_2$ [16] (see Figure 1.3), additional physical
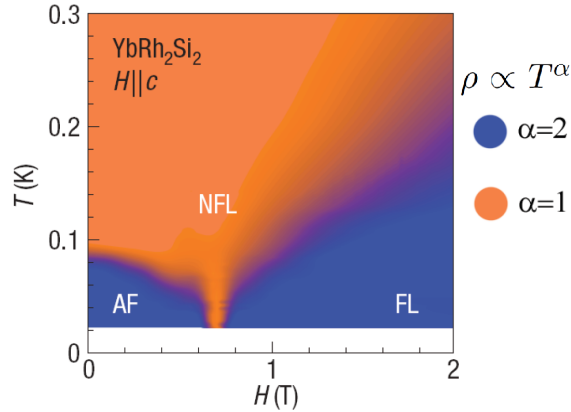
Figure 1.3: **Non-Fermi-liquid behaviour in the vicinity of quantum criticality.** Temperature-magnetic field phase diagram of $YbRh_2Si_2$. Upon application of a magnetic field the antiferromagnetic (AF) transition temperature is suppressed to zero Kelvin. Above this quantum critical point a non-Fermi-liquid (NFL) arises. This is characterised by a linear temperature dependence of the electric conductivity, ρ. Increasing the magnetic field further, the system transitions to a common paramagnetic Fermi liquid (FL). The antiferromagnetic and paramagnetic regions show the conventional quadratic temperature dependence of the resistivity of Fermi liquids. Figure from [16].

mechanisms must be accounted for.

In many experimental systems the direct observation of quantum critical points is difficult. As the supposed quantum critical point is approached, the transition turns discontinuous or new phases appear, either of which hide the quantum critical point. In fact, the emergence of exotic phases in the vicinity of quantum critical points has been observed in a number of material classes - notably non-BCS superconductivity in the cuprate [8] and pnictide compounds [21, 22]. The apparent universality of this phenomenon lead to the belief that the emergence of novel and exotic phases is directly related to the existence of the quantum critical point.

Hertz-Millis theory fails to explain these phenomena. It turns out additional aspects have to be taken into account. In Hertz-Millis theory only the lowest order correction from the coupling of electrons to the bosonic fields associated to the magnetic order are accounted for. In three spatial dimension this ansatz is valid. The lowest order vertex correction is marginal, while higher order terms are negligible. In two dimensions all higher order vertex corrections are marginal and their sum leads to a change in the universal scaling behaviour [23–25]. Of course, taking account of

an infinite number of terms is non-trivial and thus the need for novel theoretical approaches was born.

1.1.3 Fermionic quantum order by disorder

One recent approach to quantum criticality is fermionic quantum order-by-disorder. It simplifies the problem by including an infinite number of terms in the familiar second order perturbative approach. The term order by disorder was first coined by Villain in the context of degenerate spin states [26]. Zero temperature degeneracies in the mean field ground state of frustrated spin systems may be lifted by thermal fluctuations at finite temperature. This is due to a difference in the available phase space for such fluctuations. Thus, the thermal fluctuations entropically pick a particular order from the otherwise disordered ground state. Fermionic quantum order by disorder generalises this concept; the presence of an order may also enhance the available phase space for quantum fluctuations. If the entropy associated with these fluctuations is large enough, new phases may be stabilised even if they are not favoured at the classical level.

Fermionic quantum order by disorder has previously been applied to itinerant ferromagnets in two and three spatial dimensions [27–31]. In these studies quantum fluctuations drive the formation of a variety of exotic phases, such as spiral ferromagnets, spin nematics and p-wave superconductivity.

In this thesis we apply the fermionic quantum order by disorder approach to the quantum critical itinerant antiferromagnet. One of the most fundamental models for itinerant antiferromagnetism is the Hubbard model.

1.1.4 Hubbard model

Within months of the discovery of high temperature superconductivity in the cuprates, Anderson proposed that their essential physics is captured by the Hubbard model [8]. The Hubbard model is one of the seemingly simplest models of correlated electrons in condensed matter physics. The model itself was independently introduced by Anderson [32], Hubbard [33], Kanamori [34] and Gutzwiller [35]. It reduces the

energetics of particles on a lattice to two principal components: inter-site hopping and on-site interaction.
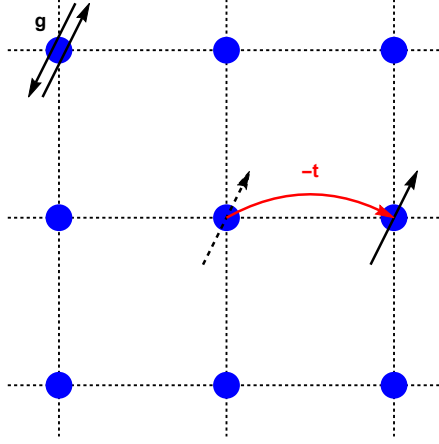
Figure 1.4: **Depiction of the Hubbard model on a square lattice.** Double occupation of lattice sites costs energy g and hopping to nearest neighbours is associated with an energy gain of t.

In certain materials electrons are so tightly bound to their respective atom that we may no longer assume them to form a gas of free electron within the solid. Instead, we replace this assumption by a picture, in which the electrons occupy discrete lattice sites. Their only mode of translation is the hopping or tunneling from one lattice site to the next. In its simplest formulation the Hubbard model allows only for the hopping between nearest neighbours. On a two dimensional square lattice this means only vertical and horizontal hops of a single lattice constant are admissible. Extensions to this simplest model may be made by inclusion of next-nearest neighbour or further hopping.

The second component of the Hubbard model is an approximate inclusion of the Coulomb repulsion between electrons. In principle, a faithful representation of the physics of solids would include the interactions of any one particle with every other one. However, the presence of positive atomic Ions screens the long range Coulomb interaction between electrons. Therefore, the Hubbard model only considers interactions between electron on the same lattice site. The inclusion of electron-electron repulsion in the model was a step forward from the non-interacting band theories at the time.

A well known consequence of the inclusion of electron-electron interaction is the Mott

insulating phase [9]. In the limit of strong interaction and one electron per site or half filling, the energetic cost of double occupation of any site becomes too large. Since there is exactly one electron per site, none of them can hop onto any other site without encountering another electron. Thus hopping is suppressed entirely and the system becomes insulating. This is in contrast to the predictions of conventional band theories, which expect any system with a finite density of states at the Fermi surface to be conducting.

In summary, the Hubbard model consists of two distinct terms: inter-site hopping and intra-site repulsion. The electrons may gain kinetic energy by hopping, but are punished for sitting on a lattice site occupied by another. This seemingly simple competition allows the Hubbard model to describe phenomena, such as metal-insulator transitions or the physics of cold-atom experiments.

1.2 *Essential concepts*

In this section we will explain and define some of the fundamental concepts used in the following chapters. First, we formally introduce key characteristics of the Hubbard model near half filling: nesting and van-Hove singularities. Secondly, we will introduce phase transitions and their description within the Ginzburg-Landau phenomenology.

1.2.1   Fermi surface nesting

A Fermi surface is nested if it possesses extended regions, that may be shifted onto one another by a single vector. This vector is called the nesting vector. Since it connects regions of the Fermi surface its start and end point are at the same energy. Consequently, in nested dispersions there exists large phase space for low energy excitation at the nesting vector $\mathbf{Q}$. This greatly enhances the system's susceptibility to the formation of order at this particular wave vector.

A common example of a nested Fermi surface is the half-filled Hubbard model with nearest neighbour hopping only. Its Fermi surface forms a diamond with perfectly parallel sections, see Figure 1.5. This makes it highly susceptible to the formation

of order at the nesting vector such as spin density waves.
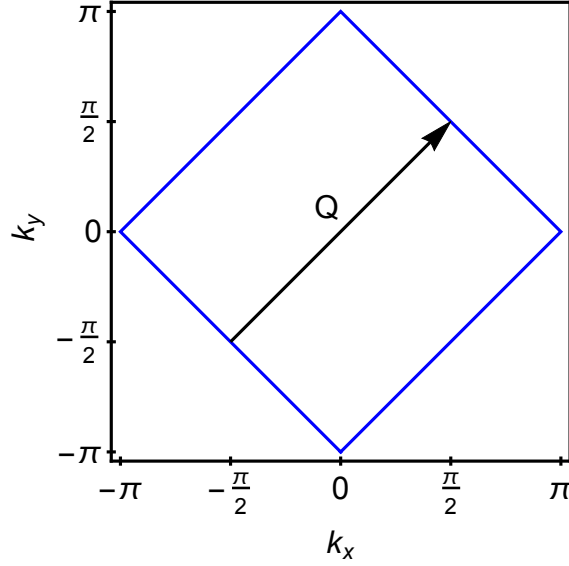
Figure 1.5: **Nesting of the Fermi surface of the half filled Hubbard model.**
The vector $\mathbf{Q} = (\pi, \pi)$ nests large regions of this diamond shaped Fermi surface.

Points on the Fermi surface that are mapped to one another by a commensurate wave vector are referred to as hot-spots.

An order is said to be commensurate if its period of spatial modulation is a rational multiple of the lattice constant of the underlying crystal structure. In case of antiferromagnetic order with $\mathbf{Q} = (\pi, \pi)$, the extrema of magnetisation lie precisely on the lattice points, thus it is commensurate. Conversely the period of spatial modulation of an incommensurate order is an irrational multiple of the lattice constant. Figure 1.6 illustrates both commensurate and incommensurate antiferromagnetic order in one spatial dimension.

1.2.2 Van Hove singularities

An additional feature, that enhances a system's susceptibility to phase formation, is a large density of states at the Fermi surface. The density of states of a system describes the number of available distinct quantum states as a function of energy. Thus, a large density of states in the vicinity of the Fermi surface enhances the available phase space for low energy excitations.
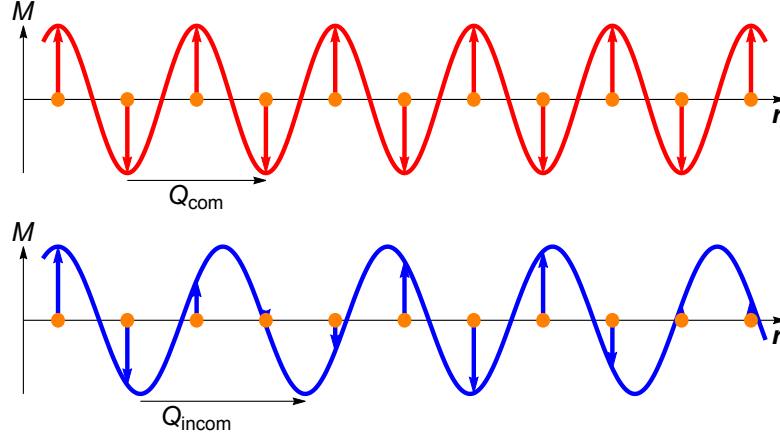
Figure 1.6: **Sketch of (in)commensurate antiferromagnetic order.** Commensurate order is sketched in red. Here λ_{com}, the wavelength of spatial modulation of magnetisation, M, is a rational multiple of the lattice spacing (orange dots). The incommensurate modulation (blue) has a scale λ_{incom} that is not a rational multiple of the lattice constant.

The density of states is a functional of gradient of the dispersion relation of the system. In particular,

$$\rho(\epsilon) \;=\; \sum_{\mathbf{k}} \delta(\epsilon - \epsilon_{\mathbf{k}}) \;\propto\; \int \frac{dS_\epsilon}{|\nabla_{\mathbf{k}}\epsilon|}, \tag{1.1}$$

where the integral is taken over the surface of constant energy ϵ. From (1.1) we conclude that the density of states may be singular at any saddle point of the dispersion. The precise form of these singularities depends on the dimensionality of the system and the nature of the saddle point. These non-analyticities in the density of states are named after Léon Van Hove, who first analysed their occurrence in phonon dispersions in 1953 [36].

1.2.3 Phase transitions

The phase of a system is its macroscopic state, in which its properties are uniform over length scales much larger than the system's microscopic components. The most familiar example are the three principal phases of water: gas, liquid and solid. The particular phase of a system at any time is a function of thermodynamic variables,

such as temperature, pressure or magnetic field.

Changing these variables across certain critical values forces the system to drastically change its macroscopic state; it undergoes a phase transition. The parameter space occupied by any particular phase may be plotted in a phase diagram, where different phases are separated by phase transition lines. Figure 1.7 illustrates these ideas for the three principle phase of water.
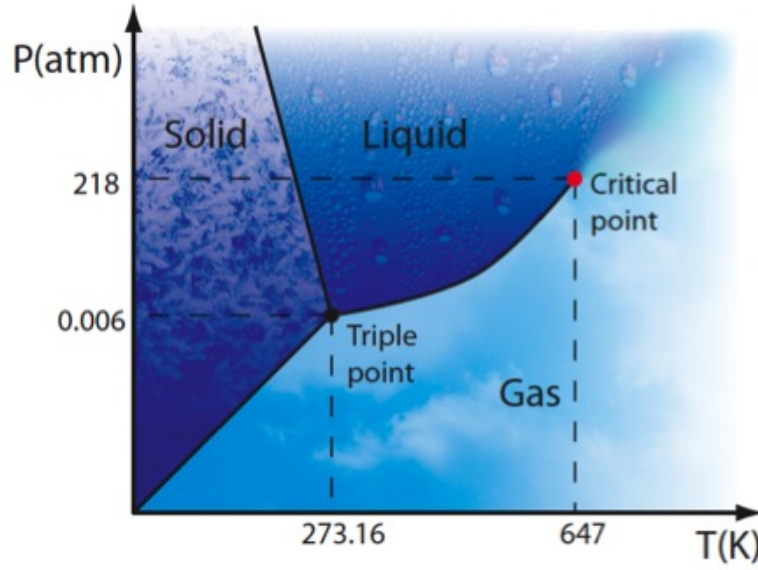
Figure 1.7: **Pressure-temperature phase diagram of water.** The solid black lines denote discontinuous first order transitions between the three principle phases. Here the mass-density changes abruptly. Above the critical point (red) the liquid-gas transition becomes a continuous second order transition. Figure from [37]

Physically, phases may be understood as the state of the system that minimise its Helmholtz free energy. The later governs the balance between minimising the system's energy, while maximising its entropy. The free energy takes the familiar form

$$\mathcal{F} = E - TS. \tag{1.2}$$

Conceptually, we may view the entropic term as arising from random thermal fluctuations, which classically work towards breaking apart ordered phases and restoring broken symmetries. Their counterpart are interactions between the system's micro-

scopic components. They try to form ordered states and break symmetries of the non-interacting model.

The degree to which a system has departed from the symmetric phase is often described by an order parameter. For example, at sufficiently low temperatures Nickel or Iron become ferromagnetic. Their electronic spins align, breaking the discrete rotational symmetry of the material. The magnetisation of the material may be used as the order parameter, as it increases dramatically as order is formed.

Since the thermodynamic parameters control the phase of a system, so do they control its macroscopic properties. In fact, the material's properties may be expressed as derivatives of the free energy with respect to particular macroscopic variables. We may divide phase transitions into two categories by the behaviour of these derivatives as a function of the external parameter.

A first order transition exhibits a discontinuous change in the first derivative of the free energy with respect to a thermodynamic variable. Consequently, first order transitions require a finite amount of latent heat. In a real material this may result in a spatially piecewise transition, as finite thermal conductivity limits the amount of heat available to different parts of the system. This piecewise process is evident in the melting of water. As water melts, its density increases step-like. Density is the first derivative of the free energy with respect to the chemical potential. Hence, this is an example of a first order transition.

Continuous or second order transitions are continuous in the first derivative of the free energy. Instead, they exhibits a discontinuous change or singularity in second or higher order derivative of the free energy with respect to a thermodynamic variable. This is evident in a divergent susceptibility. Since the transition is continuous the whole material may transition as one. Thus, the correlation length, which is the characteristic length scale at which observables co-vary, diverges at the transition. In case of a second order magnetic transition, the magnetisation increases continuously from zero as a function of an applied field. However, the magnetic susceptibility is divergent at the transition point. Magnetisation and magnetic susceptibility are the first and second derivative of the free energy with respect an applied field respectively.

1.2.4   Ginzburg-Landau expansion

In order to determine the positions of phase transitions within a parameter space, we will employ Ginzburg-Landau expansions. Originally a phenomenological ansatz to study continuous phase transitions into superconducting states [38], it was soon extended, basing phenomenological parameters on microscopic derivation [39]. The underlying concept is as follows:

In continuous transitions, the order parameter is a continuous function of thermodynamic variables. In the symmetric phase the order parameter is zero, while crossing through the transition, its value increases continuously.

By choosing a point in parameter space inside the symmetry-broken phase, but sufficiently close to the transition, the order parameter may be tuned to be arbitrarily small compared to any intrinsic scale of the model. We can then expand the free energy in powers of the order parameter and analyse the behaviour of these Landau expansion coefficients.

Let us examine the general form of a Landau expansion in the case of ferromagnetism. The free energy to sixth order in magnetisation is

$$\mathcal{F} = \alpha M^2 + \beta M^4 + \gamma M^6, \tag{1.3}$$

where we have ignored symmetry breaking effects, like an external magnetic field, $-hM$. The possible shapes of this free energy as a function of α and β are displayed in Figure 1.8. The highest order term of a Landau expansion, here γ, has to be positive to ensure a finite order parameter.

The left hand side of Figure 1.8 demonstrates the condition for a continuous transition, $\alpha = 0$. As the quadratic coefficient turns negative, two minima at finite magnetisation develop and the system spontaneously forms magnetic order.

Close to the tricritical point Landau expansions may be employed to describe first order transitions as well. The tricritical point is the position in parameter space at which a continuous transition turns discontinuous. At the tricritical point both the quadratic and quartic Landau coefficient are zero, $\alpha = \beta = 0$. Along the first order line a sufficiently negative quartic term overcomes the positive quadratic coefficient.
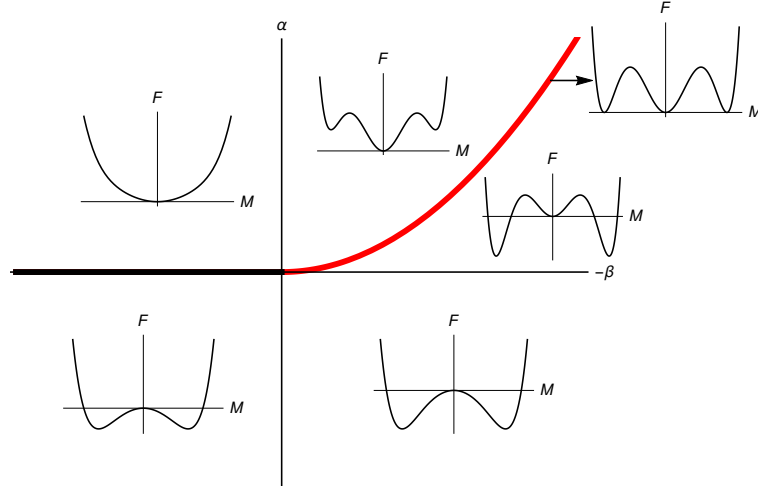
Figure 1.8: **Shapes of free energy as a function of the Landau expansion coefficients α and β.** A second order transition occurs when α turns negative (bold black line). Assuming a positive sixth order Landau term, γ, a first order transition takes place when the forth order term β becomes sufficiently negative (bold red line).

In particular, when $\beta < 0$ and $\beta^2 = 4\alpha\gamma$. This parabola is depicted in the first quadrant of Figure 1.8. Note how at the transition point local minima at finite magnetisation become degenerate with the non-magnetic minimum in the center.

Away from the tricritical point the analysis of first order transitions by a finite order Landau expansion fails. This is the result of a shrinking radius of convergence of the Landau expansion as thermal fluctuations become weaker at lower temperatures. At sufficiently low temperatures the free energy may display non-analyticities as a function of the order parameter.

In the presence of several different phases the expansion may be extended to include additional order parameters as well as the phase competition or support between them. The same principle of minimising the free energy in order to find the state of the system applies to such a multi-dimensional generalisation of the above example.

1.3 *Outline of thesis*

The remainder of this thesis is split into three parts.

In part II we analyse the mean field theory of antiferromagnetism in the Hubbard model close to half filling. Here, we already discover a surprisingly rich phase diagram including an incommensurate phase and a first order transition.

In part III we investigate the effect of quantum fluctuations in the vicinity of the antiferromagnetic quantum critical point. We start by formally introducing the fermionic quantum order by disorder approach. Next we apply this formalism to expand on the mean field phase diagram of the antiferromagnet. Having calculated the antiferromagnetic phase diagram, the next step is the inclusion of new phases. In particular, we analyse the formation of a d-wave bond density wave and d-wave superconductivity. Additionally, we consider the interaction of both of these phases with each other and antiferromagnetism.

In part IV we consider p-wave superconductivity in a model for a spin-triplet nematic. This work follows very closely the fermionic quantum order by disorder analysis in the previous chapters and earlier work on ferromagnetism [29,30].

We conclude with a discussion of the order by disorder formalism in general and its application to the antiferromagnetic and nematic order in particular. We finish by proposing several avenues for future work.

Part II

Mean field theory of the antiferromagnet

Chapter 2

Mean field theory of the antiferromagnet

2.1 *Introduction*

In this chapter we will analyse the mean field free energy of antiferromagnetism in the Hubbard model. We start off by formally defining the Hubbard model and anti-ferromagnetic order. Then we derive formal expressions for the model's Helmholtz free energy and its Ginzburg-Landau expansion.

Following work by Rice [40], we develop a heuristic picture of antiferromagnetic phase transitions. This predicts the main features of the phase diagram and guides our subsequent numerical and analytical approach.

The commonly assumed phase diagram consists of a single continuous transition to commensurate order down to zero temperature [41–43] . Surprisingly, even in mean field theory we find additional features. At low temperatures, the second order line becomes reentrant and the model supports a region of incommensurate antiferromagnetism as well as a first order transition. This is analog to the physics of LOFF states as will be explored in detail below.

2.2 *The model*

In this section we will derive formal expressions for the Helmholtz free energy of the antiferromagnetic state in the Hubbard model and its Landau expansion coefficients.

2.2.1 Hubbard Hamiltonian

In the preceding chapter we gave an intuitive picture of the Hubbard model. (See Figure 1.4)

Let us now define it formally. The Hubbard Hamiltonian takes the form;

$$\mathcal{H}_{Hubbard} = \underbrace{-t \sum_{\langle i,j \rangle,\sigma} (c^\dagger_{\mathbf{r}_i,\sigma} c_{\mathbf{r}_j,\sigma} + c^\dagger_{\mathbf{r}_j,\sigma} c_{\mathbf{r}_i,\sigma})}_{\text{kinetic}} + \underbrace{g \sum_i c^\dagger_{\mathbf{r}_i,\uparrow} c_{\mathbf{r}_i,\uparrow} c^\dagger_{\mathbf{r}_i,\downarrow} c_{\mathbf{r}_i,\downarrow}}_{\text{interaction}}, \qquad (2.1)$$

where we have identified the kinetic and interaction part of the Hamiltonian. Angled brackets, $\langle i, j \rangle$, denote summation over nearest neighbours only and t and g are the tunneling rate and on-site interaction, respectively.

This is the textbook form of the Hubbard model. It considers only the most dominant hopping term. Thereby we keep the dispersion as simple as possible. Additionally, it allows for the clear differentiation of phenomena driven by nesting and van-Hove physics, from those driven by the details of the band-structure of the cuprates, for instance the presence of hot-spots.

Fourier transforming the kinetic contribution, we obtain

$$\mathcal{H}_{Hubbard} = \sum_{\mathbf{k},\sigma} \epsilon_{\mathbf{k}} c^\dagger_{\mathbf{k},\sigma} c_{\mathbf{k},\sigma} + g \sum_i c^\dagger_{\mathbf{r}_i,\uparrow} c_{\mathbf{r}_i,\uparrow} c^\dagger_{\mathbf{r}_i,\downarrow} c_{\mathbf{r}_i,\downarrow}, \qquad (2.2)$$

where $\epsilon_{\mathbf{k}} = -2t \left(\cos k_x + \cos k_y \right)$ is the tight binding dispersion. This is plotted in Figure 2.1.
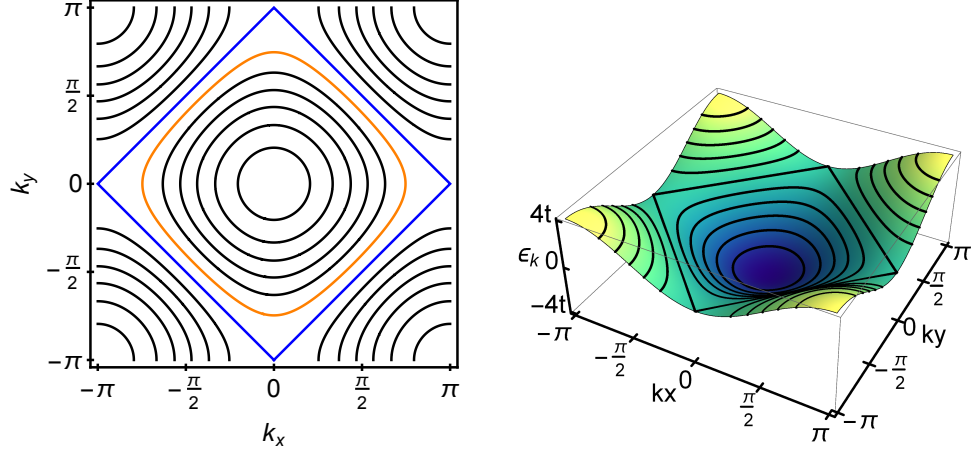
(a) The blue contour is the Fermi surface for the half filled band. The orange contour is representative of Fermi surfaces close to half filling.

(b) The contours are identical to the contour plot on the left. Note the saddle points at the corners of the half-filling contour line.

Figure 2.1: **Contour and 3D plots of the tight binding dispersion.**

Properties of the tight binding dispersion

We would like to derive the model's phase diagram close to half filling. Hence, the features of the dispersion in this range of parameters are of particular interest.

At precisely half filling, the Fermi surface of the tight binding dispersion forms a diamond shape. Translated by a vector $\mathbf{Q} = (\pi, \pi)$, the Fermi surface nests perfectly with itself and is hence highly susceptible to ordering at that scale, due the large phase space for zero energy excitations at that wave length. In addition, saddle points at half filling lead to a logarithmic van-Hove singularity in the density of states. In particular, the density of states takes the form

$$\rho(\epsilon) = \sum_{\mathbf{k}} \delta(\epsilon - \epsilon_{\mathbf{k}}) \tag{2.3}$$

$$= \frac{2K\left(1 - \left(\frac{4t}{\epsilon}\right)^2\right)}{\pi^2 |\epsilon|} \tag{2.4}$$

$$\approx -\frac{1}{2\pi^2 t} \log\left(\frac{|\epsilon|}{4t}\right) \quad \forall \quad |\epsilon| \ll t, \tag{2.5}$$

where $K(x)$ is the complete elliptic integral of the first kind.

Slightly away from half filling, nesting and van-Hove singularity play an important role. The divergent phase space at half filling may still be accessed by finite temperature fluctuations or the formation of incommensurate phases. The latter will be explored further in Sections 2.3 and 2.5.

2.2.2 The order parameter

On a lattice commensurate antiferromagnetism is an order in which any two neighbouring magnetic moments align anti-parallel. For electrons on a two dimensional square lattice, the spins of any two electrons on neighbouring sites point in opposite directions - up and down for instance. This is distinct from stripe order, where any one row of spins is aligned ferromagnetically, but spins on neighbouring rows are aligned anti-parallel. Formally, we define the magnetisation of the two sublattices of up and down spins as

$$M = \sum_{i,\sigma} \sigma \langle c_{i,\sigma}^{\dagger} c_{i,\sigma} \rangle \cos(\mathbf{Q}.\mathbf{r}_i), \tag{2.6}$$

where $\sigma = \pm 1$ labels the two spin species and we defined $\mathbf{Q}$ as the wavevector over which the spin orientation changes.

In the limit of half filling and strong coupling, the Hubbard model may be described by a Heisenberg Hamiltonian. Antiferromagnetism is not an eigenstate of the Heisenberg Hamiltonian, due to its intrinsic quantum fluctuation in the presence of antiferromagnetic order. In contrast, ferromagnetic order does not exhibit these fluctuations due to Pauli exclusion and hence is an eigenstate of the Heisenberg Hamiltonian.

2.2.3 Mean field ansatz

Interacting many body systems are hard to solve in general. Mean field theory is an ansatz to reduce the complexity of many body problems. It simplifies the Hamiltonian by treating interactions on average. This reduces the many body Hamiltonian to a one body Hamiltonian and a self-consistency relation. In effect it reduces the Hamiltonian with non-quadratic terms to a Hamiltonian only containing terms

quadratic in the electron field operators. Here, the electrons interact with the mean field, which encodes the average effect of all other particles. Deviations away from the mean field are assumed to be small.

In order to begin a mean field analysis one first has to guess an appropriate mean field. Assuming antiferromagnetic order, we define the mean field as

$$\langle n_{i,\sigma} \rangle \;\; = \;\; \frac{n}{2} + \sigma M \cos(\mathbf{Q}.\mathbf{r}_i), \tag{2.7}$$

where n denotes the average number of electrons per site and M and $\mathbf{Q}$ are the amplitude and wavevector of the antiferromagnetic order.

Adding and subtracting the mean field, we may rewrite the interaction contribution of the Hubbard model as

$$
\begin{aligned}
n_{i,\uparrow} n_{i,\downarrow} \;\; &= \;\; (n_{i,\uparrow} - \langle n_{i,\uparrow} \rangle + \langle n_{i,\uparrow} \rangle)(n_{i,\downarrow} - \langle n_{i,\downarrow} \rangle + \langle n_{i,\downarrow} \rangle) \\
&= \;\; n_{i,\uparrow} \langle n_{i,\downarrow} \rangle + n_{i,\downarrow} \langle n_{i,\uparrow} \rangle - \langle n_{i,\uparrow} \rangle \langle n_{i,\downarrow} \rangle,
\end{aligned}
\tag{2.8}
$$

where we expanded to leading order in deviations from the mean field, $(n_{i,\sigma} - \langle n_{i,\sigma} \rangle)$. The Hamiltonian may now be written as

$$\mathcal{H} - \mu \mathcal{N} = \sum_{\mathbf{k},\sigma} \xi_{\mathbf{k}} n_{\mathbf{k},\sigma} + g \sum_{i,\sigma} \left(n_{i,\sigma} \langle n_{i,\sigma} \rangle - \frac{\langle n_{i,\sigma} \rangle \langle n_{i,\bar{\sigma}} \rangle}{2} \right), \tag{2.9}$$

where $\xi_{\mathbf{k}} = \epsilon_{\mathbf{k}} - \mu$. Next, we insert our mean field assumption from equation (2.7). Fourier transforming we arrive at

$$\mathcal{H} - \mu \mathcal{N} = \frac{1}{2} \sum_{k,\sigma} \begin{pmatrix} c^\dagger_{\mathbf{k}-\frac{\mathbf{Q}}{2},\sigma} \\ c^\dagger_{\mathbf{k}+\frac{\mathbf{Q}}{2},\sigma} \end{pmatrix}^T \begin{pmatrix} \xi_{\mathbf{k}-\frac{\mathbf{Q}}{2}} & gM \\ gM & \xi_{\mathbf{k}+\frac{\mathbf{Q}}{2}} \end{pmatrix} \begin{pmatrix} c_{\mathbf{k}-\frac{\mathbf{Q}}{2},\sigma} \\ c_{\mathbf{k}+\frac{\mathbf{Q}}{2},\sigma} \end{pmatrix} + \frac{gM^2}{2}. \tag{2.10}$$

2.2.4 Diagonalisation

The Hamiltonian in equation (2.10) may be diagonalised by a rotation of the basis states,

$$\begin{pmatrix} \gamma_{\mathbf{k},\sigma} \\ \gamma_{\mathbf{k},\bar{\sigma}} \end{pmatrix} = \begin{pmatrix} u_{\mathbf{k}} & v_{\mathbf{k}} \\ -v_{\mathbf{k}} & u_{\mathbf{k}} \end{pmatrix} \begin{pmatrix} c_{\mathbf{k}-\frac{\mathbf{Q}}{2},\sigma} \\ c_{\mathbf{k}+\frac{\mathbf{Q}}{2},\sigma} \end{pmatrix}, \tag{2.11}$$

with

$$u_{\mathbf{k}}^2 = \frac{1}{2}\left(1 + \frac{\epsilon_{\mathbf{k}-\frac{\mathbf{Q}}{2}} - \epsilon_{\mathbf{k}+\frac{\mathbf{Q}}{2}}}{\sqrt{(\epsilon_{\mathbf{k}-\frac{\mathbf{Q}}{2}} - \epsilon_{\mathbf{k}+\frac{\mathbf{Q}}{2}})^2 + (2gM)^2}}\right) \tag{2.12}$$

$$v_{\mathbf{k}}^2 = \frac{1}{2}\left(1 - \frac{\epsilon_{\mathbf{k}-\frac{\mathbf{Q}}{2}} - \epsilon_{\mathbf{k}+\frac{\mathbf{Q}}{2}}}{\sqrt{(\epsilon_{\mathbf{k}-\frac{\mathbf{Q}}{2}} - \epsilon_{\mathbf{k}+\frac{\mathbf{Q}}{2}})^2 + (2gM)^2}}\right). \tag{2.13}$$

The Hamiltonian in terms of the rotated basis takes the form

$$\mathcal{H} - \mu\mathcal{N} = \sum_{\mathbf{k},\sigma} \xi_{\mathbf{k},\sigma}\gamma_{\mathbf{k},\sigma}^\dagger \gamma_{\mathbf{k},\sigma} + g\frac{M^2}{2}. \tag{2.14}$$

The dispersion in the presence of antiferromagnetism is

$$\xi_{\mathbf{k},\sigma} = \frac{1}{2}\left(\epsilon_{\mathbf{k}-\frac{\mathbf{Q}}{2}} + \epsilon_{\mathbf{k}+\frac{\mathbf{Q}}{2}} + \sigma\sqrt{(\epsilon_{\mathbf{k}-\frac{\mathbf{Q}}{2}} - \epsilon_{\mathbf{k}+\frac{\mathbf{Q}}{2}})^2 + 4g^2M^2}\right) - \mu. \tag{2.15}$$

With exception of Sections 2.3 and 2.5, this thesis will assume commensurate antiferromagnetism with $\mathbf{Q} = (\pi, \pi)$. It is instructive to highlight the effect of commensurate ordering at this point. Recall, the tight binding dispersion, $\epsilon_{\mathbf{k}} = -2t(\cos k_x + \cos k_y)$, then

$$\left.\begin{aligned} \epsilon_{\mathbf{k}+\frac{\mathbf{Q}}{2}} &= -\epsilon_{\mathbf{k}-\frac{\mathbf{Q}}{2}} \\ \epsilon_{\mathbf{k}+\mathbf{Q}} &= -\epsilon_{\mathbf{k}} \end{aligned}\right\} \quad \forall \ \mathbf{Q} = (\pm i\pi, \pm j\pi) \ \& \ i, j \in \mathbb{N}. \tag{2.16}$$

This reduces the dispersion in Equation (2.15) to

$$\xi_{\mathbf{k},\sigma} = \sigma\sqrt{\epsilon_{\mathbf{k}}^2 + g^2M^2} - \mu. \tag{2.17}$$
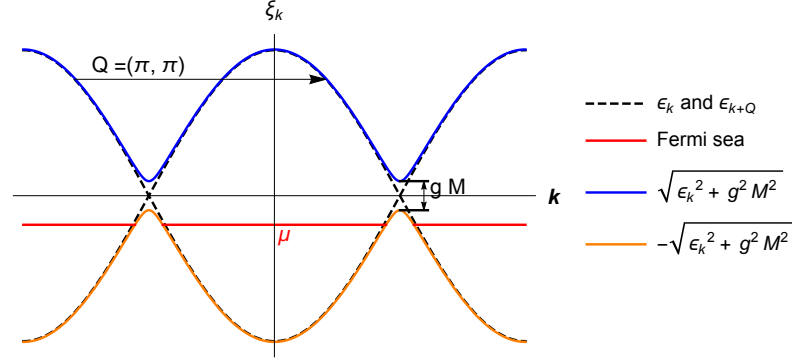
Figure 2.2: **Cross section of the dispersion in the presence of antiferromagnetic order.** The antiferromagnetic wavevector was chosen as $\mathbf{Q} = (\pi, \pi)$.

A cross section of the dispersion in the presence of commensurate antiferromagnetic order is plotted in Figure 2.2. Note how the size of the gap changes the size of the Fermi sea. In particular, when the gap is larger than the chemical potential, the lower band is completely filled and the Fermi surface disappears. The significance of this will be explored at a later stage.

2.2.5 Free energy

At mean field level the Helmholtz free energy is defined as:

$$\mathcal{F} = -\frac{1}{\beta} \log \mathcal{Z}, \tag{2.18}$$

where $\mathcal{Z}$ is the partition function of non-interacting Fermions in the grand canonical ensemble, given by:

$$\mathcal{Z} = \sum_n (e^{-\beta(\epsilon_n - \mu)} + 1) \tag{2.19}$$

$$= \text{Tr}\left(e^{-\beta(\mathcal{H} - \mu\mathcal{N})} + 1\right). \tag{2.20}$$

Combining (2.18) and (2.20) we find

$$\mathcal{F} = -\frac{1}{\beta} \text{Tr} \log \left(e^{-\beta(\mathcal{H} - \mu\mathcal{N})} + 1\right) \tag{2.21}$$

$$= -\frac{1}{\beta} \sum_{\mathbf{k}} \log \left(e^{-\beta(\epsilon_{\mathbf{k}} - \mu)} + 1\right). \tag{2.22}$$

Having derived the formal expression, we may now write down the mean field free energy of the Hubbard model in the presence of antiferromagnetic order:

$$\mathcal{F} \;\; = \;\; -T \sum_{\mathbf{k},\sigma} \log \left(e^{-\frac{\xi_{\mathbf{k},\sigma}}{T}} + 1 \right) + \frac{gM^2}{2}, \tag{2.23}$$

where $\xi_{\mathbf{k},\sigma}$ is the dispersion in the presence of antiferromagnetism, Equation (2.15).

2.2.6 Landau expansion

Next, we derive formal expressions for the mean field Landau coefficients. In the present case, we may simplify the calculation significantly. Instead of expanding in the order parameter M, we expand in M^2:

$$\alpha^{(2n)} \;\; = \;\; \frac{1}{2n!} \left. \frac{\partial^{2n} \mathcal{F}}{\partial M^{2n}} \right|_{M=0} = \frac{1}{n!} \left. \frac{\partial^n \mathcal{F}}{\partial (M^2)^n} \right|_{M=0}, \tag{2.24}$$

with

$$\mathcal{F} = \sum_{n=1}^{\infty} \alpha^{(2n)} M^{2n} = \alpha M^2 + \beta M^4 + \gamma M^6 + O(M^8). \tag{2.25}$$

We have introduced the usual notational convention for the first three coefficients. Calculating the derivatives we find

$$\alpha = g^2 \sum_{\mathbf{k}} \frac{f(\xi_{\mathbf{k}-\frac{\mathbf{Q}}{2}}) - f(\xi_{\mathbf{k}+\frac{\mathbf{Q}}{2}})}{\xi_{\mathbf{k}-\frac{\mathbf{Q}}{2}} - \xi_{\mathbf{k}+\frac{\mathbf{Q}}{2}}} + \frac{g}{2} \tag{2.26}$$

$$\beta = g^4 \sum_{\mathbf{k}} \left[-\frac{f(\xi_{\mathbf{k}-\frac{\mathbf{Q}}{2}}) - f(\xi_{\mathbf{k}+\frac{\mathbf{Q}}{2}})}{(\xi_{\mathbf{k}-\frac{\mathbf{Q}}{2}} - \xi_{\mathbf{k}+\frac{\mathbf{Q}}{2}})^3} + \frac{f'(\xi_{\mathbf{k}-\frac{\mathbf{Q}}{2}}) + f'(\xi_{\mathbf{k}+\frac{\mathbf{Q}}{2}})}{2(\xi_{\mathbf{k}-\frac{\mathbf{Q}}{2}} - \xi_{\mathbf{k}+\frac{\mathbf{Q}}{2}})^2} \right] \tag{2.27}$$

$$\gamma = g^6 \sum_{\mathbf{k}} \left[2\frac{f(\xi_{\mathbf{k}-\frac{\mathbf{Q}}{2}}) - f(\xi_{\mathbf{k}+\frac{\mathbf{Q}}{2}})}{(\xi_{\mathbf{k}-\frac{\mathbf{Q}}{2}} - \xi_{\mathbf{k}+\frac{\mathbf{Q}}{2}})^5} - \frac{f'(\xi_{\mathbf{k}-\frac{\mathbf{Q}}{2}}) + f'(\xi_{\mathbf{k}+\frac{\mathbf{Q}}{2}})}{(\xi_{\mathbf{k}-\frac{\mathbf{Q}}{2}} - \xi_{\mathbf{k}+\frac{\mathbf{Q}}{2}})^4} + \frac{f''(\xi_{\mathbf{k}-\frac{\mathbf{Q}}{2}}) - f''(\xi_{\mathbf{k}+\frac{\mathbf{Q}}{2}})}{6(\xi_{\mathbf{k}-\frac{\mathbf{Q}}{2}} - \xi_{\mathbf{k}+\frac{\mathbf{Q}}{2}})^3} \right], \tag{2.28}$$

where the Fermi distribution function is defined as $f(x) = (e^{x/T} + 1)^{-1}$.

The complexity of terms grows from order to order. In particular, note the increasing order of derivatives of Fermi functions. Their highly oscillatory behaviour at small

temperatures $(T < |\mu|)$ is further amplified by higher and higher order denominators. This is suggestive of non-analytic behaviour below the tricritical point.

Assuming commensurate order and using the discrete translational antisymmetry of the dispersion, we may simplify these expressions. In general, we obtain

$$\alpha^{(2n)}\big|_{\mathbf{Q}=(\pi,\pi)} = \frac{1}{n!} \sum_{\mathbf{k}} \left(\frac{g^2}{2\epsilon_{\mathbf{k}}} \frac{\partial}{\partial\epsilon_{\mathbf{k}}} \right)^{n-1} \left(g^2 \frac{f(\epsilon_{\mathbf{k}} - \mu) - f(-\epsilon_{\mathbf{k}} - \mu)}{2\epsilon_{\mathbf{k}}} + \frac{g}{2} \right). \quad (2.29)$$

2.3 *Heuristic picture*

Having derived formal expressions, we would now like to calculate the phase diagram.

In this section, we will discuss a heuristic picture of the mean field theory of the antiferromagnet. This will serve to develop some physical intuition as well as a guide to the analytical and numerical analysis.

2.3.1 Antiferromagnetic order

The simplest case to consider is a second order transition to commensurate order. Here, the Fermi surface close to half filling takes the form plotted in Figure 2.3.
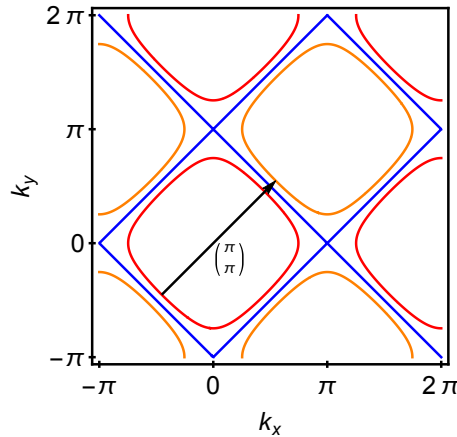
Figure 2.3: **Fermi surface in the presence of commensurate antiferromagnetic order.** The original Fermi surface is red, while the shifted Fermi surface is depicted in orange. The blue contour is the half filling Fermi surface serving as a guide to the eye.

For high temperatures $(T > |\mu|)$ the phase transition behaves as expected. The canonical picture here is of competition between thermal fluctuations and the electron-electron interactions. The transition temperature increases monotonically with the interaction strength.

In this temperature range the occupation of states in momentum space is not cut off sharply at the Fermi energy. Instead, thermal fluctuations allow partial occupation above the Fermi surface at a distance proportional to temperature. Therefore, we may picture the Fermi surface as a band of finite width $\frac{T}{v_F}$ (See Figure 2.4). This relaxes the geometric requirements for nesting, so the original and shifted Fermi surface in Figure 2.3 may be considered well nested for $T > |\mu|$.
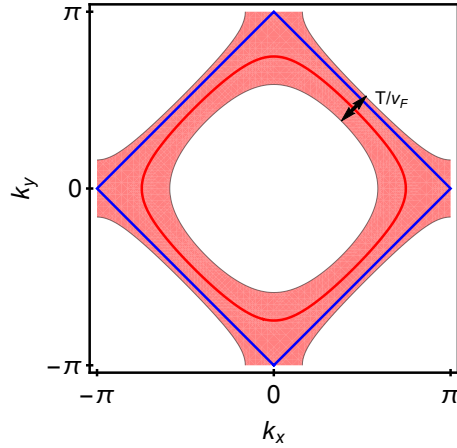
Figure 2.4: **Sketch of the Fermi surface at finite temperature.** The zero temperature Fermi surface is in red, while the thermal widening is depicted in light red. The blue line is the half filling Fermi surface for orientation.

For temperatures below this threshold the quality of nesting diminishes with decreasing temperature. Hence, the transition line becomes reentrant, in the sense that smaller temperatures require stronger interactions for the transition to occur. The reduction in nesting may also be viewed as a shrinking of the available phase space for a given value of the electron-electron interaction.

To avoid this reentrance of the second order transition, we consider incommensurate wave vectors. Incommensurate order allows for nesting even for vanishingly small temperatures. In general we may write our new ordering vector as $\mathbf{Q} = (\pi, \pi) + \delta\mathbf{Q}$, where $|\delta\mathbf{Q}| \approx \frac{\mu}{v_F}$. The broken circular symmetry of the Fermi surface suggests two independent directions of $\delta\mathbf{Q}$. Without loss of generality we consider $(1, 1)$ and $(1, 0)$.

Other symmetry related directions of $\delta\mathbf{Q}$, such as $(-1, 1)$ or $(0, 1)$, are equivalent choices. Figure 2.5 displays both possibilities. Figure 2.5 indicates a larger degree of nesting for an incommensurate wave vector $\mathbf{Q} = (\pi - \delta Q, \pi)$.

(a) Fermi surface in the presence of incommensurate antiferromagnetic order with wave vector $\mathbf{Q}=(\pi-\delta Q, \pi)$.

(b) Fermi surface in the presence of incommensurate antiferromagnetic order with wave vector $\mathbf{Q}=(\pi-\delta Q, \pi-\delta Q)$.
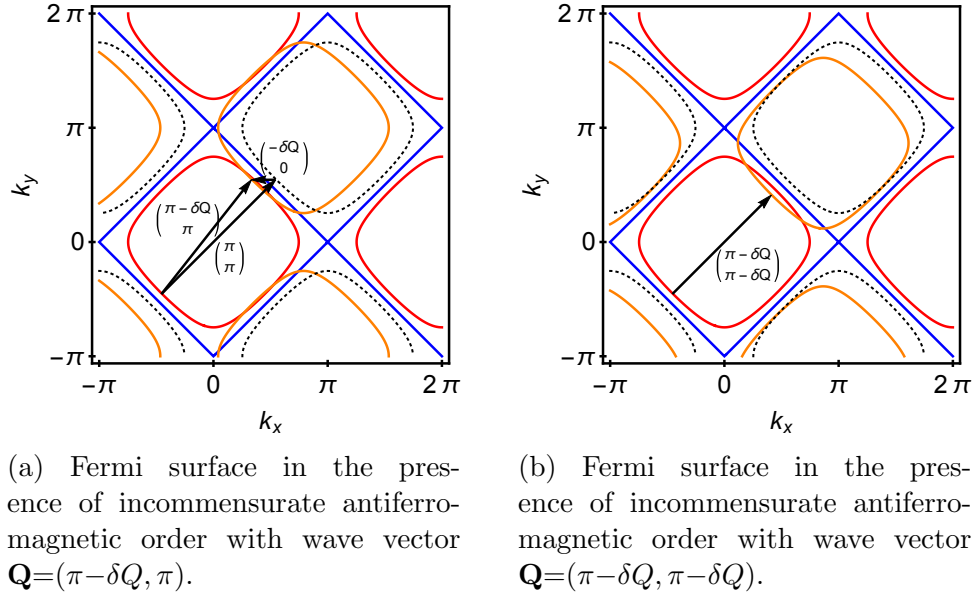
Figure 2.5: **Plots of the shifted Fermi surfaces for incommensurate antiferromagnetic order.** The red contour is the original Fermi surface. The black and dotted contour is the Fermi surface shifted by $\mathbf{Q} = (\pi, \pi)$. The orange contour is the Fermi surface shifted by an incommensurate wave vector. The blue contour is the Fermi surface at half filling serving as a guide to the eye.

Up to this point we have been thinking about the change in Fermi surface in the presence of antiferromagnetic order with regards to a second order transition. We found that the geometry of the system suggests different ordering vectors depending upon the relative size of temperature and chemical potential. Assuming a second order transition implied that we could take magnetisation to be much smaller than the Fermi energy, $|gM| < |\mu|$. Hence, effects due to the size of the finite magnetisation could be ignored.

However, from Figure 2.2 it is clear, that an increase in magnetisation enlarges the Fermi sea. In fact, for magnetisation larger than the Fermi energy, $|gM| > |\mu|$, the gap pushes through the Fermi level and the original and shifted Fermi surface join at the half filling line. Hence, for sufficiently large magnetisation the nesting behaves identical to the Hubbard model at half filling. The enhanced phase space at half filling due to perfect nesting and the logarithmic van-Hove singularity makes

the system highly susceptible to ordering at commensurate wave vectors. We may therefore envisage a first order transition towards magnetisations larger than the chemical potential.

2.3.2 Rice's LOFF analogy

The predictions gathered from the heuristics above may be reinforced by examining the phase diagram of superconductivity. In 1970 Maurice Rice showed, that antiferromagnetism and superconductivity map to one another by a particle-hole transformation of one spin [40]. Particle-hole pairs forming the antiferromagnet are mapped to Cooper pairs of particles that form the superconductivity.

In the antiferromagnet the nested Fermi surfaces are those of particles and holes, whose relative size is determined by the chemical potential. In the superconductor the paired Fermi surfaces are those of spin up and down particles, whose relative size may be changed by applying an external magnetic field.
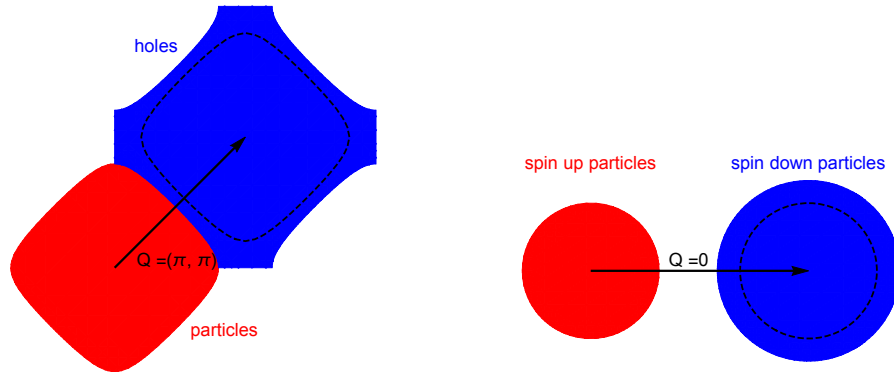
(a) Fermi surface of particle and holes in the tight binding model below half filling.

(b) Fermi surface of spin up and down particles in an external magnetic field.

Figure 2.6: **Sketch of the nested Fermi surfaces of the incommensurate antiferromagnet and LOFF superconductor.** The 2 Fermi surfaces are coloured in Red and Blue. The dashed contours are the shifted Fermi surfaces in case of commensurate and BCS order, respectively.

Lastly incommensurate antiferromagnetism is mapped onto superconductivity with non-zero pairing momentum - the LOFF state [44–46].

The behaviour of the antiferromagnet close to half filling is therefore mirrored by a superconductor in an external magnetic or spin exchange field, the later being the starting point of both Larkin and Ovchinnikov, and Fulde and Ferrell. In this model one finds similar features predicted by the heuristic picture above: A reentrant second order transition to ordinary BCS superconductivity, which is preempted by both a first order transition to zero momentum pairing as well as a second order transition to the LOFF phase.
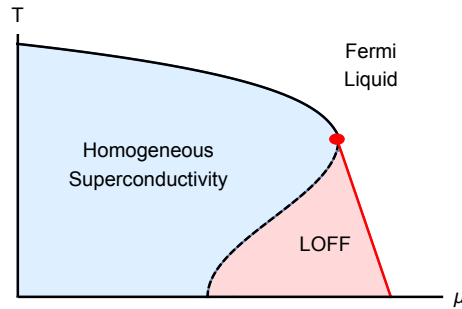
Figure 2.7: **Sketch of doping-temperature phase diagram of the LOFF phase.** The second order transition from the Fermi liquid to homogeneous superconductivity (black line) is reentrant. Below the tricritical temperature (red dot) the transition turns first order. Here, the reentrance becomes preemted by a transition to the LOFF state (red region). Figure adapted from [46]

However, the LOFF model further exhibits a first order transition to the LOFF phase which preempts the second order transition to the same. The LOFF phase diagram is sketched in Figure 2.7. The discrepancy between LOFF and incommensurate antiferromagnetism can be explained by considering the different model's dispersions. The LOFF model uses simple spherical free electron Fermi surfaces for both spins, whose geometry is fundamentally independent of the size of the superconducting gap. In contrast, the tight binding dispersion's geometry changes drastically when one introduces a gap larger than the chemical potential. This is a result of introducing a lattice into the model. Hence, in the present system Rice's analogy is only reliable for a sufficiently small order parameter.

	Antiferromagnet	Superconductor
Order parameter	$c_{\mathbf{k},\uparrow}^{\dagger} c_{\mathbf{k+Q},\downarrow}$	$c_{\mathbf{k},\uparrow}^{\dagger} c_{-\mathbf{k},\downarrow}^{\dagger}$
Control of relative size of paired Fermi surfaces	chemical potential	external magnetic field
Deviation in pairing momentum leads to	incommensurate antiferromagnet	LOFF state

Table 2.1: **Summary of the mapping between antiferromagnetism and superconductivity**

2.4   *Commensurate second order phase transition*

2.4.1   Overview

In this section we calculate the second order phase transition line from paramagnetic to commensurate antiferromagnetic order. For temperatures greater than the chemical potential we expect the classical monotonic increase of the transition temperature with interaction strength. For temperatures lower than the Fermi energy, nesting is reduced (see Figure 2.3) and we predict a reentrance.

The onset of a second order phase transition is marked by the continuous appearance of a finite order parameter. The Landau-Ginzburg formalism expresses this as a sign change of the lowest order expansion coefficient α (see Figure 2.8) The objective of this section is to find the zeros of α, as a function of interaction strength and temperature. We will start by performing a numerical analysis, which will be confirmed by analytical tools in the appropriate limits.

2.4.2   Numerical approach

The condition for second order transitions, $\alpha = 0$, gives us an expression for the interaction strength as a function of temperature and chemical potential:

$$g = -\left(\sum_{\mathbf{k}} \frac{f(\epsilon_{\mathbf{k}} - \mu) - f(-\epsilon_{\mathbf{k}} - \mu)}{\epsilon_{\mathbf{k}}} \right)^{-1}. \tag{2.30}$$
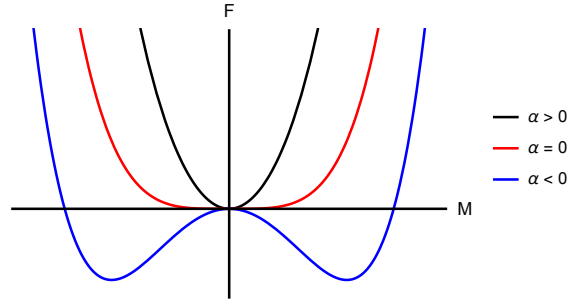
Figure 2.8: **Sketch of the Free energy as a function of magnetisation for different signs of α.** The red line represents the second order phase transition point between the symmetric phase in black and the broken symmetry phase in blue.

The numerical approach consists of evaluating the integral for α for a fixed chemical potential, $|\mu| \ll t$, and varying temperature. The result is displayed in Figure 2.9.
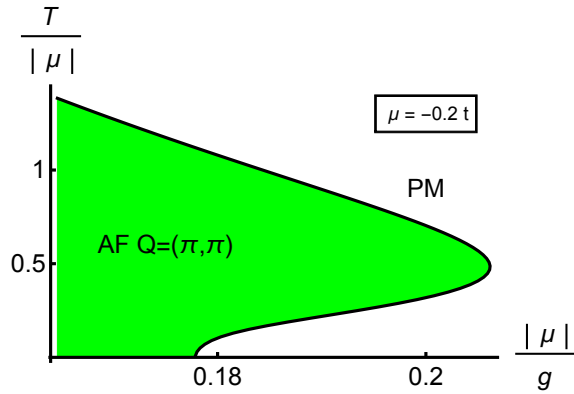
Figure 2.9: **Second order transition line of commensurate antiferromagnetic order in the Hubbard model close to half filling.** The green area (AF) denotes the commensurate antiferromagnetic phase. PM denotes the paramagnetic phase. Reentrance appears at $T \approx |\mu|/2$.

As expected, we find a reentrant second order transition to commensurate antiferromagnetism.

In the limits of temperature being much smaller or larger than the chemical potential, we may confirm these findings analytically.

2.4.3 Analytic approach

Analytical solutions for the location of the commensurate second order transition may be formed in two limits: temperatures smaller or larger than the chemical potential.

High temperature limit

In the limit of high temperatures we may expand the Fermi distributions functions in orders of $\frac{\xi}{T}$. Then the quadratic coefficient is given by

$$\alpha \;=\; 0 \;=\; g^2 \sum_{\mathbf{k}} \frac{f(\epsilon_{\mathbf{k}} - \mu) - f(-\epsilon_{\mathbf{k}} - \mu)}{2\epsilon_{\mathbf{k}}} + \frac{g}{2} \tag{2.31}$$

$$\approx \;-g^2 \sum_{\mathbf{k}} \frac{1}{T} + \frac{g}{2}. \tag{2.32}$$

Solving for the interaction we obtain

$$g \;=\; \frac{T}{2}. \tag{2.33}$$

This is in good agreement with the numerical result. For temperatures larger than the Fermi energy the numerical phase transition line approaches the analytical result asymptotically. This approach may be extended to higher orders. However, the reentrant behaviour of the second order phase transition can not be analysed with this expansion, since its temperature is outside the radius of convergence.

Low temperature limit

In the limit of small temperature we may perform a Sommerfeld expansion. To quadratic order in temperature a Sommerfeld expansion takes the form

$$\int_{-\infty}^{\infty} \frac{H(\epsilon)}{e^{\beta(\epsilon - \mu)} + 1} d\epsilon = \int_{-\infty}^{\mu} H(\epsilon) d\epsilon + T^2 \frac{\pi^2}{6} H'(\mu) + O(T^4). \tag{2.34}$$

Expressing the quadratic coefficient α as an energy integral by introduction of the density of states we obtain

$$\alpha \;\; = \;\; g^2 \sum_\epsilon \rho(\epsilon) \frac{f(\epsilon - \mu)}{\epsilon} \; + \frac{g}{2}. \tag{2.35}$$

Here, we identify $H(\epsilon) = \frac{\rho(\epsilon)}{\epsilon}$, so that the Sommerfeld expansion of α becomes

$$\alpha = g^2 \left(\int_{-4t}^{\mu} \frac{\rho(\epsilon)}{\epsilon} d\epsilon - T^2 \frac{\pi^2}{6} \left(\frac{\rho(\mu)}{\mu^2} - \frac{\rho'(\mu)}{\mu} \right) \right) + \frac{g}{2}. \tag{2.36}$$

The integration is cut of by the electron bandwidth below and by the Fermi energy above. Solving $\alpha = 0$ for g we find

$$g = \frac{1}{-2 \left(\int_{-4t}^{\mu} \frac{\rho(\epsilon)}{\epsilon} d\epsilon - T^2 \frac{\pi^2}{6} \left(\frac{\rho(\mu)}{\mu^2} - \frac{\rho'(\mu)}{\mu} \right) \right)}. \tag{2.37}$$

Evaluating the integral and derivatives with the approximate, logarithmic density of states, equation (2.5), we arrive at

$$g = \frac{1}{\rho(\mu)(-\log(\frac{|\mu|}{4t}) + T^2 \frac{\pi^2}{3\mu^2})}, \tag{2.38}$$

where we have omitted subleading contributions.

This confirms the reentrant behaviour found through numerical means as seen in Figure 2.10. As for the high temperature limit, a finite number of higher order terms is not sufficient to reproduce the phase transition line in the vicinity of intermediate temperature ($T \approx \mu/2$). This area is beyond the radius of convergence. Higher order terms merely exhibit more and more extreme behaviour in this region.

2.5 *Incommensurate second order phase transition*

2.5.1 Turning the heuristic picture into a calculation

In Section 2.3 we discussed how the reentrance of the commensurate second order transition may be preempted by incommensurate antiferromagnetic order. This may
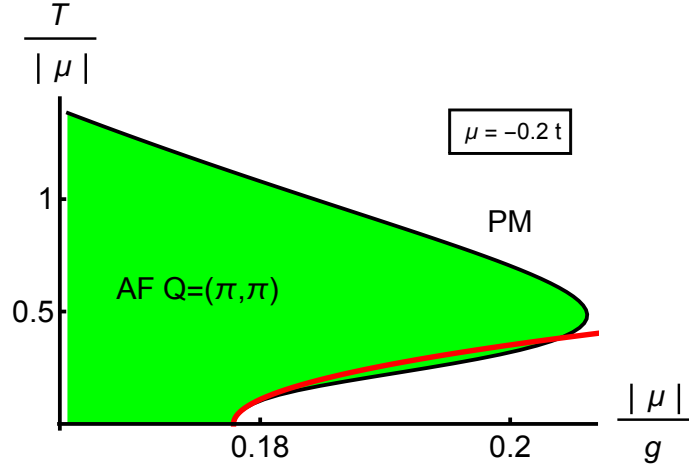
Figure 2.10: **Mean field second order transition line to commensurate antiferromagnetism including its Sommerfeld approximation.** The exact numerics are depicted as the black line, while the Sommerfeld approximation is red.

occur because a change in wavevector improves nesting at temperatures lower than the chemical potential. Below, we will analyse the precise form of this incommensurate antiferromagnetic order and calculate its phase transition line.

We will start by analysing the second order Landau coefficient as a function of antiferromagnetic ordering wave vector $\mathbf{Q}$. This will give us insight into the preferred direction of $\delta\mathbf{Q} = \mathbf{Q} - (\pi, \pi)$.

Having thus reduced the dimensionality of the parameter space, we continue by calculating the phase transition line of the incommensurate antiferromagnet.

2.5.2 Direction of $\delta\mathbf{Q}$

In order to determine the preferred direction of $\delta\mathbf{Q}$ we calculate and plot the Lindhard functions as a function of antiferromagnetic wave vector. The Lindhard function takes the form:

$$\chi(\mathbf{Q}, \omega = 0) = \sum_{\mathbf{k}} \frac{f(\xi_{\mathbf{k}-\frac{\mathbf{Q}}{2}}) - f(\xi_{\mathbf{k}+\frac{\mathbf{Q}}{2}})}{\xi_{\mathbf{k}-\frac{\mathbf{Q}}{2}} - \xi_{\mathbf{k}+\frac{\mathbf{Q}}{2}}}. \tag{2.39}$$

This is nothing other than the integral in the second order Landau coefficient in equation (2.26). Physically it measures the susceptibility of electrons to particle-

hole excitations of energy ω and momentum $\mathbf{Q}$.

The result of the numerical integration, close to half filling and temperature much lower than the chemical potential, $T \ll |\mu| \ll t$, is displayed in Figure 2.11. Close inspection reveals, that the preferred direction of the incommensurate phase is $\delta\mathbf{Q} = \delta Q(1,0)$.
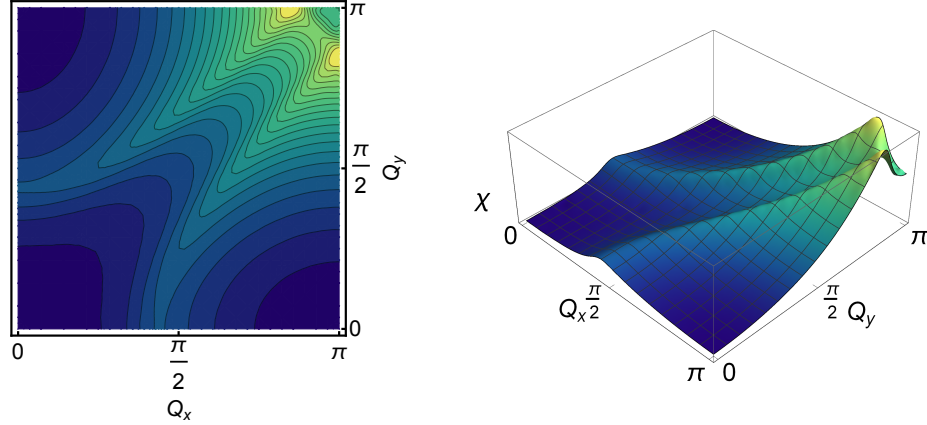
Figure 2.11: **Contour and 3D plots of the Lindhardt function of antiferromagnetism in the Hubbard model.** Identical shading was used for both Plots. See also [47, 48].

Figure 2.13 shows the shifted Fermi surface for such a wave vector. Note, that the direction of $\delta\mathbf{Q}$ is independent of temperature or chemical potential, since neither change the band symmetry. They do however change the length of $\delta\mathbf{Q}$. In particular we find that for temperatures much smaller than the Fermi energy

$$|\delta\mathbf{Q}| \approx \frac{\mu}{v_F}\pi, \tag{2.40}$$

where $v_F = 2\sqrt{2}t$ is the Fermi velocity at $\mathbf{k} = (\frac{\pi}{2}, \frac{\pi}{2})$. The accuracy of this relationship close to half filling is demonstrated in Figure 2.12.

This is consistent with neutron scattering data collected from LSCO [49–51] and YBCO [52] samples. In both these compounds the incommensurability is a linear function of doping. Further the preferred direction of $\delta\mathbf{Q}$ in these samples is identical to the one determined here. However, in LSCO the orientation only agrees for superconducting samples, while at lower doping the incommensurate vector component re-orientates by $\pi/4$. Thus the form of the antiferromagnetic wave vector seems
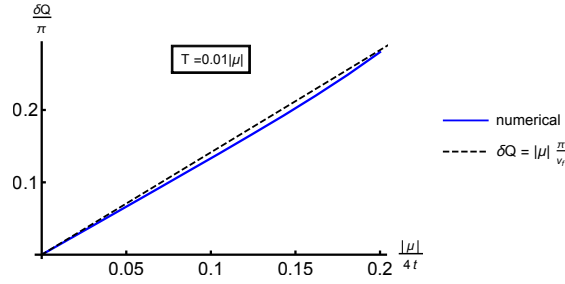
Figure 2.12: **Incommensurability, $\delta \mathbf{Q}$, as a function of the chemical potential.** In blue is the numerical result of maximising the Lindhardt-function. The black dashed line is $|\delta \mathbf{Q}| \approx \frac{\mu}{v_F}\pi$. Temperature was choosen much smaller than the chemical potential, $T = 0.01|\mu|$

intimately related to the occurrence of superconductivity. Figure 2.14 summarises this experimental data.

The method of measuring the antiferromagnetic ordering wavevector employed by [49–52] is neutron scattering. Neutrons posses zero charge and due to their spin a small magnetic moment. Thus neutrons only interact with the atomic nuclei of samples via the short-ranged strong force and with magnetic moments via a dipole interaction. This makes neutrons only weakly interacting and therefore ideal candidates to probe the bulk properties of samples and samples inside an experimental casing as required for cryogenics or application of pressure. However, this weak interaction necessitate large single crystal samples and does not allow for powder diffraction experiments. Due to their interaction with the atomic nuclei, neutrons are used to probe the lattice structure and its excitations - phonons. The spin of the neutrons interacts with unpaired electrons and thus neutrons are employed to probe the magnetic structure and magnetic excitations of samples.

Since, the cross-section of the neutron-magnetic scattering is comparable to the neutron-nuclear scattering cross-section, the scattering of neutrons off magnetic structure provides sufficiently strong signals in the diffraction pattern. This diffraction pattern is governed by Bragg's law, highly repetitive structures result in bright Bragg diffraction peaks. To distinguish between features in the diffraction pattern caused by nuclear or magnetic scattering, one may first analyse the crystal structure in the absence of magnetic order, for instance at sufficiently high temperature. Subsequently, one can cool the sample and measure any changes in the diffraction pattern due to the formation of order. The diffraction pattern is a map of the sam-
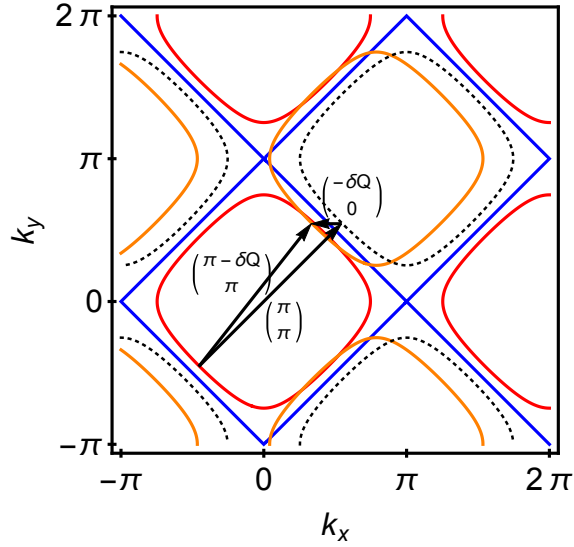
Figure 2.13: **Fermi surface in the presence of incommensurate antiferro-magnetism.** The wave vector is of the form $\mathbf{Q} = (\pi + \delta Q, \pi)$. The red contour is the original Fermi surface. The orange and black dotted contour are the incommensurately and commensurately shifter Fermi surfaces respectively. The blue contour is the half filling diamond for reference.

ple's crystal and magnetic phase structure and thus allows for direct measurement of the magnetic ordering wavevector.

2.5.3 Phase diagram of the incommensurate antiferromagnet

Above, we demonstrated the preferred direction of the incommensurate component, $\delta\mathbf{Q}$, of the antiferromagnetic order. Our next task is to determine its length. Earlier, we argued that nesting of the commensurate order is improved by an increase in temperature. Hence the degree to which the system prefers incommensurate order should decrease as temperature rises. Therefore, we hypothesised, that $\delta\mathbf{Q}$ tends to zero as temperature approaches the Fermi energy.

Our task in this section is to determine the ordering wave vector as a function of temperature and from that calculate the incommensurate phase transition line.

In general this may be done by expanding α in $\delta\mathbf{Q}$ and solving the simultaneous

(a) YBCO   (b) LSCO
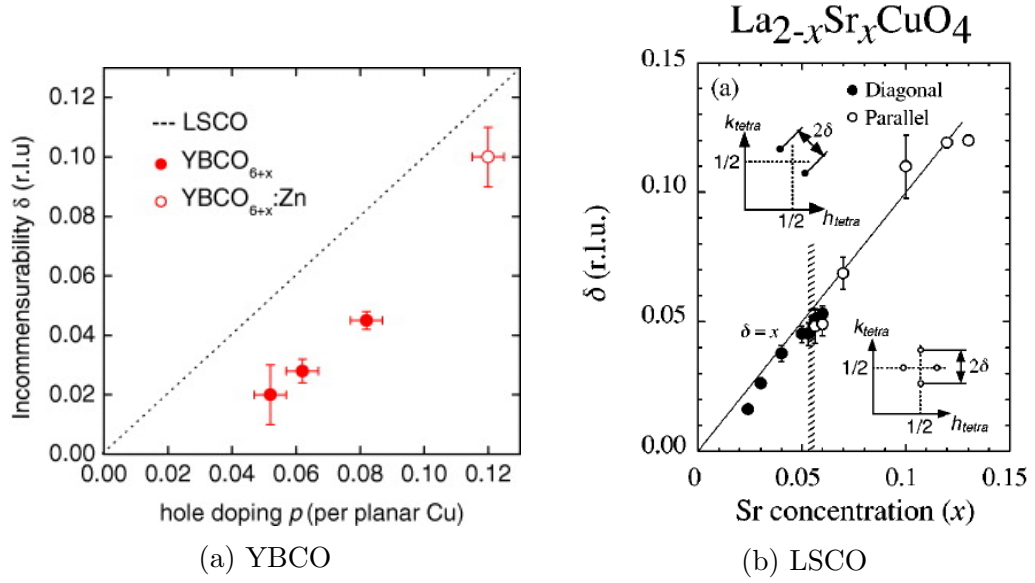
Figure 2.14: **Incommensurability of the antiferromagnetic wave vector as a function of hole-doping in cuprates.** In case of LSCO, the direction of incommensurability changes with the onset of superconductivity around $x = 0.05$. Panel (a) and (b) adapted from [52] and [50] respectively.

equations

$$\alpha = \quad \alpha_0 + \alpha_2 \delta \mathbf{Q^2} + \alpha_4 \delta \mathbf{Q^4} + \alpha_6 \delta \mathbf{Q^6} + .. \quad = 0 \tag{2.41}$$

$$\partial_{\delta \mathbf{Q}} \alpha = \quad 2\alpha_2 \delta \mathbf{Q} + 4\alpha_4 \delta \mathbf{Q^3} + 6\alpha_6 \delta \mathbf{Q^5} + .. \quad = 0. \tag{2.42}$$

However, even knowing the preferred direction of $\delta \mathbf{Q}$, the form of these expansion coefficients is sufficiently non-trivial to prevent an accurate analytical solution.

Instead, we determine the preferred $\delta \mathbf{Q}$ as function of temperature numerically. That is to say, we perform numerical integration and find the maxima of the Lindhardt function. The result is plotted in Figure 2.15. As expected, $\delta \mathbf{Q}$ tends to zero as temperature approaches the Fermi energy.

Surprisingly, $\delta \mathbf{Q}$ does not increase monotonically as temperature tends towards zero. This can be understood by examining the degree of nesting at a smaller scale than the Brillouin zone as displayed in Figure 2.16.

Figure 2.16a sketches the optimal nesting for intermediate temperatures ($T \approx .2|\mu|$). In this regime we may consider the Fermi surface as a band of finite width T. Hence,
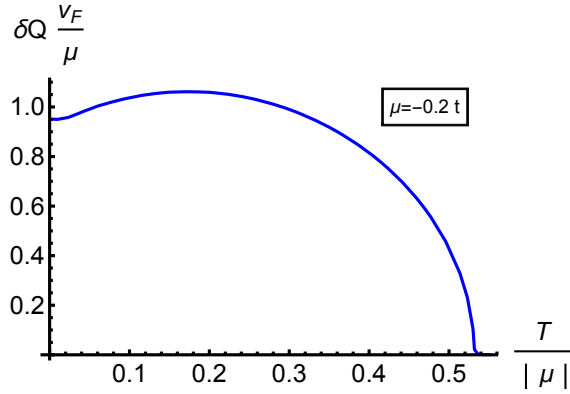
Figure 2.15: **Incommensurability, $\delta\mathbf{Q}$, as a function of temperature.** Note that the incommensurability is not growing monotonically as temperature is lowered.

the best nesting is achieved by crossing the two Fermi surfaces. This weighted overlap of Fermi surfaces results in maximal incommensurability around $T = .17|\mu|$.

As temperature approaches zero this is no longer the optimal manner to nest. Nesting would only be achieved at the two crossing points as the width of the Fermi surface is proportional to temperature. Instead, optimal nesting is achieved by the two Fermi surface touching. To achieve this $\delta\mathbf{Q}$ has to shrink slightly as temperature tends towards zero. Figure 2.16b sketches the optimal nesting in the limit of temperatures approaching zero.

Having determined the optimal ordering wave vector as a function of temperature we may now calculate the phase transition line to incommensurate antiferromagnetic order.

This is done by numerical evaluation of

$$g = -\frac{1}{2}\left(\sum_{\mathbf{k}} \frac{f(\epsilon_{\mathbf{k}-\frac{\mathbf{Q}}{2}} - \mu) - f(\epsilon_{\mathbf{k}+\frac{\mathbf{Q}}{2}} - \mu)}{\epsilon_{\mathbf{k}-\frac{\mathbf{Q}}{2}} - \epsilon_{\mathbf{k}+\frac{\mathbf{Q}}{2}}}\right)^{-1}, \qquad (2.43)$$

for general temperature and with the optimal ordering wave vector determined at that temperature.

The resulting phase diagram is plotted in Figure 2.17. As expected, the re-entrance of the commensurate antiferromagnet is preempted by the incommensurate order. Note, that the ordering wave vector inside the area of incommensurate antiferromagnetism (shown in orange) is not a constant. The antiferromagnetic wave vector
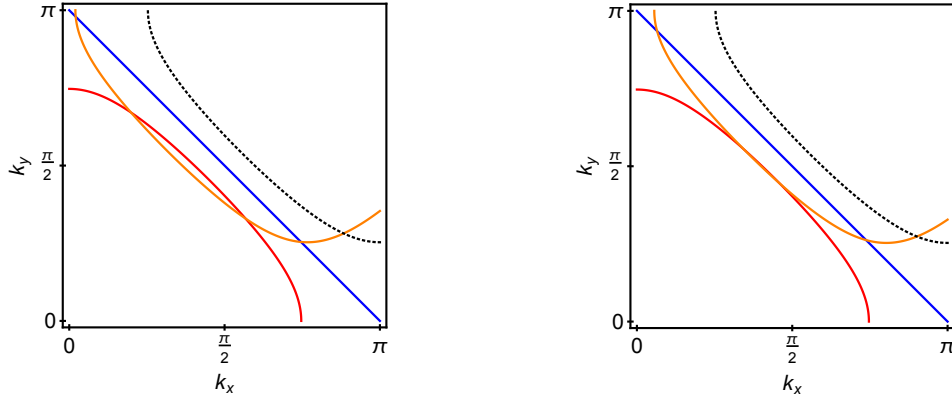
(a) Sketch of optimal nesting at intermediate temperatures ($T \approx .2|\mu|$). This scenario allows for large regions of nesting for intermediate temperatures, while for $T \approx 0$ this geometry only nests at the two crossing points.

(b) Sketch of optimal nesting as temperature approaches zero ($T \ll .1|\mu|$). This scenario allows for Fermi surface nesting along a section of finite length for $T \ll .1|\mu|$. At intermediate temperatures this geometry has reduced nesting away from middle of the Fermi surface sides.

Figure 2.16: **Detail of the Fermi surface around $\mathbf{k} = (\frac{\pi}{2}, \frac{\pi}{2})$ in the presence of incommensurate antiferromagnetism of wave vector $\mathbf{Q} = (\pi + \delta Q, \pi)$.** The red contour is the original Fermi surface. The black solid and dotted contours are the incommensurately and commensurately shifted Fermi surfaces respectively. The blue contour is the half filling "diamond" for reference.

is a function of temperature as displayed in Figure 2.15. The interaction strength, g, does not change the incommensurability. Hence, away from the tricritical point the ordering wave vector changes discontinuously between the commensurate and incommensurate phase regions.

2.6 *First order transition*

2.6.1 Introduction

The last aspect of the mean-field antiferromagnetic phase diagram we would like to explore is the possibility of a first order transition. This is again motivated by Rice's analogy between antiferromagnetism and superconductivity.

In the case of superconductivity, one may calculate a first order transition line
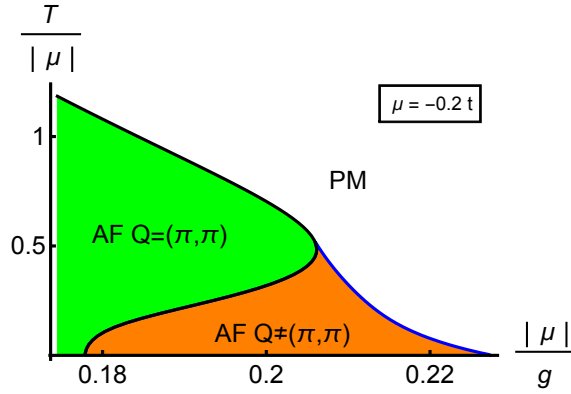
Figure 2.17: **Second order transition lines to antiferromagnetic order in the Hubbard model close to half filling.** The two coloured regions are commensurate order in green and incommensurate order in orange.

to the homogeneous phase. The later is ultimately preempted by considering the incommensurate or LOFF phase. The transition to the LOFF phase is found to be first order, too. Hence, we would like to investigate the existence of a first order transition in the antiferromagnet.

A first order transition consists of a discontinuous jump in the order parameter from zero to a finite value. A quadratic Landau expansion is insufficient to capture this behaviour. Instead, we must expand to sixth order and track the behaviour of the fourth order term, β in relation to the other two (see Figure 1.8). To be exact we aim to find the line of temperature and interaction on which

$$\beta^2 = 4\alpha\gamma. \tag{2.44}$$

2.6.2 Tricritical temperature

The first step in analysing the possibility of a first order transition is to determine the existence of a tricritical temperature. That is the temperature at which

$$\beta = g^4 \sum_{\mathbf{k}} \left\{ -\frac{f(\xi_{\mathbf{k}-\frac{\mathbf{Q}}{2}}) - f(\xi_{\mathbf{k}+\frac{\mathbf{Q}}{2}})}{(\xi_{\mathbf{k}-\frac{\mathbf{Q}}{2}} - \xi_{\mathbf{k}+\frac{\mathbf{Q}}{2}})^3} + \frac{f'(\xi_{\mathbf{k}-\frac{\mathbf{Q}}{2}}) + f'(\xi_{\mathbf{k}+\frac{\mathbf{Q}}{2}})}{2(\xi_{\mathbf{k}-\frac{\mathbf{Q}}{2}} - \xi_{\mathbf{k}+\frac{\mathbf{Q}}{2}})^2} \right\} = 0. \tag{2.45}$$

The point at which this line crosses the second order transition, $\alpha = 0$, is the tricritical point. In Figure 2.19 the tricritical point is depicted as a red dot.
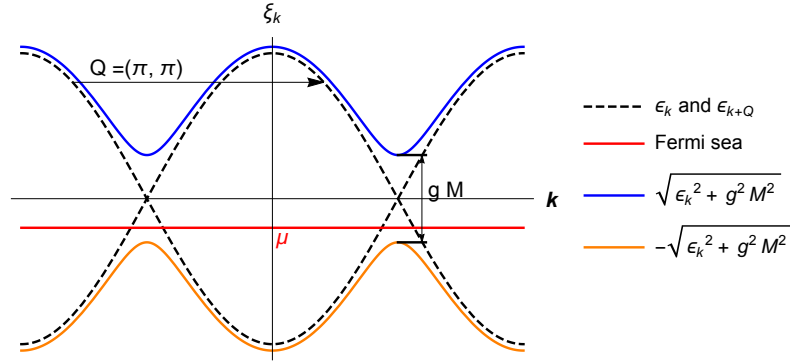
Figure 2.18: **Cross section of the dispersion in the presence of antiferromagnetic order with $g|M| > |\mu|$.** The antiferromagnetic wavevector was chosen as $\mathbf{Q} = (\pi, \pi)$.

2.6.3 Non-analytic behaviour of free energy

It turns out that further analysis of the Landau expansion is not feasible. Below the tricritical point the wild behaviour of the fourth and higher order coefficients makes even their numerical evaluation difficult. This is symptomatic of the non-analytic behaviour of the free energy as temperature approaches zero.

Numerical evaluation of the free energy as a function of magnetisation exposes the origin of the Landau expansion's downfall. For temperatures much smaller than the Fermi energy, the systems exhibits a first order transition to values of magnetisation larger than the chemical potential, $g|M| > |\mu|$. Hence, the chemical potential now lives inside the gap, see Figure 2.18. This is in contrast to the usual scenario of small magnetisation, $g|M| < |\mu|$, displayed in Figure 2.2.

Since the Fermi energy is the intrinsic scale of the model, the antiferromagnetic order parameter can no longer be considered small and a Landau expansion is not an appropriate tool to study the first order transition.

Additionally, since the Fermi energy is situated inside the gap, the band structure for large magnetisation is equivalent to the Hubbard model at half filling in the presence of antiferromagnetic order. Hence, the Fermi surface is perfectly square and deviations away from commensurate ordering are disfavoured.

This behaviour is in contrast to the LOFF phase. In the LOFF model the system transitions to finite momentum superconductivity via a first order transition. The

opening of a gap does not change the fundamental geometry of its spherical dispersion. Hence for sufficiently low temperatures the LOFF model prefers ordering at finite momentum regardless of the size of its ordering parameter.

2.6.4 Numerical approach

We may investigate the position of the first order line by numerical means. For fixed chemical potential, and varying temperature and interaction, we find the global minimum of the free energy with respect to magnetisation. The first order transition is then identified as the line at which magnetisation jumps to a finite value. The resulting phase diagram is plotted in Figures 2.19 and 2.20.
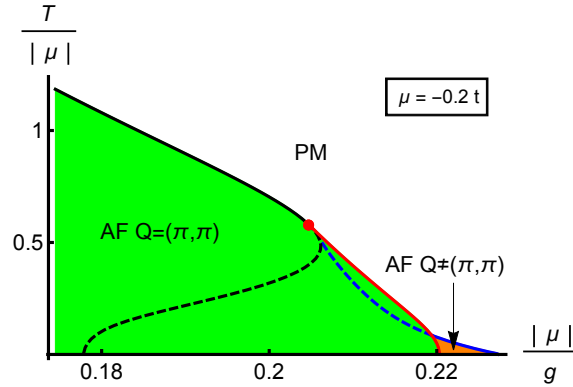
Figure 2.19: **Mean field phase diagram of antiferromagnetism in the Hubbard model close to half filling.** The two coloured regions are commensurate order in green and incommensurate order in orange. The solid and dashed lines depict actual and avoided transition lines. The black and blue lines are second order transitions to commensurate and incommensurate order respectively. The red line is the first order transition and the red dot shows the position of the tricritical point.

As predicted, the first order transition preempts the second order transition to incommensurate antiferromagnetism in general.

Surprisingly, for sufficiently small temperatures there remains a small patch of incommensurate order. Here, the strength of magnetisation is small compared to the chemical potential. The transition between commensurate and incommensurate order is a first order metamagnetic transition. The value of magnetisation jumps to values larger than the Fermi energy and the ordering wave vector changes discontinuously to $\mathbf{Q} = (\pi, \pi)$.
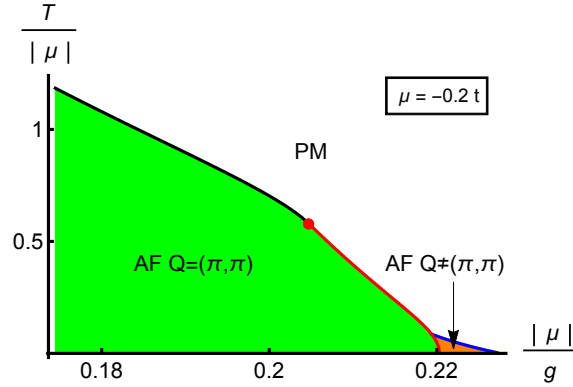
Figure 2.20: **Mean field phase diagram of antiferromagnetism in the Hubbard model close to half filling.** The two coloured regions are commensurate order in green and incommensurate order in orange. The black and blue lines are second order transitions to commensurate and incommensurate order respectively. The red line is the first order transition and the red dot shows the position of the tricritical point.

The free energy gained inside the remaining incommensurate pocket is very small compared to the commensurate region. so it is extremely fragile. However, incommensurate antiferromagnetic order has been proposed in numerous numerical studies [53–55]. Furthermore, there is evidence for incommensurate antiferrogmagnetism in the cuprates, notably in LSCO [49–51, 56, 57] and YBCO [52, 58, 59].

2.7   *Summary*

In this chapter we formally introduced, calculated and analysed the mean field Helmholtz free energy of the Hubbard model in the presence of antiferromagnetic order. We developed a heuristic picture of the model, that explains and predicts the main features of the phase diagram. The latter was determined through analytical and numerical methods, confirming the heuristic predictions in general.

The mean field phase diagram of antiferromagnetism in the Hubbard model was found to be surprisingly rich. Although much of this detail is in the literature, it is often overlooked and assumed the transition will be continuously second order. Instead, the second order transition to commensurate order is reentrant and preempted by incommensurate order as well as a first order transition.

To our surprise, a pocket of incommensurate order survives at low temperatures. This is consistent with the theoretical literature and in fact reproduces experimental phenomena in the cuprate superconductors.

Our next step is to include the effects of quantum fluctuations and new phases such as bond density waves and superconductivity. These will be the topics of the following chapters.

Part III

Quantum order by disorder of the antiferromagnet

Chapter 3

Fermionic quantum order-by-disorder: Formalism

In this chapter we introduce the fermionic quantum order by disorder formalism. We start by illustrating the physics with the help of classical analogies and a simple quantum mechanical example. Then, we explicitly derive the fermionic quantum order-by-disorder formalism from second order perturbation theory, as well as field theoretically, and highlight some properties of the expressions.

3.1 *Concept*

Order-by-disorder describes phenomena in which fluctuations stabilise particular states of a system. This is a familiar mechanism in classical physics. Noise stabilises acrobats on a tight ropes and the ground state in rubber bands is selected entropically by thermal fluctuations. In the Casimir effect, a change in the boundary conditions, imposed by the parallel plates, alters the allowed spectrum of fluctuations, which self-consistently drives the two plates towards each other. Furthermore, order-by-disorder is a familiar concept in high energy physics. The Coleman-Weinberg mechanism describes spontaneous symmetry breaking due to low-energy fluctuations coupling to the order parameter [60].

In condensed matter theory, order-by-disorder is best know in frustrated magnets

[61–64]. Here, the degeneracy of ground states may be lifted by taking into account differences in the spin-wave excitation spectrum. It was in this context, that Villain coined the term order-by-disorder [26]. Albeit in this context it refers to effects driven by thermal fluctuations.

3.1.1 A simple Quantum illustration

The possibly simplest example of fluctuations lifting a classically degenerate ground state is the two-site half filled Hubbard model, see Figure 3.1. In the limit of strong on-site repulsion double occupation of a site is energetically disfavoured. Hence, the classical ground state consists of one spin on either site. Since there is no inter-site interaction, the relative orientation of the two spins leads to a degeneracy.

Fluctuations, in the form of virtual hopping, lift this degeneracy. In case of ferromagnetic ordering, virtual hops are forbidden by the Fermi exclusion principle, Figure 3.1a. However, in case of antiferromagnetic ordering, spin fluctuations are allowed, Figure 3.1b. These virtual hops lower the free energy of the antiferromagnetic state and break the degeneracy.

This simple example contains all the physical ingredients of the more complicated models studied in this thesis. Namely, the determination of the fluctuation spectrum through Pauli blocking by the ground state Fermi surface.

(a) Virtual hopping is forbidden by Fermi exclusion in ferromagnetically aligned spins.

(b) Virtual hopping lowering the free energy in antiferromagnetically aligned spins.
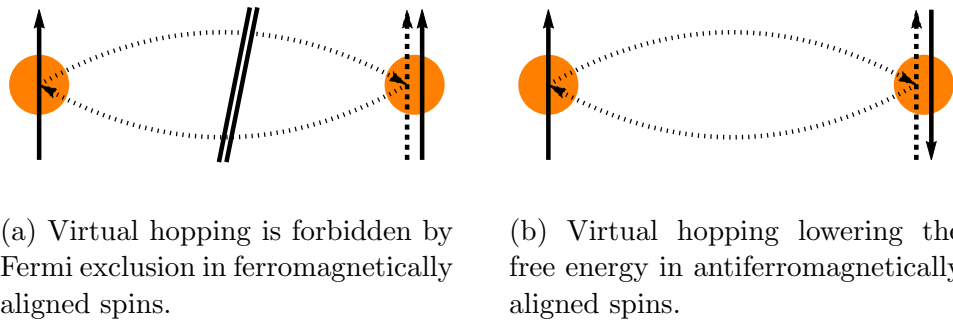
Figure 3.1: **Virtual hopping of spins between two sites.**

In addition to lifting degeneracies, fluctuations may also drive new types of order. Quantum order-by-disorder is an intuitive formalism describing this effect. The presence of particular novel orders changes the shape of the Fermi surface. This in

turn modifies the available phase space for fluctuations, which may self-consistently lower the free energy of the new order. Especially in the vicinity of putative quantum critical points, these fluctuations can be strong enough to drive the system towards novel phases, even if they are not supported in mean field theory.

In fermionic quantum order-by-disorder, the underlying statistic are fermionic. This is in contrast to the conventional order-by-disorder formalism, which analyses bosonic excitations. Hence, the Pauli exclusion principle plays a central role in the fermionic quantum order-by-disorder formalism.

Quantum order-by-disorder expands around the saddle point in the presence of fluctuation driven orders. Thus perturbative corrections due to the interaction are taken into account self-consistently. The broken symmetry phases may in principle change the shape of the Fermi surface, which in turn changes the spectrum of fluctuations, this is automatically taken into account by the self-consistent treatment.

These effects may be treated in a slightly different but equivalent formalism by self-consistent renormalisation starting in the symmetric phase. Here the renormalisation flows towards a fixed point whose Fermi surface shape has changed as a result of perturbative corrections due to the interaction. Neumayr and Metzner perform such renormalisation calculations for an itinerant antiferromagnet and found that it leads to Fermi surface deformations which break the underlying lattice symmetry. Further, they found lower superconducting transition temperatures as compared to similar calculations, which neglect self-consistent Fermi surface deformations [65]. Thus, a complete treatment of itinerant antiferromagnetism and the related superconducting and charge orders should treat the interaction self-consistently.

3.2 *Formal derivation of the fermionic quantum order-by-disorder corrections to the free energy*

Having introduced a physical framework, we now derive fermionic quantum order-by-disorder from self-consistent second order perturbation theory. The derivation is followed by an analysis of the underlying fluctuations. Finally, we present an equivalent field theoretical approach.

3.2.1 Self-consistent perturbative corrections to the free energy

We calculate the corrections to the free energy self-consistently in the presence of the novel order.

The first order perturbative correction to the free energy is zero. The second order perturbative correction to the free energy is given by

$$\delta\mathcal{F} = \sum_m \frac{\langle T|\mathcal{H}_{int}|m\rangle\langle m|\mathcal{H}_{int}|T\rangle}{\epsilon_T - \epsilon_m}, \tag{3.1}$$

where $|T\rangle$ is a thermal state and $|m\rangle$ is a virtual intermediate state.

The interaction Hamiltonian is taken to be the on-site interaction

$$\mathcal{H}_{int} = g\sum_{\mathbf{k}_1..\mathbf{k}_4}' c^\dagger_{\mathbf{k}_1,\uparrow}c^\dagger_{\mathbf{k}_2,\downarrow}c_{\mathbf{k}_3,\uparrow}c_{\mathbf{k}_4,\downarrow}, \tag{3.2}$$

where the $'$ over the sum sign indicates momentum conservation. In this case $\mathbf{k}_1 + \mathbf{k}_2 = \mathbf{k}_3 + \mathbf{k}_4$.

Non-zero terms are given by

$$|m\rangle = \sum_{\substack{\mathbf{k}_1\neq\mathbf{k}_4,\\ \mathbf{k}_2\neq\mathbf{k}_3}} c_{\mathbf{k}_1,\uparrow}c_{\mathbf{k}_2,\downarrow}c^\dagger_{\mathbf{k}_3,\uparrow}c^\dagger_{\mathbf{k}_4,\downarrow}|0\rangle. \tag{3.3}$$

Which leads to

$$\mathcal{F}_{\text{fluct}} = g^2\sum_{\substack{\mathbf{k}_1\neq\mathbf{k}_4,\\ \mathbf{k}_2\neq\mathbf{k}_3}} \frac{|_0\langle\mathbf{k}_1\uparrow,\mathbf{k}_2\downarrow|\mathcal{H}_{int}|\mathbf{k}_3\uparrow,\mathbf{k}_4\downarrow\rangle_0|^2}{\epsilon^\uparrow_{\mathbf{k}_1} + \epsilon^\downarrow_{\mathbf{k}_2} - \epsilon^\uparrow_{\mathbf{k}_3} - \epsilon^\downarrow_{\mathbf{k}_4}}, \tag{3.4}$$

where $|\mathbf{k}_3\uparrow,\mathbf{k}_4\downarrow\rangle_0$ are the two-particle bare electron states. We may write equivalently

$$\mathcal{F}_{\text{fluct}} = g^2\sum_{\substack{\mathbf{k}_1...\mathbf{k}_4,\\ \mathbf{p}_1...\mathbf{p}_4,\\ m}}' \frac{\langle c^\dagger_{\mathbf{k}_1,\uparrow}c^\dagger_{\mathbf{k}_2,\downarrow}c_{\mathbf{k}_3,\uparrow}c_{\mathbf{k}_4,\downarrow}|m\rangle\langle m|c^\dagger_{\mathbf{p}_1,\uparrow}c^\dagger_{\mathbf{p}_2,\downarrow}c_{\mathbf{p}_3,\uparrow}c_{\mathbf{p}_4,\downarrow}\rangle}{\epsilon^\uparrow_{\mathbf{k}_1} + \epsilon^\downarrow_{\mathbf{k}_2} - \epsilon^\uparrow_{\mathbf{k}_3} - \epsilon^\downarrow_{\mathbf{k}_4}} \quad + \quad \text{c.c..} \tag{3.5}$$

Expressing the expectation value in terms of Fermi distribution functions we find

$$\delta\mathcal{F} = -2g^2 \sideset{}{'}\sum_{\mathbf{k}_1..\mathbf{k}_2} \frac{f^{\uparrow}_{\mathbf{k}_1} f^{\downarrow}_{\mathbf{k}_2} (1 - f^{\uparrow}_{\mathbf{k}_3})(1 - f^{\downarrow}_{\mathbf{k}_4})}{\epsilon^{\uparrow}_{\mathbf{k}_1} + \epsilon^{\downarrow}_{\mathbf{k}_2} - \epsilon^{\uparrow}_{\mathbf{k}_3} - \epsilon^{\downarrow}_{\mathbf{k}_4}}, \tag{3.6}$$

where the four Fermi function term

$$\sideset{}{'}\sum_{\mathbf{k}_1..\mathbf{k}_2} \frac{f^{\uparrow}_{\mathbf{k}_1} f^{\downarrow}_{\mathbf{k}_2} f^{\uparrow}_{\mathbf{k}_3} f^{\downarrow}_{\mathbf{k}_4}}{\epsilon^{\uparrow}_{\mathbf{k}_1} + \epsilon^{\downarrow}_{\mathbf{k}_2} - \epsilon^{\uparrow}_{\mathbf{k}_3} - \epsilon^{\downarrow}_{\mathbf{k}_4}} = 0, \tag{3.7}$$

because it is odd under exchange of dummy momentum labels, $(\mathbf{k}_1, \mathbf{k}_2) \to (\mathbf{k}_3, \mathbf{k}_4)$. Additionally, the two Fermi function term,

$$\delta\mathcal{F}_\infty = -2g^2 \sideset{}{'}\sum_{\mathbf{k}_1..\mathbf{k}_2} \frac{f^{\uparrow}_{\mathbf{k}_1} f^{\downarrow}_{\mathbf{k}_2}}{\epsilon^{\uparrow}_{\mathbf{k}_1} + \epsilon^{\downarrow}_{\mathbf{k}_2} - \epsilon^{\uparrow}_{\mathbf{k}_3} - \epsilon^{\downarrow}_{\mathbf{k}_4}}, \tag{3.8}$$

is divergent. Hence, we include a renormalisation of the states to avoid this unphysical divergence:

$$|\mathbf{k}\uparrow,\mathbf{l}\downarrow\rangle \; = \; |\mathbf{k}\uparrow,\mathbf{l}\downarrow\rangle_0 + \sum_{\mathbf{p}\neq\mathbf{k},\mathbf{q}\neq\mathbf{l}} \frac{{}_0\langle\mathbf{p}\uparrow,\mathbf{q}\downarrow|\mathcal{H}^{\mathrm{int}}|\mathbf{k}\uparrow,\mathbf{l}\downarrow\rangle_0}{\epsilon^{+}_{\mathbf{k}} + \epsilon^{-}_{\mathbf{l}} - \epsilon^{+}_{\mathbf{p}} - \epsilon^{-}_{\mathbf{q}}}|\mathbf{p}\uparrow,\mathbf{q}\downarrow\rangle_0 \quad (3.9)$$

where $|\mathbf{k}\uparrow,\mathbf{l}\downarrow\rangle$ is the two-particle state corrected to first order in the interaction g. With this identification, we must also make a corresponding alteration to the matrix element g,

$$g_{\mathbf{k}_1,\mathbf{k}_2} \to g - 2g^2 \sideset{}{'}\sum_{\mathbf{k}_3,\mathbf{k}_4} \frac{1}{\epsilon^{+}_{\mathbf{k}_1} + \epsilon^{-}_{\mathbf{k}_2} - \epsilon^{+}_{\mathbf{k}_3} - \epsilon^{-}_{\mathbf{k}_4}}. \tag{3.10}$$

The remaining contribution to the free energy is

$$\delta\mathcal{F} = 2g^2 \sideset{}{'}\sum_{\mathbf{k}_1..\mathbf{k}_2} \frac{f^{\uparrow}_{\mathbf{k}_1} f^{\downarrow}_{\mathbf{k}_2} (f^{\uparrow}_{\mathbf{k}_3} + f^{\downarrow}_{\mathbf{k}_4})}{\epsilon^{\uparrow}_{\mathbf{k}_1} + \epsilon^{\downarrow}_{\mathbf{k}_2} - \epsilon^{\uparrow}_{\mathbf{k}_3} - \epsilon^{\downarrow}_{\mathbf{k}_4}}. \tag{3.11}$$

This perturbative correction is evaluated self-consistently in the presence of a new order. The dispersions inside the Fermi functions are the mean-field dispersions in the presence of this order. Since second order corrections are always negative,

particular orders may enhance the phase space for these fluctuations and thus are self-consistently stabilised by these fluctuations.

Orders, such as superconductivity or bond density wave order, change the form of the original interaction vertex. This change leads to an additional modification of the fluctuation spectrum, which in turn may lower the free energy. Formally, this generates additional terms in equation (3.11). Chapters 5 and 6 will explore this scenario in greater detail.

3.2.2 Fluctuation corrections in terms of particle-hole density of states

We now introduce a reformulation of the second order perturbative correction to the free energy derived in the previous section. We express the fluctuation correction in terms of particle-hole densities of states. This allows for an intuitive physical interpretation of the expressions and simplifies their evaluation.

Inspecting equation (3.6) we note that the fluctuations form pairs of particle-hole pairs of spin up and down. The integral in (3.6) effectively counts these pairs weighed by the inverse of their energy.

Starting with equation (3.11) we may write

$$
\delta\mathcal{F} = 2g^2 \sum_{\epsilon_1,\epsilon_2,\mathbf{k_3}} \left(\frac{\sum_{\mathbf{k}_1} f^{\uparrow}_{\mathbf{k}_1} f^{\uparrow}_{\mathbf{k}_3} \delta(\epsilon_1 - \epsilon^{\uparrow}_{\mathbf{k}_1} + \epsilon^{\uparrow}_{\mathbf{k}_3}) \sum_{\mathbf{k}_2} f^{\downarrow}_{\mathbf{k}_2} \delta(\epsilon_2 - \epsilon^{\downarrow}_{\mathbf{k}_2} + \epsilon^{\downarrow}_{\mathbf{k}_4})}{\epsilon_1 + \epsilon_2} \right.
$$
$$
\left. + \frac{\sum_{\mathbf{k}_2} f^{\downarrow}_{\mathbf{k}_2} f^{\downarrow}_{\mathbf{k}_4} \delta(\epsilon_2 - \epsilon^{\downarrow}_{\mathbf{k}_2} + \epsilon^{\downarrow}_{\mathbf{k}_4}) \sum_{\mathbf{k}_1} f^{\uparrow}_{\mathbf{k}_1} \delta(\epsilon_1 - \epsilon^{\uparrow}_{\mathbf{k}_1} + \epsilon^{\uparrow}_{\mathbf{k}_3})}{\epsilon_1 + \epsilon_2} \right), \quad (3.12)
$$

where we identified

$$
\frac{1}{\epsilon^{\uparrow}_{\mathbf{k}_1} + \epsilon^{\downarrow}_{\mathbf{k}_2} - \epsilon^{\uparrow}_{\mathbf{k}_3} - \epsilon^{\downarrow}_{\mathbf{k}_4}} = \sum_{\epsilon_1,\epsilon_2} \delta(\epsilon_2 - \epsilon^{\downarrow}_{\mathbf{k}_2} + \epsilon^{\downarrow}_{\mathbf{k}_4}) \delta(\epsilon_1 - \epsilon^{\uparrow}_{\mathbf{k}_1} + \epsilon^{\uparrow}_{\mathbf{k}_3}) \frac{1}{\epsilon_1 + \epsilon_2}. \quad (3.13)
$$

Shifting momentum labels such that

$$
\begin{align}
\mathbf{k}_3 &\rightarrow \mathbf{q} = \mathbf{k}_1 - \mathbf{k}_3 \tag{3.14}\\
\mathbf{k}_1 &\rightarrow \mathbf{k}_1 + \frac{\mathbf{q}}{2} \tag{3.15}\\
\mathbf{k}_2 &\rightarrow \mathbf{k}_1 + \frac{\mathbf{q}}{2}, \tag{3.16}
\end{align}
$$

we may write the fluctuation corrections as

$$
\delta\mathcal{F} = 2g^2 \sum_{\epsilon_1,\epsilon_1,\mathbf{q},\sigma} \frac{\Delta\rho^\sigma(\epsilon_1,\mathbf{q})\tilde{\rho}^\sigma(\epsilon_2,-\mathbf{q})}{\epsilon_1 + \epsilon_2}, \tag{3.17}
$$

with

$$
\begin{align}
\Delta\rho^\sigma(\epsilon,\mathbf{q}) &= \sum_{\mathbf{k}} f^\sigma_{\mathbf{k}-\frac{\mathbf{q}}{2}} \delta(\epsilon - \epsilon^\sigma_{\mathbf{k}+\frac{\mathbf{q}}{2}} + \epsilon^\sigma_{\mathbf{k}-\frac{\mathbf{q}}{2}}) \tag{3.18}\\
\tilde{\rho}^\sigma(\epsilon,\mathbf{q}) &= \sum_{\mathbf{k}} f^\sigma_{\mathbf{k}-\frac{\mathbf{q}}{2}} f^\sigma_{\mathbf{k}+\frac{\mathbf{q}}{2}} \delta(\epsilon - \epsilon^\sigma_{\mathbf{k}+\frac{\mathbf{q}}{2}} + \epsilon^\sigma_{\mathbf{k}-\frac{\mathbf{q}}{2}}). \tag{3.19}
\end{align}
$$

The difference between these two expression is the particle-hole density of states:

$$
\begin{align}
\rho^\sigma_{ph}(\epsilon,\mathbf{q}) &= \Delta\rho^\sigma(\epsilon,\mathbf{q}) - \tilde{\rho}^\sigma(\epsilon,\mathbf{q}) \tag{3.20}\\
&= \sum_{\mathbf{k}} f^\sigma_{\mathbf{k}-\frac{\mathbf{q}}{2}} (1 - f^\sigma_{\mathbf{k}+\frac{\mathbf{q}}{2}}) \delta(\epsilon - \epsilon^\sigma_{\mathbf{k}+\frac{\mathbf{q}}{2}} + \epsilon^\sigma_{\mathbf{k}-\frac{\mathbf{q}}{2}}). \tag{3.21}
\end{align}
$$

Properties of the particle-hole density of states

In order to understand the particle-hole density of states it is instructive to remind ourselves of the single-particle density of states,

$$
\rho(\epsilon) = \sum_{\mathbf{k}} \delta(\epsilon - \epsilon_{\mathbf{k}}). \tag{3.22}
$$

This expression measures the available phase space for particles within an infinitesimal band of energy $\epsilon + \delta\epsilon$. Hence, the single particle density of states is largest wherever the slope of the dispersion is smallest, see Figure 3.2. This may also be

concluded from an expansion of the density of states to leading order in momentum:

$$\rho(\epsilon)_{\text{local}} \;=\; \sum_{\mathbf{k}} \delta(\epsilon - \mathbf{k}.(\nabla_{\mathbf{k}}\epsilon_{\mathbf{k}})) \tag{3.23}$$

$$=\; \sum_{S_{\mathbf{k}}(\epsilon)} \frac{1}{|\nabla_{\mathbf{k}}\epsilon_{\mathbf{k}}|}, \tag{3.24}$$

that is the average of $\frac{1}{|\nabla_{\mathbf{k}}\epsilon_{\mathbf{k}}|}$ over the surface $S_{\mathbf{k}}(\epsilon)$ at constant energy ϵ.
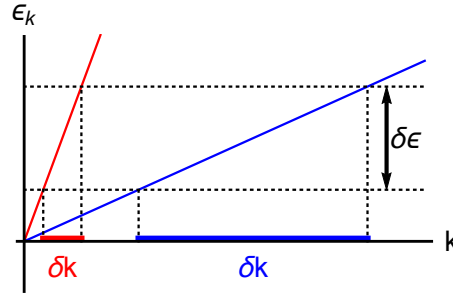
Figure 3.2: **Single-particle momentum states within an energy interval** $\delta\epsilon$ **for two different dispersions.** This plot demonstrates, that the number of single-particle momentum states, $\delta\mathbf{k}$, in an energy interval $\delta\epsilon$ is inversely proportional to the slope of the dispersion.

The particle-hole density of states at energy ϵ and momentum $\mathbf{q}$ is given by

$$\rho^{\sigma}_{ph}(\epsilon, \mathbf{q}) \;=\; \sum_{\mathbf{k}} f^{\sigma}_{\mathbf{k}-\frac{\mathbf{q}}{2}}(1 - f^{\sigma}_{\mathbf{k}+\frac{\mathbf{q}}{2}})\delta(\epsilon - \epsilon^{\sigma}_{\mathbf{k}+\frac{\mathbf{q}}{2}} + \epsilon^{\sigma}_{\mathbf{k}-\frac{\mathbf{q}}{2}}). \tag{3.25}$$

This expression describes the available phase space for particle-hole excitations. These excitations consist of taking an electron from inside the Fermi sea at energy $\epsilon_{\mathbf{k}-\frac{\mathbf{q}}{2}}$ and putting it outside the Fermi sea into a state of energy $\epsilon_{\mathbf{k}+\frac{\mathbf{q}}{2}}$. (This is equivalent to creating a hole at energy $\epsilon_{\mathbf{k}-\frac{\mathbf{q}}{2}}$ and simultaneously creating an electron at energy $\epsilon_{\mathbf{k}+\frac{\mathbf{q}}{2}}$.) The distance between the old and the new state in momentum space is $\mathbf{q}$, while their energy difference is $\epsilon = \epsilon_{\mathbf{k}+\frac{\mathbf{q}}{2}} - \epsilon_{\mathbf{k}-\frac{\mathbf{q}}{2}}$. See Figure 3.3. Hence, we may state more specifically: the particle-hole density of states measures the available phase space for particle-hole excitations of energy ϵ and momentum $\mathbf{q}$ within an infinitesimal band of energy $\delta\epsilon$.

In parallel to the analysis of the single-particle density of states, we may construct a local approximation to the particle-hole density of states assuming small particle-
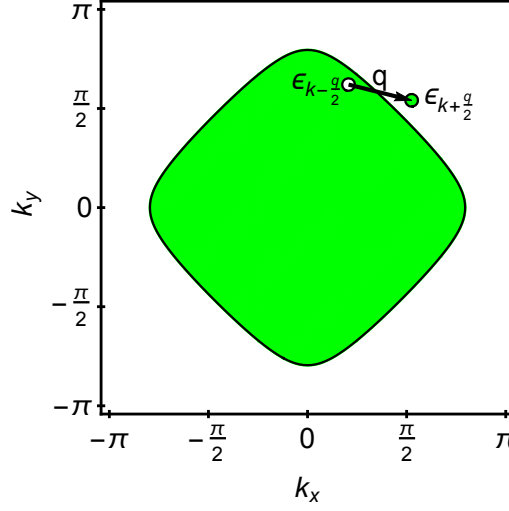
Figure 3.3: **Sketch of a particle hole excitation.** The large green area depicts the Fermi sea. Sketched is the excitation of an electron at energy $\epsilon_{\mathbf{k}-\frac{\mathbf{q}}{2}}$ to a state at a distance $\mathbf{q}$ and energy $\epsilon_{\mathbf{k}+\frac{\mathbf{q}}{2}}$.

hole momentum:

$$\rho_{ph}(\epsilon, \mathbf{q})_{\text{local}} = \sum_{\mathbf{k}} \delta(\epsilon - \mathbf{q}.(\nabla_{\mathbf{k}}\epsilon_{\mathbf{k}})) \tag{3.26}$$

$$= \sum_{\mathbf{k}} \delta(\epsilon - \mathbf{q}.\mathbf{k}\nabla_{\mathbf{k}}^2\epsilon_{\mathbf{k}}) \tag{3.27}$$

$$= \sum_{S_{\mathbf{k}}(\epsilon)} \frac{1}{|\mathbf{q}.\mathbf{k}\nabla_{\mathbf{k}}^2\epsilon_{\mathbf{k}}|}, \tag{3.28}$$

where we again average over the surface $S_{\mathbf{k}}(\epsilon)$ at energy ϵ.

From equation (3.28) we conclude, that the particle-hold density of states is maximal for dispersions with minimal curvature and small particle-hole momenta. Further, we obtain from equation (3.26), that the maximal particle hole energy for a given momentum is determined by the largest slope in the direction of $\mathbf{q}$ within the support.

Hence, the particle-hole density of states is inversely proportional to both the curvature of the dispersion as well as the length of the particle-hole momentum. These effects are plotted in Figures 3.4a and 3.4b, respectively.

As noted in equation (3.17), some of the later algebra is simplified by identifying

(a) **Particle-hole states in an energy interval $\delta\epsilon$ for different curvatures of the dispersion.** All four particle-hole momenta **q** are of equal length. The number of states, $\delta\mathbf{k}$, is inversely proportional to the curvature of the dispersion.

(b) **Particle-hole states in an energy interval for different particle-hole momenta q.** The number of states, $\delta\mathbf{k}$, is inversely proportional to the length of the particle-hole momentum **q**.

Figure 3.4: **Particle-hole states in an energy interval for different curvatures of the dispersion and particle-hole momenta.** The energy intervals $\delta\epsilon$ is identical within Figure 3.4a and 3.4b. The particle-hole momenta **q** of the excitations with energy zero and $\delta\epsilon$ are pairwise equal in length and direction. They are merely shifted in k-space with respect to one another.

the modified particle-hole density of states $\tilde{\rho}$ and $\Delta\rho$:

$$\tilde{\rho}(\epsilon, \mathbf{q})^\sigma = \sum_{\mathbf{k}} f^\sigma(\epsilon^\sigma_{\mathbf{k}-\frac{\mathbf{q}}{2}} - \mu)\delta(\epsilon - \epsilon^\sigma_{\mathbf{k}+\frac{\mathbf{q}}{2}} + \epsilon^\sigma_{\mathbf{k}-\frac{\mathbf{q}}{2}}) \tag{3.29}$$

$$\Delta\rho(\epsilon, \mathbf{q})^\sigma = \sum_{\mathbf{k}} f(\epsilon^\sigma_{\mathbf{k}-\frac{\mathbf{q}}{2}} - \mu)f(\epsilon^\sigma_{\mathbf{k}+\frac{\mathbf{q}}{2}} - \mu)\delta(\epsilon - \epsilon^\sigma_{\mathbf{k}+\frac{\mathbf{q}}{2}} + \epsilon^\sigma_{\mathbf{k}-\frac{\mathbf{q}}{2}}), \tag{3.30}$$

such that

$$\rho^\sigma_{ph}(\epsilon, \mathbf{q}) = \tilde{\rho}^\sigma(\epsilon, \mathbf{q}) - \Delta\rho^\sigma(\epsilon, \mathbf{q}). \tag{3.31}$$

$\Delta\rho^\sigma(\epsilon, \mathbf{q})$ may be though of as a measure for the number of vectors of length and direction equal to **q**, that fit into the Fermi sea. This can be seen easily by considering the product of two Fermi functions inside its integrand. In order to get a non-zero contribution to $\Delta\rho(\epsilon, \mathbf{q})$, both the start and end point of the vector **q**, at $\epsilon_{\mathbf{k}-\frac{\mathbf{q}}{2}}$ and $\epsilon_{\mathbf{k}+\frac{\mathbf{q}}{2}}$, have to lie within the Fermi sea. Hence, we conclude that particle-hole momenta around **q** = **0** result in the largest $\Delta\rho(\epsilon, \mathbf{q})$.

$\tilde{\rho}^\sigma(\epsilon, \mathbf{q})$ on the other hand only contains one Fermi function shifted by $\frac{\mathbf{q}}{2}$. Hence,

its support as a function of particle-hole momentum does not change in size, but is merely shifted in momentum space.

Finally, in the limit of $\mathbf{q} \to 0$ we note that $\tilde{\rho}^{\sigma}(\epsilon, \mathbf{q}) \to \Delta\rho(\epsilon, \mathbf{q})$.

3.2.3   Field-theoretical derivation of fluctuation corrections

Finally, we would like to derive the self-consistent second order perturbative correction to the free energy from a quantum field theory ansatz.

We start by decoupling the interaction in charge and spin channels. The static component is included in the definition of the propagator, so that we expand around the ordered phase. We integrate out fermions and finite frequency spin and charge fluctuations, while keeping the leading order in the interaction.

The fermionic partition function and action are give by:

$$\mathcal{Z} = \int \mathcal{D}(\bar{\psi}, \psi) e^{-S[\bar{\psi}, \psi]}, \tag{3.32}$$

$$S[\bar{\psi}, \psi] = \int_0^{\beta} d\tau \int d\mathbf{r}^3 \left[\bar{\psi} \partial_{\tau} \psi + \mathcal{H}(\bar{\psi}, \psi) \right], \tag{3.33}$$

where $\psi = (\psi_{\uparrow}, \psi_{\downarrow})$ are fermionic fields and $\mathcal{H}$ is the Hubbard Hamiltonian containing the contact interaction term

$$\mathcal{H}_{int} = g \int_0^{\beta} d\tau \int d\mathbf{r}^3 \bar{\psi}_{\uparrow}(\mathbf{r}, \tau) \psi_{\uparrow}(\mathbf{r}, \tau) \bar{\psi}_{\downarrow}(\mathbf{r}, \tau) \psi_{\downarrow}(\mathbf{r}, \tau). \tag{3.34}$$

In order to diagonalise the Hamiltonian, we perform a Hubbard-Stratonovich decoupling in spin ϕ and charge ρ channel, which are defined as

$$\rho(\mathbf{r}, \tau) = -\frac{1}{2} \bar{\psi}(\mathbf{r}, \tau) \psi(\mathbf{r}, \tau) \tag{3.35}$$

$$\phi(\mathbf{r}, \tau) = \frac{1}{2} \bar{\psi}(\mathbf{r}, \tau) \boldsymbol{\sigma} \psi(\mathbf{r}, \tau), \tag{3.36}$$

where $\boldsymbol{\sigma}$ denotes the set of Pauli matrices. For instance, if one only decoupled in

the charge channel, the Hubbard-Stratonovich transformation is:

$$e^{g\bar{\psi}_\uparrow \psi_\uparrow \bar{\psi}_\downarrow \psi_\downarrow} = \int D(\rho) e^{-g\rho^2 + g\rho\bar{\psi}\psi}, \quad (3.37)$$

as may be confirmed by Gaussian integration over the charge field, ρ.

The partition function and action may now be written as

$$\mathcal{Z} = \int \mathcal{D}(\bar{\psi}, \psi, \phi, \rho) e^{-S[\bar{\psi}, \psi, \phi, \rho]}, \quad (3.38)$$

$$S[\bar{\psi}, \psi, \phi, \rho] = \int d\tau d\mathbf{r}^3 \left[\bar{\psi} \left(\mathcal{G}_0^{-1} + g(\rho - \boldsymbol{\sigma}.\phi) \right) \psi + g(\phi^2 - \rho^2) \right], \quad (3.39)$$

where $\mathcal{G}_0^{-1}$ is the bare electron Green's function. We separate spin and charge into zero and finite-frequency components:

$$\rho = \rho_0 + \tilde{\rho} \quad (3.40)$$

$$\phi = \mathbf{M} + \tilde{\phi} \quad (3.41)$$

$\mathbf{M}$ and ρ_0 are the static background orders, while $\tilde{\phi}$ and $\tilde{\rho}$ are fluctuations around the static order.

Work by Conduit *et al.* [66], and Chubukov and Maslov [67] has shown that contributions from charge fluctuations have to be taken into account. This is in contrast to earlier work on quantum phase transitions by Hertz [17] and Millis [18], who only decoupled in the spin channel [41, 68].

In the grand canonical ensemble we absorb ρ_0 into the chemical potential. The action becomes

$$S[\bar{\psi}, \psi, \phi, \rho] = \int d\tau d\mathbf{r}^3 \left[\bar{\psi} \left(\mathcal{G}_\sigma^{-1} + g(\tilde{\rho} - \boldsymbol{\sigma}.\tilde{\phi}) \right) \psi + g(M^2 + \tilde{\phi}^2 - \tilde{\rho}^2) \right] (3.42)$$

where we identified the propagator in the presence of the order as $\mathcal{G}_\sigma^{-1} = \mathcal{G}_0^{-1} - g\boldsymbol{\sigma}.\mathbf{M}$. This amounts to self-consistent perturbation theory around a saddle point in the presence of order. This effectively sums a set of diagrams, that would have to be computed explicitly if one expanded around a saddle point in the symmetric phase.

Now we would like to integrate out the fermions. There are two integrands to be

considered: the Green's function, $\mathcal{G}_\sigma^{-1}$, and the fluctuation fields, $g(\tilde{\rho} - \boldsymbol{\sigma}.\tilde{\phi})$. The former follows the usual Gaussian integration over the Grassmann fields. The later term is more interesting. It describes the interaction between electrons and fluctuations. This contribution to the action may be Fourier transformed to momentum space. It reads

$$S_{int}[\bar{\psi}, \psi, \phi, \rho] = g \sum_{\substack{\omega,\omega_q \\ \mathbf{k},\mathbf{q}}} \bar{\psi}(\mathbf{k}, \omega) \left(\tilde{\rho}(\mathbf{q}, \omega_q) - \boldsymbol{\sigma}\tilde{\phi}(\mathbf{q}, \omega_q) \right) \psi(\mathbf{k} + \mathbf{q}, \omega + \omega_q), \quad (3.43)$$

where ω_q and ω are bosonic and fermionic Matsubara frequencies respectively.

After integration over the fermion fields, this term corresponds to fermion bubble-diagrams. The two principle possibilities are spin-symmetric and spin-anti-symmetric. These are the longitudinal and transverse fluctuations, respectively. The relevant diagrams are
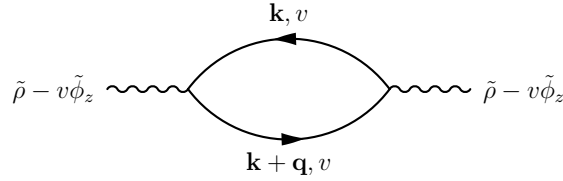
and
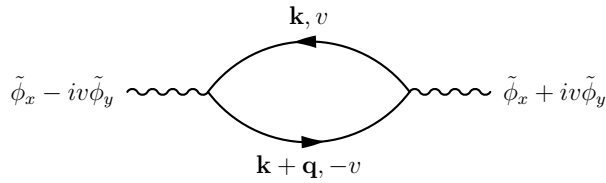
where v labels spin.

Treating S_{int} as a perturbation to the remaining action we may expand the partition

function. The lowest order non-zero contribution is

$$\langle e^{-S_{int}[\bar{\psi},\psi,\phi,\rho]}\rangle = \langle \frac{1}{2} S_{int}[\bar{\psi},\psi,\phi,\rho]^2 \rangle. \tag{3.44}$$

$$= -g^2 \sum_{\substack{\omega,\omega_q \\ \mathbf{k},\mathbf{q},v,v'}} \mathcal{G}_v(\mathbf{k})\mathcal{G}_{v'}(\mathbf{k}+\mathbf{q}) \left(\tilde{\rho}(\mathbf{q}) - \boldsymbol{\sigma}\tilde{\phi}(\mathbf{q}) \right) \left(\tilde{\rho}(-\mathbf{q}) - \boldsymbol{\sigma}\tilde{\phi}(-\mathbf{q}) \right) \tag{3.45}$$

The propagators themselves are functions of the static order and the interaction. The quadratic contribution in equation (3.45) corresponds to diagrams of the form
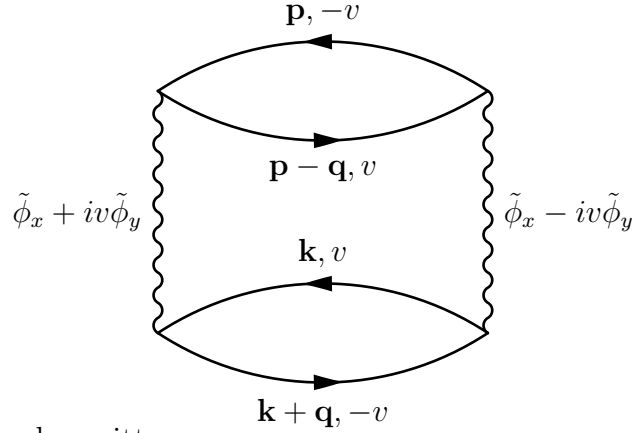
The action may now be written as

$$S[\tilde{\rho},\tilde{\phi}] = \int d\tau d\mathbf{r}^3 \left(\log\left(G_\sigma^{-1}\right) + gM^2 \right)$$

$$+ \sum_{\mathbf{q},\omega_q} \begin{pmatrix} \tilde{\rho} \\ \tilde{\phi}_z \end{pmatrix}^T \left\{ \begin{pmatrix} -g & 0 \\ 0 & g \end{pmatrix} + \frac{g^2}{2} \begin{pmatrix} \Pi^{++} + \Pi^{--} & \Pi^{++} - \Pi^{--} \\ \Pi^{--} - \Pi^{++} & \Pi^{++} + \Pi^{--} \end{pmatrix} \right\} \begin{pmatrix} \tilde{\rho} \\ \tilde{\phi}_z \end{pmatrix}$$

$$+ \sum_{\mathbf{q},\omega_q} \begin{pmatrix} \tilde{\phi}_x \\ \tilde{\phi}_y \end{pmatrix}^T \left\{ \begin{pmatrix} g & 0 \\ 0 & g \end{pmatrix} + \frac{g^2}{2} \begin{pmatrix} \Pi^{+-} + \Pi^{-+} & 0 \\ 0 & \Pi^{+-} + \Pi^{-+} \end{pmatrix} \right\} \begin{pmatrix} \tilde{\phi}_x \\ \tilde{\phi}_y \end{pmatrix}, \tag{3.46}$$

where we shortened notation by defining

$$\Pi^{\sigma\bar{\sigma}}(\mathbf{q},\omega_q) = \sum_{\mathbf{k},\omega} \mathcal{G}_\sigma(\mathbf{k},\omega)\mathcal{G}_{\bar{\sigma}}(\mathbf{k}+\mathbf{q},\omega+\omega_q). \tag{3.47}$$

Finally, we are in position to perform the integration over the finite frequency fluctuation fields. After expanding the logarithms to leading order the action takes the

form

$$S \;=\; g \int dr^3 M^2 + \mathrm{Tr}(\mathcal{G}_v^{-1}) + \mathrm{Tr}\left(g(\Pi^{+-} + \Pi^{-+}) - g^2(\Pi^{++}\Pi^{--} + \Pi^{+-}\Pi^{-+})\right).$$

$$(3.48)$$

Diagrammatically the integration over the fluctuations corresponds to contracting the bosonic lines in the above diagram. Thus, we find
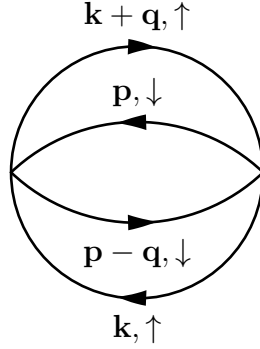
Finally we may write the free energy as

$$\mathcal{F} = -T \log \mathcal{Z}, \tag{3.49}$$

such that

$$\mathcal{F} \;=\; \underbrace{g \int dr^3 M^2 - \mathrm{Tr} \log \mathcal{G}_\sigma^{-1}}_{\mathcal{F}_{MF}} + \underbrace{\mathrm{Tr}(g\Pi^{\sigma\bar\sigma} + \frac{g^2}{2}\Pi^{\sigma\bar\sigma}\Pi^{\bar\sigma\sigma})}_{\delta\mathcal{F}_\parallel}$$
$$- \underbrace{\frac{g^2}{2}\mathrm{Tr}\Pi^{\sigma\sigma}\Pi^{\bar\sigma\bar\sigma}}_{\delta\mathcal{F}_\perp}, \tag{3.50}$$

where we have identified the mean field free energy, $\mathcal{F}_{MF}$, and the longitudinal and transverse fluctuation contribution, $\delta\mathcal{F}_\parallel$ and $\delta\mathcal{F}_\perp$, respectively.

The expression above was derived by decoupling in both the charge and spin channel. Their zero frequency component is included in the definition of the propagator. This means we are expanding self-consistently in the presence of finite static order. The finite frequency components of these charge and spin fluctuations are integrated out after the integration of fermions.

The trace in equation (3.50) contains a Matsubara sum. Evaluating this sum re-

produces the free energy in terms of Fermi distribution functions, expressed in equation(3.11).

3.3   Summary

In this chapter we introduced the fermionic quantum order-by-disorder formalism. We first illustrated the concept with the help of a simple toy model and then formally derived it in two equivalent ways. The main idea of this ansatz is a self-consistent expansion around a saddle point inside the broken-symmetry phase. This choice of saddle point is equivalent to the resummation of an infinite set of diagrams. Furthermore, the formulation in terms of particle-hole density of states allows for a direct physical interpretation as well as easier evaluation compared to the diagrammatic alternative. [27, 28, 30].

In the following chapters we will apply the fermionic quantum order-by-disorder approach to extend the mean field phase diagram of the antiferromagnet. We start by including fluctuation corrections to the antiferromagnet itself. Later, we investigate d-wave bond density and d-wave superconducting order as well as the intertwining of pairs of these phases with each other and the antiferromagnetic background.

Chapter 4

Fermionic quantum order by disorder: Explicit calculation in the antiferromagnet

We now wish to evaluate the fluctuation corrections to the free energy of the antiferromagnet. In Chapter 3 we derived the formal expression for the fluctuation corrections in terms of particle-hole density of states. We then introduced the general properties of these particle-hole densities to give an intuitive picture of their characteristics. Here we start off by applying these findings specifically to the Hubbard model. This will guide the subsequent explicit calculation of the fluctuation corrections to the antiferromagnet.

Ultimately, this calculation is not as straightforward as in the case of ferromagnetism [30]. We restrict our analysis to commensurate antiferromagnetism, leaving aside the possibility of incommensurate antiferromagnetic order, and consider only the lowest order in magnetisation. The antiferromagnetic fluctuation corrections shift the mean field phase transitions to smaller interactions, but do not change the topology of the phase diagram. Orders that change the interaction vertex exhibit more dramatic fluctuation corrections. This will be explored in Chapters 5 and 6, which investigate superconductivity and bond density wave order.

4.1 *Analysis of the fluctuation corrections in the antiferromagnet*

In this section we analyse the fluctuation corrections to the free energy of antiferromagnetism in the Hubbard model. The goal is to develop an appropriate approximation scheme to allow their explicit evaluation. We start by developing a physical picture of the dominant contribution. The analytical predictions are then verified by numerical means.

4.1.1 Heuristic analysis

The perturbative correction to the free energy in terms of particle-hole densities is given by

$$\delta \mathcal{F} = 2g^2 \sum_{\epsilon_1, \epsilon_1, \mathbf{q}, \sigma} \frac{\Delta \rho^\sigma(\epsilon_1, \mathbf{q}) \tilde{\rho}^\sigma(\epsilon_2, -\mathbf{q})}{\epsilon_1 + \epsilon_2}. \tag{4.1}$$

From this expression, we conclude that it is dominated by particle hole excitations near zero energy, such that $\epsilon_1 + \epsilon_2 = 0$.

Therefore, we would like to find particle-hole momenta for which the particle-hole density of states is largest at zero energy. The results of chapter 3 suggest, that the dominant contribution comes from particle-hole momenta near $\mathbf{q} = \mathbf{0}$. Further, we should find, that their largest support is in regions of vanishing curvature.

In the tight-binding dispersion $\mathbf{k} = (\frac{\pi}{2}, \frac{\pi}{2})$ and the three symmetry related points exhibit zero curvature regardless of direction. Hence, we expect the dominant contribution to particle-hole excitations to arise in their vicinity. The slope at $\mathbf{k} = (\frac{\pi}{2}, \frac{\pi}{2})$ will determine the principal energy associated with a particle-hole excitation of a particular momentum. Hence, we can identify the direction of the particle-hole momenta that correspond to zero-energy peaks in the density of states. That is, for $\mathbf{k} = (\frac{\pi}{2}, \frac{\pi}{2})$, zero energy excitations are only possible if the particle-hole momentum is parallel to $(1, -1)$ or $(-1, 1)$.

We are assuming, that the dominant contribution to the free energy comes from

static or zero-frequency fluctuations, thus we restrict ourselves to the zero energy component of the particle-hole densities of states. A treatment of both, the full momentum space dependence and finite frequency components is beyond the scope of the current work.

4.1.2 Numerical analysis

Our physical intuition is confirmed by numerical evaluation of the particle-hole density of states as a function of the length and direction of particle-hole momenta.

$$\Delta\rho(\epsilon, \mathbf{q}) = \sum_{\mathbf{k}} f(\epsilon_{\mathbf{k}-\frac{\mathbf{q}}{2}} - \mu) f(\epsilon_{\mathbf{k}+\frac{\mathbf{q}}{2}} - \mu) \delta(\epsilon - \epsilon_{\mathbf{k}+\frac{\mathbf{q}}{2}} + \epsilon_{\mathbf{k}-\frac{\mathbf{q}}{2}}) \tag{4.2}$$

$$\tilde{\rho}(\epsilon, \mathbf{q}) = \sum_{\mathbf{k}} f(\epsilon_{\mathbf{k}-\frac{\mathbf{q}}{2}} - \mu) \delta(\epsilon - \epsilon_{\mathbf{k}+\frac{\mathbf{q}}{2}} + \epsilon_{\mathbf{k}-\frac{\mathbf{q}}{2}}) \tag{4.3}$$

In order to perform the numerical integration of the particle-hole density of states we first integrate analytically over the delta function. The remaining one dimensional integral is then performed numerically in Mathematica. The results are plotted in Figure 4.1.

(a) $\mathbf{q} \parallel (-1, 1)$ (b) $\mathbf{q} \parallel (-0.5, 1)$ (c) $\mathbf{q} \parallel (0, 1)$
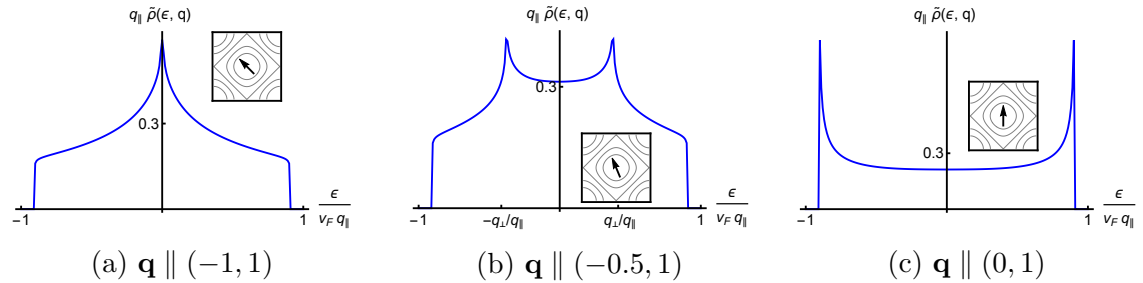
Figure 4.1: $\tilde{\rho}(\epsilon, \mathbf{q})$ **as a function of particle-hole energy for different directions of particle-hole momenta.** Note the position of the peaks as a function of the direction of the particle-hole momentum. The direction is indicated in the plot's insets with respect to the first Brillouin zone of the tight binding dispersion.

The three plots in Figure 4.1 are evaluated at the same temperature and chemical potential, such that $T \ll |\mu| \ll t$, and with the same length of the particle-hole momentum; they differ only in the chosen direction of $\mathbf{q}$.

The most striking feature of these plots are the peaks. Their location in energy is determined by the direction of $\mathbf{q}$. The largest contribution to zero energy particle-

hole excitations come from momenta parallel to $(k_x, k_y) = (-1, 1)$ and symmetry related directions.

The height of these peaks as well as the rest of the particle-hole density of states is inversely proportional to the length of $\mathbf{q}$. This follows exactly from the analysis in Section 3.2.2. The height of the peaks is also determined by the smallest curvature accessible to the particle-hole excitations within their support. Zero curvature is found exactly at half filling, leading to logarithmically divergent particle-hole density of states. Below half filling, the logarithmic peaks in the particle-hole density of states are cut off by the chemical potential.

The width of $\tilde{\rho}$ scales with the length of one the component of $\mathbf{q}$. In Figure 4.1 this component is parallel to $(k_x, k_y) = (-1, 1)$. The width of the particle hole density of states is proportional to the maximal slope within its support. Hence, below half filling the width is slightly less than its maximal possible value, $v_F = \nabla_{\mathbf{k}} \epsilon_{\mathbf{k}}|_{\mathbf{k}=(\frac{\pi}{2}, \frac{\pi}{2})}$.

In fact, we may identify $\mathbf{k} = (\frac{\pi}{2}, \frac{\pi}{2})$ as a point of zero curvature independent of the direction of $\mathbf{q}$, too. Thus, $\mathbf{k} = (\frac{\pi}{2}, \frac{\pi}{2})$ will lead to a logarithmic divergence of the particle-hole density of states at half filling. It can therefore be thought of as the particle-hole analog of saddle points in the single-particle density of states.

This is of particular importance close to half filling. For sufficiently small chemical potential one may approximate the single-particle density of states by expanding around a saddle point. A similar approximation of the particle-hole density of states is given by an expansion around $\mathbf{k} = (\frac{\pi}{2}, \frac{\pi}{2})$. We will investigate this idea in detail in Section 4.2.1.

So far we have confirmed that the dominant contribution to zero-energy particle-hole excitations comes from particle-hole pairs with momenta near $\mathbf{q} = \mathbf{0}$. Furthermore we confirmed that the zero-energy particle hole excitations are strongest, when the particle-hole momentum lies parallel to $(k_x, k_y) = (-1, 1)$.

Next, we analyse the support of the particle-hole excitations in the Brillouin zone. We plot particle-hole energy contours for different direction of particle-hole momentum, see Figure 4.2. The contours are the zeros of the delta function in the definition

(a) $\mathbf{q} \parallel (-1, 1)$

(b) $\mathbf{q} \parallel (-1, 1 + \delta)$, where $0 < \delta \ll 1$

(c) $\mathbf{q} \parallel (\delta, 1)$, where $0 < \delta \ll 1$

(d) $\mathbf{q} \parallel (0, 1)$
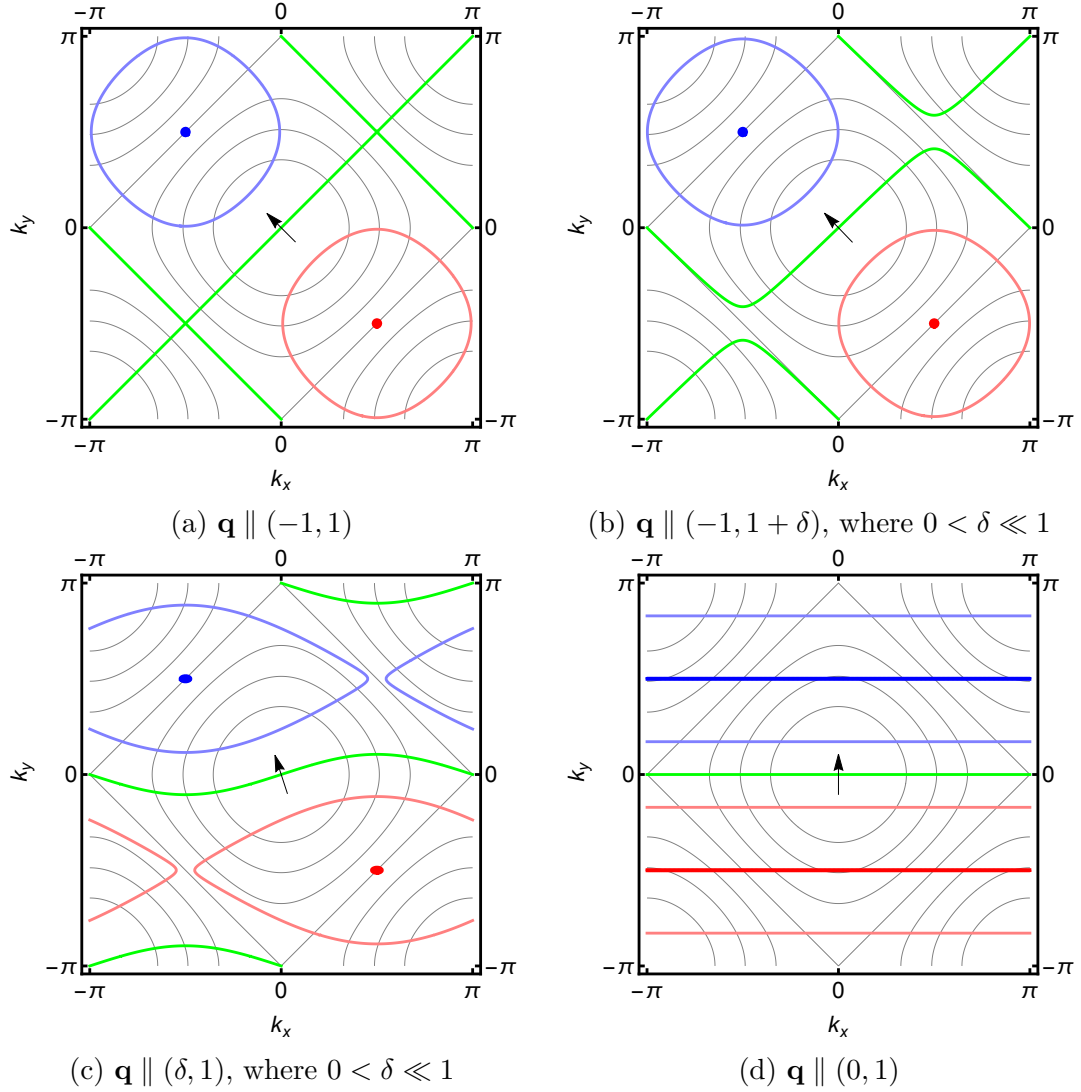
Figure 4.2: **Particle-hole energy contours in the tight binding dispersion for different directions of the particle-hole momentum.** The green line is the zero energy contour. The red and blue line are the maximal negative and positive energy contour, respectively. The light red and light blue lines are halfway between zero and maximal energy. The black lines are a contour plot of the tight binding dispersion for reference (See Figure 2.1 for a 3D plot). The arrows in the center indicate the direction of the particle-hole momentum chosen for each plot.

of the particle-hole density of states, equation (4.3),

$$\epsilon = \epsilon_{\mathbf{k}+\frac{\mathbf{q}}{2}} - \epsilon_{\mathbf{k}-\frac{\mathbf{q}}{2}}. \tag{4.4}$$

The contribution to the particle-hole density of states is not homogeneous along these contours, but inversely proportional to the local curvature.

Figure 4.2a and 4.2b are of particular interest. Here the particle-hole momentum is (almost) parallel to $(k_x, k_y) = (-1, 1)$, where the dominant contribution to zero-energy particle-hole excitations is found. The zero-energy contours themselves run in close proximity to $\mathbf{k} = (\pm\frac{\pi}{2}, \pm\frac{\pi}{2})$ in both of these figures.

Similarly Figure 4.2d explains, why $\mathbf{q} \parallel (0, 1)$ and symmetry related directions correspond to peaks at extremal energies in the particle-hole density of states. In this scenario the zero-energy contour lies along a path of strong curvature, while the contours for minimal and maximal energy cross the zero curvature points at $\mathbf{k} = (\pm\frac{\pi}{2}, \pm\frac{\pi}{2})$ and $\mathbf{k} = (\pm\frac{\pi}{2}, \mp\frac{\pi}{2})$.

This further substantiates the claim, that an expansion around these points captures the dominant contribution to particle-hole excitations close to half filling.

4.2   *Calculation of fluctuation corrections*

In the previous section we developed an understanding of the particle-hole density of states and determined their dominant contribution to the fluctuation correction to the free energy. Now we derive an analytical expression for the particle-hole density of states and from this calculate the leading fluctuation corrections.

4.2.1   Analytic particle hole density of states of the antiferromagnet

The leading contribution to the fluctuation correction to the free energy stems from zero-energy particle-hole excitations. These in turn are dominated by particle-hole pairs with momenta that are near $\mathbf{q} = \mathbf{0}$ and parallel to the $(1, 1)$ or symmetry
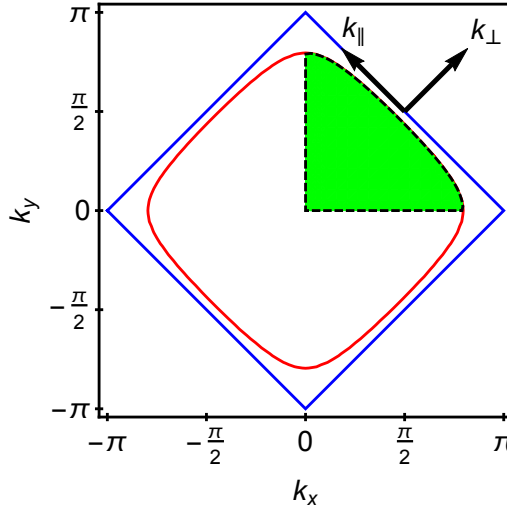
Figure 4.3: **Plot of the area of integration and rotated coordinates.** The green area denotes the are of integration, which is approximated in the calculation of the particle-hole density of states. The black arrows indicate the origin and direction of the rotated coordinate system $\mathbf{k} = (k_\parallel, k_\perp)$.

related directions. Further, we found that the areas close to the zero curvature points at $\mathbf{k} = (\pm\frac{\pi}{2}, \pm\frac{\pi}{2})$ and $\mathbf{k} = (\pm\frac{\pi}{2}, \mp\frac{\pi}{2})$ lead to logarithmic peaks in the particle-hole density of states. Finally we know that for sufficiently small particle-hole momenta $\tilde{\rho}(\epsilon, \mathbf{q}) \approx \Delta\rho(\epsilon, \mathbf{q})$.

We will now derive an analytic expression for the particle-hole density of states at zero temperature by expanding to leading order in $\mathbf{k}$ and $\mathbf{q}$ around $\mathbf{k} = (\frac{\pi}{2}, \frac{\pi}{2})$. We first introduce a $\pi/4$ rotated coordinate system $(k_\parallel, k_\perp) = \frac{1}{\sqrt{2}}(k_y - k_x, k_y + k_x)$, illustrated in Figure 4.3.

In the shifted and rotates coordinates the tight-binding dispersion becomes

$$\epsilon_{\mathbf{k}} \approx v_F\, k_\perp \left(1 - \frac{k_\parallel^2}{4}\right), \qquad (4.5)$$

where $v_F = 2\sqrt{2}t$ is the local Fermi velocity.

Using the Fermi functions at zero temperature to change the limits of integration

$\Delta\rho(\epsilon, \mathbf{q})$ takes the form

$$
\Delta\rho(\epsilon, \mathbf{q}) = \sum_{\mathbf{k}} f(\epsilon_{\mathbf{k}-\frac{\mathbf{q}}{2}} - \mu) f(\epsilon_{\mathbf{k}+\frac{\mathbf{q}}{2}} - \mu) \delta(\epsilon - \epsilon_{\mathbf{k}+\frac{\mathbf{q}}{2}} + \epsilon_{\mathbf{k}-\frac{\mathbf{q}}{2}}) \tag{4.6}
$$

$$
= \frac{2}{(2\pi)^2} \int_{-\frac{\pi}{\sqrt{2}}}^{\frac{\pi}{\sqrt{2}}} dk_{\parallel} \int_{-\frac{\pi}{\sqrt{2}}+|k_{\parallel}|}^{\frac{\mu}{v_F}+\frac{|q_{\perp}|}{2}} dk_{\perp} \delta\left(\epsilon - v_F\left(q_{\perp} - k_{\perp}\frac{q_{\parallel}k_{\parallel}}{2}\right)\right). \tag{4.7}
$$

Figure 4.3 depicts the range of integration.

The leading contribution near zero-energy particle-hole excitations stems from $|q_{\perp}| \ll |q_{\parallel}|$. Hence, there is an equal contribution to the particle-hole density near $\mathbf{k} = (-\frac{\pi}{2}, -\frac{\pi}{2})$, which is included by a factor of two. The other two quadrant only contribute in the limit of $|q_{\perp}| \approx |q_{\parallel}|$. This sub-leading contribution to the zero-energy excitations may be neglected.

Next we integrate over $k_{\perp}$ using the delta function and find

$$
\Delta\rho(\epsilon, \mathbf{q}) = \frac{1}{\pi^2} \int_{-\frac{\pi}{\sqrt{2}}}^{\frac{\pi}{\sqrt{2}}} \frac{dk_{\parallel}}{v_F |k_{\parallel}q_{\parallel}|} \theta\left(\frac{\pi}{\sqrt{2}} - |k_+| - 2\frac{\frac{\epsilon}{v_F} - q_{\perp}}{k_{\parallel}q_{\parallel}}\right) \theta\left(\frac{\mu}{v_F} + \frac{|q_{\perp}|}{2} + 2\frac{\frac{\epsilon}{v_F} - q_{\perp}}{k_{\parallel}q_{\parallel}}\right)
$$
$$
\tag{4.8}
$$

The resultant step functions may be rearranged to limit the range of integration of $k_{\parallel}$. Keeping only contributions close to $k_{\parallel} = 0$ we arrive at

$$
\Delta\rho(\epsilon, \mathbf{q}) = \frac{2}{\pi^2} \int_0^{\frac{\pi}{\sqrt{2}}} \frac{dk_{\parallel}}{v_F k_{\parallel}|q_{\parallel}|} \theta\left(-k_{\parallel} - 2\frac{\frac{\epsilon}{v_F} - q_{\perp}}{q_{\parallel}\left(\frac{\mu}{v_F} + \frac{|q_{\perp}|}{2}\right)}\right) \theta\left(k_{\parallel} - \frac{4\sqrt{2}}{\pi}\frac{\frac{\epsilon}{v_F} - q_{\perp}}{q_{\parallel}}\right)
$$
$$
\tag{4.9}
$$

Keeping the leading contribution to this expression requires both step functions to lie within the range of integration. We perform the final integration to yield:

$$
\Delta\rho(\epsilon, \mathbf{q}) = \frac{-2}{v_F \pi^2 |q_{\parallel}|} \log\left|\frac{2\sqrt{2}}{\pi}\left(\frac{\mu}{v_F} + \frac{q_{\perp}}{2}\right)\right| \theta\left(\frac{\pi}{\sqrt{2}} - 2\left|\frac{\frac{\epsilon}{v_F} - q_{\perp}}{q_{\parallel}\left(\frac{\mu}{v_F} + \frac{q_{\perp}}{2}\right)}\right|\right). \tag{4.10}
$$

Now we rearrange the step function to give limits on the particle-hole energy:

$$\Delta\rho(\epsilon, \mathbf{q}) = \frac{-2}{v_F \pi^2 |q_\parallel|} \log \left| \frac{2\sqrt{2}}{\pi} \left(\frac{\mu}{v_F} + \frac{q_\perp}{2} \right) \right| \left\{ \theta \left(\frac{\epsilon}{v_F} - q_\perp - \frac{q_\parallel}{2} \frac{\pi}{\sqrt{2}} \left(\frac{\mu}{v_F} + \frac{q_\perp}{2} \right) \right) \right.$$
$$\theta \left(-\frac{\epsilon}{v_F} + q_\perp - \frac{q_\parallel}{2} \frac{\pi}{\sqrt{2}} \left(\frac{\mu}{v_F} + \frac{q_\perp}{2} \right) \right)$$
$$\left. +\epsilon \rightarrow -\epsilon \right\} \tag{4.11}$$

These step functions form two top-hats, that are constant approximations to the logarithmic peaks seen in Figure 4.1. Their behaviour mirrors that of the numerical peaks. Their position in energy is given by $\epsilon = \pm v_F q_\perp$ and their height scales as $1/q_\parallel$. This is in good agreement with the numerical evaluation.

Low energy particle-hole excitations result in the dominant contributions to the fluctuation corrections. Hence, we only consider the two peaks in the vicinity of zero energy. This simplifies our expressions further:

$$\Delta\rho(\epsilon, \mathbf{q}) = \frac{-4}{v_F \pi^2 |q_\parallel|} \log \left| \frac{2\sqrt{2}}{\pi} \frac{\mu}{v_F} \right| \theta \left(-\epsilon - v_F q_\perp - q_\parallel \frac{\pi}{2\sqrt{2}} \left(\mu - v_F \frac{q_\perp}{2} \right) \right)$$
$$\theta \left(\epsilon - v_F q_\perp - q_\parallel \frac{\pi}{2\sqrt{2}} \left(\mu - v_F \frac{q_\perp}{2} \right) \right) \tag{4.12}$$

The condition, that the peaks overlap around zero energy, is simply a constraint on the direction of $\mathbf{q}$. In particular,

$$0 > v_F q_\parallel + q_\parallel \frac{\pi}{2\sqrt{2}} (\mu - v_F \frac{q_\perp}{2}) \tag{4.13}$$

$$|q_\perp| < \frac{\pi |\mu|}{2\sqrt{2} v_F} |q_\parallel|, \tag{4.14}$$

where close to half filling $|\mu| \ll v_F$. As expected this constrains $\mathbf{q}$ to lie approximately parallel to the Fermi surface.

4.2.2 Antiferromagnetic fluctuation corrections

Having derived an analytical approximation to the particle-hole density of states we now calculate the leading contribution to the fluctuation correction to the free

energy. The later is calculated from

$$\delta\mathcal{F} = g^2 \sum_{\mathbf{q},\epsilon_{1/2}} \frac{\tilde{\rho}(\epsilon_1,\mathbf{q})\Delta\rho(\epsilon_2,-\mathbf{q})}{\epsilon_1+\epsilon_2} \tag{4.15}$$

$$= g^2 \sum_{\mathbf{q},\epsilon_{1/2}} \frac{\tilde{\rho}(\epsilon_1,\mathbf{q})\Delta\rho(\epsilon_2,\mathbf{q})}{\epsilon_1+\epsilon_2}, \tag{4.16}$$

where we used the time-reversal symmetry of $\Delta\rho(\epsilon,\mathbf{q})$. Additionally, we use $\tilde{\rho}(\epsilon,\mathbf{q}) \approx \Delta\rho(\epsilon,\mathbf{q})$ for sufficiently small particle-hole momenta. We insert the analytic expression for the particle-hole densities, equation (4.12), and perform the energy integrals. The limits on these integrals are given by the step-functions in the expressions for the particle-hole densities. After integration and neglecting sub-leading contributions we arrive at

$$\delta\mathcal{F} = g^2 \sum_{\mathbf{q}} \frac{8q_\perp}{v_F\pi^3\sqrt{2}|q_\parallel|} \log^2\left|\frac{2\sqrt{2}\mu}{\pi v_F}\right| \log\left(1 - \frac{2v_F q_\perp + \frac{\pi}{\sqrt{2}}\mu q_\parallel}{v_F\frac{\pi}{2\sqrt{2}}q_\parallel q_\perp}\right). \tag{4.17}$$

Next, we integrate over $q_\perp$, where we use the fact that the dominant particle-hole momenta lie near parallel to the Fermi surface, such that $|q_\perp| < \frac{\pi|\mu|}{2\sqrt{2}v_F}|q_\parallel|$. Then

$$\delta\mathcal{F} = -\frac{g^2\mu^2}{v_F^3 2\sqrt{2}\pi} \log^2\left|\frac{4\sqrt{2}\mu}{\pi v_F}\right| \sum_{q_\parallel} q_\parallel \left(\frac{1}{\frac{4\sqrt{2}q_\parallel}{\pi}-1} + \frac{\log\left(\frac{4\sqrt{2}}{q_\parallel\pi}\right)}{\left(\frac{4\sqrt{2}q_\parallel}{\pi}-1\right)^2}\right) \tag{4.18}$$

Finally we integrate over $q_\parallel$ for $q_\parallel < 1$. The result of this last integral is just a number that is roughly $\frac{1}{4}$. Hence we arrive at the final expression for the fluctuation correction to the free energy:

$$\delta\mathcal{F} = -\frac{g^2\mu^2}{v_F^3 8\sqrt{2}\pi} \log^2\left|\frac{4\sqrt{2}\mu}{\pi v_F}\right| \tag{4.19}$$

4.2.3 Fluctuation corrections to the Landau coefficients

The goal of this chapter is to calculate perturbative corrections to the mean field phase diagram of the antiferromagnet. Therefore, we must calculate the above ex-

pressions self-consistently, using the dispersion in the presence of antiferromagnetic order and subsequently expand in powers of the order parameter. A simpler approach is to consider the effect of finite magnetisation on the Fermi surface. As noticed in chapter 2, finite magnetisation effectively shifts the chemical potential towards half filling by opening a gap. Hence, instead of expanding in the magnetic order parameter, we expand appropriately in the chemical potential.

The dispersion in the presence of antiferromagnetic order is given by

$$\xi_{\mathbf{k}}^{\sigma} = \sigma \sqrt{\epsilon_{\mathbf{k}}^2 + g^2 M^2} - \mu. \tag{4.20}$$

Expanding a general function $f(\xi_{\mathbf{k}}^{\sigma})$ in powers of the antiferromagnetic order takes the form:

$$\partial_{M^2} f(\xi_{\mathbf{k}}^{\sigma})|_{M=0} = \frac{g^2}{\epsilon_{\mathbf{k}}} \partial_{\epsilon_{\mathbf{k}}} f(\xi_{\mathbf{k}}). \tag{4.21}$$

At zero temperature all physical processes are constraint to the Fermi surface. Then, any function of the dispersion is evaluated at the chemical potential. Furthermore, the magnetic order parameter always appears in conjunction with the chemical potential. Thus we approximate:

$$\partial_{M^2} = \frac{g^2}{\mu} \partial_{\mu}. \tag{4.22}$$

Now we are equipped to evaluate the perturbative correction to the Landau coefficients of antiferromagnetic order. Taking derivatives of equation (4.19) we find

$$\alpha_{fluct} = \partial_{M^2} \delta \mathcal{F} \tag{4.23}$$

$$= -\frac{g^4}{v_F^3 4\sqrt{2}\pi} \log^2 \left| \frac{4\sqrt{2}\mu}{\pi v_F} \right| \tag{4.24}$$

In chapter 2 we analysed the mean field Landau expansion of the antiferromagnet. We found that an evaluation of the Landau coefficients was only feasible to quadratic order. Higher order terms were increasingly hard to evaluate, which suggests non-analytic behaviour of the free energy below the tricritical point. Furthermore, the minimum of the free energy with respect to magnetisation was found at values too large to allow expansion. The fluctuation corrections to quartic or higher order

Landau coefficients are meaningless without the supporting mean field expansion.

4.3 *Phase diagram*

We are now in a position to analyse the effect of fluctuation corrections on the phase diagram and in particular the second order transition to commensurate antiferromagnetism. The quadratic Landau coefficient may be written as the sum of mean field and fluctuation correction coefficient

$$\mathcal{F} \; = \; \alpha M^2 + O(M^4) \tag{4.25}$$

$$= \; (\alpha_{MF} + \alpha_{fluct})M^2 + O(M^4). \tag{4.26}$$

Thus, we may compute the fluctuation corrected second order phase transition line to commensurate antiferromagnetism by finding the zeros of $\alpha_{MF} + \alpha_{fluct}$. The result is plotted in Figure 4.4. Since α_{fluct} is negative, the fluctuations self-consistently increase the transition temperature to commensurate antiferromagnetic order.
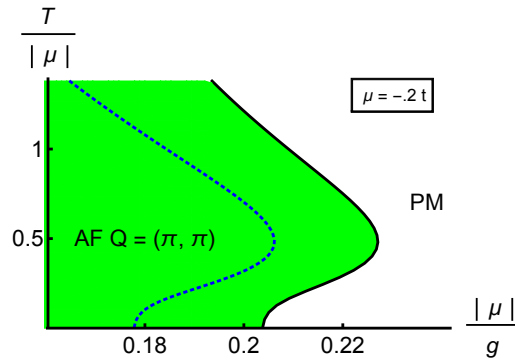
Figure 4.4: **Fluctuation corrected second order phase transition to commensurate antiferromagnetism.** The dashed blue line is the mean field second order transition. The black line is the fluctuation corrected second order transition. The Green area denotes the region of commensurate antiferromagnetic order.

The calculation of the fluctuation corrections to the antiferromagnet was done at zero temperature. However, with increasing temperature the relative importance of quantum fluctuations diminishes, so the observed shift of the second order transition line should be less pronounced as temperature increases. This may in fact weaken or even destroy the reentrant behaviour of the second order transition. That would be

in line with the simple physical picture of phase transitions; increasing temperature and thereby the strength of thermal fluctuations, usually drives the system towards the disordered state.

Further, we expect the first order line to shift in a similar manner to the second order line and thereby preserve the overall topology of the phase diagram. In Figure 4.5 we have added a hand-drawn first order line as a guide to the eye.
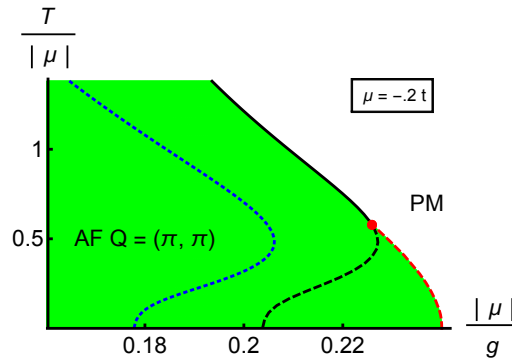
Figure 4.5: **Sketch of the fluctuation corrected phase diagram of commensurate antiferromagnetic order.** The dashed blue line is the mean field second order transition. The black line is the fluctuation corrected second order transition. Below the tricritical point (red) the second order line is preempted by a sketched first order transition. The dashed black line denotes the preempted second order transition. The green area denotes the region of commensurate antiferromagnetic order.

The calculation of the fluctuation corrections to the antiferromagnet was further limited to commensurate order. Further research is required to determine the fate of incommensurate order in this model.

Finally, we would like to comment on the fate of Fermi liquid physics in the vicinity of the antiferromagnetic quantum critical point. In the limit of small interaction, far away from the phase transition, the system is conventionally assumed to behave analogous to a free electron gas, whose dynamical properties are renormalised by the effects of interactions - a Fermi liquid. Thus the Fermi liquid is adiabatically connected to the non-interacting Fermi gas. This physics breaks down in the immediate vicinity of quantum critical points due to the proliferation of quantum fluctuations. Here, collective excitations replace the single particle excitations. This fundamental change in the character of excitations breaks the adiabatic connection to the non-interacting model. Fermi liquid physics is often assumed to reemerge

inside the broken symmetry phase. However, Vekhter and Chubukov demonstrate that even inside the symmetry broken region of the itinerant antiferromagnet Fermi liquid theory may be invalid [69]. Their analysis involves a calculation of frequency dependent fluctuations inside the ordered phase. They find that low frequency, large wave-vector, overdamped fluctuations give rise to non-Fermi liquid behaviour insider the antiferromagnetically ordered phase. This thesis is self-consistently calculated in the static limit. Thus the investigation of such dynamic effects is beyond the scope of the current work yet presents an exciting direction for future calculations.

4.4   *Summary*

In this chapter we analysed and calculated the particle-hole density of states in the Hubbard model. We then derived analytical corrections to the mean field free energy of commensurate antiferromagnetic order and demonstrated their effect on the mean field phase diagram.

This analysis was limited to corrections to the commensurate second order transition. The effects of fluctuations on the first order line as well as incommensurate order were discussed.

Next, we will incorporate bond density wave and d-wave superconducting order into the formalism and compute a more complete phase diagram.

Chapter 5

Quantum order-by-disorder of the anti-ferromagnet: bond density wave instability

In this chapter we will analyse how the presence of a d-wave bond density wave order affects the free energy of the antiferromagnet. The starting point will be a variational ansatz to the mean field theory of the bond density wave. We then calculate the bond density wave order's effect on the anti-ferromagnetic fluctuations and its interaction with the antiferromagnetic order.

5.1 *Mean field theory of the bond density wave*

5.1.1 Hamiltonian

Consider the following Hamiltonian:

$$\mathcal{H} - \mu\mathcal{N} = \underbrace{\sum_{\mathbf{k},\sigma} \xi_{\mathbf{k}} c_{\mathbf{k},\sigma}^{\dagger} c_{\mathbf{k},\sigma}}_{\text{kinetic}} + \underbrace{\sum_{\mathbf{k},\mathbf{p},\mathbf{q}} V_{\mathbf{q}} c_{\mathbf{k},\uparrow}^{\dagger} c_{\mathbf{p},\downarrow}^{\dagger} c_{\mathbf{p}-\mathbf{q},\downarrow} c_{\mathbf{k}+\mathbf{q},\uparrow}}_{\text{interaction}}, \tag{5.1}$$

where $\xi_{\mathbf{k}} = \epsilon_{\mathbf{k}} - \mu$ and we make the usual identifications; the first term is the kinetic contribution $\mathcal{H}_{kin}$ and the second term is the interaction Hamiltonian $\mathcal{H}_{int}$.

Our task is to construct the free energy of this Hamiltonian in the presence of d-wave bond density wave order.

5.1.2   The order parameter

We define the d-wave bond density wave order parameter as

$$D_{\mathbf{k}} = \theta_{\mathbf{k}} \sum_{\mathbf{p},\sigma} (c^{\dagger}_{\mathbf{p}-\frac{\mathbf{Q}}{2},\sigma} c_{\mathbf{p}+\frac{\mathbf{Q}}{2},\sigma} + c.c.), \tag{5.2}$$

with $\theta_{\mathbf{k}} = cos(k_x) - cos(k_y)$ encoding the d-wave symmetry and $\mathbf{Q}$ being the wave vector of the bond density modulation.

In contrast to a conventional charge density wave, the bond density wave does not change the charge density on each lattice site. Instead, a bond density wave modulates the charge density in between lattice sites, on the bonds between them. This modulation has a length scale set by the wave vector $\mathbf{Q}$. In addition, the bond order considered here is modulated by a d-wave symmetry factor $\theta_{\mathbf{k}} = cos(k_x) - cos(k_y)$. As a result, the order is symmetric under rotation by π and time reversal, and antisymmetric under rotation by $\frac{\pi}{2}$, thus breaking the discrete $\frac{\pi}{2}$ rotational symmetry of the lattice.

5.1.3   Variational ansatz

The bond density wave is included in the Hamiltonian by a variational ansatz. We add and subtract a term,

$$\mathcal{H}_{var} = \frac{g}{2} \sum_{\mathbf{k},\sigma} \left(D_{\mathbf{k}} c^{\dagger}_{\mathbf{k}+\frac{\mathbf{Q}}{2},\sigma} c_{\mathbf{k}-\frac{\mathbf{Q}}{2},\sigma} + \bar{D}_{\mathbf{k}} c^{\dagger}_{\mathbf{k}-\frac{\mathbf{Q}}{2},\sigma} c_{\mathbf{k}+\frac{\mathbf{Q}}{2},\sigma} \right), \tag{5.3}$$

to the Hamiltonian, where $\bar{D}$ is the complex conjugate of $\bar{D}$. The Hamiltonian now reads

$$\mathcal{H} - \mu\mathcal{N} = \underbrace{\mathcal{H}_{kin} + \mathcal{H}_{var}}_{\text{diagonalise}} \underbrace{-\mathcal{H}_{var} + \mathcal{H}_{int}}_{\text{perturbation}}. \tag{5.4}$$

The first two terms will be diagonalised and the second two terms are treated a perturbative correction. Including the positive contribution in the kinetic Hamiltonian, we may write

$$\mathcal{H}_{kin} + \mathcal{H}_{var} = \frac{1}{2}\sum_{\mathbf{k},\sigma} \begin{pmatrix} c^{\dagger}_{\mathbf{k}+\frac{\mathbf{Q}}{2},\sigma} \\ c^{\dagger}_{\mathbf{k}-\frac{\mathbf{Q}}{2},\sigma} \end{pmatrix}^{T} \begin{pmatrix} \xi_{\mathbf{k}+\frac{\mathbf{Q}}{2},\sigma} & gD_{\mathbf{k}} \\ g\bar{D}_{\mathbf{k}} & \xi_{\mathbf{k}-\frac{\mathbf{Q}}{2},\sigma} \end{pmatrix} \begin{pmatrix} c_{\mathbf{k}+\frac{\mathbf{Q}}{2},\sigma} \\ c_{\mathbf{k}-\frac{\mathbf{Q}}{2},\sigma} \end{pmatrix}. \tag{5.5}$$

The introduction of variational terms is similar to the counter-terms used by Neumayr and Metzner in their self-consistent renormalisation treatment of the interaction in the two dimensional Hubbard model [65]. This highlights the equivalence of the self-consistent treatment of interaction effects on the dispersion and the self-consistent treatment of perturbative corrections via the quantum order-by-disorder approach. D-wave superconducting order will be included into the model in the same way in Chapter 6.

5.1.4 Diagonalisation

A simple rotation of basis vectors, coupling pairs of operators shifted by $\mathbf{Q}$ relative to each other, will diagonalise this expression.

$$\begin{pmatrix} c_{\mathbf{k}+\frac{\mathbf{Q}}{2},\sigma} \\ c_{\mathbf{k}-\frac{\mathbf{Q}}{2},\sigma} \end{pmatrix} = \begin{pmatrix} u_{\mathbf{k}} & v_{\mathbf{k}} \\ -v^{*}_{\mathbf{k}} & u^{*}_{\mathbf{k}} \end{pmatrix} \begin{pmatrix} \alpha_{\mathbf{k}+\frac{\mathbf{Q}}{2},\sigma} \\ \alpha_{\mathbf{k}-\frac{\mathbf{Q}}{2},\sigma} \end{pmatrix}, \tag{5.6}$$

where to quadratic order in D,

$$u^{2}_{\mathbf{k}} \approx 1 - \frac{g^{2}|D_{\mathbf{k}}|^{2}}{(\epsilon_{\mathbf{k}-\frac{\mathbf{Q}}{2}} - \epsilon_{\mathbf{k}+\frac{\mathbf{Q}}{2}})^{2}} \quad \text{and} \quad v_{\mathbf{k}} \approx \frac{gD_{\mathbf{k}}}{\epsilon_{\mathbf{k}-\frac{\mathbf{Q}}{2}} - \epsilon_{\mathbf{k}+\frac{\mathbf{Q}}{2}}}. \tag{5.7}$$

In order to transform an operator of the form $c_{\mathbf{k},\sigma}$, one may shift the above transformation matrix by $+\frac{\mathbf{Q}}{2}$ or $-\frac{\mathbf{Q}}{2}$. Since the system is symmetric under the exchange

$\mathbf{Q} \to -\mathbf{Q}$, we use a linear superposition of both shifted transformations:

$$c_{\mathbf{k},\sigma} = \frac{1}{2}(u_{\mathbf{k}+\frac{\mathbf{Q}}{2}}\alpha_{\mathbf{k}} + u^*_{\mathbf{k}-\frac{\mathbf{Q}}{2}}\alpha_{\mathbf{k}} - v^*_{\mathbf{k}+\frac{\mathbf{Q}}{2}}\alpha_{\mathbf{k}+\mathbf{Q}} + v_{\mathbf{k}-\frac{\mathbf{Q}}{2}}\alpha_{\mathbf{k}-\mathbf{Q}}) \tag{5.8}$$

$$c^\dagger_{\mathbf{k},\sigma} = \frac{1}{2}(u^*_{\mathbf{k}+\frac{\mathbf{Q}}{2}}\alpha^\dagger_{\mathbf{k}} + u_{\mathbf{k}-\frac{\mathbf{Q}}{2}}\alpha^\dagger_{\mathbf{k}} - v_{\mathbf{k}+\frac{\mathbf{Q}}{2}}\alpha^\dagger_{\mathbf{k}+\mathbf{Q}} + v^*_{\mathbf{k}-\frac{\mathbf{Q}}{2}}\alpha^\dagger_{\mathbf{k}-\mathbf{Q}}). \tag{5.9}$$

The diagonalised kinetic Hamiltonian takes the form

$$\mathcal{H}_{kin} + \mathcal{H}_{var} = \sum_{\mathbf{k},\sigma} \xi_{\mathbf{k},\sigma} n_{\mathbf{k},\sigma}, \tag{5.10}$$

where

$$\xi_{\mathbf{k},\sigma} = \frac{1}{2}\left(\epsilon_{\mathbf{k}-\frac{\mathbf{Q}}{2}} + \epsilon_{\mathbf{k}+\frac{\mathbf{Q}}{2}} + \sigma\sqrt{(\epsilon_{\mathbf{k}-\frac{\mathbf{Q}}{2}} - \epsilon_{\mathbf{k}+\frac{\mathbf{Q}}{2}})^2 + 4g^2|D_{\mathbf{k}}|^2}\right) - \mu \tag{5.11}$$

is the dispersion in the presence of bond density wave order.

5.1.5   Free energy

Having diagonalised the non-interacting part of the Hamiltonian we now construct the free energy. The partition function is given by

$$Z = \mathrm{Tr}\, e^{-\beta\mathcal{H}} \tag{5.12}$$

$$= \mathrm{Tr}\, e^{-\beta(\mathcal{H}_{kin}+\mathcal{H}_{var}-\mathcal{H}_{var}+\mathcal{H}_{int})} \tag{5.13}$$

$$= \mathrm{Tr}\, e^{-\beta(\mathcal{H}_{kin}+\mathcal{H}_{var})}\langle e^{-\beta(-\mathcal{H}_{var}+\mathcal{H}_{int})}\rangle, \tag{5.14}$$

where $\langle ...\rangle$ indicate the thermal expectation taken over the normal modes of $\mathcal{H}_{kin} + \mathcal{H}_{var}$. Using $F = -T\log Z$, we obtain the mean field contribution to the free energy

$$\mathcal{F}_{MF} = -T\sum_{\mathbf{k},\sigma}\log\left(1 + e^{-\frac{\xi_{\mathbf{k},\sigma}}{T}}\right). \tag{5.15}$$

Corrections to this are given by

$$-T\log\langle e^{-\beta(-\mathcal{H}_{var}+\mathcal{H}_{int})}\rangle \approx \langle -\mathcal{H}_{var} + \mathcal{H}_{int}\rangle. \tag{5.16}$$

This second contribution is calculated by rotating it into the diagonal basis of $\mathcal{H}_{kin}+\mathcal{H}_{var}$ and keeping terms to order D^2. After collecting terms and simplifying, the first term of this contribution to the free energy takes the form of a susceptibility.

$$\mathcal{F}(D) = \mathcal{F}_{MF} - \langle\mathcal{H}_{var}\rangle + \langle\mathcal{H}_{int}\rangle \tag{5.17}$$

$$= -T\sum_{\mathbf{k},\sigma}\log\left(1 + e^{-\frac{\xi_{\mathbf{k},\sigma}}{T}}\right) - g^2\sum_{\mathbf{k},\sigma}|D_{\mathbf{k}}|^2\frac{f_{\mathbf{k}-\frac{\mathbf{Q}}{2}} - f_{\mathbf{k}+\frac{\mathbf{Q}}{2}}}{\epsilon_{\mathbf{k}-\frac{\mathbf{Q}}{2}} - \epsilon_{\mathbf{k}+\frac{\mathbf{Q}}{2}}} + \langle\mathcal{H}_{int}\rangle. \tag{5.18}$$

Note that the D^2-contribution of the mean field term is of the same form as the variational contribution up to multiplicative factors. It is important to keep these second order contributions to the free energy in order to capture the effects that we seek.

An important consequence of the transformation used to diagonalise the combination of kinetic and variational Hamiltonian, $\mathcal{H}_{kin}+\mathcal{H}_{var}$, is that the form of the interaction vertex changes. This will be fully accounted for in the calculation of the interaction term's contribution to the free energy. Its origin has physical significance - the bare interaction does not have any weight in the bond density wave channel. This shows up in the Hubbard-Stratonovich decoupling of the interaction used in the analysis of the antiferromagnet; for the bond density wave, this decoupling leads to an unstable expansion. In other words the field integral after Hubbard-Stratonovich decoupling is not convergent due to the wrong sign of the Gaussian weight. Interactions that support pairing in the bond density channel are only generated by fluctuations.

In the following section will calculate this fluctuation contribution to the free energy to second order in the bond density wave order parameter.

5.2 *Fluctuation corrections to the antiferromagnet in the presence of bond density wave order*

5.2.1 Overview of calculation

In the preceding section, we derived the mean field free energy of bond density order in our model. As expected, we showed that bond density wave order is not

supported in mean field theory. In this section we will derive corrections to the free energy from self-consistent second order perturbation theory.

The principal idea is that *an order, even if not supported in mean field theory, may be self consistently stabilised by low energy fluctuations. That is to say, the presence of an order may enhance the available state space for fluctuations and these in turn lower the free energy.*

We will derive corrections to the free energy of the Hubbard model in the presence of bond density wave order. These will show whether fluctuations can self consistently stabilise bond density wave order in the model. Furthermore, we will investigate how the antiferromagnetic and bond density wave order interact. For this purpose we will treat the bond density wave order as a weak perturbation in the background of antiferromagnetic order and neglect the effect of the presence of bond density wave order on the antiferromagnetic fluctuations. However, the antiferromagnetic order will change the Fermi surface shape and so influences the bond density fluctuations. Therefore we will be able to conclude whether the presence of antiferromagnetism supports or hinders the formation of bond density waves.

In the following we give a short outline of the main steps of the derivation. It should serve as an overview before the messy detail of the calculation and as a summary for later reference.

The second order change in the free energy, which we will refer to as fluctuation corrections, is given by

$$\langle \mathcal{H}_{int} \rangle = \mathcal{F}_{\text{fluct}} = g^2 \sum_{\substack{\mathbf{k}_1 \ldots \mathbf{k}_4, \\ \mathbf{p}_1 \ldots \mathbf{p}_4, \\ m}}^{\prime} \frac{\langle c_{\mathbf{k}_1,\uparrow}^{\dagger} c_{\mathbf{k}_2,\downarrow}^{\dagger} c_{\mathbf{k}_3,\downarrow} c_{\mathbf{k}_4,\uparrow} | m \rangle \langle m | c_{\mathbf{p}_1,\uparrow}^{\dagger} c_{\mathbf{p}_2,\downarrow}^{\dagger} c_{\mathbf{p}_3,\downarrow} c_{\mathbf{p}_4,\uparrow} \rangle}{\epsilon_{\mathbf{k}_1}^+ + \epsilon_{\mathbf{k}_2}^- - \epsilon_{\mathbf{k}_3}^+ - \epsilon_{\mathbf{k}_4}^-} + \text{c.c.} \quad (5.19)$$

Following on from Section 5.1, the expectations must be calculated in the diagonal basis of $\mathcal{H}_{kin} + \mathcal{H}_{var}$. The first step will be to rotate the creation and annihilation operators to this basis. Correct momentum matching of pairs of transformed operators ensures only non-zero expectations. These expectations are then expressed in terms of Fermi distribution functions of electrons and holes. Finally, we collect terms and simplify the expressions as much as possible.

Since the rotation of operators into the new basis generates a large number of terms,

we would like to keep notation as clean as possible. Conveniently there are symmetries, that we may exploit to identify a smaller set of independent terms. Firstly, we note that the bond density wave order as defined above is independent of the sign of its wave vector $\mathbf{Q}$. Secondly, the order is symmetric under spin flips. Hence, the free energy of bond density wave order is likewise unaltered under those transformations. We should therefore be able to identify pairs of terms, that correspond to either of these two transformations, and simplify appropriately.

5.2.2 Fluctuation corrections to the antiferromagnet in the presence of bond density wave order

The result of replacing all of the field operators in equation 5.19 by their form in the diagonal basis is:

$$
\mathcal{F}_{fluct}(D) = g^2 \sum_{\mathbf{k,p,q}}
$$

$$
\underbrace{|u_{\mathbf{k+q}+\frac{\mathbf{Q}}{2}}|^2 |u_{\mathbf{p-q}+\frac{\mathbf{Q}}{2}}|^2 |u_{\mathbf{p}+\frac{\mathbf{Q}}{2}}|^2 |u_{\mathbf{k}+\frac{\mathbf{Q}}{2}}|^2 \frac{\langle \alpha^\dagger_{\mathbf{k+q},\uparrow} \alpha^\dagger_{\mathbf{p-q},\downarrow} \alpha_{\mathbf{p},\downarrow} \alpha_{\mathbf{k},\uparrow} \alpha^\dagger_{\mathbf{k},\uparrow} \alpha^\dagger_{\mathbf{p},\downarrow} \alpha_{\mathbf{p-q},\downarrow} \alpha_{\mathbf{k+q},\uparrow} \rangle}{\epsilon^\uparrow_{\mathbf{k+q}} + \epsilon^\downarrow_{\mathbf{p-q}} - \epsilon^\uparrow_{\mathbf{k}} - \epsilon^\downarrow_{\mathbf{p}}}}_{\textbf{A. regular contribution}}
$$

$$
+ \frac{g^2}{4} \sum_{\substack{\mathbf{k,p,q} \\ \mathbf{k',p',q'}}} (\{[
$$

$$
\underbrace{
\begin{aligned}
& v_{\mathbf{k+q}+\frac{\mathbf{Q}}{2}} v^*_{\mathbf{k'+q'}+\frac{\mathbf{Q}}{2}} \frac{\langle \alpha^\dagger_{\mathbf{k+q+Q},\uparrow} \alpha^\dagger_{\mathbf{p-q},\downarrow} \alpha_{\mathbf{p},\downarrow} \alpha_{\mathbf{k},\uparrow} \alpha^\dagger_{\mathbf{k'},\uparrow} \alpha^\dagger_{\mathbf{p'},\downarrow} \alpha_{\mathbf{p'-q'},\downarrow} \alpha_{\mathbf{k'+q'+Q},\uparrow} \rangle}{\epsilon^\uparrow_{\mathbf{k+q}} + \epsilon^\downarrow_{\mathbf{p-q}} - \epsilon^\uparrow_{\mathbf{k}} - \epsilon^\downarrow_{\mathbf{p}}} \\[4pt]
& + v^*_{\mathbf{k}+\frac{\mathbf{Q}}{2}} v_{\mathbf{k'}+\frac{\mathbf{Q}}{2}} \frac{\langle \alpha_{\mathbf{k+q},\uparrow} \alpha^\dagger_{\mathbf{p-q},\downarrow} \alpha_{\mathbf{p},\downarrow} \alpha_{\mathbf{k+Q},\uparrow} \alpha^\dagger_{\mathbf{k'+Q},\uparrow} \alpha^\dagger_{\mathbf{p'},\downarrow} \alpha_{\mathbf{p'-q'},\downarrow} \alpha_{\mathbf{k'+q'},\uparrow} \rangle}{\epsilon^\uparrow_{\mathbf{k+q}} + \epsilon^\downarrow_{\mathbf{p-q}} - \epsilon^\uparrow_{\mathbf{k}} - \epsilon^\downarrow_{\mathbf{p}}} \\[4pt]
& + v_{\mathbf{k+q}+\frac{\mathbf{Q}}{2}} v^*_{\mathbf{k}+\frac{\mathbf{Q}}{2}} \frac{\langle \alpha^\dagger_{\mathbf{k+q+Q},\uparrow} \alpha^\dagger_{\mathbf{p-q},\downarrow} \alpha_{\mathbf{p},\downarrow} \alpha_{\mathbf{k+Q},\uparrow} \alpha^\dagger_{\mathbf{k'},\uparrow} \alpha^\dagger_{\mathbf{p'},\downarrow} \alpha_{\mathbf{p'-q'},\downarrow} \alpha_{\mathbf{k'+q'},\uparrow} \rangle}{\epsilon^\uparrow_{\mathbf{k+q}} + \epsilon^\downarrow_{\mathbf{p-q}} - \epsilon^\uparrow_{\mathbf{k}} - \epsilon^\downarrow_{\mathbf{p}}} \\[4pt]
& + v^*_{\mathbf{k'}-\frac{\mathbf{Q}}{2}} v_{\mathbf{k'+q'}-\frac{\mathbf{Q}}{2}} \frac{\langle \alpha^\dagger_{\mathbf{k+q},\uparrow} \alpha^\dagger_{\mathbf{p-q},\downarrow} \alpha_{\mathbf{p},\downarrow} \alpha_{\mathbf{k},\uparrow} \alpha^\dagger_{\mathbf{k'-Q},\uparrow} \alpha^\dagger_{\mathbf{p'},\downarrow} \alpha_{\mathbf{p'-q'},\downarrow} \alpha_{\mathbf{k'+q'-Q},\uparrow} \rangle}{\epsilon^\uparrow_{\mathbf{k+q}} + \epsilon^\downarrow_{\mathbf{p-q}} - \epsilon^\uparrow_{\mathbf{k}} - \epsilon^\downarrow_{\mathbf{p}}} \\[4pt]
& - v_{\mathbf{k+q}+\frac{\mathbf{Q}}{2}} v^*_{\mathbf{k'}-\frac{\mathbf{Q}}{2}} \frac{\langle \alpha^\dagger_{\mathbf{k+q+Q},\uparrow} \alpha^\dagger_{\mathbf{p-q},\downarrow} \alpha_{\mathbf{p},\downarrow} \alpha_{\mathbf{k},\uparrow} \alpha^\dagger_{\mathbf{k'-Q},\uparrow} \alpha^\dagger_{\mathbf{p'},\downarrow} \alpha_{\mathbf{p'-q'},\downarrow} \alpha_{\mathbf{k'+q'},\uparrow} \rangle}{\epsilon^\uparrow_{\mathbf{k+q}} + \epsilon^\downarrow_{\mathbf{p-q}} - \epsilon^\uparrow_{\mathbf{k}} - \epsilon^\downarrow_{\mathbf{p}}} \\[4pt]
& - v^*_{\mathbf{k}+\frac{\mathbf{Q}}{2}} v_{\mathbf{k'+q'}-\frac{\mathbf{Q}}{2}} \frac{\langle \alpha^\dagger_{\mathbf{k+q},\uparrow} \alpha^\dagger_{\mathbf{p-q},\downarrow} \alpha_{\mathbf{p},\downarrow} \alpha_{\mathbf{k+Q},\uparrow} \alpha^\dagger_{\mathbf{k'},\uparrow} \alpha^\dagger_{\mathbf{p'},\downarrow} \alpha_{\mathbf{p'-q'},\downarrow} \alpha_{\mathbf{k'+q'-Q},\uparrow} \rangle}{\epsilon^\uparrow_{\mathbf{k+q}} + \epsilon^\downarrow_{\mathbf{p-q}} - \epsilon^\uparrow_{\mathbf{k}} - \epsilon^\downarrow_{\mathbf{p}}}
\end{aligned}
}_{\textbf{B. transformed pairs of spin-up operators}}
$$

$$
] + [\mathbf{Q} \to -\mathbf{Q}]\} + \{\uparrow \leftrightarrow \uparrow\})
$$

$$
+ \frac{g^2}{4} \sum_{\substack{\mathbf{k,p,q} \\ \mathbf{k',p',q'}}} \Bigg(\Bigg[
$$

$$
- v_{\mathbf{k+q}+\frac{\mathbf{Q}}{2}} v^*_{\mathbf{p-q}-\frac{\mathbf{Q}}{2}} \frac{\langle \alpha^\dagger_{\mathbf{k+q+Q},\uparrow} \alpha^\dagger_{\mathbf{p-q-Q},\downarrow} \alpha_{\mathbf{p},\downarrow} \alpha_{\mathbf{k},\uparrow} \alpha^\dagger_{\mathbf{k'},\uparrow} \alpha^\dagger_{\mathbf{p'},\downarrow} \alpha_{\mathbf{p'-q'},\downarrow} \alpha_{\mathbf{k'+q'},\uparrow} \rangle}{\epsilon^\uparrow_{\mathbf{k+q}} + \epsilon^\downarrow_{\mathbf{p-q}} - \epsilon^\uparrow_{\mathbf{k}} - \epsilon^\downarrow_{\mathbf{p}}}
$$

$$+ v_{\mathbf{k}+\mathbf{q}+\frac{\mathbf{Q}}{2}} v^*_{\mathbf{p}+\frac{\mathbf{Q}}{2}} \frac{\langle \alpha^\dagger_{\mathbf{k}+\mathbf{q}+\mathbf{Q},\uparrow} \alpha^\dagger_{\mathbf{p}-\mathbf{q},\downarrow} \alpha_{\mathbf{p}+\mathbf{Q},\downarrow} \alpha_{\mathbf{k},\uparrow} \alpha^\dagger_{\mathbf{k}',\uparrow} \alpha^\dagger_{\mathbf{p}',\downarrow} \alpha_{\mathbf{p}'-\mathbf{q}',\downarrow} \alpha_{\mathbf{k}'+\mathbf{q}',\uparrow} \rangle}{\epsilon^\uparrow_{\mathbf{k}+\mathbf{q}} + \epsilon^\downarrow_{\mathbf{p}-\mathbf{q}} - \epsilon^\uparrow_{\mathbf{k}} - \epsilon^\downarrow_{\mathbf{p}}} \tag{5.20}$$

$$- v_{\mathbf{k}+\mathbf{q}+\frac{\mathbf{Q}}{2}} v^*_{\mathbf{p}'-\frac{\mathbf{Q}}{2}} \frac{\langle \alpha^\dagger_{\mathbf{k}+\mathbf{q}+\mathbf{Q},\uparrow} \alpha^\dagger_{\mathbf{p}-\mathbf{q},\downarrow} \alpha_{\mathbf{p},\downarrow} \alpha_{\mathbf{k},\uparrow} \alpha^\dagger_{\mathbf{k}',\uparrow} \alpha^\dagger_{\mathbf{p}'-\mathbf{Q},\downarrow} \alpha_{\mathbf{p}'-\mathbf{q}',\downarrow} \alpha_{\mathbf{k}'+\mathbf{q}',\uparrow} \rangle}{\epsilon^\uparrow_{\mathbf{k}+\mathbf{q}} + \epsilon^\downarrow_{\mathbf{p}-\mathbf{q}} - \epsilon^\uparrow_{\mathbf{k}} - \epsilon^\downarrow_{\mathbf{p}}}$$

$$+ v_{\mathbf{k}+\mathbf{q}+\frac{\mathbf{Q}}{2}} v^*_{\mathbf{p}'-\mathbf{q}'+\frac{\mathbf{Q}}{2}} \frac{\langle \alpha^\dagger_{\mathbf{k}+\mathbf{q}+\mathbf{Q},\uparrow} \alpha^\dagger_{\mathbf{p}-\mathbf{q},\downarrow} \alpha_{\mathbf{p},\downarrow} \alpha_{\mathbf{k},\uparrow} \alpha^\dagger_{\mathbf{k}',\uparrow} \alpha^\dagger_{\mathbf{p}',\downarrow} \alpha_{\mathbf{p}'-\mathbf{q}'+\mathbf{Q},\downarrow} \alpha_{\mathbf{k}'+\mathbf{q}',\uparrow} \rangle}{\epsilon^\uparrow_{\mathbf{k}+\mathbf{q}} + \epsilon^\downarrow_{\mathbf{p}-\mathbf{q}} - \epsilon^\uparrow_{\mathbf{k}} - \epsilon^\downarrow_{\mathbf{p}}}$$

$$+ v_{\mathbf{p}-\mathbf{q}+\frac{\mathbf{Q}}{2}} v^*_{\mathbf{k}+\frac{\mathbf{Q}}{2}} \frac{\langle \alpha^\dagger_{\mathbf{k}+\mathbf{q},\uparrow} \alpha^\dagger_{\mathbf{p}-\mathbf{q}+\mathbf{Q},\downarrow} \alpha_{\mathbf{p},\downarrow} \alpha_{\mathbf{k}+\mathbf{Q},\uparrow} \alpha^\dagger_{\mathbf{k}',\uparrow} \alpha^\dagger_{\mathbf{p}',\downarrow} \alpha_{\mathbf{p}'-\mathbf{q}',\downarrow} \alpha_{\mathbf{k}'+\mathbf{q}',\uparrow} \rangle}{\epsilon^\uparrow_{\mathbf{k}+\mathbf{q}} + \epsilon^\downarrow_{\mathbf{p}-\mathbf{q}} - \epsilon^\uparrow_{\mathbf{k}} - \epsilon^\downarrow_{\mathbf{p}}}$$

$$- v_{\mathbf{p}-\frac{\mathbf{Q}}{2}} v^*_{\mathbf{k}+\frac{\mathbf{Q}}{2}} \frac{\langle \alpha^\dagger_{\mathbf{k}+\mathbf{q},\uparrow} \alpha^\dagger_{\mathbf{p}-\mathbf{q},\downarrow} \alpha_{\mathbf{p}-\mathbf{Q},\downarrow} \alpha_{\mathbf{k}+\mathbf{Q},\uparrow} \alpha^\dagger_{\mathbf{k}',\uparrow} \alpha^\dagger_{\mathbf{p}',\downarrow} \alpha_{\mathbf{p}'-\mathbf{q}',\downarrow} \alpha_{\mathbf{k}'+\mathbf{q}',\uparrow} \rangle}{\epsilon^\uparrow_{\mathbf{k}+\mathbf{q}} + \epsilon^\downarrow_{\mathbf{p}-\mathbf{q}} - \epsilon^\uparrow_{\mathbf{k}} - \epsilon^\downarrow_{\mathbf{p}}}$$

$$+ v^*_{\mathbf{k}+\frac{\mathbf{Q}}{2}} v_{\mathbf{p}'+\frac{\mathbf{Q}}{2}} \frac{\langle \alpha^\dagger_{\mathbf{k}+\mathbf{q},\uparrow} \alpha^\dagger_{\mathbf{p}-\mathbf{q},\downarrow} \alpha_{\mathbf{p},\downarrow} \alpha_{\mathbf{k}+\mathbf{Q},\uparrow} \alpha^\dagger_{\mathbf{k}',\uparrow} \alpha^\dagger_{\mathbf{p}'+\mathbf{Q},\downarrow} \alpha_{\mathbf{p}'-\mathbf{q}',\downarrow} \alpha_{\mathbf{k}'+\mathbf{q}',\uparrow} \rangle}{\epsilon^\uparrow_{\mathbf{k}+\mathbf{q}} + \epsilon^\downarrow_{\mathbf{p}-\mathbf{q}} - \epsilon^\uparrow_{\mathbf{k}} - \epsilon^\downarrow_{\mathbf{p}}}$$

$$- v^*_{\mathbf{k}+\frac{\mathbf{Q}}{2}} v_{\mathbf{p}'-\mathbf{q}'-\frac{\mathbf{Q}}{2}} \frac{\langle \alpha^\dagger_{\mathbf{k}+\mathbf{q},\uparrow} \alpha^\dagger_{\mathbf{p}-\mathbf{q},\downarrow} \alpha_{\mathbf{p},\downarrow} \alpha_{\mathbf{k}+\mathbf{Q},\uparrow} \alpha^\dagger_{\mathbf{k}',\uparrow} \alpha^\dagger_{\mathbf{p}',\downarrow} \alpha_{\mathbf{p}'-\mathbf{q}'-\mathbf{Q},\downarrow} \alpha_{\mathbf{k}'+\mathbf{q}',\uparrow} \rangle}{\epsilon^\uparrow_{\mathbf{k}+\mathbf{q}} + \epsilon^\downarrow_{\mathbf{p}-\mathbf{q}} - \epsilon^\uparrow_{\mathbf{k}} - \epsilon^\downarrow_{\mathbf{p}}}$$

$$- v^*_{\mathbf{p}-\mathbf{q}-\frac{\mathbf{Q}}{2}} v_{\mathbf{k}'+\frac{\mathbf{Q}}{2}} \frac{\langle \alpha^\dagger_{\mathbf{k}+\mathbf{q},\uparrow} \alpha^\dagger_{\mathbf{p}-\mathbf{q}-\mathbf{Q},\downarrow} \alpha_{\mathbf{p},\downarrow} \alpha_{\mathbf{k},\uparrow} \alpha^\dagger_{\mathbf{k}'+\mathbf{Q},\uparrow} \alpha^\dagger_{\mathbf{p}',\downarrow} \alpha_{\mathbf{p}'-\mathbf{q}',\downarrow} \alpha_{\mathbf{k}'+\mathbf{q}',\uparrow} \rangle}{\epsilon^\uparrow_{\mathbf{k}+\mathbf{q}} + \epsilon^\downarrow_{\mathbf{p}-\mathbf{q}} - \epsilon^\uparrow_{\mathbf{k}} - \epsilon^\downarrow_{\mathbf{p}}}$$

$$+ v^*_{\mathbf{p}+\frac{\mathbf{Q}}{2}} v_{\mathbf{k}'+\frac{\mathbf{Q}}{2}} \frac{\langle \alpha^\dagger_{\mathbf{k}+\mathbf{q},\uparrow} \alpha^\dagger_{\mathbf{p}-\mathbf{q},\downarrow} \alpha_{\mathbf{p}+\mathbf{Q},\downarrow} \alpha_{\mathbf{k},\uparrow} \alpha^\dagger_{\mathbf{k}'+\mathbf{Q},\uparrow} \alpha^\dagger_{\mathbf{p}',\downarrow} \alpha_{\mathbf{p}'-\mathbf{q}',\downarrow} \alpha_{\mathbf{k}'+\mathbf{q}',\uparrow} \rangle}{\epsilon^\uparrow_{\mathbf{k}+\mathbf{q}} + \epsilon^\downarrow_{\mathbf{p}-\mathbf{q}} - \epsilon^\uparrow_{\mathbf{k}} - \epsilon^\downarrow_{\mathbf{p}}}$$

$$- v_{\mathbf{k}'+\frac{\mathbf{Q}}{2}} v^*_{\mathbf{p}'-\frac{\mathbf{Q}}{2}} \frac{\langle \alpha^\dagger_{\mathbf{k}+\mathbf{q},\uparrow} \alpha^\dagger_{\mathbf{p}-\mathbf{q},\downarrow} \alpha_{\mathbf{p},\downarrow} \alpha_{\mathbf{k},\uparrow} \alpha^\dagger_{\mathbf{k}'+\mathbf{Q},\uparrow} \alpha^\dagger_{\mathbf{p}'-\mathbf{Q},\downarrow} \alpha_{\mathbf{p}'-\mathbf{q}',\downarrow} \alpha_{\mathbf{k}'+\mathbf{q}',\uparrow} \rangle}{\epsilon^\uparrow_{\mathbf{k}+\mathbf{q}} + \epsilon^\downarrow_{\mathbf{p}-\mathbf{q}} - \epsilon^\uparrow_{\mathbf{k}} - \epsilon^\downarrow_{\mathbf{p}}}$$

$$+ v_{\mathbf{k}'+\frac{\mathbf{Q}}{2}} v^*_{\mathbf{p}'-\mathbf{q}'+\frac{\mathbf{Q}}{2}} \frac{\langle \alpha^\dagger_{\mathbf{k}+\mathbf{q},\uparrow} \alpha^\dagger_{\mathbf{p}-\mathbf{q},\downarrow} \alpha_{\mathbf{p},\downarrow} \alpha_{\mathbf{k},\uparrow} \alpha^\dagger_{\mathbf{k}'+\mathbf{Q},\uparrow} \alpha^\dagger_{\mathbf{p}',\downarrow} \alpha_{\mathbf{p}'-\mathbf{q}'+\mathbf{Q},\downarrow} \alpha_{\mathbf{k}'+\mathbf{q}',\uparrow} \rangle}{\epsilon^\uparrow_{\mathbf{k}+\mathbf{q}} + \epsilon^\downarrow_{\mathbf{p}-\mathbf{q}} - \epsilon^\uparrow_{\mathbf{k}} - \epsilon^\downarrow_{\mathbf{p}}}$$

$$+ v_{\mathbf{p}-\mathbf{q}+\frac{\mathbf{Q}}{2}} v^*_{\mathbf{k}'+\mathbf{q}'+\frac{\mathbf{Q}}{2}} \frac{\langle \alpha^\dagger_{\mathbf{k}+\mathbf{q},\uparrow} \alpha^\dagger_{\mathbf{p}-\mathbf{q}+\mathbf{Q},\downarrow} \alpha_{\mathbf{p},\downarrow} \alpha_{\mathbf{k},\uparrow} \alpha^\dagger_{\mathbf{k}',\uparrow} \alpha^\dagger_{\mathbf{p}',\downarrow} \alpha_{\mathbf{p}'-\mathbf{q}',\downarrow} \alpha_{\mathbf{k}'+\mathbf{q}'+\mathbf{Q},\uparrow} \rangle}{\epsilon^\uparrow_{\mathbf{k}+\mathbf{q}} + \epsilon^\downarrow_{\mathbf{p}-\mathbf{q}} - \epsilon^\uparrow_{\mathbf{k}} - \epsilon^\downarrow_{\mathbf{p}}}$$

$$- v_{\mathbf{p}-\frac{\mathbf{Q}}{2}} v^*_{\mathbf{k}'+\mathbf{q}'+\frac{\mathbf{Q}}{2}} \frac{\langle \alpha^\dagger_{\mathbf{k}+\mathbf{q},\uparrow} \alpha^\dagger_{\mathbf{p}-\mathbf{q},\downarrow} \alpha_{\mathbf{p}-\mathbf{Q},\downarrow} \alpha_{\mathbf{k},\uparrow} \alpha^\dagger_{\mathbf{k}',\uparrow} \alpha^\dagger_{\mathbf{p}',\downarrow} \alpha_{\mathbf{p}'-\mathbf{q}',\downarrow} \alpha_{\mathbf{k}'+\mathbf{q}'+\mathbf{Q},\uparrow} \rangle}{\epsilon^\uparrow_{\mathbf{k}+\mathbf{q}} + \epsilon^\downarrow_{\mathbf{p}-\mathbf{q}} - \epsilon^\uparrow_{\mathbf{k}} - \epsilon^\downarrow_{\mathbf{p}}}$$

$$+ v_{\mathbf{p}'+\frac{\mathbf{Q}}{2}} v^*_{\mathbf{k}'+\mathbf{q}'+\frac{\mathbf{Q}}{2}} \frac{\langle \alpha^\dagger_{\mathbf{k}+\mathbf{q},\uparrow} \alpha^\dagger_{\mathbf{p}-\mathbf{q},\downarrow} \alpha_{\mathbf{p},\downarrow} \alpha_{\mathbf{k},\uparrow} \alpha^\dagger_{\mathbf{k}',\uparrow} \alpha^\dagger_{\mathbf{p}'+\mathbf{Q},\downarrow} \alpha_{\mathbf{p}'-\mathbf{q}',\downarrow} \alpha_{\mathbf{k}'+\mathbf{q}'+\mathbf{Q},\uparrow} \rangle}{\epsilon^\uparrow_{\mathbf{k}+\mathbf{q}} + \epsilon^\downarrow_{\mathbf{p}-\mathbf{q}} - \epsilon^\uparrow_{\mathbf{k}} - \epsilon^\downarrow_{\mathbf{p}}}$$

$$- v_{\mathbf{p}'-\mathbf{q}'-\frac{\mathbf{Q}}{2}} v^*_{\mathbf{k}'+\mathbf{q}'+\frac{\mathbf{Q}}{2}} \frac{\langle \alpha^\dagger_{\mathbf{k}+\mathbf{q},\uparrow} \alpha^\dagger_{\mathbf{p}-\mathbf{q},\downarrow} \alpha_{\mathbf{p},\downarrow} \alpha_{\mathbf{k},\uparrow} \alpha^\dagger_{\mathbf{k}',\uparrow} \alpha^\dagger_{\mathbf{p}',\downarrow} \alpha_{\mathbf{p}'-\mathbf{q}'-\mathbf{Q},\downarrow} \alpha_{\mathbf{k}'+\mathbf{q}'+\mathbf{Q},\uparrow} \rangle}{\epsilon^\uparrow_{\mathbf{k}+\mathbf{q}} + \epsilon^\downarrow_{\mathbf{p}-\mathbf{q}} - \epsilon^\uparrow_{\mathbf{k}} - \epsilon^\downarrow_{\mathbf{p}}} \Bigg]$$

C. transformed pairs of operator with one spin-up and down each

$$+ [\mathbf{Q} \to -\mathbf{Q}]) \tag{5.21}$$

The first line, **A**, consists of the regular, unrotated fluctuation contribution or second order perturbative correction to the free energy. Here, momentum matching is trivial and has been performed already to shorten the expression. The following six lines, **B**, are rotations of momentum-paired spin-up electrons and holes. Hence, there is a symmetric contribution from spin-down pairs, which is trivially found by switching the spin labels on theses 6 terms. The final terms, **C**, are all remaining pairs with one spin-up and one spin-down operator.

For ease of reading, any factors of $u_{\mathbf{k}} = \sqrt{1 - \frac{g^2 |D_{\mathbf{k}}|^2}{(\epsilon_{\mathbf{k}-\frac{\mathbf{Q}}{2}} - \epsilon_{\mathbf{k}+\frac{\mathbf{Q}}{2}})^2}}$ have been set to 1 in the anomalous terms. Their D^2 contribution stems from factors of $v_{\mathbf{k}} = \frac{g D_{\mathbf{k}}}{\epsilon_{\mathbf{k}-\frac{\mathbf{Q}}{2}} - \epsilon_{\mathbf{k}+\frac{\mathbf{Q}}{2}}}$.

One may express these contributions in terms of diagrams as well. Below, we draw three examples - one for each of the first lines of the three blocks of terms identified above.

A. Regular term:

$$g^2 \langle \alpha^{\dagger}_{\mathbf{k}+\mathbf{q},\uparrow} \alpha^{\dagger}_{\mathbf{p}-\mathbf{q},\downarrow} \alpha_{\mathbf{p},\downarrow} \alpha_{\mathbf{k},\uparrow} \alpha^{\dagger}_{\mathbf{k},\uparrow} \alpha^{\dagger}_{\mathbf{p},\downarrow} \alpha_{\mathbf{p}-\mathbf{q},\downarrow} \alpha_{\mathbf{k}+\mathbf{q},\uparrow} \rangle$$

$$(5.22)$$

B. First term of rotated pairs of spin-up electron and hole:

$$g^2 v_{\mathbf{k}+\mathbf{q}+\frac{\mathbf{Q}}{2}} v^{*}_{\mathbf{k}'+\mathbf{q}'+\frac{\mathbf{Q}}{2}} \langle \alpha^{\dagger}_{\mathbf{k}+\mathbf{q}+\mathbf{Q},\uparrow} \alpha^{\dagger}_{\mathbf{p}-\mathbf{q},\downarrow} \alpha_{\mathbf{p},\downarrow} \alpha_{\mathbf{k},\uparrow} \alpha^{\dagger}_{\mathbf{k}',\uparrow} \alpha^{\dagger}_{\mathbf{p}',\downarrow} \alpha_{\mathbf{p}'-\mathbf{q}',\downarrow} \alpha_{\mathbf{k}'+\mathbf{q}'+\mathbf{Q},\uparrow} \rangle$$

$$(5.23)$$

C. First term of rotated pairs of spin-up and spin-down field operator:

$$-g^2 v_{\mathbf{k}+\mathbf{q}+\frac{\mathbf{Q}}{2}} v^*_{\mathbf{p}-\mathbf{q}-\frac{\mathbf{Q}}{2}} \langle \alpha^\dagger_{\mathbf{k}+\mathbf{q}+\mathbf{Q},\uparrow} \alpha^\dagger_{\mathbf{p}-\mathbf{q}-\mathbf{Q},\downarrow} \alpha_{\mathbf{p},\downarrow} \alpha_{\mathbf{k},\uparrow} \alpha^\dagger_{\mathbf{k}',\uparrow} \alpha^\dagger_{\mathbf{p}',\downarrow} \alpha_{\mathbf{p}'-\mathbf{q}',\downarrow} \alpha_{\mathbf{k}'+\mathbf{q}',\uparrow} \rangle$$

$$(5.24)$$

Next we explicitly calculate the expectation in the diagonal basis. Non-zero contributions are formed by matching creation and annihilation operators of identical momentum and spin, which yield Fermi distribution functions, $\langle \alpha^\dagger_{\mathbf{k},\sigma} \alpha_{\mathbf{k},\sigma} \rangle = f^\sigma_{\mathbf{k}}$. Diagrams of the form shown above are helpful in determining which pairings are non-zero. After carrying out all of these contractions, we obtain

$$\mathcal{F}_{fluct}(D) = 2g^2 \sum_{\mathbf{k},\mathbf{p},\mathbf{q}}$$

$$\underbrace{\left(|v_{\mathbf{k}-\frac{\mathbf{Q}}{2}}|^2 + |v_{\mathbf{p}-\frac{\mathbf{Q}}{2}}|^2 + |v_{\mathbf{k}+\mathbf{q}-\frac{\mathbf{Q}}{2}}|^2 + |v_{\mathbf{p}-\mathbf{q}-\frac{\mathbf{Q}}{2}}|^2 \right) \frac{f^\uparrow_{\mathbf{k}+\mathbf{q}} f^\downarrow_{\mathbf{p}-\mathbf{q}}(1 - f^\downarrow_{\mathbf{p}})(1 - f^\uparrow_{\mathbf{k}})}{\epsilon^\uparrow_{\mathbf{k}+\mathbf{q}} + \epsilon^\downarrow_{\mathbf{p}-\mathbf{q}} - \epsilon^\uparrow_{\mathbf{k}} - \epsilon^\downarrow_{\mathbf{p}}}}_{\textbf{A. regular contribution}}$$

$$\underbrace{+\frac{g^2}{4} \sum_{\mathbf{k},\mathbf{p},\mathbf{q}} \left\{ \left[|v_{\mathbf{k}+\mathbf{q}+\frac{\mathbf{Q}}{2}}|^2 \frac{f^\uparrow_{\mathbf{k}+\mathbf{q}+\mathbf{Q}} f^\downarrow_{\mathbf{p}-\mathbf{q}}(1 - f^\downarrow_{\mathbf{p}})(1 - f^\uparrow_{\mathbf{k}})}{\epsilon^\uparrow_{\mathbf{k}+\mathbf{q}} + \epsilon^\downarrow_{\mathbf{p}-\mathbf{q}} - \epsilon^\uparrow_{\mathbf{k}} - \epsilon^\downarrow_{\mathbf{p}}} \right. \right.}$$

$$+ |v_{\mathbf{k}+\frac{\mathbf{Q}}{2}}|^2 \frac{f^\uparrow_{\mathbf{k}+\mathbf{q}} f^\downarrow_{\mathbf{p}-\mathbf{q}}(1 - f^\downarrow_{\mathbf{p}})(1 - f^\uparrow_{\mathbf{k}+\mathbf{Q}})}{\epsilon^\uparrow_{\mathbf{k}+\mathbf{q}} + \epsilon^\downarrow_{\mathbf{p}-\mathbf{q}} - \epsilon^\uparrow_{\mathbf{k}} - \epsilon^\downarrow_{\mathbf{p}}}$$

$$+ v_{\mathbf{k}+\mathbf{q}+\frac{\mathbf{Q}}{2}} v^*_{\mathbf{k}+\frac{\mathbf{Q}}{2}} \frac{f^\uparrow_{\mathbf{k}+\mathbf{q}+\mathbf{Q}} f^\downarrow_{\mathbf{p}-\mathbf{q}}(1 - f^\downarrow_{\mathbf{p}})(1 - f^\uparrow_{\mathbf{k}+\mathbf{Q}})}{\epsilon^\uparrow_{\mathbf{k}+\mathbf{q}} + \epsilon^\downarrow_{\mathbf{p}-\mathbf{q}} - \epsilon^\uparrow_{\mathbf{k}} - \epsilon^\downarrow_{\mathbf{p}}}$$

$$+ v^*_{\mathbf{k}+\frac{\mathbf{Q}}{2}} v_{\mathbf{k}+\mathbf{q}+\frac{\mathbf{Q}}{2}} \frac{f^\uparrow_{\mathbf{k}+\mathbf{q}} f^\downarrow_{\mathbf{p}-\mathbf{q}}(1 - f^\downarrow_{\mathbf{p}})(1 - f^\uparrow_{\mathbf{k}})}{\epsilon^\uparrow_{\mathbf{k}+\mathbf{q}} + \epsilon^\downarrow_{\mathbf{p}-\mathbf{q}} - \epsilon^\uparrow_{\mathbf{k}} - \epsilon^\downarrow_{\mathbf{p}}}$$

$$- v_{\mathbf{k}+\mathbf{q}+\frac{\mathbf{Q}}{2}} v^*_{\mathbf{k}+\frac{\mathbf{Q}}{2}} \frac{f^\uparrow_{\mathbf{k}+\mathbf{q}} f^\downarrow_{\mathbf{p}-\mathbf{q}}(1 - f^\downarrow_{\mathbf{p}})(1 - f^\uparrow_{\mathbf{k}+\mathbf{Q}})}{\epsilon^\uparrow_{\mathbf{k}+\mathbf{q}} + \epsilon^\downarrow_{\mathbf{p}-\mathbf{q}} - \epsilon^\uparrow_{\mathbf{k}} - \epsilon^\downarrow_{\mathbf{p}}}$$

$$\underbrace{\left. \left. - v_{\mathbf{k}+\mathbf{q}+\frac{\mathbf{Q}}{2}} v^*_{\mathbf{k}+\frac{\mathbf{Q}}{2}} \frac{f^\uparrow_{\mathbf{k}+\mathbf{q}+\mathbf{Q}} f^\downarrow_{\mathbf{p}-\mathbf{q}}(1 - f^\downarrow_{\mathbf{p}})(1 - f^\uparrow_{\mathbf{k}})}{\epsilon^\uparrow_{\mathbf{k}+\mathbf{q}} + \epsilon^\downarrow_{\mathbf{p}-\mathbf{q}} - \epsilon^\uparrow_{\mathbf{k}} - \epsilon^\downarrow_{\mathbf{p}}} \right] + [\uparrow \leftrightarrow \downarrow] \right.}_{\textbf{B. rotated pairs of spin-up operator}}$$

$$-v_{\mathbf{k+q}+\frac{\mathbf{Q}}{2}}v^*_{\mathbf{p-q}-\frac{\mathbf{Q}}{2}}\frac{f^{\uparrow}_{\mathbf{k+q+Q}}f^{\downarrow}_{\mathbf{p-q-Q}}(1-f^{\downarrow}_{\mathbf{p}})(1-f^{\uparrow}_{\mathbf{k}})}{\epsilon^{\uparrow}_{\mathbf{k+q}}+\epsilon^{\downarrow}_{\mathbf{p-q}}-\epsilon^{\uparrow}_{\mathbf{k}}-\epsilon^{\downarrow}_{\mathbf{p}}}$$

$$+v_{\mathbf{k+q}+\frac{\mathbf{Q}}{2}}v^*_{\mathbf{p}+\frac{\mathbf{Q}}{2}}\frac{f^{\uparrow}_{\mathbf{k+q-Q}}f^{\downarrow}_{\mathbf{p-q}}(1-f^{\downarrow}_{\mathbf{p+Q}})(1-f^{\uparrow}_{\mathbf{k}})}{\epsilon^{\uparrow}_{\mathbf{k+q}}+\epsilon^{\downarrow}_{\mathbf{p-q}}-\epsilon^{\uparrow}_{\mathbf{k}}-\epsilon^{\downarrow}_{\mathbf{p}}}$$

$$-v_{\mathbf{k+q}+\frac{\mathbf{Q}}{2}}v^*_{\mathbf{p}+\frac{\mathbf{Q}}{2}}\frac{f^{\uparrow}_{\mathbf{k+q+Q}}f^{\downarrow}_{\mathbf{p-q}}(1-f^{\downarrow}_{\mathbf{p}})(1-f^{\uparrow}_{\mathbf{k}})}{\epsilon^{\uparrow}_{\mathbf{k+q}}+\epsilon^{\downarrow}_{\mathbf{p-q}}-\epsilon^{\uparrow}_{\mathbf{k}}-\epsilon^{\downarrow}_{\mathbf{p}}}$$

$$+v_{\mathbf{k+q}+\frac{\mathbf{Q}}{2}}v^*_{\mathbf{p-q}-\frac{\mathbf{Q}}{2}}\frac{f^{\uparrow}_{\mathbf{k+q+Q}}f^{\downarrow}_{\mathbf{p-q}}(1-f^{\downarrow}_{\mathbf{p}})(1-f^{\uparrow}_{\mathbf{k}})}{\epsilon^{\uparrow}_{\mathbf{k+q}}+\epsilon^{\downarrow}_{\mathbf{p-q}}-\epsilon^{\uparrow}_{\mathbf{k}}-\epsilon^{\downarrow}_{\mathbf{p}}}$$

$$+v^*_{\mathbf{k}+\frac{\mathbf{Q}}{2}}v_{\mathbf{p-q}+\frac{\mathbf{Q}}{2}}\frac{f^{\uparrow}_{\mathbf{k+q}}f^{\downarrow}_{\mathbf{p-q+Q}}(1-f^{\downarrow}_{\mathbf{p}})(1-f^{\uparrow}_{\mathbf{k+Q}})}{\epsilon^{\uparrow}_{\mathbf{k+q}}+\epsilon^{\downarrow}_{\mathbf{p-q}}-\epsilon^{\uparrow}_{\mathbf{k}}-\epsilon^{\downarrow}_{\mathbf{p}}}$$

$$-v^*_{\mathbf{k}+\frac{\mathbf{Q}}{2}}v_{\mathbf{p}-\frac{\mathbf{Q}}{2}}\frac{f^{\uparrow}_{\mathbf{k+q}}f^{\downarrow}_{\mathbf{p-q}}(1-f^{\downarrow}_{\mathbf{p-Q}})(1-f^{\uparrow}_{\mathbf{k+Q}})}{\epsilon^{\uparrow}_{\mathbf{k+q}}+\epsilon^{\downarrow}_{\mathbf{p-q}}-\epsilon^{\uparrow}_{\mathbf{k}}-\epsilon^{\downarrow}_{\mathbf{p}}}$$

$$+v^*_{\mathbf{k}+\frac{\mathbf{Q}}{2}}v_{\mathbf{p}-\frac{\mathbf{Q}}{2}}\frac{f^{\uparrow}_{\mathbf{k+q}}f^{\downarrow}_{\mathbf{p-q}}(1-f^{\downarrow}_{\mathbf{p}})(1-f^{\uparrow}_{\mathbf{k+Q}})}{\epsilon^{\uparrow}_{\mathbf{k+q}}+\epsilon^{\downarrow}_{\mathbf{p-q}}-\epsilon^{\uparrow}_{\mathbf{k}}-\epsilon^{\downarrow}_{\mathbf{p}}}$$

$$-v^*_{\mathbf{k}+\frac{\mathbf{Q}}{2}}v_{\mathbf{p-q}+\frac{\mathbf{Q}}{2}}\frac{f^{\uparrow}_{\mathbf{k+q}}f^{\downarrow}_{\mathbf{p-q}}(1-f^{\downarrow}_{\mathbf{p}})(1-f^{\uparrow}_{\mathbf{k+Q}})}{\epsilon^{\uparrow}_{\mathbf{k+q}}+\epsilon^{\downarrow}_{\mathbf{p-q}}-\epsilon^{\uparrow}_{\mathbf{k}}-\epsilon^{\downarrow}_{\mathbf{p}}}$$

$$-v_{\mathbf{k}-\frac{\mathbf{Q}}{2}}v^*_{\mathbf{p-q}-\frac{\mathbf{Q}}{2}}\frac{f^{\uparrow}_{\mathbf{k+q}}f^{\downarrow}_{\mathbf{p-q-Q}}(1-f^{\downarrow}_{\mathbf{p}})(1-f^{\uparrow}_{\mathbf{k}})}{\epsilon^{\uparrow}_{\mathbf{k+q}}+\epsilon^{\downarrow}_{\mathbf{p-q}}-\epsilon^{\uparrow}_{\mathbf{k}}-\epsilon^{\downarrow}_{\mathbf{p}}}$$

$$+v_{\mathbf{k}-\frac{\mathbf{Q}}{2}}v^*_{\mathbf{p}+\frac{\mathbf{Q}}{2}}\frac{f^{\uparrow}_{\mathbf{k+q}}f^{\downarrow}_{\mathbf{p-q}}(1-f^{\downarrow}_{\mathbf{p+Q}})(1-f^{\uparrow}_{\mathbf{k}})}{\epsilon^{\uparrow}_{\mathbf{k+q}}+\epsilon^{\downarrow}_{\mathbf{p-q}}-\epsilon^{\uparrow}_{\mathbf{k}}-\epsilon^{\downarrow}_{\mathbf{p}}}$$

$$-v_{\mathbf{k}-\frac{\mathbf{Q}}{2}}v^*_{\mathbf{p}+\frac{\mathbf{Q}}{2}}\frac{f^{\uparrow}_{\mathbf{k+q}}f^{\downarrow}_{\mathbf{p-q}}(1-f^{\downarrow}_{\mathbf{p}})(1-f^{\uparrow}_{\mathbf{k}})}{\epsilon^{\uparrow}_{\mathbf{k+q}}+\epsilon^{\downarrow}_{\mathbf{p-q}}-\epsilon^{\uparrow}_{\mathbf{k}}-\epsilon^{\downarrow}_{\mathbf{p}}}$$

$$\underbrace{+v_{\mathbf{k}-\frac{\mathbf{Q}}{2}}v^*_{\mathbf{p-q}-\frac{\mathbf{Q}}{2}}\frac{f^{\uparrow}_{\mathbf{k+q}}f^{\downarrow}_{\mathbf{p-q}}(1-f^{\downarrow}_{\mathbf{p}})(1-f^{\uparrow}_{\mathbf{k}})}{\epsilon^{\uparrow}_{\mathbf{k+q}}+\epsilon^{\downarrow}_{\mathbf{p-q}}-\epsilon^{\uparrow}_{\mathbf{k}}-\epsilon^{\downarrow}_{\mathbf{p}}}}_{\substack{\textbf{C.} \text{ rotated pairs of operator with} \\ \text{one spin-up and down each}}} \tag{5.25}$$

It is helpful at this point to step back for a moment and look at where all these terms came from. This morass of terms is given by all possible contractions of vertices formed by the rotation of operators. Again, we would like to show a few examples corresponding to the first term of each block of terms.

A. Regular term:

$$
\left\langle \quad\right\rangle = \qquad\qquad (5.26)
$$

B. First term of rotated pairs of spin-up electron and hole:

$$
\left\langle \quad\right\rangle = \qquad\qquad (5.27)
$$

C. First term of rotated pairs of spin-up and spin-down field operator:

$$
\left\langle \quad\right\rangle = \qquad\qquad (5.28)
$$

We may further simplify the fluctuation corrections by collecting terms and shifting momentum labels where appropriate:

$$
\mathcal{F}_{fluct}(D) =
$$

$$
\frac{g^2}{4} \sum_{\mathbf{k},\mathbf{p},\mathbf{q}} \left\{ \left[\left(\left\{ v^*_{\mathbf{k+q}-\frac{\mathbf{Q}}{2}} \left(f^{\uparrow}_{\mathbf{k+q-Q}} - f^{\uparrow}_{\mathbf{k+q}} \right) v_{\mathbf{k}-\frac{\mathbf{Q}}{2}} \left(f^{\uparrow}_{\mathbf{k}} - f^{\uparrow}_{\mathbf{k-Q}} \right) \frac{f^{\downarrow}_{\mathbf{p-q}} \left(1 - f^{\downarrow}_{\mathbf{p}}\right)}{\epsilon^{\uparrow}_{\mathbf{k+q}} + \epsilon^{\downarrow}_{\mathbf{p-q}} - \epsilon^{\uparrow}_{\mathbf{k}} - \epsilon^{\downarrow}_{\mathbf{p}}} \right.\right.\right.
$$

$$
\left.\left.\left. + |v_{\mathbf{k}+\frac{\mathbf{Q}}{2}}|^2 \left(f^{\uparrow}_{\mathbf{k}} - f^{\uparrow}_{\mathbf{k+Q}} \right) \frac{f^{\uparrow}_{\mathbf{k+q}} f^{\downarrow}_{\mathbf{p-q}} \left(1 - f^{\downarrow}_{\mathbf{p}}\right) + \left(1 - f^{\uparrow}_{\mathbf{k+q}}\right)\left(1 - f^{\downarrow}_{\mathbf{p-q}}\right) f^{\downarrow}_{\mathbf{p}}}{\epsilon^{\uparrow}_{\mathbf{k+q}} + \epsilon^{\downarrow}_{\mathbf{p-q}} - \epsilon^{\uparrow}_{\mathbf{k}} - \epsilon^{\downarrow}_{\mathbf{p}}} \right\} + \{\uparrow \leftrightarrow \downarrow\} \right)
$$

$$
+ v^*_{\mathbf{k}+\frac{\mathbf{Q}}{2}} \left(f^{\uparrow}_{\mathbf{k}} - f^{\uparrow}_{\mathbf{k+Q}} \right) v_{\mathbf{p}-\frac{\mathbf{Q}}{2}} \left(f^{\downarrow}_{\mathbf{p-Q}} - f^{\downarrow}_{\mathbf{p}} \right) \frac{f^{\downarrow}_{\mathbf{p-q}} + f^{\uparrow}_{\mathbf{k+q}} - 1}{\epsilon^{\uparrow}_{\mathbf{k+q}} + \epsilon^{\downarrow}_{\mathbf{p-q}} - \epsilon^{\uparrow}_{\mathbf{k}} - \epsilon^{\downarrow}_{\mathbf{p}}}
$$

$$
- v^*_{\mathbf{k}+\frac{\mathbf{Q}}{2}} \left(f^{\uparrow}_{\mathbf{k}} - f^{\uparrow}_{\mathbf{k+Q}} \right) v_{\mathbf{p-q}+\frac{\mathbf{Q}}{2}} \left(f^{\downarrow}_{\mathbf{p-q+Q}} - f^{\downarrow}_{\mathbf{p-q}} \right) \frac{f^{\uparrow}_{\mathbf{k+q}} - f^{\downarrow}_{\mathbf{p}}}{\epsilon^{\uparrow}_{\mathbf{k+q}} + \epsilon^{\downarrow}_{\mathbf{p-q}} - \epsilon^{\uparrow}_{\mathbf{k}} - \epsilon^{\downarrow}_{\mathbf{p}}} \right] + [Q \to -Q] \right\}
$$

$$
(5.29)
$$

Now we insert the definitions of the off diagonal rotation elements, $v_{\mathbf{k}} = \frac{gD_{\mathbf{k}}}{\epsilon_{\mathbf{k}} - \epsilon_{\mathbf{k+Q}}}$

and use the $\mathbf{Q} \to -\mathbf{Q}$ symmetry;

$$
\mathcal{F}_{fluct}(D) =
$$

$$
\frac{g^4}{2} \sum_{\mathbf{k},\mathbf{p},\mathbf{q}} \Bigg\{ \Bigg(\Bigg\{ \overline{D}_{\mathbf{k}+\mathbf{q}-\frac{\mathbf{Q}}{2}} \frac{f^{\uparrow}_{\mathbf{k}+\mathbf{q}-\mathbf{Q}} - f^{\uparrow}_{\mathbf{k}+\mathbf{q}}}{\epsilon_{\mathbf{k}+\mathbf{q}-\mathbf{Q}} - \epsilon_{\mathbf{k}+\mathbf{q}}} D_{\mathbf{k}-\frac{\mathbf{Q}}{2}} \frac{f^{\uparrow}_{\mathbf{k}} - f^{\uparrow}_{\mathbf{k}-\mathbf{Q}}}{\epsilon_{\mathbf{k}-\mathbf{Q}} - \epsilon_{\mathbf{k}}} \frac{f^{\downarrow}_{\mathbf{p}-\mathbf{q}} (1 - f^{\downarrow}_{\mathbf{p}})}{\epsilon^{\uparrow}_{\mathbf{k}+\mathbf{q}} + \epsilon^{\downarrow}_{\mathbf{p}-\mathbf{q}} - \epsilon^{\uparrow}_{\mathbf{k}} - \epsilon^{\downarrow}_{\mathbf{p}}}
$$

$$
+ |D_{\mathbf{k}+\frac{\mathbf{Q}}{2}}|^2 \frac{f^{\uparrow}_{\mathbf{k}} - f^{\uparrow}_{\mathbf{k}+\mathbf{Q}}}{(\epsilon_{\mathbf{k}} - \epsilon_{\mathbf{k}+\mathbf{Q}})^2} \frac{f^{\uparrow}_{\mathbf{k}+\mathbf{q}} f^{\downarrow}_{\mathbf{p}-\mathbf{q}} (1 - f^{\downarrow}_{\mathbf{p}}) + (1 - f^{\uparrow}_{\mathbf{k}+\mathbf{q}})(1 - f^{\downarrow}_{\mathbf{p}-\mathbf{q}}) f^{\downarrow}_{\mathbf{p}}}{\epsilon^{\uparrow}_{\mathbf{k}+\mathbf{q}} + \epsilon^{\downarrow}_{\mathbf{p}-\mathbf{q}} - \epsilon^{\uparrow}_{\mathbf{k}} - \epsilon^{\downarrow}_{\mathbf{p}}} \Bigg\} + \{\uparrow \leftrightarrow \downarrow\} \Bigg)
$$

$$
+ \overline{D}_{\mathbf{k}+\frac{\mathbf{Q}}{2}} \frac{f^{\uparrow}_{\mathbf{k}} - f^{\uparrow}_{\mathbf{k}+\mathbf{Q}}}{\epsilon_{\mathbf{k}} - \epsilon_{\mathbf{k}+\mathbf{Q}}} D_{\mathbf{p}-\frac{\mathbf{Q}}{2}} \frac{f^{\downarrow}_{\mathbf{p}-\mathbf{Q}} - f^{\downarrow}_{\mathbf{p}}}{\epsilon_{\mathbf{p}-\mathbf{Q}} - \epsilon_{\mathbf{p}}} \frac{f^{\downarrow}_{\mathbf{p}-\mathbf{q}} + f^{\uparrow}_{\mathbf{k}+\mathbf{q}} - 1}{\epsilon^{\uparrow}_{\mathbf{k}+\mathbf{q}} + \epsilon^{\downarrow}_{\mathbf{p}-\mathbf{q}} - \epsilon^{\uparrow}_{\mathbf{k}} - \epsilon^{\downarrow}_{\mathbf{p}}}
$$

$$
- \overline{D}_{\mathbf{k}+\frac{\mathbf{Q}}{2}} \frac{f^{\uparrow}_{\mathbf{k}} - f^{\uparrow}_{\mathbf{k}+\mathbf{Q}}}{\epsilon_{\mathbf{k}} - \epsilon_{\mathbf{k}+\mathbf{Q}}} D_{\mathbf{p}-\mathbf{q}+\frac{\mathbf{Q}}{2}} \frac{f^{\downarrow}_{\mathbf{p}-\mathbf{q}+\mathbf{Q}} - f^{\downarrow}_{\mathbf{p}-\mathbf{q}}}{\epsilon_{\mathbf{p}-\mathbf{q}} - \epsilon_{\mathbf{p}-\mathbf{q}+\mathbf{Q}}} \frac{f^{\uparrow}_{\mathbf{k}+\mathbf{q}} - f^{\downarrow}_{\mathbf{p}}}{\epsilon^{\uparrow}_{\mathbf{k}+\mathbf{q}} + \epsilon^{\downarrow}_{\mathbf{p}-\mathbf{q}} - \epsilon^{\uparrow}_{\mathbf{k}} - \epsilon^{\downarrow}_{\mathbf{p}}} \Bigg\} \qquad (5.30)
$$

Using the standard form of antiferromagnetic susceptibility $\chi^{\downarrow\downarrow}_{AF}$, superconducting susceptibility $\chi^{\uparrow\downarrow}_{SC}$ and self-energy Σ;

$$
\chi^{\downarrow\downarrow}_{AF}(\mathbf{q}, \epsilon^{\uparrow}_{\mathbf{k}} - \epsilon^{\uparrow}_{\mathbf{k}+\mathbf{q}}) = \sum_{\mathbf{p}} \frac{f^{\downarrow}_{\mathbf{p}-\mathbf{q}} - f^{\downarrow}_{\mathbf{p}}}{\epsilon^{\uparrow}_{\mathbf{k}+\mathbf{q}} + \epsilon^{\downarrow}_{\mathbf{p}-\mathbf{q}} - \epsilon^{\uparrow}_{\mathbf{k}} - \epsilon^{\downarrow}_{\mathbf{p}}} \qquad (5.31)
$$

$$
\chi^{\uparrow\downarrow}_{SC}(\mathbf{p}+\mathbf{k}, \epsilon^{\uparrow}_{\mathbf{k}} + \epsilon^{\downarrow}_{\mathbf{p}}) = \sum_{\mathbf{p}} \frac{f^{\downarrow}_{\mathbf{p}-\mathbf{q}} + f^{\uparrow}_{\mathbf{k}+\mathbf{q}} - 1}{\epsilon^{\uparrow}_{\mathbf{k}+\mathbf{q}} + \epsilon^{\downarrow}_{\mathbf{p}-\mathbf{q}} - \epsilon^{\uparrow}_{\mathbf{k}} - \epsilon^{\downarrow}_{\mathbf{p}}} \qquad (5.32)
$$

$$
\Sigma(\mathbf{k}, \epsilon_{\mathbf{k}}) = g^2 \sum_{\mathbf{p},\mathbf{q}} \frac{f^{\uparrow}_{\mathbf{k}+\mathbf{q}} f^{\downarrow}_{\mathbf{p}-\mathbf{q}} (1 - f^{\downarrow}_{\mathbf{p}}) + (1 - f^{\uparrow}_{\mathbf{k}+\mathbf{q}})(1 - f^{\downarrow}_{\mathbf{p}-\mathbf{q}}) f^{\downarrow}_{\mathbf{p}}}{\epsilon^{\uparrow}_{\mathbf{k}+\mathbf{q}} + \epsilon^{\downarrow}_{\mathbf{p}-\mathbf{q}} - \epsilon^{\uparrow}_{\mathbf{k}} - \epsilon^{\downarrow}_{\mathbf{p}}}, \qquad (5.33)
$$

we can rewrite equation (5.30) as

$$
\mathcal{F}_{fluct}(D) = \frac{g^4}{2} \sum_{\mathbf{k}} \Bigg(\Bigg\{ |D_{\mathbf{k}+\frac{\mathbf{Q}}{2}}|^2 \frac{f^{\uparrow}_{\mathbf{k}} - f^{\uparrow}_{\mathbf{k}+\mathbf{Q}}}{(\epsilon_{\mathbf{k}} - \epsilon_{\mathbf{k}+\mathbf{Q}})^2} \Sigma(\mathbf{k}, \epsilon_{\mathbf{k}}) \Bigg\} + \{\uparrow \leftrightarrow \downarrow\} \Bigg)
$$

$$
- \frac{g^4}{4} \sum_{\mathbf{k},\mathbf{q}} \Bigg(\Bigg\{ \overline{D}_{\mathbf{k}+\mathbf{q}-\frac{\mathbf{Q}}{2}} \frac{f^{\uparrow}_{\mathbf{k}+\mathbf{q}-\mathbf{Q}} - f^{\uparrow}_{\mathbf{k}+\mathbf{q}}}{\epsilon_{\mathbf{k}+\mathbf{q}-\mathbf{Q}} - \epsilon_{\mathbf{k}+\mathbf{q}}} D_{\mathbf{k}-\frac{\mathbf{Q}}{2}} \frac{f^{\uparrow}_{\mathbf{k}-\mathbf{Q}} - f^{\uparrow}_{\mathbf{k}}}{\epsilon_{\mathbf{k}-\mathbf{Q}} - \epsilon_{\mathbf{k}}} \chi^{\downarrow\downarrow}_{AF}(\mathbf{q}, \epsilon^{\uparrow}_{\mathbf{k}} - \epsilon^{\uparrow}_{\mathbf{k}+\mathbf{q}}) \Bigg\} + \{\uparrow \leftrightarrow \downarrow\} \Bigg)
$$

$$
+ \frac{g^4}{2} \sum_{\mathbf{k},\mathbf{p}} \overline{D}_{\mathbf{k}+\frac{\mathbf{Q}}{2}} \frac{f^{\uparrow}_{\mathbf{k}} - f^{\uparrow}_{\mathbf{k}+\mathbf{Q}}}{\epsilon_{\mathbf{k}} - \epsilon_{\mathbf{k}+\mathbf{Q}}} D_{\mathbf{p}-\frac{\mathbf{Q}}{2}} \frac{f^{\downarrow}_{\mathbf{p}-\mathbf{Q}} - f^{\downarrow}_{\mathbf{p}}}{\epsilon_{\mathbf{p}-\mathbf{Q}} - \epsilon_{\mathbf{p}}} \chi^{\uparrow\downarrow}_{SC}(\mathbf{p}+\mathbf{k}, \epsilon^{\uparrow}_{\mathbf{k}} + \epsilon^{\downarrow}_{\mathbf{p}})
$$

$$
+ \frac{g^4}{2} \sum_{\mathbf{k},\mathbf{p},\mathbf{q}} \overline{D}_{\mathbf{k}+\frac{\mathbf{Q}}{2}} \frac{f^{\uparrow}_{\mathbf{k}} - f^{\uparrow}_{\mathbf{k}+\mathbf{Q}}}{\epsilon_{\mathbf{k}} - \epsilon_{\mathbf{k}+\mathbf{Q}}} D_{\mathbf{p}-\mathbf{q}+\frac{\mathbf{Q}}{2}} \frac{f^{\downarrow}_{\mathbf{p}-\mathbf{q}} - f^{\downarrow}_{\mathbf{p}-\mathbf{q}+\mathbf{Q}}}{\epsilon_{\mathbf{p}-\mathbf{q}} - \epsilon_{\mathbf{p}-\mathbf{q}+\mathbf{Q}}} \frac{f^{\downarrow}_{\mathbf{p}} - f^{\uparrow}_{\mathbf{k}+\mathbf{q}}}{\epsilon^{\uparrow}_{\mathbf{k}+\mathbf{q}} + \epsilon^{\downarrow}_{\mathbf{p}-\mathbf{q}} - \epsilon^{\uparrow}_{\mathbf{k}} - \epsilon^{\downarrow}_{\mathbf{p}}}, \qquad (5.34)
$$

The last term requires further manipulation before one may identify its character.

The diagrams corresponding to the spin susceptibility and electron self-energy are given by

$$\chi_{AF}^{\downarrow\downarrow}(\mathbf{q}, \epsilon_{\mathbf{k}}^{\uparrow} - \epsilon_{\mathbf{k}+\mathbf{q}}^{\uparrow}) \quad = \quad \tag{5.35}$$

$$\chi_{SC}^{\uparrow\downarrow}(\mathbf{p} + \mathbf{k}, \epsilon_{\mathbf{k}}^{\uparrow} + \epsilon_{\mathbf{p}}^{\downarrow}) \quad = \quad \tag{5.36}$$

$$\Sigma(\mathbf{k}, \epsilon_{\mathbf{k}}) \quad = \quad \tag{5.37}$$

The self-energy-like term may be integrated by parts while assuming a constant density of states at the Fermi energy. This allows us to rewrite this term with an

energy derivative on the self-energy factor as follows:

$$
\begin{aligned}
\mathcal{F}_{fluct}(D) = \\
-\frac{g^4}{4}\sum_{\mathbf{k},\mathbf{q}} &\left(\left\{ \overline{D}_{\mathbf{k}+\mathbf{q}-\frac{\mathbf{Q}}{2}} \frac{f^{\uparrow}_{\mathbf{k}+\mathbf{q}-\mathbf{Q}}-f^{\uparrow}_{\mathbf{k}+\mathbf{q}}}{\epsilon_{\mathbf{k}+\mathbf{q}-\mathbf{Q}}-\epsilon_{\mathbf{k}+\mathbf{q}}} D_{\mathbf{k}-\frac{\mathbf{Q}}{2}} \frac{f^{\uparrow}_{\mathbf{k}-\mathbf{Q}}-f^{\uparrow}_{\mathbf{k}}}{\epsilon_{\mathbf{k}-\mathbf{Q}}-\epsilon_{\mathbf{k}}} \chi^{\downarrow\downarrow}_{AF}(\mathbf{q},\epsilon^{\uparrow}_{\mathbf{k}}-\epsilon^{\uparrow}_{\mathbf{k}+\mathbf{q}}) \right\} + \{\uparrow\leftrightarrow\downarrow\} \right) \\
+\frac{g^4}{2}\sum_{\mathbf{k},\mathbf{p}} &\overline{D}_{\mathbf{k}+\frac{\mathbf{Q}}{2}} \frac{f^{\uparrow}_{\mathbf{k}}-f^{\uparrow}_{\mathbf{k}+\mathbf{Q}}}{\epsilon_{\mathbf{k}}-\epsilon_{\mathbf{k}+\mathbf{Q}}} D_{\mathbf{p}-\frac{\mathbf{Q}}{2}} \frac{f^{\downarrow}_{\mathbf{p}-\mathbf{Q}}-f^{\downarrow}_{\mathbf{p}}}{\epsilon_{\mathbf{p}-\mathbf{Q}}-\epsilon_{\mathbf{p}}} \chi^{\uparrow\downarrow}_{SC}(\mathbf{p}+\mathbf{k},\epsilon^{\uparrow}_{\mathbf{k}}+\epsilon^{\downarrow}_{\mathbf{p}}) \\
-\frac{g^4}{2}\sum_{\mathbf{k}} &\left(\left\{ 2|D_{\mathbf{k}+\frac{\mathbf{Q}}{2}}|^2 \frac{f^{\uparrow}_{\mathbf{k}}-f^{\uparrow}_{\mathbf{k}+\mathbf{Q}}}{\epsilon_{\mathbf{k}}-\epsilon_{\mathbf{k}+\mathbf{Q}}} \partial_{\epsilon_{\mathbf{k}}}\Sigma(\mathbf{k},\epsilon_{\mathbf{k}}) \right\} + \{\uparrow\leftrightarrow\downarrow\} \right) \\
+\frac{g^4}{2}\sum_{\mathbf{k},\mathbf{p},\mathbf{q}} &\overline{D}_{\mathbf{k}+\frac{\mathbf{Q}}{2}} \frac{f^{\uparrow}_{\mathbf{k}}-f^{\uparrow}_{\mathbf{k}+\mathbf{Q}}}{\epsilon_{\mathbf{k}}-\epsilon_{\mathbf{k}+\mathbf{Q}}} D_{\mathbf{p}-\mathbf{q}+\frac{\mathbf{Q}}{2}} \frac{f^{\downarrow}_{\mathbf{p}-\mathbf{q}}-f^{\downarrow}_{\mathbf{p}-\mathbf{q}+\mathbf{Q}}}{\epsilon_{\mathbf{p}-\mathbf{q}}-\epsilon_{\mathbf{p}-\mathbf{q}+\mathbf{Q}}} \frac{f^{\downarrow}_{\mathbf{p}}-f^{\uparrow}_{\mathbf{k}+\mathbf{q}}}{\epsilon^{\uparrow}_{\mathbf{k}+\mathbf{q}}+\epsilon^{\downarrow}_{\mathbf{p}-\mathbf{q}}-\epsilon^{\uparrow}_{\mathbf{k}}-\epsilon^{\downarrow}_{\mathbf{p}}}
\end{aligned}
\tag{5.38}
$$

The diagrams corresponding to these fluctuation corrections to the free energy are

$$
-\frac{g^4}{4}\sum_{\mathbf{k},\mathbf{q}} \overline{D}_{\mathbf{k}+\mathbf{q}-\frac{\mathbf{Q}}{2}} \frac{f^{\uparrow}_{\mathbf{k}+\mathbf{q}-\mathbf{Q}}-f^{\uparrow}_{\mathbf{k}+\mathbf{q}}}{\epsilon_{\mathbf{k}+\mathbf{q}-\mathbf{Q}}-\epsilon_{\mathbf{k}+\mathbf{q}}} D_{\mathbf{k}-\frac{\mathbf{Q}}{2}} \frac{f^{\uparrow}_{\mathbf{k}-\mathbf{Q}}-f^{\uparrow}_{\mathbf{k}}}{\epsilon_{\mathbf{k}-\mathbf{Q}}-\epsilon_{\mathbf{k}}} \chi^{\downarrow\downarrow}_{AF}(\mathbf{q},\epsilon^{\uparrow}_{\mathbf{k}}-\epsilon^{\uparrow}_{\mathbf{k}+\mathbf{q}})
$$

$$
= \tag{5.39}
$$

$$
\frac{g^4}{2}\sum_{\mathbf{k},\mathbf{p}} \overline{D}_{\mathbf{k}+\frac{\mathbf{Q}}{2}} \frac{f^{\uparrow}_{\mathbf{k}}-f^{\uparrow}_{\mathbf{k}+\mathbf{Q}}}{\epsilon_{\mathbf{k}}-\epsilon_{\mathbf{k}+\mathbf{Q}}} D_{\mathbf{p}-\frac{\mathbf{Q}}{2}} \frac{f^{\downarrow}_{\mathbf{p}-\mathbf{Q}}-f^{\downarrow}_{\mathbf{p}}}{\epsilon_{\mathbf{p}-\mathbf{Q}}-\epsilon_{\mathbf{p}}} \chi^{\uparrow\downarrow}_{SC}(\mathbf{p}+\mathbf{k},\epsilon^{\uparrow}_{\mathbf{k}}+\epsilon^{\downarrow}_{\mathbf{p}})
$$

$$
= \tag{5.40}
$$

$$g^2 \sum_{\mathbf{k}} |D_{\mathbf{k}+\frac{\mathbf{Q}}{2}}|^2 \frac{f_{\mathbf{k}}^{\uparrow} - f_{\mathbf{k}+\mathbf{Q}}^{\uparrow}}{(\epsilon_{\mathbf{k}} - \epsilon_{\mathbf{k}+\mathbf{Q}})^2} \Sigma(\mathbf{k}, \epsilon_{\mathbf{k}})$$

$$= \qquad\qquad\qquad\qquad\qquad\qquad (5.41)$$

$$\frac{g^4}{2} \sum_{\mathbf{k},\mathbf{p},\mathbf{q}} \overline{D}_{\mathbf{k}+\frac{\mathbf{Q}}{2}} \frac{f_{\mathbf{k}}^{\uparrow} - f_{\mathbf{k}+\mathbf{Q}}^{\uparrow}}{\epsilon_{\mathbf{k}} - \epsilon_{\mathbf{k}+\mathbf{Q}}} D_{\mathbf{p}-\mathbf{q}+\frac{\mathbf{Q}}{2}} \frac{f_{\mathbf{p}-\mathbf{q}}^{\downarrow} - f_{\mathbf{p}-\mathbf{q}+\mathbf{Q}}^{\downarrow}}{\epsilon_{\mathbf{p}-\mathbf{q}} - \epsilon_{\mathbf{p}-\mathbf{q}+\mathbf{Q}}} \frac{f_{\mathbf{p}}^{\downarrow} - f_{\mathbf{k}+\mathbf{q}}^{\uparrow}}{\epsilon_{\mathbf{k}+\mathbf{q}}^{\uparrow} + \epsilon_{\mathbf{p}-\mathbf{q}}^{\downarrow} - \epsilon_{\mathbf{k}}^{\uparrow} - \epsilon_{\mathbf{p}}^{\downarrow}}$$

$$=$$

In fact, using these diagrams makes it easier to identify a re-labeling of momenta. In the final diagram above we may rename dummy momentum labels such that

$$= \qquad\qquad\qquad\qquad\qquad , \qquad (5.42)$$

$$= \frac{g^4}{2} \sum_{\mathbf{k},\mathbf{p},\mathbf{q}} \overline{D}_{\mathbf{k}+\frac{\mathbf{Q}}{2}} \frac{f_{\mathbf{k}}^{\uparrow} - f_{\mathbf{k}+\mathbf{Q}}^{\uparrow}}{\epsilon_{\mathbf{k}} - \epsilon_{\mathbf{k}+\mathbf{Q}}} D_{\mathbf{k}+\mathbf{q}+\frac{\mathbf{Q}}{2}} \frac{f_{\mathbf{k}+\mathbf{q}}^{\downarrow} - f_{\mathbf{k}+\mathbf{q}+\mathbf{Q}}^{\downarrow}}{\epsilon_{\mathbf{k}+\mathbf{q}} - \epsilon_{\mathbf{k}+\mathbf{q}+\mathbf{Q}}} \frac{f_{\mathbf{p}}^{\downarrow} - f_{\mathbf{p}-\mathbf{q}}^{\uparrow}}{\epsilon_{\mathbf{p}-\mathbf{q}}^{\uparrow} + \epsilon_{\mathbf{k}+\mathbf{q}}^{\downarrow} - \epsilon_{\mathbf{k}}^{\uparrow} - \epsilon_{\mathbf{p}}^{\downarrow}}. \qquad (5.43)$$

A further simplification follows from the identification

$$\chi_{AF}^{\downarrow\uparrow}(\mathbf{q}, \epsilon_{\mathbf{k}}^{\uparrow} - \epsilon_{\mathbf{k}+\mathbf{q}}^{\downarrow}) = \sum_{\mathbf{p}} \frac{f_{\mathbf{p}-\mathbf{q}}^{\uparrow} - f_{\mathbf{p}}^{\downarrow}}{\epsilon_{\mathbf{k}+\mathbf{q}}^{\downarrow} + \epsilon_{\mathbf{p}-\mathbf{q}}^{\uparrow} - \epsilon_{\mathbf{k}}^{\uparrow} - \epsilon_{\mathbf{p}}^{\downarrow}}. \qquad (5.44)$$

Using the above definition, we write the formal expression of the free energy of the

bond density wave as

$$
\begin{aligned}
\mathcal{F}(D) \;=\; & \mathcal{F}_{MF} + \mathcal{F}_{fluct} = \\
& -T \sum_{\mathbf{k},\sigma} \ln\left(e^{-\frac{\xi_{\mathbf{k},\sigma}-\mu}{T}}+1\right) + g^2 \sum_{\mathbf{k},\sigma} |D_{\mathbf{k}}|^2 \frac{f_{\mathbf{k}-\frac{\mathbf{Q}}{2}} - f_{\mathbf{k}+\frac{\mathbf{Q}}{2}}}{\epsilon_{\mathbf{k}-\frac{\mathbf{Q}}{2}} - \epsilon_{\mathbf{k}+\frac{\mathbf{Q}}{2}}} \\
& + \left\{ \frac{g^4}{4} \sum_{\mathbf{k},\mathbf{q}} -\overline{D}_{\mathbf{k}+\mathbf{q}-\frac{\mathbf{Q}}{2}} \frac{f^{\uparrow}_{\mathbf{k}+\mathbf{q}-\mathbf{Q}} - f^{\uparrow}_{\mathbf{k}+\mathbf{q}}}{\epsilon_{\mathbf{k}+\mathbf{q}-\mathbf{Q}} - \epsilon_{\mathbf{k}+\mathbf{q}}} D_{\mathbf{k}-\frac{\mathbf{Q}}{2}} \frac{f^{\uparrow}_{\mathbf{k}-\mathbf{Q}} - f^{\uparrow}_{\mathbf{k}}}{\epsilon_{\mathbf{k}-\mathbf{Q}} - \epsilon_{\mathbf{k}}} \; \chi^{\downarrow\downarrow}_{AF}(\mathbf{q}, \epsilon^{\uparrow}_{\mathbf{k}} - \epsilon^{\uparrow}_{\mathbf{k}+\mathbf{q}}) \right. \\
& + \frac{g^4}{4} \sum_{\mathbf{k},\mathbf{q}} -\overline{D}_{\mathbf{k}+\mathbf{q}-\frac{\mathbf{Q}}{2}} \frac{f^{\uparrow}_{\mathbf{k}+\mathbf{q}-\mathbf{Q}} - f^{\uparrow}_{\mathbf{k}+\mathbf{q}}}{\epsilon_{\mathbf{k}+\mathbf{q}-\mathbf{Q}} - \epsilon_{\mathbf{k}+\mathbf{q}}} D_{\mathbf{k}-\frac{\mathbf{Q}}{2}} \frac{f^{\downarrow}_{\mathbf{k}-\mathbf{Q}} - f^{\downarrow}_{\mathbf{k}}}{\epsilon_{\mathbf{k}-\mathbf{Q}} - \epsilon_{\mathbf{k}}} \; \chi^{\downarrow\uparrow}_{AF}(\mathbf{q}, \epsilon^{\uparrow}_{\mathbf{k}} - \epsilon^{\downarrow}_{\mathbf{k}+\mathbf{q}}) \\
& + \frac{g^4}{4} \sum_{\mathbf{k},\mathbf{p}} \overline{D}_{\mathbf{k}+\frac{\mathbf{Q}}{2}} \frac{f^{\uparrow}_{\mathbf{k}} - f^{\uparrow}_{\mathbf{k}+\mathbf{Q}}}{\epsilon_{\mathbf{k}} - \epsilon_{\mathbf{k}+\mathbf{Q}}} D_{\mathbf{p}-\frac{\mathbf{Q}}{2}} \frac{f^{\downarrow}_{\mathbf{p}-\mathbf{Q}} - f^{\downarrow}_{\mathbf{p}}}{\epsilon_{\mathbf{p}-\mathbf{Q}} - \epsilon_{\mathbf{p}}} \; \chi^{\uparrow\downarrow}_{SC}(\mathbf{p}+\mathbf{k}, \epsilon^{\uparrow}_{\mathbf{k}} + \epsilon^{\downarrow}_{\mathbf{p}}) \\
& \left. -g^2 \sum_{\mathbf{k}} |D_{\mathbf{k}+\frac{\mathbf{Q}}{2}}|^2 \frac{f^{\uparrow}_{\mathbf{k}-\mathbf{Q}} - f^{\uparrow}_{\mathbf{k}}}{\epsilon_{\mathbf{k}-\mathbf{Q}} - \epsilon_{\mathbf{k}}} \partial_{\epsilon_{\mathbf{k}}}\Sigma(\mathbf{k}, \epsilon_{\mathbf{k}}) \right\} + \{\uparrow\leftrightarrow\downarrow\}.
\end{aligned}
\tag{5.45}
$$

Note, that the term including the superconducting susceptibility $\chi^{\uparrow\downarrow}_{SC}$ is sub-leading compared to the terms that feature antiferromagnetic susceptibilities - $\chi^{\uparrow\uparrow}_{AF}$ and $\chi^{\uparrow\downarrow}_{AF}$. In fact $\chi^{\uparrow\downarrow}_{SC}$ is suppressed exponentially for finite momentum and hence the integration over this momentum results in a negligible contribution [70]. We will therefore neglect this term.

5.2.3 Regularising the interaction

The Hamiltonian, equation (5.1), harbours an unphysical, singular contribution to the free energy. This is revealed by following the usual renormalisation procedure of writing the free energy in terms of physically observable renormalised quantities. We carry out this renormalisation to first order by making the following shift in the definition of the two particle eigenstates [27]:

$$
|\mathbf{k}\uparrow, \mathbf{l}\downarrow\rangle \;=\; |\mathbf{k}\uparrow, \mathbf{l}\downarrow\rangle_0 + \sum_{\mathbf{p}\neq\mathbf{k},\mathbf{q}\neq\mathbf{l}} \frac{{}_0\langle\mathbf{p}\uparrow,\mathbf{q}\downarrow|\mathcal{H}^{\mathrm{int}}|\mathbf{k}\uparrow,\mathbf{l}\downarrow\rangle_0}{\epsilon^{+}_{\mathbf{k}} + \epsilon^{-}_{\mathbf{l}} - \epsilon^{+}_{\mathbf{p}} - \epsilon^{-}_{\mathbf{q}}} |\mathbf{p}\uparrow,\mathbf{q}\downarrow\rangle_0, \tag{5.46}
$$

where $|\mathbf{k}\uparrow, \mathbf{l}\downarrow\rangle_0$ labels the bare two-particle electron state, and $|\mathbf{k}\uparrow, \mathbf{l}\downarrow\rangle$ the *two-particle state corrected to first order in the interaction g*. $\epsilon^{\sigma}_{\mathbf{k}}$ are taken self-consistently to be the mean-field electron dispersions and $\mathcal{H}^{\mathrm{int}}$ represents the inter-

action Hamiltonian. With this identification, we must also make a corresponding alteration to the matrix element g,

$$g_{\mathbf{k}_1,\mathbf{k}_2} \rightarrow g - 2g^2 {\sum_{\mathbf{k}_3,\mathbf{k}_4}}' \frac{1}{\epsilon^+_{\mathbf{k}_1} + \epsilon^-_{\mathbf{k}_2} - \epsilon^+_{\mathbf{k}_3} - \epsilon^-_{\mathbf{k}_4}}. \tag{5.47}$$

This leads to a corresponding correction to the free energy

$$\delta\mathcal{F}_{\text{fluct}} = 2g^2_{eff} {\sum_{\mathbf{k}_1\ldots\mathbf{k}_4}}' \frac{\langle c^\dagger_{\mathbf{k}_1,\uparrow} c_{\mathbf{k}_1,\uparrow} c^\dagger_{\mathbf{k}_2,\downarrow} c_{\mathbf{k}_2,\downarrow}\rangle}{\epsilon^+_{\mathbf{k}_1} + \epsilon^-_{\mathbf{k}_2} - \epsilon^+_{\mathbf{k}_3} - \epsilon^-_{\mathbf{k}_4}}, \tag{5.48}$$

Following the variational Ansatz, we may then calculate an additional $|D|^2$ contribution to the free energy by transforming the operators in equation (5.48) to the diagonal basis. This is done analogously to the derivation of the fluctuation corrections to the free energy above;

$$\delta\mathcal{F}(D) = 2g^4 \sum_{\mathbf{k},\mathbf{p},\mathbf{q}} \left\{ |D_{\mathbf{k}+\frac{\mathbf{Q}}{2}}|^2 \frac{f^\uparrow_{\mathbf{k}} - f^\uparrow_{\mathbf{k}+\mathbf{Q}}}{\left(\epsilon^\uparrow_{\mathbf{k}} - \epsilon^\uparrow_{\mathbf{k}+\mathbf{Q}}\right)^2} \frac{f^\downarrow_{\mathbf{p}}}{\epsilon^\uparrow_{\mathbf{k}+\mathbf{p}} + \epsilon^\downarrow_{\mathbf{q}-\mathbf{p}} - \epsilon^\uparrow_{\mathbf{k}} - \epsilon^\downarrow_{\mathbf{q}}} + \uparrow\leftrightarrow\downarrow \right\}. \tag{5.49}$$

As expected, these terms give an additional contribution to the wavefunction renormalization - the shift to the effective coupling g_{eff} is simply a wavefunction regularization. We include the regularisation by redefining the self energy, $\Sigma \rightarrow \Sigma'$.

The resulting free energy, upon which we will base our subsequent calculations, is given by

$$\begin{aligned}
\mathcal{F}(D) &= -T\sum_{\mathbf{k},\sigma} \ln\left(e^{-\frac{\xi_{\mathbf{k},\sigma}-\mu}{T}} + 1\right) + g^2 \sum_{\mathbf{k},\sigma} |D_{\mathbf{k}}|^2 \frac{f_{\mathbf{k}-\frac{\mathbf{Q}}{2}} - f_{\mathbf{k}+\frac{\mathbf{Q}}{2}}}{\epsilon_{\mathbf{k}-\frac{\mathbf{Q}}{2}} - \epsilon_{\mathbf{k}+\frac{\mathbf{Q}}{2}}} \\
&+ \left\{ \frac{g^4}{4}\sum_{\mathbf{k},\mathbf{q}} -\overline{D}_{\mathbf{k}+\mathbf{q}-\frac{\mathbf{Q}}{2}} \frac{f^\uparrow_{\mathbf{k}+\mathbf{q}-\mathbf{Q}} - f^\uparrow_{\mathbf{k}+\mathbf{q}}}{\epsilon_{\mathbf{k}+\mathbf{q}-\mathbf{Q}} - \epsilon_{\mathbf{k}+\mathbf{q}}} D_{\mathbf{k}-\frac{\mathbf{Q}}{2}} \frac{f^\uparrow_{\mathbf{k}-\mathbf{Q}} - f^\uparrow_{\mathbf{k}}}{\epsilon_{\mathbf{k}-\mathbf{Q}} - \epsilon_{\mathbf{k}}} \chi^{\downarrow\downarrow}_{AF}(\mathbf{q}, \epsilon^\uparrow_{\mathbf{k}} - \epsilon^\uparrow_{\mathbf{k}+\mathbf{q}}) \right. \\
&+ \frac{g^4}{4}\sum_{\mathbf{k},\mathbf{q}} -\overline{D}_{\mathbf{k}+\mathbf{q}-\frac{\mathbf{Q}}{2}} \frac{f^\uparrow_{\mathbf{k}+\mathbf{q}-\mathbf{Q}} - f^\uparrow_{\mathbf{k}+\mathbf{q}}}{\epsilon_{\mathbf{k}+\mathbf{q}-\mathbf{Q}} - \epsilon_{\mathbf{k}+\mathbf{q}}} D_{\mathbf{k}-\frac{\mathbf{Q}}{2}} \frac{f^\downarrow_{\mathbf{k}-\mathbf{Q}} - f^\downarrow_{\mathbf{k}}}{\epsilon_{\mathbf{k}-\mathbf{Q}} - \epsilon_{\mathbf{k}}} \chi^{\downarrow\uparrow}_{AF}(\mathbf{q}, \epsilon^\uparrow_{\mathbf{k}} - \epsilon^\downarrow_{\mathbf{k}+\mathbf{q}}) \\
&\left. - g^2\sum_{\mathbf{k}} |D_{\mathbf{k}+\frac{\mathbf{Q}}{2}}|^2 \frac{f^\uparrow_{\mathbf{k}-\mathbf{Q}} - f^\uparrow_{\mathbf{k}}}{\epsilon_{\mathbf{k}-\mathbf{Q}} - \epsilon_{\mathbf{k}}} \partial_{\epsilon_{\mathbf{k}}} \Sigma'(\mathbf{k}, \epsilon_{\mathbf{k}}) \right\} + \{\uparrow\leftrightarrow\downarrow\}.
\end{aligned} \tag{5.50}$$

5.3   *Saddle point equation of bond density wave order*

We may now find the formal expression of the Eliashberg-equation. From the free energy of the bond density wave - equation (5.50) - we set $\partial_{D_{\mathbf{k}+\frac{\mathbf{Q}}{2}}} \mathcal{F}(D) = 0$ and rearrange to find the saddle point equation;

$$\bar{D}_{\mathbf{k}+\frac{\mathbf{Q}}{2}} \left(1 + \Sigma'(\mathbf{k}, \epsilon_{\mathbf{k}})\right) = g^2 \sum_{\mathbf{q}} -\bar{D}_{\mathbf{k}+\mathbf{q}+\frac{\mathbf{Q}}{2}} \left[\frac{f^{\uparrow}_{\mathbf{k}+\mathbf{q}} - f^{\uparrow}_{\mathbf{k}+\mathbf{q}+\mathbf{Q}}}{\epsilon^{\uparrow}_{\mathbf{k}+\mathbf{q}} - \epsilon^{\uparrow}_{\mathbf{k}+\mathbf{q}+\mathbf{Q}}} \chi^{\uparrow\uparrow}_{AF}(\mathbf{q}, \epsilon^{\uparrow}_{\mathbf{k}} - \epsilon^{\uparrow}_{\mathbf{k}+\mathbf{q}}) \right.$$
$$\left. + \frac{f^{\downarrow}_{\mathbf{k}+\mathbf{q}} - f^{\downarrow}_{\mathbf{k}+\mathbf{q}+\mathbf{Q}}}{\epsilon^{\downarrow}_{\mathbf{k}+\mathbf{q}} - \epsilon^{\downarrow}_{\mathbf{k}+\mathbf{q}+\mathbf{Q}}} \chi^{\uparrow\downarrow}_{AF}(\mathbf{q}, \epsilon^{\uparrow}_{\mathbf{k}} - \epsilon^{\downarrow}_{\mathbf{k}+\mathbf{q}}) \right] \quad (5.51)$$

5.4   *Evaluation of the free energy of bond density wave order*

Having derived the formal expression of the free energy of bond density wave order, we now would like to evaluate these integrals.

5.4.1   Overview of the calculation

Before diving into the detail of the integration we would like to discuss the assumptions and approximations used repeatedly to simplify our task. They amount to assuming that all relevant physics happens near to the Fermi surface.

We are interested in the low temperature phase diagram of the Hubbard model close to half filling. We therefore assume that temperature is lower than the chemical potential, which in turn is smaller than the band width: $T \ll |\mu| \ll t$.

Additionally, we note that the mean field free energy and fluctuation corrections share common factors of the form

$$\frac{f^{\sigma}_{\mathbf{k}} - f^{\sigma}_{\mathbf{k}+\mathbf{Q}}}{\xi^{\sigma}_{\mathbf{k}} - \xi^{\sigma}_{\mathbf{k}+\mathbf{Q}}}. \quad (5.52)$$

These terms correspond to the susceptibility to bond density wave order. They

are dominated by a bond density wave vector of $\mathbf{Q} = (\pi, \pi)$ - identical to the antiferromagnet. Since $\epsilon^\sigma_{\mathbf{k}+(\pi,\pi)} = -\epsilon^\sigma_{\mathbf{k}}$, we may simplify these terms to:

$$\frac{f^\sigma_{\mathbf{k}} - f^\sigma_{\mathbf{k}+\mathbf{Q}}}{\xi^\sigma_{\mathbf{k}} - \xi^\sigma_{\mathbf{k}+\mathbf{Q}}} = \frac{f(\epsilon^\sigma_{\mathbf{k}} - \mu) - f(-\epsilon^\sigma_{\mathbf{k}} - \mu)}{2\epsilon^\sigma_{\mathbf{k}}} \tag{5.53}$$
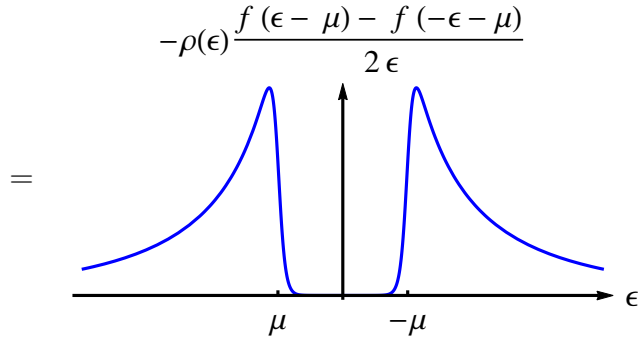
These factors are dominated by peaks at $\epsilon^\sigma_{\mathbf{k}} = \pm\mu$, whose width is set by temperature. In the limit of $\mu \to 0$ these peaks merge and the susceptibility to d-wave bond density order is the same as that to d-wave superconductivity. This was first pointed out by Sachdev and Metlitski [71]. For temperatures larger than the Fermi energy these two peaks merge into a single peak situated at half filling. However, for finite chemical potential and temperature smaller than this energy scale, the peaks are distinct and may be used to constrict the integrations to the vicinity of the Fermi surface. Hence, we may treat such factors as weighted delta functions, while keeping in mind that their neglected temperature dependence might be of use in cutting off divergences;

$$\frac{f^\sigma_{\mathbf{k}} - f^\sigma_{\mathbf{k}+\mathbf{Q}}}{\xi^\sigma_{\mathbf{k}} - \xi^\sigma_{\mathbf{k}+\mathbf{Q}}} \approx \frac{\delta(|\epsilon^\sigma_{\mathbf{k}}| - \mu)}{\rho(\mu)} \int_{\mu+T}^{4t} d\epsilon \frac{\rho(\epsilon)}{\epsilon} \tag{5.54}$$

such that

$$\boxed{\frac{f^\sigma_{\mathbf{k}} - f^\sigma_{\mathbf{k}+\mathbf{Q}}}{\xi^\sigma_{\mathbf{k}} - \xi^\sigma_{\mathbf{k}+\mathbf{Q}}} \approx \delta(|\epsilon^\sigma_{\mathbf{k}}| - \mu) \log\left(\frac{|\mu - T|}{4t}\right)} \ , \tag{5.55}$$

where we inserted the density of states, $\rho(\epsilon) = \frac{-1}{2\pi^2 t} \log\left(\frac{|\epsilon|}{4t}\right)$.

For convenience we split the free energy into various parts that we calculate sep-

arately. The free energy as derived in Sections 5.1 and 5.2 separated into parts is

$$\mathcal{F}(D) = \mathcal{F}_{MF} + \underbrace{\delta\mathcal{F}_{\chi_{AF}^{\downarrow\downarrow}} + \delta\mathcal{F}_{\chi_{AF}^{\downarrow\uparrow}} + \delta\mathcal{F}_{\Sigma}}_{\mathcal{F}_{fluct}}, \tag{5.56}$$

with

$$\mathcal{F}_{MF} = -T\sum_{\mathbf{k},\sigma} \ln\left(e^{-\frac{\xi_{\mathbf{k},\sigma}-\mu}{T}} + 1\right) + g^2 \sum_{\mathbf{k},\sigma} |D_{\mathbf{k}}|^2 \frac{f_{\mathbf{k}-\frac{\mathbf{Q}}{2}} - f_{\mathbf{k}+\frac{\mathbf{Q}}{2}}}{\epsilon_{\mathbf{k}-\frac{\mathbf{Q}}{2}} - \epsilon_{\mathbf{k}+\frac{\mathbf{Q}}{2}}}$$

$$\delta\mathcal{F}_{\chi_{AF}^{\downarrow\downarrow}} = \frac{g^4}{4} \sum_{\mathbf{k},\mathbf{q}} \left(\left\{ -\overline{D}_{\mathbf{k}+\mathbf{q}-\frac{\mathbf{Q}}{2}} \frac{f_{\mathbf{k}+\mathbf{q}-\mathbf{Q}}^{\uparrow} - f_{\mathbf{k}+\mathbf{q}}^{\uparrow}}{\epsilon_{\mathbf{k}+\mathbf{q}-\mathbf{Q}} - \epsilon_{\mathbf{k}+\mathbf{q}}} D_{\mathbf{k}-\frac{\mathbf{Q}}{2}} \frac{f_{\mathbf{k}-\mathbf{Q}}^{\uparrow} - f_{\mathbf{k}}^{\uparrow}}{\epsilon_{\mathbf{k}-\mathbf{Q}} - \epsilon_{\mathbf{k}}} \; \chi_{AF}^{\downarrow\downarrow}(\mathbf{q}, \epsilon_{\mathbf{k}}^{\uparrow} - \epsilon_{\mathbf{k}+\mathbf{q}}^{\uparrow}) \right\} \right.$$

$$\left. + \{\uparrow\leftrightarrow\downarrow\} \right)$$

$$\delta\mathcal{F}_{\chi_{AF}^{\downarrow\uparrow}} = \frac{g^4}{4} \sum_{\mathbf{k},\mathbf{q}} \left(\left\{ -\overline{D}_{\mathbf{k}+\mathbf{q}-\frac{\mathbf{Q}}{2}} \frac{f_{\mathbf{k}+\mathbf{q}-\mathbf{Q}}^{\uparrow} - f_{\mathbf{k}+\mathbf{q}}^{\uparrow}}{\epsilon_{\mathbf{k}+\mathbf{q}-\mathbf{Q}} - \epsilon_{\mathbf{k}+\mathbf{q}}} D_{\mathbf{k}-\frac{\mathbf{Q}}{2}} \frac{f_{\mathbf{k}-\mathbf{Q}}^{\downarrow} - f_{\mathbf{k}}^{\downarrow}}{\epsilon_{\mathbf{k}-\mathbf{Q}} - \epsilon_{\mathbf{k}}} \; \chi_{AF}^{\downarrow\uparrow}(\mathbf{q}, \epsilon_{\mathbf{k}}^{\uparrow} - \epsilon_{\mathbf{k}+\mathbf{q}}^{\downarrow}) \right\} \right.$$

$$\left. + \{\uparrow\leftrightarrow\downarrow\} \right)$$

$$\delta\mathcal{F}_{\Sigma} = -g^2 \sum_{\mathbf{k}} \left(\left\{ |D_{\mathbf{k}+\frac{\mathbf{Q}}{2}}|^2 \frac{f_{\mathbf{k}-\mathbf{Q}}^{\uparrow} - f_{\mathbf{k}}^{\uparrow}}{\epsilon_{\mathbf{k}-\mathbf{Q}} - \epsilon_{\mathbf{k}}} \partial_{\epsilon_{\mathbf{k}}} \Sigma'(\mathbf{k}, \epsilon_{\mathbf{k}}) \right\} + \{\uparrow\leftrightarrow\downarrow\} \right). \tag{5.57}$$

We will first analyse the mean field and then the fluctuation contribution, which in turn will be treated term by term.

5.4.2   Evaluation of mean field contribution

The simplest term is the mean field free energy contribution,

$$\mathcal{F}_{MF}(D) \;=\; -T\sum_{\mathbf{k},\sigma} \ln\left(e^{-\frac{\xi_{\mathbf{k},\sigma}-\mu}{T}} + 1\right) + g^2 \sum_{\mathbf{k},\sigma} |D_{\mathbf{k}}|^2 \frac{f_{\mathbf{k}-\frac{\mathbf{Q}}{2}} - f_{\mathbf{k}+\frac{\mathbf{Q}}{2}}}{\epsilon_{\mathbf{k}-\frac{\mathbf{Q}}{2}} - \epsilon_{\mathbf{k}+\frac{\mathbf{Q}}{2}}}. \tag{5.58}$$

To quadratic order, using $D_{\mathbf{k}} = D\theta_{\mathbf{k}}$, this takes the form

$$\partial_{|D|^2}\mathcal{F}_{MF}(D)|_{D=0} = -g^2 \sum_{\mathbf{k},\sigma} |\theta_{\mathbf{k}}|^2 \frac{f_{\mathbf{k}-\frac{\mathbf{Q}}{2}} - f_{\mathbf{k}+\frac{\mathbf{Q}}{2}}}{\epsilon_{\mathbf{k}-\frac{\mathbf{Q}}{2}} - \epsilon_{\mathbf{k}+\frac{\mathbf{Q}}{2}}}. \tag{5.59}$$

In the limit of $\mathbf{Q} \to (\pi, \pi)$ and using the Fermi functions to restrict the range of integration over energy we find

$$\partial_{|D|^2} \mathcal{F}_{MF}(D) = -\frac{g^2}{2} \langle\langle \theta_{\mathbf{k}}^2 \rangle\rangle \rho(\mu - T) \log\left(\frac{|\mu - T|}{4t}\right), \tag{5.60}$$

where $\langle\langle \theta_{\mathbf{k}}^2 \rangle\rangle$ denotes the angular average around the Fermi surface of the d-wave factor squared.

This Landau coefficient is positive. Therefore we may conclude, that there is no mean field drive to a second order transition to bond density wave order.

5.4.3 Evaluation of the fluctuation contribution

Next, we will calculate the various fluctuation terms one by one.

Evaluation of the $\delta\mathcal{F}_{\chi_{AF}^{\uparrow\uparrow}}$ term

Let us start with the susceptibility like terms, in particular with the $\chi_{AF}^{\uparrow\uparrow}$ term:

$$\delta\mathcal{F}_{\chi_{AF}^{\uparrow\uparrow}} = -\frac{g^4}{4} \sum_{\mathbf{k},\mathbf{q}} \overline{D}_{\mathbf{k}+\mathbf{q}-\frac{\mathbf{Q}}{2}} \frac{f_{\mathbf{k}+\mathbf{q}-\mathbf{Q}}^{\uparrow} - f_{\mathbf{k}+\mathbf{q}}^{\uparrow}}{\epsilon_{\mathbf{k}+\mathbf{q}-\mathbf{Q}}^{\uparrow} - \epsilon_{\mathbf{k}+\mathbf{q}}^{\uparrow}} D_{\mathbf{k}-\frac{\mathbf{Q}}{2}} \frac{f_{\mathbf{k}-\mathbf{Q}}^{\uparrow} - f_{\mathbf{k}}^{\uparrow}}{\epsilon_{\mathbf{k}-\mathbf{Q}}^{\uparrow} - \epsilon_{\mathbf{k}}^{\uparrow}} \chi_{AF}^{\uparrow\uparrow}(\mathbf{q}, \epsilon_{\mathbf{k}}^{\uparrow} - \epsilon_{\mathbf{k}+\mathbf{q}}^{\uparrow}) \tag{5.61}$$

where

$$\chi_{AF}^{\uparrow\uparrow}(\mathbf{q}, \epsilon_{\mathbf{k}}^{\uparrow} - \epsilon_{\mathbf{k}+\mathbf{q}}^{\uparrow}) = \sum_{\mathbf{p}} \frac{f_{\mathbf{p}}^{\downarrow} - f_{\mathbf{p}-\mathbf{q}}^{\downarrow}}{\epsilon_{\mathbf{p}-\mathbf{q}}^{\downarrow} + \epsilon_{\mathbf{k}+\mathbf{q}}^{\uparrow} - \epsilon_{\mathbf{k}}^{\uparrow} - \epsilon_{\mathbf{p}}^{\downarrow}}. \tag{5.62}$$

Setting $\mathbf{Q} = (\pi, \pi)$, we use the bond density susceptibility factors to simplify this expression. Their delta-function-like nature places certain constraints onto the frequency and momentum of $\chi_{AF}^{\uparrow\uparrow}$. We note that they set $\epsilon_{\mathbf{k}}^{\uparrow} = \pm\mu$ and $\epsilon_{\mathbf{k}+\mathbf{q}}^{\uparrow} = \pm\mu$ and hence $\epsilon_{\mathbf{k}+\mathbf{q}}^{\uparrow} = \pm\epsilon_{\mathbf{k}}^{\uparrow}$. This therefore, restricts the supported momentum of $\chi_{AF}^{\uparrow\uparrow}$. In particular, they allow $\mathbf{q}$ to be either zero or (π, π) (or any symmetry related choice) and $\epsilon_{\mathbf{k}}^{\uparrow} - \epsilon_{\mathbf{k}+\mathbf{q}}^{\uparrow}$ is limited to zero or $\pm 2\mu$.

Numerical analysis of $\chi_{AF}^{\uparrow\uparrow}$ shows that it is largest in the vicinity of $\mathbf{q} = (\pi, \pi)$ and

$\epsilon_{\mathbf{k}}^{\uparrow} - \epsilon_{\mathbf{k+q}}^{\uparrow} = \pm 2\mu$. Combining these observations we may write

$$\delta\mathcal{F}_{\chi_{AF}^{\uparrow\uparrow}} = \frac{g^4}{2}\langle\langle|D_{\mathbf{k}}|^2\rangle\rangle\rho(\mu-T)^2\log^2\left(\frac{|\mu-T|}{4t}\right)\chi_{AF}^{\uparrow\uparrow}((\pi,\pi),2\mu), \qquad (5.63)$$

where we have used $D_{\mathbf{k}+(\pi,\pi)} = -D_{\mathbf{k}}$. The antiferromagnetic susceptibility may be evaluated close to its most divergent contribution;

$$\chi_{AF}^{\uparrow\uparrow}((\pi,\pi),2\mu) = \sum_{\epsilon}\rho(\epsilon)\frac{f(\epsilon-\mu)-f(-\epsilon-\mu)}{-2\epsilon-2\mu} \qquad (5.64)$$

$$= \int_{-\mu+T}^{4t}\frac{\rho(\mu-T)}{2(\epsilon+\mu)}d\epsilon \qquad (5.65)$$

$$= \frac{1}{2}\rho(\mu-T)\log\left(\frac{T}{4t}\right). \qquad (5.66)$$

Hence the $\chi_{AF}^{\uparrow\uparrow}$ term of the bond density wave fluctuation corrections takes the form:

$$\delta\mathcal{F}_{\chi_{AF}^{\uparrow\uparrow}} = \frac{g^4}{4}\langle\langle|D_{\mathbf{k}}|^2\rangle\rangle\rho(\mu-T)^3\log^2\left(\frac{|\mu-T|}{4t}\right)\log\left(\frac{T}{4t}\right) \qquad (5.67)$$

Evaluation of the $\delta\mathcal{F}_{\chi_{AF}^{\uparrow\downarrow}}$ term

Next, let us examine the $\chi_{AF}^{\uparrow\downarrow}$ -term.

$$\delta\mathcal{F}_{\chi_{AF}^{\uparrow\downarrow}} = -\frac{g^4}{2}\sum_{\mathbf{k,q}}\overline{D}_{\mathbf{k}+\frac{\mathbf{Q}}{2}}\frac{f_{\mathbf{k}}^{\uparrow}-f_{\mathbf{k+Q}}^{\uparrow}}{\epsilon_{\mathbf{k}}-\epsilon_{\mathbf{k+Q}}}D_{\mathbf{k+q}+\frac{\mathbf{Q}}{2}}\frac{f_{\mathbf{k+q}}^{\downarrow}-f_{\mathbf{k+q+Q}}^{\downarrow}}{\epsilon_{\mathbf{k+q}}-\epsilon_{\mathbf{k+q+Q}}}\chi_{AF}^{\uparrow\downarrow}(\mathbf{q},\epsilon_{\mathbf{k}}^{\uparrow}-\epsilon_{\mathbf{k+q}}^{\downarrow}), \quad (5.68)$$

where

$$\chi_{AF}^{\uparrow\downarrow}(\mathbf{q},\epsilon_{\mathbf{k}}^{\uparrow}-\epsilon_{\mathbf{k+q}}^{\downarrow}) = \sum_{\mathbf{p}}\frac{f_{\mathbf{p}}^{\downarrow}-f_{\mathbf{p-q}}^{\uparrow}}{\epsilon_{\mathbf{p-q}}^{\uparrow}+\epsilon_{\mathbf{k+q}}^{\downarrow}-\epsilon_{\mathbf{k}}^{\uparrow}-\epsilon_{\mathbf{p}}^{\downarrow}}. \qquad (5.69)$$

Bond density wave order preserves spin rotation symmetry. Since in the absence of spin symmetry breaking $\epsilon_{\mathbf{k}}^{\uparrow} = \epsilon_{\mathbf{k}}^{\downarrow}$, the $\delta\mathcal{F}_{\chi_{AF}^{\uparrow\downarrow}}$ term is equal to $\delta\mathcal{F}_{\chi_{AF}^{\uparrow\uparrow}}$.

Evaluation of the $\delta \mathcal{F}_\Sigma$ term

Lastly let us evaluate the self-energy-like term,

$$\delta \mathcal{F}_\Sigma = g^2 \sum_{\mathbf{k}} \left(\left\{ |D_{\mathbf{k}+\frac{\mathbf{Q}}{2}}|^2 \frac{f_{\mathbf{k}}^\uparrow - f_{\mathbf{k}+\mathbf{Q}}^\uparrow}{\epsilon_{\mathbf{k}} - \epsilon_{\mathbf{k}+\mathbf{Q}}} \partial_{\epsilon_{\mathbf{k}}} \Sigma(\mathbf{k}, \epsilon_{\mathbf{k}}) \right\} + \{\uparrow \leftrightarrow \downarrow\} \right), \qquad (5.70)$$

where

$$\Sigma(\mathbf{k}, \epsilon_{\mathbf{k}}) = g^2 \sum_{\mathbf{p},\mathbf{q}} \frac{f_{\mathbf{k}+\mathbf{q}}^\uparrow f_{\mathbf{p}-\mathbf{q}}^\downarrow \left(1 - f_{\mathbf{p}}^\downarrow\right) + \left(1 - f_{\mathbf{k}+\mathbf{q}}^\uparrow\right) \left(1 - f_{\mathbf{p}-\mathbf{q}}^\downarrow\right) f_{\mathbf{p}}^\downarrow}{\epsilon_{\mathbf{k}+\mathbf{q}}^\uparrow + \epsilon_{\mathbf{p}-\mathbf{q}}^\downarrow - \epsilon_{\mathbf{k}}^\uparrow - \epsilon_{\mathbf{p}}^\downarrow}. \qquad (5.71)$$

Using the result of a calculation by Abanov et al [41] we write

$$\Sigma(\mathbf{k}, \epsilon_{\mathbf{k}}) = \frac{3g^2 \chi(\mathbf{Q}, 0)}{4\pi\mu} \epsilon_{\mathbf{k}}, \qquad (5.72)$$

where the susceptibility takes the usual form in the limit of $\mathbf{Q} \to (\pi, \pi)$ and small
temperatures. So that

$$\chi(\mathbf{Q}, 0) = \sum_{\mathbf{k}} \frac{f(\epsilon_{\mathbf{k}} - \mu) - f(\epsilon_{\mathbf{k}-\mathbf{Q}} - \mu)}{\epsilon_{\mathbf{k}} - \epsilon_{\mathbf{k}-\mathbf{Q}}} \qquad (5.73)$$

$$= \sum_{\mathbf{k}} \frac{f(\epsilon_{\mathbf{k}} - \mu) - f(-\epsilon_{\mathbf{k}} - \mu)}{2\epsilon_{\mathbf{k}}} \qquad (5.74)$$

$$= \frac{1}{2} \rho(\mu - T) \log\left(\frac{|\mu - T|}{4t}\right). \qquad (5.75)$$

Hence,

$$\delta \mathcal{F}_\Sigma = \frac{3g^4}{16\pi\mu} \langle\langle |D_{\mathbf{k}}|^2 \rangle\rangle \rho(\mu - T)^2 \log^2\left(\frac{|\mu - T|}{4t}\right) \qquad (5.76)$$

In summary, contributions to the free energy due to fluctuations are negative at
this level. This is in contrast to the mean field results, which disfavour symmetry
breaking. Thus, fluctuations support the formation of d-wave bond density order.
Moreover, $\delta \mathcal{F}_{\chi_{AF}^{\uparrow\uparrow}}$ and $\delta \mathcal{F}_{\chi_{AF}^{\uparrow\downarrow}}$ are divergent as temperature approaches zero. Hence, at
sufficiently low temperatures fluctuations self-consistently drive the system towards
formation of bond density wave order.

5.5 *Interplay of bond density wave and antiferromagnetism*

Having calculated the free energy of bond density wave order, we now would like to analyse its interaction with a static antiferromagnetic background. The magnitude of the bond density wave order parameter is taken to be much smaller than that of the antiferromagnetic order. Hence, the bond density wave is treated as a small perturbation, whose back action onto the antiferromagnetic fluctuations may be neglected.

We formally expand the free energy to order $D^2 M^2$. The sign of this expansion coefficient determines whether antiferromagnetic order supports or hinders the formation of bond density wave order.

5.5.1 Overview of calculation

As in the previous section we use the principle, that all physics happens around the Fermi surface. This restricts the supported momentum space and thereby simplifies the integrations.

Assuming a static background order allows us to simply replace all dispersions in the expression of the bond density wave's free energy by the dispersion in the presence of commensurate antiferromagnetism:

$$\xi_{\mathbf{k}}^{\sigma} = \sigma \sqrt{\epsilon_{\mathbf{k}}^2 + g^2 M^2} - \mu \tag{5.77}$$

In principle we may also consider incommensurate antiferromagnetism interacting with bond density wave order. Previous studies of incommensurate antiferromagnetism interacting with charge or superconducting order are rare and suggest coexistence, but with negligible effects on the superconducting or charge order due to the weakness of the incommensurate antiferromagnetic order [55]. Unfortunately the analysis of incommensurate antiferromagnetic order does not allow for the same symmetry related simplifications, making its treatment considerably harder. To the best knowledge of the author, an analysis of leading order perturbative corrections

to the free energy in the simultaneous presence of incommensurate antiferromagnetic order and superconducting or charge order in the Hubbard model has not been performed to date.

As in the previous section we split the free energy of bond density wave order into similar parts and evaluate them separately. We will first analyse the mean field and then the fluctuation contribution, which in turn will be treated term by term.

5.5.2 Expanding the mean field free energy in orders of magnetisation

The mean field free energy of bond density wave up to order D^2 takes the form

$$\mathcal{F}_{MF}(D) = -\frac{g^2}{2} \sum_{\mathbf{k},\sigma} |D_{\mathbf{k}}^2| \frac{f_{\mathbf{k}-\frac{\mathbf{Q}}{2}}^{\sigma} - f_{\mathbf{k}+\frac{\mathbf{Q}}{2}}^{\sigma}}{\epsilon_{\mathbf{k}-\frac{\mathbf{Q}}{2}}^{\sigma} - \epsilon_{\mathbf{k}+\frac{\mathbf{Q}}{2}}^{\sigma}}. \tag{5.78}$$

Choosing a bond density ordering wave vector of $\mathbf{Q} = (\pi, \pi)$ and introducing the antiferromagnetic order we arrive at

$$\mathcal{F}_{MF}(D, M) = -\frac{g^2}{2} \sum_{\mathbf{k},\sigma} |D_{\mathbf{k}}^2| \frac{f(\sigma\sqrt{\epsilon_{\mathbf{k}}^2 + g^2 M^2} - \mu) - f(-\sigma\sqrt{\epsilon_{\mathbf{k}}^2 + g^2 M^2} - \mu)}{2\sigma\sqrt{\epsilon_{\mathbf{k}}^2 + g^2 M^2}} \tag{5.79}$$

The sum over σ simply introduces a factor of 2, since the expression is symmetric in this band label. Next, we expand in magnetisation:

$$\partial_{M^2}\mathcal{F}_{MF}(D, M)|_{M=0} = g^4 \sum_{\mathbf{k}} |D_{\mathbf{k}}^2| \left\{ \frac{f(\epsilon_{\mathbf{k}} - \mu) - f(-\epsilon_{\mathbf{k}} - \mu)}{4\epsilon_{\mathbf{k}}^3} \right.$$
$$\left. - \frac{f'(\epsilon_{\mathbf{k}} - \mu) + f'(-\epsilon_{\mathbf{k}} - \mu)}{4\epsilon_{\mathbf{k}}^2} \right\} \tag{5.80}$$

Integrating by parts in the limit of zero temperature and neglecting the sub-leading term arising from the action of the derivative on the density of states, we arrive at:

$$
\partial_{M^2} \mathcal{F}_{MF}(D, M)|_{M=0} = -g^4 \sum_{\mathbf{k}} |D_{\mathbf{k}}^2| \frac{f(\epsilon_{\mathbf{k}} - \mu) - f(-\epsilon_{\mathbf{k}} - \mu)}{4\epsilon_{\mathbf{k}}^3} \tag{5.81}
$$

$$
= g^4 \langle\langle |D_{\mathbf{k}}|^2 \rangle\rangle \int_{\mu-T}^{4t} \frac{\rho(\epsilon)}{2\epsilon^3} d\epsilon \tag{5.82}
$$

$$
= -\frac{g^4 \rho(\mu - T)}{4\mu^2} \langle\langle |D_{\mathbf{k}}|^2 \rangle\rangle. \tag{5.83}
$$

5.5.3 Expanding the fluctuation corrections in orders of magnetisation

The expansion of the fluctuation corrections to the free energy in powers of the antiferromagnetic background order will be split into its individual terms.

Expansion of the $\delta\mathcal{F}_{\chi_{AF}^{\uparrow\uparrow}}$ term in M^2

Let us start with the $\chi_{AF}^{\uparrow\uparrow}$-term,

$$
\delta\mathcal{F}_{\chi_{AF}^{\uparrow\uparrow}} = -\frac{g^4}{4} \sum_{\mathbf{k},\mathbf{q}} \overline{D}_{\mathbf{k}+\mathbf{q}-\frac{\mathbf{Q}}{2}} \frac{f_{\mathbf{k}+\mathbf{q}-\mathbf{Q}}^{\uparrow} - f_{\mathbf{k}+\mathbf{q}}^{\uparrow}}{\epsilon_{\mathbf{k}+\mathbf{q}-\mathbf{Q}}^{\uparrow} - \epsilon_{\mathbf{k}+\mathbf{q}}^{\uparrow}} D_{\mathbf{k}-\frac{\mathbf{Q}}{2}} \frac{f_{\mathbf{k}-\mathbf{Q}}^{\uparrow} - f_{\mathbf{k}}^{\uparrow}}{\epsilon_{\mathbf{k}-\mathbf{Q}}^{\uparrow} - \epsilon_{\mathbf{k}}^{\uparrow}} \chi_{AF}^{\uparrow\uparrow}(\mathbf{q}, \epsilon_{\mathbf{k}}^{\uparrow} - \epsilon_{\mathbf{k}+\mathbf{q}}^{\uparrow}) \tag{5.84}
$$

where

$$
\chi_{AF}^{\uparrow\uparrow}(\mathbf{q}, \epsilon_{\mathbf{k}}^{\uparrow} - \epsilon_{\mathbf{k}+\mathbf{q}}^{\uparrow}) = \sum_{\mathbf{p}} \frac{f_{\mathbf{p}}^{\downarrow} - f_{\mathbf{p}-\mathbf{q}}^{\downarrow}}{\epsilon_{\mathbf{p}-\mathbf{q}}^{\downarrow} + \epsilon_{\mathbf{k}+\mathbf{q}}^{\uparrow} - \epsilon_{\mathbf{k}}^{\uparrow} - \epsilon_{\mathbf{p}}^{\downarrow}}. \tag{5.85}
$$

As discussed in the previous section we take the limit of $\mathbf{Q} \to (\pi, \pi)$ and use the bond density susceptibility factors to simplify the expression. That is to say, we keep the leading contribution, $\mathbf{q} = (\pi, \pi)$ and $\epsilon_{\mathbf{k}}^{\uparrow} - \epsilon_{\mathbf{k}+\mathbf{q}}^{\uparrow} = 2\mu$. Finally, we introduce

the antiferromagnetic order parameter:

$$\delta \mathcal{F}_{\chi_{AF}^{\uparrow\uparrow}}(M) = \frac{g^4}{16} \langle\langle |D_{\mathbf{k}}|^2 \rangle\rangle \rho (\mu - T)^2 \log \left(\frac{|\mu - T|}{4t} \right)^2$$
$$\sum_{\mathbf{p}} \frac{f(-\sqrt{\epsilon_{\mathbf{p}}^2 + g^2 M^2} - \mu) - f(\sqrt{\epsilon_{\mathbf{p}}^2 + g^2 M^2} - \mu)}{2\sqrt{\epsilon_{\mathbf{p}}^2 + g^2 M^2} + 2\mu} \quad (5.86)$$

Expanding this expression, we arrive at:

$$\partial_{M^2} \delta \mathcal{F}_{\chi_{AF}^{\uparrow\uparrow}}(M)|_{M=0}$$
$$= \frac{g^4}{16} \langle\langle |D_{\mathbf{k}}|^2 \rangle\rangle \rho (\mu - T)^2 \log \left(\frac{|\mu - T|}{4t} \right)^2$$
$$\sum_{\mathbf{p}} \left(\frac{f'(-\epsilon_{\mathbf{p}} - \mu) + f'(\epsilon_{\mathbf{p}} - \mu)}{4(\epsilon_{\mathbf{p}} + \mu)\epsilon_{\mathbf{p}}} + \frac{f(-\epsilon_{\mathbf{p}} - \mu) - f(\epsilon_{\mathbf{p}} - \mu)}{4(\epsilon_{\mathbf{p}} + \mu)^2 \epsilon_{\mathbf{p}}} \right) \} \quad (5.87)$$

The next step is to integrate by parts and use the Fermi functions to restrict the range of integration.

$$\partial_{M^2} \delta \mathcal{F}_{\chi_{AF}^{\uparrow\uparrow}}(M)|_{M=0}$$
$$= \frac{g^4}{32} \langle\langle |D_{\mathbf{k}}|^2 \rangle\rangle \rho (\mu - T)^2 \log \left(\frac{|\mu - T|}{4t} \right)^2 \int_{-\mu+T}^{4t} d\epsilon \frac{\rho(\epsilon)}{\epsilon^2(\epsilon + \mu)} \quad (5.88)$$

We have elected to keep some temperature dependence to cut off divergences. Lastly, we perform the integration and arrive at:

$$\partial_{M^2} \delta \mathcal{F}_{\chi_{AF}^{\uparrow\uparrow}}(M)|_{M=0} = -\frac{g^6}{32} \langle\langle |D_{\mathbf{k}}|^2 \rangle\rangle \frac{\rho(\mu-T)^3}{(\mu-T)^2} \log \left(\frac{|\mu-T|}{4t} \right)^2 \log \left(\frac{T}{|\mu|} \right) \quad (5.89)$$

Expansion of the $\delta \mathcal{F}_{\chi_{AF}^{\uparrow\downarrow}}$ term in M^2

Next, let us examine the $\chi_{AF}^{\uparrow\downarrow}$-term,

$$\delta \mathcal{F}_{\chi_{AF}^{\uparrow\downarrow}} = -\frac{g^4}{2} \sum_{\mathbf{k},\mathbf{q}} \overline{D}_{\mathbf{k}+\frac{\mathbf{Q}}{2}} \frac{f_{\mathbf{k}}^{\uparrow} - f_{\mathbf{k}+\mathbf{Q}}^{\uparrow}}{\epsilon_{\mathbf{k}} - \epsilon_{\mathbf{k}+\mathbf{Q}}} D_{\mathbf{k}+\mathbf{q}+\frac{\mathbf{Q}}{2}} \frac{f_{\mathbf{k}+\mathbf{q}}^{\downarrow} - f_{\mathbf{k}+\mathbf{q}+\mathbf{Q}}^{\downarrow}}{\epsilon_{\mathbf{k}+\mathbf{q}} - \epsilon_{\mathbf{k}+\mathbf{q}+\mathbf{Q}}} \chi_{AF}^{\uparrow\downarrow}(\mathbf{q}, \epsilon_{\mathbf{k}}^{\uparrow} - \epsilon_{\mathbf{k}+\mathbf{q}}^{\downarrow}), \quad (5.90)$$

where

$$\chi_{AF}^{\uparrow\downarrow}(\mathbf{q}, \epsilon_{\mathbf{k}}^{\uparrow} - \epsilon_{\mathbf{k+q}}^{\downarrow}) = \sum_{\mathbf{p}} \frac{f_{\mathbf{p}}^{\downarrow} - f_{\mathbf{p-q}}^{\uparrow}}{\epsilon_{\mathbf{p-q}}^{\uparrow} + \epsilon_{\mathbf{k+q}}^{\downarrow} - \epsilon_{\mathbf{k}}^{\uparrow} - \epsilon_{\mathbf{p}}^{\downarrow}}. \tag{5.91}$$

In the limit of $\mathbf{Q} \to (\pi, \pi)$ the bond density wave susceptibility factors only support a few momenta and frequencies of $\chi_{AF}^{\uparrow\downarrow}(\mathbf{q}, \epsilon_{\mathbf{k}}^{\uparrow} - \epsilon_{\mathbf{k+q}}^{\downarrow})$. In particular, these are $\mathbf{q} = \mathbf{0}$ or $\mathbf{q} = (\pi, \pi)$ and $\epsilon_{\mathbf{k}}^{\uparrow} - \epsilon_{\mathbf{k+q}}^{\downarrow} = 0$ or $\epsilon_{\mathbf{k}}^{\uparrow} - \epsilon_{\mathbf{k+q}}^{\downarrow} = \pm\mu$. One might guess that this terms behaves identically to $\chi_{AF}^{\uparrow\uparrow}$. However, note that the difference in spin labels introduces relative minus signs in the presence of antiferromagnetic order. In fact the leading contribution of $\chi_{AF}^{\uparrow\downarrow}$ in the presence of antiferromagnetic order stems from $\mathbf{q} = \mathbf{0}$, such that

$$\chi_{AF}^{\uparrow\downarrow}(\mathbf{0}, \omega, M) = \chi_{AF}^{\uparrow\uparrow}((\pi, \pi), \omega, M) \tag{5.92}$$

and hence,

$$\delta\mathcal{F}_{\chi_{AF}^{\uparrow\downarrow}}(M) = \delta\mathcal{F}_{\chi_{AF}^{\uparrow\uparrow}}(M) \tag{5.93}$$

$$\partial_{M^2}\delta\mathcal{F}_{\chi_{AF}^{\uparrow\downarrow}}(M)|_{M=0} = \partial_{M^2}\delta\mathcal{F}_{\chi_{AF}^{\uparrow\uparrow}}(M)|_{M=0} \tag{5.94}$$

Expansion of the $\mathcal{F}_\Sigma$ term in M^2

Lastly, we would like to expand the self-energy term,

$$\delta\mathcal{F}_\Sigma = g^4 \sum_{\mathbf{k}} \left(\left\{ |D_{\mathbf{k}+\frac{\mathbf{Q}}{2}}|^2 \frac{f_{\mathbf{k-Q}}^{\uparrow} - f_{\mathbf{k}}^{\uparrow}}{\epsilon_{\mathbf{k-Q}} - \epsilon_{\mathbf{k}}} \partial_{\epsilon_{\mathbf{k}}}\Sigma'(\mathbf{k}, \epsilon_{\mathbf{k}}) \right\} + \{\uparrow\leftrightarrow\downarrow\} \right). \tag{5.95}$$

From Abanov *et al* [41] we know the form of the self-energy,

$$\Sigma'(\mathbf{k}, \epsilon_{\mathbf{k}}) = \frac{3\chi(\mathbf{Q}, 0)}{4\pi\mu} \epsilon_{\mathbf{k}} \tag{5.96}$$

so that,

$$\partial_{\epsilon_{\mathbf{k}}}\Sigma'(\mathbf{k}, \epsilon_{\mathbf{k}}) = \frac{3\chi(\mathbf{Q}, 0)}{4\pi\mu}. \tag{5.97}$$

In the same limits as taken previously $\chi(\mathbf{Q}, 0) \to \frac{1}{2}\rho(\mu - T) \log\left(\frac{-\mu + T}{4t}\right)$. We conclude that the self-energy is independent of magnetisation and therefore all dependence on magnetisation comes from the bond density susceptibility factor.

$$\delta \mathcal{F}_\Sigma(M) = g^4 \frac{3\chi(\mathbf{Q}, 0)}{4\pi\mu} \sum_{\mathbf{k}} |D_{\mathbf{k}}|^2 \frac{f(\sqrt{\epsilon_{\mathbf{k}}^2 + g^2 M^2} - \mu) - f(-\sqrt{\epsilon_{\mathbf{k}}^2 + g^2 M^2} - \mu)}{\sqrt{\epsilon_{\mathbf{k}}^2 + g^2 M^2}}$$

(5.98)

Expanding in magnetisation to leading order we arrive at:

$$|\partial_{M^2}\delta\mathcal{F}_\Sigma(M)|_{M=0} =$$
$$g^6 \frac{3\chi(\mathbf{Q}, 0)}{8\pi\mu} \sum_{\mathbf{k}} |D_{\mathbf{k}}|^2 \left\{ \frac{f'(\epsilon_{\mathbf{k}} - \mu) + f'(-\epsilon_{\mathbf{k}} - \mu)}{\epsilon_{\mathbf{k}}^2} - \frac{f(\epsilon_{\mathbf{k}} - \mu) - f(-\epsilon_{\mathbf{k}} - \mu)}{\epsilon_{\mathbf{k}}^3} \right\}$$

(5.99)

Introducing the density of states and integrating by parts;

$$|\partial_{M^2}\delta\mathcal{F}_\Sigma(M)|_{M=0} = -g^6 \frac{3}{16\pi\mu} \frac{\rho(\mu - T)^2}{(\mu - T)^2} \log\left(\frac{|\mu - T|}{4t}\right) \langle\langle|D_{\mathbf{k}}|^2\rangle\rangle \quad (5.100)$$

In principle we may also consider mode-mode coupling between incommensurate antiferromagnetism and bond density wave order. However, the analysis of incommensurate antiferromagnetism in Chapter 2 showed that incommensurate order is very weak and thus its effect on the bond density wave order should be insignificant. Moreover, calculations involving incommensurate order do not allow for the same symmetry related simplifications, making its inclusion highly non-trivial.

5.6 *Phase diagram*

In the previous sections we evaluated the fluctuation corrected free energy of bond density wave order in the Hubbard model. Further, we analysed the leading terms in the interaction of the bond density wave with commensurate antiferromagnetism. Now we will use the derived expressions to extend the phase diagram of the antiferromagnet.

The free energy of the bond density wave takes the general form

$$\mathcal{F}(D) \;=\; \left(\alpha + \beta M^2\right) D^2,\tag{5.101}$$

where α and β are the sum of the previously derived contributions to the free energy in the absence and presence of commensurate antiferromagnetic order, respectively. In particular, α is the sum of equations (5.60), 2×(5.67) and (5.76), while β is the sum of equations (5.83), 2×(5.89) and (5.100).

The second order transition is found by determining the zeros of this quadratic coefficient of the bond density order parameter. In the absence of antiferromagnetic order (M=0) the transition temperature as a function of interaction strength takes the familiar form of a BCS-like exponential:

$$T_c = 4t\; exp\left(\frac{1 - g^2 \frac{3}{8\pi\mu}\rho(\mu - T)}{g^2\rho(\mu - T)^2 \log\left(\frac{|\mu - T|}{4t}\right)}\right).\tag{5.102}$$

The resulting phase diagram is plotted in Figure 5.1.

The position of the antiferromagnetic transition line is shifted relative to Figure 4.5. This difference is a result of the discrepancy between the real density of states of the tight binding dispersion and its logarithmic approximation. The transition to bond density wave order was derived assuming a logarithmic density of states. Hence, in order to ensure consistency, the antiferromagnetic transition in Figure 5.1 has been computed using the same logarithmic density of states. The first order transition to antiferromagnetic order as well as the incommensurate region were included by hand in order to retain the topology of the antiferromagnetic phase transitions. Hence, there is ambiguity in the exact position of these phase transition lines and the phase diagrams should be viewed as a qualitative summary of the results.

In the presence of commensurate antiferromagnetic order the analysis is less straight forward. The $M^2 D^2$ coefficient is positive in general. Thus, the two phases compete. From the investigation of antiferromagnetic order, we may numerically determine the magnetisation as a function of interaction strength and temperature. Then, we may evaluate $\alpha + \beta M^2$ for any point in the phase diagram and determine whether bond density wave order is present.
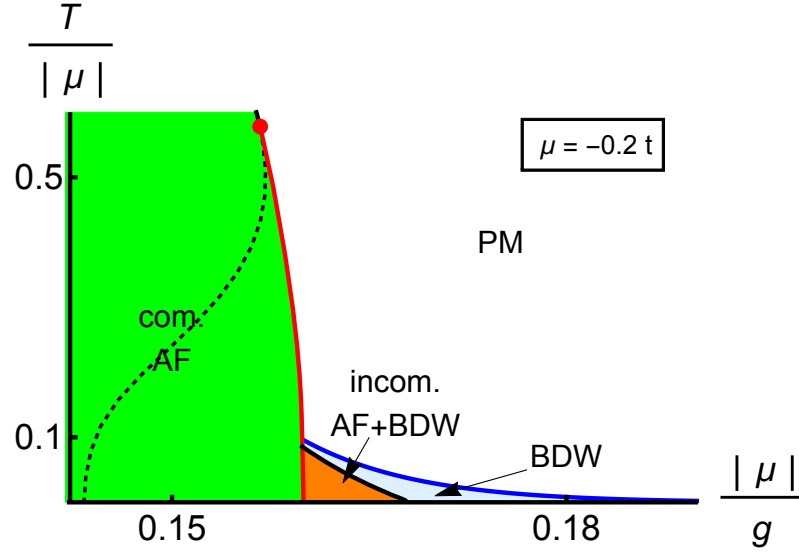
Figure 5.1: **Phase diagram of bond density wave order and antiferromagnetism.** The orders in this diagram are commensurate antiferromagnetism (com. AF), bond density wave (BDW) and the paramagnetic phase (PM). Additionally, bond density wave order coexists with incommensurate antiferromagnetism (incom. AF) in orange region, respectively. As a guide to the eye we have we left the preempted second order transition into the commensurate antiferromagnet as dotted line inside the commensurate phase.

Magnetisation and interaction strength in the relevant region of the phase diagram are large. Hence, the two phases only coexist in a small region of the phase diagram. This is consistent with our heuristic picture of the antiferromagnet. For large magnetisation the Fermi surface is completely gapped. In that case there is no phase space for the formation of bond density wave order. This may also be viewed as the onset of Mott insulator physics.

This is in contrast to incommensurate order. Here, the gap is small and the Fermi surface persists. In fact the incommensurate order parameter is so small, that we may neglect its interaction with other orders and propose their coexistence. The resulting phase diagram is plotted in Figure 5.1.

In the analysis of the antiferromagnetic phase we found, that for sufficiently low temperatures below the tricritical point the Landau expansion in magnetisation fails, due to non-analyticities in the free energy (section 2.6.3). Hence, the treatment of the mode-mode coupling between antiferromagnetic and bond density wave order should be extended to higher order in magnetisation to ensure a fully consistent
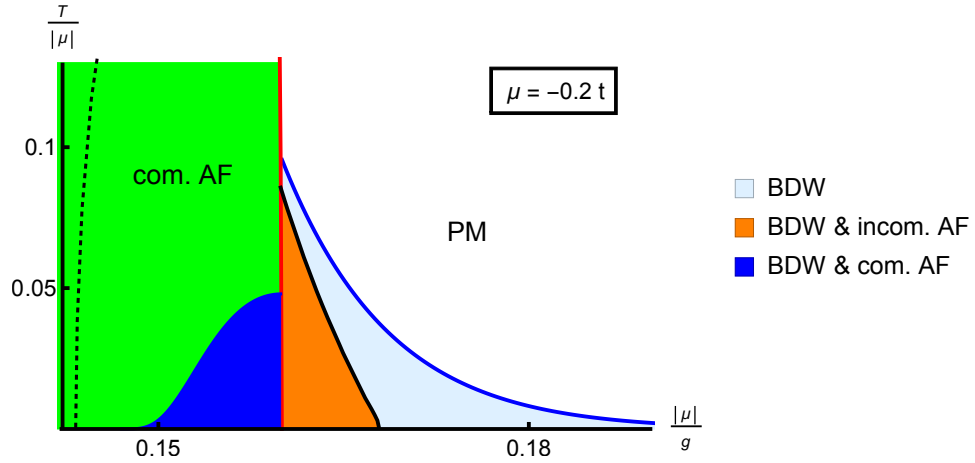
Figure 5.2: **Phase diagram of bond density wave order and antiferromagnetism.** The orders in this diagram are commensurate antiferromagnetism (com. AF), bond density wave (BDW) and the paramagnetic phase (PM). Additionally, bond density wave order coexists with commensurate (com. AF) and incommensurate antiferromagnetism (incom. AF) in the dark blue and orange region, respectively. As a guide to the eye we have we left the preempted second order transition into the commensurate antiferromagnet as dotted line inside the commensurate phase.

treatment below the tri-critical point or deep within the antiferromagnetic phase region. That is wherever magnetisation is comparable to the intrinsic scale of the model, μ.

5.7 *Variational ansatz vs Legendre transformation*

As an alternative to the above analysis one may also use a Legendre transformation to investigate bond density wave order. The approaches are equivalent as we now demonstrate.

5.7.1 Variational ansatz

First we present the variational approach, after which we show the Legendre transformation.

Starting with the Hubbard model:

$$\mathcal{H} - \mu\mathcal{N} = \underbrace{\sum_{\mathbf{k},\sigma}(\epsilon_{\mathbf{k}} - \mu)\hat{n}_{\mathbf{k},\sigma}}_{\mathcal{H}_{kin}} + \underbrace{g\sum_{\mathbf{r}}\hat{n}_{\mathbf{r},\uparrow}\hat{n}_{\mathbf{r},\downarrow}}_{\mathcal{H}_{int}}, \tag{5.103}$$

where we have identified the kinetic and interaction contribution, we add and subtract a term

$$\mathcal{H}_{var} = \frac{g}{2}\sum_{\mathbf{k},\sigma}\left(D_{\mathbf{k}}c^{\dagger}_{\mathbf{k}+\frac{\mathbf{Q}}{2},\sigma}c_{\mathbf{k}-\frac{\mathbf{Q}}{2},\sigma} + \bar{D}_{\mathbf{k}}c^{\dagger}_{\mathbf{k}-\frac{\mathbf{Q}}{2},\sigma}c_{\mathbf{k}+\frac{\mathbf{Q}}{2},\sigma}\right), \tag{5.104}$$

such that

$$\mathcal{H} - \mu\mathcal{N} = \underbrace{\mathcal{H}_{kin} + \mathcal{H}_{var}}_{diagonalise} - \underbrace{\mathcal{H}_{var} + \mathcal{H}_{int}}_{perturbation}. \tag{5.105}$$

The first two terms will be treated as the original Hamiltonian and diagonalized. The remaining terms are treated as a perturbation to this Hamiltonian.

We may now construct the Helmholtz free energy and expand it in powers of the order parameter to form a Landau-Ginzburg expansion. This takes the general form

$$\mathcal{F}(|D|^2) = \alpha|D|^2 + \beta|D|^4 + \gamma|D|^6 - \langle\mathcal{H}_{var}\rangle \tag{5.106}$$

where the thermal expectation $\langle...\rangle$ is taken over the diagonal basis of the original Hamiltonian.

5.7.2 Legendre transformation

Next, let us examine the Legendre transformation.

We start with the same Hamiltonian as for the variational ansatz:

$$\mathcal{H} - \mu\mathcal{N} = \underbrace{\sum_{\mathbf{k},\sigma}(\epsilon_{\mathbf{k}} - \mu)\hat{n}_{\mathbf{k},\sigma}}_{\mathcal{H}_{kin}} + \underbrace{g\sum_{\mathbf{r}}\hat{n}_{\mathbf{r},\uparrow}\hat{n}_{\mathbf{r},\downarrow}}_{\mathcal{H}_{int}}. \tag{5.107}$$

Introducing a field $j_{\mathbf{k}}$ conjugate to the bond density wave order,

$$\mathcal{H}_{leg} = \frac{g}{2} \sum_{\mathbf{k},\sigma} \left(j_{\mathbf{k}} c^\dagger_{\mathbf{k}+\frac{\mathbf{Q}}{2},\sigma} c_{\mathbf{k}-\frac{\mathbf{Q}}{2},\sigma} + \bar{j}_{\mathbf{k}} c^\dagger_{\mathbf{k}-\frac{\mathbf{Q}}{2},\sigma} c_{\mathbf{k}+\frac{\mathbf{Q}}{2},\sigma} \right), \tag{5.108}$$

such that

$$\mathcal{H} - \mu\mathcal{N} = \underbrace{\mathcal{H}_{kin} + \mathcal{H}_{leg}}_{diagonalise} + \underbrace{\mathcal{H}_{int}}_{perturbation}. \tag{5.109}$$

The first two terms will be treated as the original Hamiltonian and will be diagonalised. The remaining term will be treated as a perturbation.

Again we may now construct the free energy and expand it in powers of the conjugate field. By construction the Landau-Ginzburg coefficients will be the same as for the variational ansatz.

$$\Gamma(|j|^2) = \alpha|j|^2 + \beta|j|^4 + \gamma|j|^6 \tag{5.110}$$

The last step is to perform the Legendre transformation,

$$\mathcal{F}(|D|^2) = \Gamma(|j(D)|^2) - j(D)\bar{D} - \bar{j}(\bar{D})D, \tag{5.111}$$

where

$$\bar{j}(\bar{D}) = \partial_D \mathcal{F}(|D|^2) \quad \text{and} \quad j(D) = \partial_{\bar{D}} \mathcal{F}(|D|^2) \tag{5.112}$$

$$\bar{D}(\bar{j}) = \partial_j \Gamma(|j|^2) \quad \text{and} \quad D(j) = \partial_{\bar{j}} \Gamma(|j|^2). \tag{5.113}$$

To leading order these reduce to

$$\bar{j}(\bar{D}) \propto \bar{D} \quad \text{and} \quad j(D) \propto D \tag{5.114}$$

$$\bar{D}(\bar{j}) \propto \langle c^\dagger_{\mathbf{k}+\frac{\mathbf{Q}}{2},\sigma} c_{\mathbf{k}-\frac{\mathbf{Q}}{2},\sigma} \rangle \quad \text{and} \quad D(j) \propto \langle c^\dagger_{\mathbf{k}-\frac{\mathbf{Q}}{2},\sigma} c_{\mathbf{k}+\frac{\mathbf{Q}}{2},\sigma} \rangle. \tag{5.115}$$

Including the above into equation (5.111) and rescaling D appropriately we arrive at

$$\mathcal{F}(|D|^2) = \alpha|D|^2 + \beta|D|^4 + \gamma|D|^6 - \frac{g}{2}\bar{D}\langle c^\dagger_{\mathbf{k}-\frac{\mathbf{Q}}{2},\sigma} c_{\mathbf{k}+\frac{\mathbf{Q}}{2},\sigma} \rangle - \frac{g}{2}D\langle c^\dagger_{\mathbf{k}+\frac{\mathbf{Q}}{2},\sigma} c_{\mathbf{k}-\frac{\mathbf{Q}}{2},\sigma} \rangle$$

$$\mathcal{F}(|D|^2) = \alpha|D|^2 + \beta|D|^4 + \gamma|D|^6 - \langle\mathcal{H}_{var}\rangle. \tag{5.116}$$

Which to leading order is the same Helmholtz free energy as the from the variational ansatz.

5.8   *Summary*

In this chapter we analysed bond density wave order in the Hubbard model. We began by deriving the fluctuation corrected free energy of the bond density wave and its intertwining with antiferromagnetism. From there we constructed the joined phase diagram. Even though bond density wave oder is not supported in mean field theory, fluctuation self-consistently stabilise the phase. This leads to a region of bond density wave order in the vicinity of the antiferromagnetic quantum critical point. Additionally, we found phase competition between spin and charge order. The later results in a drop of the bond density transition temperature inside the antiferromagnetic phase.

We finished this chapter by demonstrating the equivalence of the variational and Legendre transformation ansatz in the context of bond density wave order.

Chapter 6

Quantum order-by-disorder of the antiferromagnet: d-wave superconducting instability

In this chapter we include leading order effects of the presence of d-wave supercon-ducting order in the free energy of the antiferromagnet. d-wave superconductivity is introduced to the mean field theory via a variational ansatz. As expected super-conducting order is not supported at mean field level, so we calculate the effect of superconducting order on the anti-ferromagnetic fluctuations. Finally we consider the intertwining of d-wave superconducting order and background antiferromagnetic order.

Much of this calculation is very similar to the calculation of the d-wave bond density wave order's free energy presented in the previous chapter. Hence, details of the derivations present in the last chapter are often omitted in the treatment of the d-wave superconductivity below. To allow for easier comparison and clarity, despite the lack of detail, this chapter is arranged in the same format as the previous one.

6.1 *Mean field theory of the d-wave superconductor*

6.1.1 Hamiltonian

Consider the following Hamiltonian

$$\underbrace{\mathcal{H} - \mu\mathcal{N} = \sum_{\mathbf{k},\sigma} \xi_{\mathbf{k}} c_{\mathbf{k},\sigma}^{\dagger} c_{\mathbf{k},\sigma}}_{\text{kinetic}} + \underbrace{\sum_{\mathbf{k},\mathbf{p},\mathbf{q}} V_{\mathbf{q}} c_{\mathbf{k},\uparrow}^{\dagger} c_{\mathbf{p},\downarrow}^{\dagger} c_{\mathbf{p}-\mathbf{q},\downarrow} c_{\mathbf{k}+\mathbf{q},\uparrow}}_{\text{interaction}}, \tag{6.1}$$

where $\xi_{\mathbf{k}} = \epsilon_{\mathbf{k}} - \mu$ and the kinetic, $\mathcal{H}_{kin}$, and interaction, $\mathcal{H}_{int}$, part of the Hamiltonian have been identified.

Our task is to construct the free energy of this Hamiltonian in the presence of d-wave superconducting order.

6.1.2 The order parameter

We define the d-wave superconducting order as

$$\Delta_{\mathbf{k}} = \theta_{\mathbf{k}} \sum_{\mathbf{k},\sigma} c_{\mathbf{k},\sigma}^{\dagger} c_{-\mathbf{k},-\sigma}^{\dagger}, \tag{6.2}$$

with $\theta_{\mathbf{k}} = cos(k_x) - cos(k_y)$ encoding the d-wave symmetry.

D-wave superconductivity is symmetric under time reversal $\Delta_{\mathbf{k}} = \Delta_{-\mathbf{k}}$ and antisymmetric under rotations of $\frac{\pi}{2}$. Furthermore d-wave superconductivity as defined above is antisymmetric under spin character switching. This can be concluded from drawing the form of the gap for up and down electrons and considering how $\mathbf{k}$ maps to $-\mathbf{k}$ in this picture.

6.1.3 Variational ansatz

We include superconducting order by adding and subtracting a variational term,

$$\mathcal{H}_{var} = \sum_{\mathbf{k}} \left(\Delta_{\mathbf{k}} c^{\dagger}_{-\mathbf{k},\uparrow} c^{\dagger}_{\mathbf{k},\downarrow} + \bar{\Delta}_{\mathbf{k}} c_{\mathbf{k},\downarrow} c_{-\mathbf{k},\uparrow} \right), \tag{6.3}$$

to the Hamiltonian. Such that

$$\mathcal{H} - \mu \mathcal{N} = \underbrace{\mathcal{H}_{kin} + \mathcal{H}_{var}}_{\text{diagonalise}} \underbrace{-\mathcal{H}_{var} + \mathcal{H}_{int}}_{\text{perturbation}}. \tag{6.4}$$

The first two terms will be diagonalised and the remaining terms will be treated perturbatively.

We may now formally derive the order's symmetry under spin flip. We split the variational term in the above Hamiltonian in two by switching momentum label $\mathbf{k} \leftrightarrow -\mathbf{k}$:

$$\mathcal{H}_{var} = \frac{1}{2} \sum_{\mathbf{k}} \left(\Delta_{\mathbf{k}} c^{\dagger}_{-\mathbf{k},\uparrow} c^{\dagger}_{\mathbf{k},\downarrow} + \Delta_{-\mathbf{k}} c^{\dagger}_{\mathbf{k},\uparrow} c^{\dagger}_{-\mathbf{k},\downarrow} + \bar{\Delta}_{\mathbf{k}} c_{\mathbf{k},\downarrow} c_{-\mathbf{k},\uparrow} + \bar{\Delta}_{-\mathbf{k}} c_{-\mathbf{k},\downarrow} c_{\mathbf{k},\uparrow} \right). \tag{6.5}$$

Exchanging the operators of the last two terms, which introduces minus signs, we arrive at:

$$\mathcal{H}_{var} = \frac{1}{2} \sum_{\mathbf{k}} \left(\Delta_{\mathbf{k}} c^{\dagger}_{-\mathbf{k},\uparrow} c^{\dagger}_{\mathbf{k},\downarrow} - \Delta_{\mathbf{k}} c^{\dagger}_{-\mathbf{k},\downarrow} c^{\dagger}_{\mathbf{k},\uparrow} + \bar{\Delta}_{\mathbf{k}} c_{\mathbf{k},\downarrow} c_{-\mathbf{k},\uparrow} - \bar{\Delta}_{\mathbf{k}} c_{\mathbf{k},\uparrow} c_{-\mathbf{k},\downarrow} \right). \tag{6.6}$$

From the line above we can conclude that the d-wave gap is odd under spin character switching.

6.1.4 Diagonalisation

We will now derive the diagonal Hamiltonian in the presence of d-wave superconductivity with help of an appropriate Bogoliubov transformation.

Adding the positive contribution to the kinetic Hamiltonian, we write:

$$\mathcal{H}_{kin} + \mathcal{H}_{var} = \sum_{\mathbf{k},\sigma} \xi_{\mathbf{k}} c^{\dagger}_{\mathbf{k},\sigma} c_{\mathbf{k},\sigma} + \sum_{\mathbf{k}} \left(\Delta_{\mathbf{k}} c^{\dagger}_{-\mathbf{k},\uparrow} c^{\dagger}_{\mathbf{k},\downarrow} + \bar{\Delta}_{\mathbf{k}} c_{\mathbf{k},\downarrow} c_{-\mathbf{k},\uparrow}. \right) \quad (6.7)$$

Which, after expanding the expressions for all spin, may be written in matrix form;

$$\mathcal{H}_{kin} + \mathcal{H}_{var} = \frac{1}{2} \sum_{\mathbf{k}} \begin{pmatrix} c^{\dagger}_{-\mathbf{k},\sigma} \\ c_{\mathbf{k},-\sigma} \end{pmatrix}^{T} \begin{pmatrix} \xi_{\mathbf{k}} & \sigma \Delta_{\mathbf{k}} \\ \sigma \bar{\Delta}_{\mathbf{k}} & -\xi_{\mathbf{k}} \end{pmatrix} \begin{pmatrix} c_{-\mathbf{k},\sigma} \\ c^{\dagger}_{\mathbf{k},-\sigma} \end{pmatrix},$$

where the spin label is

$$\sigma = \pm 1 \text{ or } \uparrow / \downarrow \quad (6.8)$$

This Hamiltonian may be diagonalised by a Bogoliubov transformation of the form

$$\begin{pmatrix} c_{-\mathbf{k},\sigma} \\ c^{\dagger}_{\mathbf{k},-\sigma} \end{pmatrix} = \begin{pmatrix} u^{*} & -\sigma v^{*} \\ \sigma v & u \end{pmatrix} \begin{pmatrix} \alpha_{-\mathbf{k},\sigma} \\ \alpha^{\dagger}_{\mathbf{k},-\sigma} \end{pmatrix}, \quad (6.9)$$

where the matrix elements are

$$u_{\mathbf{k}}^{2}(v_{\mathbf{k}}^{2}) = \frac{1}{2} \left(1 + (-) \frac{\xi_{\mathbf{k}}}{\sqrt{\xi_{\mathbf{k}}^{2} + |\Delta_{\mathbf{k}}|^{2}}} \right)$$

$$u_{\mathbf{k}}^{2} \approx 1 - \frac{|\Delta_{\mathbf{k}}|^{2}}{4\xi_{\mathbf{k}}^{2}}, \quad v_{\mathbf{k}} \approx \frac{\Delta_{\mathbf{k}}}{2\xi_{\mathbf{k}}}. \quad (6.10)$$

The diagonalised kinetic Hamiltonian takes the form

$$\mathcal{H}_{kin} + \mathcal{H}_{var} = \sum_{\mathbf{k},\sigma} \xi_{\mathbf{k},\sigma} n_{\mathbf{k},\sigma}, \quad (6.11)$$

where the dispersion in the presence of superconducting order is given by

$$\xi_{\mathbf{k},\sigma} = \sigma \sqrt{(\epsilon_{\mathbf{k}} - \mu)^{2} + |\Delta_{\mathbf{k}}|^{2}}. \quad (6.12)$$

The structure of the order parameter determines the form of the transformation. The bond density wave is a simple momentum translation and hence the diagonalisation only alters the momentum of the rotated operators. The superconductor on the other hand requires a Bogoliubov transformation, which not only changes the momentum,

but also the particle and spin character of the transformed operators. This can also be viewed as a reflection of their inherent symmetries. The bond density wave is spin symmetric, while the superconductor is particle-hole and time reversal invariant. The transformation have to obey these same symmetries.

6.1.5   Free energy

Having diagonalised the Hamiltonian the mean field free energy is given by

$$\mathcal{F}_{MF} = -T \sum_{\mathbf{k},\sigma} \log\left(1 + e^{-\frac{\xi_{\mathbf{k},\sigma}}{T}}\right). \tag{6.13}$$

Corrections to this are given by

$$-T \log\langle e^{-\beta(-\mathcal{H}_{var} + \mathcal{H}_{int})}\rangle \approx \langle -\mathcal{H}_{var} + \mathcal{H}_{int}\rangle. \tag{6.14}$$

After applying the Bogoliubov transformation, Equation 6.9, this terms gives an additional contribution. We keep the leading, quadratic correction to the free energy of d-wave superconductivity. $\langle \mathcal{H}_{var}\rangle$ now takes the form of a superconducting susceptibility. We obtain

$$\begin{aligned}
\mathcal{F}(\Delta) &= \mathcal{F}_{MF} - \langle\mathcal{H}_{var}\rangle + \langle\mathcal{H}_{int}\rangle \tag{6.15}\\
&= -T \sum_{\mathbf{k},\sigma} \ln\left(e^{-\xi_{\mathbf{k},\sigma}/T} + 1\right) - \sum_{\mathbf{k}} |\Delta_{\mathbf{k}}|^2 \frac{2f_{\mathbf{k}} - 1}{\xi_{\mathbf{k}}} + \langle\mathcal{H}_{int}\rangle. \tag{6.16}
\end{aligned}$$

The Δ^2-term of the mean field and variational contribution have the same form up to multiplicative factors.

The Bogoliubov transformation, Equation 6.9, changes the form of the interaction vertex. This in turn affects the free energy contribution of the interaction term, which is accounted for in the analysis of the fluctuation corrections. As for the d-wave bond density wave, the bare interaction has no weight in the d-wave superconducting channel. Fluctuation contributions to the free energy that drive superconducting order are calculated in the following section.

6.2 *Fluctuation corrections to the antiferromagnet in the presence of d-wave superconductivity*

6.2.1 Overview of calculation

As in the previous section the following treatment of d-wave superconducting order is very similar to that in the chapter on d-wave bond density wave order, Chapter 5. We will derive corrections to the mean field free energy from self-consistent second order perturbation theory. We will demonstrate, that d-wave superconductivity is self-consistently stabilised by fluctuations. Moreover, we will treat superconducting order as a weak perturbation to the background antiferromagnetic phase and thereby determine whether the presence of antiferromagnetic order drives or suppresses fluctuations, which support the formation of Cooper pairs. As for the bond density wave the antiferromagnetic background order is assumed to be unaffected by the presence of superconductivity.

The second order change in the free energy is given by

$$
\langle \mathcal{H}_{int} \rangle = \mathcal{F}_{\text{fluct}} = g^2 \sum_{\substack{\mathbf{k}_1 \ldots \mathbf{k}_4, \\ \mathbf{p}_1 \ldots \mathbf{p}_4, \\ m}}' \frac{\langle c_{\mathbf{k}_1,\uparrow}^\dagger c_{\mathbf{k}_2,\downarrow}^\dagger c_{\mathbf{k}_3,\downarrow} c_{\mathbf{k}_4,\uparrow} | m \rangle \langle m | c_{\mathbf{p}_1,\uparrow}^\dagger c_{\mathbf{p}_2,\downarrow}^\dagger c_{\mathbf{p}_3,\downarrow} c_{\mathbf{p}_4,\uparrow} \rangle}{\epsilon_{\mathbf{k}_1}^+ + \epsilon_{\mathbf{k}_2}^- - \epsilon_{\mathbf{k}_3}^+ - \epsilon_{\mathbf{k}_4}^-} + \text{c.c.} \quad (6.17)
$$

The expectations, $\langle .. \rangle$, are calculated in the diagonal basis of $\mathcal{H}_{kin} + \mathcal{H}_{var}$ by application of the Bogoliubov transformation, Equation 6.9, onto the creation and annihilation operators. Non-zero expectations are formed by matching momenta between creation and annihilation operators and thus forming number operators, which are expressed as Fermi distribution functions. Finally, we collect terms and simplify the expressions as much as possible.

As in the calculation of the fluctuation corrections due to bond density wave order, the transformation of operators creates a large number of terms.

In contrast to the rotation of operators performed for the bond density wave, the Bogoliubov transformation not only changes the momentum of the operators, but also their particle and spin character. That is to say it transforms electrons into holes, spin up operators into spin down operators and vice versa. This is founded

in the very definition of the order parameter. As a consequence the pairing of operators in case of the bond density wave is simpler, only the momentum matching is non-trivial. In case of the superconductor, all three quantum numbers have to be considered carefully.

6.2.2 Fluctuation corrections to the antiferromagnet in the presence of d-wave superconducting order

The result of transforming the operators in Equation (6.17) into their form in the diagonal basis is:

$$
\mathcal{F}_{\text{fluct}}(\Delta) =
$$

$$
\underbrace{g^2 \sum_{\mathbf{k},\mathbf{p},\mathbf{q}} |u_{\mathbf{k}+\mathbf{q}}|^2 |u_{\mathbf{p}-\mathbf{q}}|^2 |u_{\mathbf{p}}|^2 |u_{\mathbf{k}}|^2 \frac{\langle \alpha^\dagger_{\mathbf{k}+\mathbf{q},\uparrow} \alpha^\dagger_{\mathbf{p}-\mathbf{q},\downarrow} \alpha_{\mathbf{p},\downarrow} \alpha_{\mathbf{k},\uparrow} \alpha^\dagger_{\mathbf{k},\uparrow} \alpha^\dagger_{\mathbf{p},\downarrow} \alpha_{\mathbf{p}-\mathbf{q},\downarrow} \alpha_{\mathbf{k}+\mathbf{q},\uparrow} \rangle}{\epsilon^\uparrow_{\mathbf{k}+\mathbf{q}} + \epsilon^\downarrow_{\mathbf{p}-\mathbf{q}} - \epsilon^\uparrow_{\mathbf{k}} - \epsilon^\downarrow_{\mathbf{p}}} + \text{c.c.}}_{\textbf{A. regular contribution}}
$$

$$
+g^2 \sum_{\substack{\mathbf{k},\mathbf{p},\mathbf{q} \\ \mathbf{k}',\mathbf{p}',\mathbf{q}'}} v_{\mathbf{k}+\mathbf{q}} v^*_{\mathbf{k}'} \frac{\langle \alpha_{-\mathbf{k}-\mathbf{q},\downarrow} \alpha^\dagger_{\mathbf{p}-\mathbf{q},\downarrow} \alpha_{\mathbf{p},\downarrow} \alpha_{\mathbf{k},\uparrow} \alpha^\dagger_{\mathbf{k}'+\mathbf{q}',\uparrow} \alpha^\dagger_{\mathbf{p}'-\mathbf{q}',\downarrow} \alpha_{\mathbf{p}',\downarrow} \alpha^\dagger_{-\mathbf{k}',\downarrow} \rangle}{\epsilon^\uparrow_{\mathbf{k}+\mathbf{q}} + \epsilon^\downarrow_{\mathbf{p}-\mathbf{q}} - \epsilon^\uparrow_{\mathbf{k}} - \epsilon^\downarrow_{\mathbf{p}}} + \text{c.c.}
$$

$$
+g^2 \sum_{\substack{\mathbf{k},\mathbf{p},\mathbf{q} \\ \mathbf{k}',\mathbf{p}',\mathbf{q}'}} v_{\mathbf{p}-\mathbf{q}} v^*_{\mathbf{p}'} \frac{\langle \alpha^\dagger_{\mathbf{k}+\mathbf{q},\uparrow} \alpha_{-\mathbf{p}+\mathbf{q},\uparrow} \alpha_{\mathbf{p},\downarrow} \alpha_{\mathbf{k},\uparrow} \alpha^\dagger_{\mathbf{k}'+\mathbf{q}',\uparrow} \alpha^\dagger_{\mathbf{p}'-\mathbf{q}',\downarrow} \alpha^\dagger_{\mathbf{p}',\uparrow} \alpha_{\mathbf{k}',\uparrow} \rangle}{\epsilon^\uparrow_{\mathbf{k}+\mathbf{q}} + \epsilon^\downarrow_{\mathbf{p}-\mathbf{q}} - \epsilon^\uparrow_{\mathbf{k}} - \epsilon^\downarrow_{\mathbf{p}}} + \text{c.c.}
$$

$$
+g^2 \sum_{\substack{\mathbf{k},\mathbf{p},\mathbf{q} \\ \mathbf{k}',\mathbf{p}',\mathbf{q}'}} v^*_{\mathbf{p}} v_{\mathbf{p}'-\mathbf{q}'} \frac{\langle \alpha^\dagger_{\mathbf{k}+\mathbf{q},\uparrow} \alpha^\dagger_{\mathbf{p}-\mathbf{q},\downarrow} \alpha^\dagger_{-\mathbf{p},\uparrow} \alpha_{\mathbf{k},\uparrow} \alpha^\dagger_{\mathbf{k}'+\mathbf{q}',\uparrow} \alpha_{-\mathbf{p}'+\mathbf{q}',\uparrow} \alpha_{\mathbf{p}',\downarrow} \alpha_{\mathbf{k}',\uparrow} \rangle}{\epsilon^\uparrow_{\mathbf{k}+\mathbf{q}} + \epsilon^\downarrow_{\mathbf{p}-\mathbf{q}} - \epsilon^\uparrow_{\mathbf{k}} - \epsilon^\downarrow_{\mathbf{p}}} + \text{c.c.}
$$

$$
\underbrace{+g^2 \sum_{\substack{\mathbf{k},\mathbf{p},\mathbf{q} \\ \mathbf{k}',\mathbf{p}',\mathbf{q}'}} v^*_{\mathbf{k}} v_{\mathbf{k}'+\mathbf{q}'} \frac{\langle \alpha^\dagger_{\mathbf{k}+\mathbf{q},\uparrow} \alpha^\dagger_{\mathbf{p}-\mathbf{q},\downarrow} \alpha_{\mathbf{p},\downarrow} \alpha^\dagger_{-\mathbf{k},\downarrow} \alpha_{-\mathbf{k}'-\mathbf{q}',\downarrow} \alpha^\dagger_{\mathbf{p}'-\mathbf{q}',\uparrow} \alpha_{\mathbf{p}',\downarrow} \alpha_{\mathbf{k}',\uparrow} \rangle}{\epsilon^\uparrow_{\mathbf{k}+\mathbf{q}} + \epsilon^\downarrow_{\mathbf{p}-\mathbf{q}} - \epsilon^\uparrow_{\mathbf{k}} - \epsilon^\downarrow_{\mathbf{p}}} + \text{c.c.}}_{\textbf{B. pairs of } \mathcal{H}_{int} \text{ perturbed to linear order in } \Delta}
$$

$$-g^2 \sum_{\substack{\mathbf{k},\mathbf{p},\mathbf{q} \\ \mathbf{k}',\mathbf{p}',\mathbf{q}'}} v_{\mathbf{k}+\mathbf{q}} v_{\mathbf{p}}^* \frac{\langle \alpha_{-\mathbf{k}-\mathbf{q},\downarrow} \alpha_{\mathbf{p}-\mathbf{q},\downarrow}^\dagger \alpha_{-\mathbf{p},\uparrow}^\dagger \alpha_{\mathbf{k},\uparrow} \alpha_{\mathbf{k}'+\mathbf{q}',\uparrow}^\dagger \alpha_{\mathbf{p}'-\mathbf{q}',\downarrow}^\dagger \alpha_{\mathbf{p}',\downarrow} \alpha_{\mathbf{k}',\uparrow} \rangle}{\epsilon_{\mathbf{k}+\mathbf{q}}^\uparrow + \epsilon_{\mathbf{p}-\mathbf{q}}^\downarrow - \epsilon_{\mathbf{k}}^\uparrow - \epsilon_{\mathbf{p}}^\downarrow} \quad + \quad \text{c.c.}$$

$$-g^2 \sum_{\substack{\mathbf{k},\mathbf{p},\mathbf{q} \\ \mathbf{k}',\mathbf{p}',\mathbf{q}'}} v_{\mathbf{p}-\mathbf{q}} v_{\mathbf{k}}^* \frac{\langle \alpha_{\mathbf{k}+\mathbf{q},\uparrow}^\dagger \alpha_{-\mathbf{p}+\mathbf{q},\uparrow} \alpha_{\mathbf{p},\downarrow} \alpha_{-\mathbf{k},\downarrow}^\dagger \alpha_{\mathbf{k}'+\mathbf{q}',\uparrow}^\dagger \alpha_{\mathbf{p}'-\mathbf{q}',\downarrow}^\dagger \alpha_{\mathbf{p}',\downarrow} \alpha_{\mathbf{k}',\uparrow} \rangle}{\epsilon_{\mathbf{k}+\mathbf{q}}^\uparrow + \epsilon_{\mathbf{p}-\mathbf{q}}^\downarrow - \epsilon_{\mathbf{k}}^\uparrow - \epsilon_{\mathbf{p}}^\downarrow} \quad + \quad \text{c.c.}$$

$$-g^2 \sum_{\substack{\mathbf{k},\mathbf{p},\mathbf{q} \\ \mathbf{k}',\mathbf{p}',\mathbf{q}'}} v_{\mathbf{k}'+\mathbf{q}'} v_{\mathbf{p}'}^* \frac{\langle \alpha_{\mathbf{k}+\mathbf{q},\uparrow}^\dagger \alpha_{\mathbf{p}-\mathbf{q},\downarrow}^\dagger \alpha_{\mathbf{p},\downarrow} \alpha_{\mathbf{k},\uparrow} \alpha_{-\mathbf{k}'-\mathbf{q}',\downarrow} \alpha_{\mathbf{p}'-\mathbf{q}',\downarrow}^\dagger \alpha_{-\mathbf{p}',\uparrow}^\dagger \alpha_{\mathbf{k}',\uparrow} \rangle}{\epsilon_{\mathbf{k}+\mathbf{q}}^\uparrow + \epsilon_{\mathbf{p}-\mathbf{q}}^\downarrow - \epsilon_{\mathbf{k}}^\uparrow - \epsilon_{\mathbf{p}}^\downarrow} \quad + \quad \text{c.c.}$$

$$-g^2 \sum_{\substack{\mathbf{k},\mathbf{p},\mathbf{q} \\ \mathbf{k}',\mathbf{p}',\mathbf{q}'}} v_{\mathbf{p}'-\mathbf{q}'} v_{\mathbf{k}'}^* \frac{\langle \alpha_{\mathbf{k}+\mathbf{q},\uparrow}^\dagger \alpha_{\mathbf{p}-\mathbf{q},\downarrow}^\dagger \alpha_{\mathbf{p},\downarrow} \alpha_{\mathbf{k},\uparrow} \alpha_{\mathbf{k}'+\mathbf{q}',\uparrow}^\dagger \alpha_{-\mathbf{p}'+\mathbf{q}',\uparrow} \alpha_{\mathbf{p}',\downarrow} \alpha_{-\mathbf{k}',\downarrow}^\dagger \rangle}{\epsilon_{\mathbf{k}+\mathbf{q}}^\uparrow + \epsilon_{\mathbf{p}-\mathbf{q}}^\downarrow - \epsilon_{\mathbf{k}}^\uparrow - \epsilon_{\mathbf{p}}^\downarrow} \quad + \quad \text{c.c.}$$

$$\underbrace{\hspace{10cm}}$$

C. pairs of the regular $\mathcal{H}_{int}$ contracted with $\mathcal{H}_{int}$ quadratic in Δ

$$(6.18)$$

The first and simplest term, the regular contribution **A**, is identical in form to the bond density wave calculation. Here, momentum matching is trivial and has been performed already to shorten the expression.

The additional terms are of a different structure compared to the bond density wave. The first set of anomalous terms, **B**, is created by perturbing both copies of $\mathcal{H}_{int}$ to linear order in the superconducting gap. The second set, **C**, is created by perturbing one $\mathcal{H}_{int}$ to quadratic order in the gap while keeping the second $\mathcal{H}_{int}$ unperturbed.

For ease of reading, factors of $u_{\mathbf{k}} = \sqrt{1 - \frac{|\Delta_{\mathbf{k}}|^2}{4\xi_{\mathbf{k}}^2}}$ have been set to 1 in the anomalous terms. Their D^2 contribution stems from factors of $v_{\mathbf{k}} = \frac{\Delta_{\mathbf{k}}}{2\xi_{\mathbf{k}}}$.

One may express these contributions in terms of diagrams as well. Below, we draw three examples - one for each of the first lines of the three blocks of terms identified above.

A. Regular term:

$$g^2\langle\alpha^\dagger_{\mathbf{k+q},\uparrow}\alpha^\dagger_{\mathbf{p-q},\downarrow}\alpha_{\mathbf{p},\downarrow}\alpha_{\mathbf{k},\uparrow}\alpha^\dagger_{\mathbf{k},\uparrow}\alpha^\dagger_{\mathbf{p},\downarrow}\alpha_{\mathbf{p-q},\downarrow}\alpha_{\mathbf{k+q},\uparrow}\rangle$$

$$\tag{6.19}$$

B. First term of the contribution from vertices linear in Δ

$$g^2 v_{\mathbf{k+q}} v^*_{\mathbf{k}'}\langle\alpha_{-\mathbf{k-q},\downarrow}\alpha^\dagger_{\mathbf{p-q},\downarrow}\alpha_{\mathbf{p},\downarrow}\alpha_{\mathbf{k},\uparrow}\alpha^\dagger_{\mathbf{k}'+\mathbf{q}',\uparrow}\alpha^\dagger_{\mathbf{p}'-\mathbf{q}',\downarrow}\alpha_{\mathbf{p}',\downarrow}\alpha^\dagger_{-\mathbf{k}',\downarrow}\rangle$$

$$\tag{6.20}$$

C. First term of the contribution from a regular vertex contracted with one quadratic in Δ

$$-g^2 v_{\mathbf{k+q}} v^*_{\mathbf{p}}\langle\alpha_{-\mathbf{k-q},\downarrow}\alpha^\dagger_{\mathbf{p-q},\downarrow}\alpha^\dagger_{-\mathbf{p},\uparrow}\alpha_{\mathbf{k},\uparrow}\alpha^\dagger_{\mathbf{k}'+\mathbf{q}',\uparrow}\alpha^\dagger_{\mathbf{p}'-\mathbf{q}',\downarrow}\alpha_{\mathbf{p}',\downarrow}\alpha_{\mathbf{k}',\uparrow}\rangle$$

$$\tag{6.21}$$

Next, we must allow for the various non-zero expectations by identifying pairs of Fermi operators with matching quantum numbers. In the regular term (**A.**) and the last four terms (**C.**) there is only one way of matching terms. In the remaining four cases (**B.**) there are two ways each to match momenta and form non-zero expectations. The diagrams shown above are helpful in determining which pairings are non-zero.

$$\mathcal{F}_{\text{fluct}}(\Delta) =$$

$$g^2 \sum_{\mathbf{k},\mathbf{p},\mathbf{q}} |u_{\mathbf{k+q}}|^2 |u_{\mathbf{p-q}}|^2 |u_{\mathbf{p}}|^2 |u_{\mathbf{k}}|^2 \frac{\langle \alpha^\dagger_{\mathbf{k+q},\uparrow} \alpha^\dagger_{\mathbf{p-q},\downarrow} \alpha_{\mathbf{p},\downarrow} \alpha_{\mathbf{k},\uparrow} \alpha^\dagger_{\mathbf{k},\uparrow} \alpha^\dagger_{\mathbf{p},\downarrow} \alpha_{\mathbf{p-q},\downarrow} \alpha_{\mathbf{k+q},\uparrow} \rangle}{\epsilon^\uparrow_{\mathbf{k+q}} + \epsilon^\downarrow_{\mathbf{p-q}} - \epsilon^\uparrow_{\mathbf{k}} - \epsilon^\downarrow_{\mathbf{p}}} \quad + \text{ c.c.}$$

$$\underbrace{\phantom{g^2 \sum_{\mathbf{k},\mathbf{p},\mathbf{q}} |u_{\mathbf{k+q}}|^2 |u_{\mathbf{p-q}}|^2 |u_{\mathbf{p}}|^2 |u_{\mathbf{k}}|^2}}_{\textbf{A. } \text{regular contribution}}$$

$$+ g^2 \sum_{\mathbf{k},\mathbf{p},\mathbf{q}} |v_{\mathbf{k+q}}|^2 \frac{\langle \alpha_{-\mathbf{k-q},\downarrow} \alpha^\dagger_{\mathbf{p-q},\downarrow} \alpha_{\mathbf{p},\downarrow} \alpha_{\mathbf{k},\uparrow} \alpha^\dagger_{\mathbf{k},\uparrow} \alpha^\dagger_{\mathbf{p},\downarrow} \alpha_{\mathbf{p-q},\downarrow} \alpha^\dagger_{-\mathbf{k-q},\downarrow} \rangle}{\epsilon^\uparrow_{\mathbf{k+q}} + \epsilon^\downarrow_{\mathbf{p-q}} - \epsilon^\uparrow_{\mathbf{k}} - \epsilon^\downarrow_{\mathbf{p}}} \quad + \text{ c.c.}$$

$$+ g^2 \sum_{\mathbf{k},\mathbf{p},\mathbf{q}} |v_{\mathbf{p-q}}|^2 \frac{\langle \alpha^\dagger_{\mathbf{k+q},\uparrow} \alpha_{-\mathbf{p+q},\uparrow} \alpha_{\mathbf{p},\downarrow} \alpha_{\mathbf{k},\uparrow} \alpha^\dagger_{\mathbf{k},\uparrow} \alpha^\dagger_{\mathbf{p},\downarrow} \alpha^\dagger_{-\mathbf{p+q},\uparrow} \alpha_{\mathbf{k+q},\uparrow} \rangle}{\epsilon^\uparrow_{\mathbf{k+q}} + \epsilon^\downarrow_{\mathbf{p-q}} - \epsilon^\uparrow_{\mathbf{k}} - \epsilon^\downarrow_{\mathbf{p}}} \quad + \text{ c.c.}$$

$$+ g^2 \sum_{\mathbf{k},\mathbf{p},\mathbf{q}} |v_{\mathbf{p}}|^2 \frac{\langle \alpha^\dagger_{\mathbf{k+q},\uparrow} \alpha^\dagger_{\mathbf{p-q},\downarrow} \alpha^\dagger_{-\mathbf{p},\uparrow} \alpha_{\mathbf{k},\uparrow} \alpha^\dagger_{\mathbf{k},\uparrow} \alpha_{-\mathbf{p},\uparrow} \alpha_{\mathbf{p-q},\downarrow} \alpha_{\mathbf{k+q},\uparrow} \rangle}{\epsilon^\uparrow_{\mathbf{k+q}} + \epsilon^\downarrow_{\mathbf{p-q}} - \epsilon^\uparrow_{\mathbf{k}} - \epsilon^\downarrow_{\mathbf{p}}} \quad + \text{ c.c.}$$

$$+ g^2 \sum_{\mathbf{k},\mathbf{p},\mathbf{q}} |v_{\mathbf{k}}|^2 \frac{\langle \alpha^\dagger_{\mathbf{k+q},\uparrow} \alpha^\dagger_{\mathbf{p-q},\downarrow} \alpha_{\mathbf{p},\downarrow} \alpha^\dagger_{-\mathbf{k},\downarrow} \alpha_{-\mathbf{k},\downarrow} \alpha^\dagger_{\mathbf{p},\downarrow} \alpha_{\mathbf{p-q},\downarrow} \alpha_{\mathbf{k+q},\uparrow} \rangle}{\epsilon^\uparrow_{\mathbf{k+q}} + \epsilon^\downarrow_{\mathbf{p-q}} - \epsilon^\uparrow_{\mathbf{k}} - \epsilon^\downarrow_{\mathbf{p}}} \quad + \text{ c.c.}$$

$$+ g^2 \sum_{\mathbf{k},\mathbf{p},\mathbf{q}} v^*_{\mathbf{k+q}} v_{\mathbf{p}} \frac{\langle \alpha_{-\mathbf{k-q},\downarrow} \alpha^\dagger_{\mathbf{p-q},\downarrow} \alpha_{\mathbf{p},\downarrow} \alpha_{\mathbf{k},\uparrow} \alpha^\dagger_{\mathbf{k},\uparrow} \alpha^\dagger_{-\mathbf{k+q},\downarrow} \alpha_{\mathbf{p-q},\downarrow} \alpha^\dagger_{\mathbf{p},\downarrow} \rangle}{\epsilon^\uparrow_{\mathbf{k+q}} + \epsilon^\downarrow_{\mathbf{p-q}} - \epsilon^\uparrow_{\mathbf{k}} - \epsilon^\downarrow_{\mathbf{p}}} \quad + \text{ c.c.}$$

$$+ g^2 \sum_{\mathbf{k},\mathbf{p},\mathbf{q}} v^*_{\mathbf{p-q}} v_{\mathbf{k}} \frac{\langle \alpha^\dagger_{\mathbf{k+q},\uparrow} \alpha_{-\mathbf{p+q},\uparrow} \alpha_{\mathbf{p},\downarrow} \alpha_{\mathbf{k},\uparrow} \alpha^\dagger_{\mathbf{p-q},\uparrow} \alpha^\dagger_{\mathbf{p},\downarrow} \alpha^\dagger_{\mathbf{k},\uparrow} \alpha_{\mathbf{k+q},\uparrow} \rangle}{\epsilon^\uparrow_{\mathbf{k+q}} + \epsilon^\downarrow_{\mathbf{p-q}} - \epsilon^\uparrow_{\mathbf{k}} - \epsilon^\downarrow_{\mathbf{p}}} \quad + \text{ c.c.}$$

$$+ g^2 \sum_{\mathbf{k},\mathbf{p},\mathbf{q}} v^*_{\mathbf{k+q}} v_{\mathbf{p}} \frac{\langle \alpha^\dagger_{\mathbf{k+q},\uparrow} \alpha^\dagger_{\mathbf{p-q},\downarrow} \alpha^\dagger_{-\mathbf{p},\uparrow} \alpha_{\mathbf{k},\uparrow} \alpha^\dagger_{\mathbf{k},\uparrow} \alpha_{\mathbf{k+q},\uparrow} \alpha_{\mathbf{p-q},\downarrow} \alpha_{-\mathbf{p},\uparrow} \rangle}{\epsilon^\uparrow_{\mathbf{k+q}} + \epsilon^\downarrow_{\mathbf{p-q}} - \epsilon^\uparrow_{\mathbf{k}} - \epsilon^\downarrow_{\mathbf{p}}} \quad + \text{ c.c.}$$

$$+ g^2 \sum_{\mathbf{k},\mathbf{p},\mathbf{q}} v^*_{\mathbf{p-q}} v_{\mathbf{k}} \frac{\langle \alpha^\dagger_{\mathbf{k+q},\uparrow} \alpha^\dagger_{\mathbf{p-q},\downarrow} \alpha_{\mathbf{p},\downarrow} \alpha^\dagger_{-\mathbf{k},\downarrow} \alpha_{\mathbf{p-q},\downarrow} \alpha^\dagger_{\mathbf{p},\downarrow} \alpha_{-\mathbf{k},\downarrow} \alpha_{\mathbf{k+q},\uparrow} \rangle}{\epsilon^\uparrow_{\mathbf{k+q}} + \epsilon^\downarrow_{\mathbf{p-q}} - \epsilon^\uparrow_{\mathbf{k}} - \epsilon^\downarrow_{\mathbf{p}}} \quad + \text{ c.c.}$$

$$\underbrace{\phantom{+ g^2 \sum_{\mathbf{k},\mathbf{p},\mathbf{q}} v^*_{\mathbf{p-q}} v_{\mathbf{k}}}}_{\textbf{B. } \text{pairs of } \mathcal{H}_{int} \text{ perturbed to linear order in } \Delta}$$

$$- g^2 \sum_{\mathbf{k},\mathbf{p},\mathbf{q}} v^*_{\mathbf{k+q}} v_{\mathbf{p}} \frac{\langle \alpha_{-\mathbf{k-q},\downarrow} \alpha^\dagger_{\mathbf{p-q},\downarrow} \alpha^\dagger_{-\mathbf{p},\uparrow} \alpha_{\mathbf{k},\uparrow} \alpha^\dagger_{\mathbf{k},\uparrow} \alpha^\dagger_{-\mathbf{k-q},\downarrow} \alpha_{\mathbf{p-q},\downarrow} \alpha_{-\mathbf{p},\uparrow} \rangle}{\epsilon^\uparrow_{\mathbf{k+q}} + \epsilon^\downarrow_{\mathbf{p-q}} - \epsilon^\uparrow_{\mathbf{k}} - \epsilon^\downarrow_{\mathbf{p}}} \quad + \text{ c.c.}$$

$$- g^2 \sum_{\mathbf{k},\mathbf{p},\mathbf{q}} v^*_{\mathbf{p-q}} v_{\mathbf{k}} u^*_{\mathbf{k}} \frac{\langle \alpha^\dagger_{\mathbf{k+q},\uparrow} \alpha_{-\mathbf{p+q},\uparrow} \alpha_{\mathbf{p},\downarrow} \alpha^\dagger_{-\mathbf{k},\downarrow} \alpha^\dagger_{-\mathbf{p+q},\uparrow} \alpha^\dagger_{\mathbf{p},\downarrow} \alpha_{-\mathbf{k},\downarrow} \alpha_{\mathbf{k+q},\uparrow} \rangle}{\epsilon^\uparrow_{\mathbf{k+q}} + \epsilon^\downarrow_{\mathbf{p-q}} - \epsilon^\uparrow_{\mathbf{k}} - \epsilon^\downarrow_{\mathbf{p}}} \quad + \text{ c.c.}$$

$$- g^2 \sum_{\mathbf{k},\mathbf{p},\mathbf{q}} v^*_{\mathbf{p-q}} v_{\mathbf{k}} \frac{\langle \alpha^\dagger_{\mathbf{k+q},\uparrow} \alpha^\dagger_{\mathbf{p-q},\downarrow} \alpha_{\mathbf{p},\downarrow} \alpha_{\mathbf{k},\uparrow} \alpha_{\mathbf{p-q},\downarrow} \alpha^\dagger_{\mathbf{p},\downarrow} \alpha^\dagger_{\mathbf{k},\uparrow} \alpha_{\mathbf{k+q},\uparrow} \rangle}{\epsilon^\uparrow_{\mathbf{k+q}} + \epsilon^\downarrow_{\mathbf{p-q}} - \epsilon^\uparrow_{\mathbf{k}} - \epsilon^\downarrow_{\mathbf{p}}} \quad + \text{ c.c.}$$

$$- g^2 \sum_{\mathbf{k},\mathbf{p},\mathbf{q}} v^*_{\mathbf{k+q}} v_{\mathbf{p}} \frac{\langle \alpha^\dagger_{\mathbf{k+q},\uparrow} \alpha^\dagger_{\mathbf{p-q},\downarrow} \alpha_{\mathbf{p},\downarrow} \alpha_{\mathbf{k},\uparrow} \alpha^\dagger_{\mathbf{k},\uparrow} \alpha_{\mathbf{k+q},\uparrow} \alpha_{\mathbf{p-q},\downarrow} \alpha^\dagger_{\mathbf{p},\downarrow} \rangle}{\epsilon^\uparrow_{\mathbf{k+q}} + \epsilon^\downarrow_{\mathbf{p-q}} - \epsilon^\uparrow_{\mathbf{k}} - \epsilon^\downarrow_{\mathbf{p}}} \quad + \text{ c.c.,} \tag{6.22}$$

$$\underbrace{\phantom{- g^2 \sum_{\mathbf{k},\mathbf{p},\mathbf{q}} v^*_{\mathbf{k+q}} v_{\mathbf{p}}}}_{\textbf{C. } \text{pairs of the regular } \mathcal{H}_{int} \text{ contracted with } \mathcal{H}_{int} \text{ quadratic in } \Delta}$$

where we have used $u_{\mathbf{k}} = u_{-\mathbf{k}}$ and $v_{\mathbf{k}} = v_{-\mathbf{k}}$. Since the matrix elements, $u_{\mathbf{k}}$ and $v_{\mathbf{k}}$, are functions of the superconducting order parameter their symmetry is determined by the d-wave form factors, which are time-reversal symmetric.

Next, we explicitly evaluate the expectation over the Bogoliubov operators by forming Fermi distribution functions, $\langle \alpha_{\mathbf{k},\sigma}^{\dagger} \alpha_{\mathbf{k},\sigma} \rangle = f_{\mathbf{k}}^{\sigma}$. Furthermore, we substitute for u and v, keeping terms to order $|\Delta|^2$. The results of these contractions is

$$\mathcal{F}_{\text{fluct}}(\Delta) =$$

$$- 2g^2 \sum_{\mathbf{k},\mathbf{p},\mathbf{q}} \left(\frac{|\Delta_{\mathbf{k}+\mathbf{q}}|^2}{(\xi_{\mathbf{k}+\mathbf{q}}^{\uparrow} + \xi_{-\mathbf{k}-\mathbf{q}}^{\downarrow})^2} + \frac{|\Delta_{\mathbf{p}-\mathbf{q}}|^2}{(\xi_{\mathbf{p}-\mathbf{q}}^{\uparrow} + \xi_{-\mathbf{p}+\mathbf{q}}^{\downarrow})^2} + \frac{|\Delta_{\mathbf{p}}|^2}{(\xi_{\mathbf{p}}^{\uparrow} + \xi_{-\mathbf{p}}^{\downarrow})^2} + \frac{|\Delta_{\mathbf{k}}|^2}{(\xi_{\mathbf{k}}^{\uparrow} + \xi_{-\mathbf{k}}^{\downarrow})^2} \right)$$

$$\times \underbrace{\frac{f_{\mathbf{k}+\mathbf{q},\uparrow} f_{\mathbf{p}-\mathbf{q},\downarrow}(1 - f_{\mathbf{p},\downarrow})(1 - f_{\mathbf{k},\uparrow})}{\epsilon_{\mathbf{k}+\mathbf{q}}^{\uparrow} + \epsilon_{\mathbf{p}-\mathbf{q}}^{\downarrow} - \epsilon_{\mathbf{k}}^{\uparrow} - \epsilon_{\mathbf{p}}^{\downarrow}}}_{\textbf{A. regular contribution}}$$

$$+ 2g^2 \sum_{\mathbf{k},\mathbf{p},\mathbf{q}} \frac{|\Delta_{\mathbf{k}+\mathbf{q}}|^2}{(\xi_{\mathbf{k}+\mathbf{q}}^{\uparrow} + \xi_{-\mathbf{k}-\mathbf{q}}^{\downarrow})^2} \frac{(1 - f_{-\mathbf{k}-\mathbf{q},\downarrow}) f_{\mathbf{p}-\mathbf{q},\downarrow}(1 - f_{\mathbf{p},\downarrow})(1 - f_{\mathbf{k},\uparrow})}{\epsilon_{\mathbf{k}+\mathbf{q}}^{\uparrow} + \epsilon_{\mathbf{p}-\mathbf{q}}^{\downarrow} - \epsilon_{\mathbf{k}}^{\uparrow} - \epsilon_{\mathbf{p}}^{\downarrow}}$$

$$+ 2g^2 \sum_{\mathbf{k},\mathbf{p},\mathbf{q}} \frac{|\Delta_{\mathbf{p}-\mathbf{q}}|^2}{(\xi_{\mathbf{p}-\mathbf{q}}^{\uparrow} + \xi_{-\mathbf{p}+\mathbf{q}}^{\downarrow})^2} \frac{f_{\mathbf{k}+\mathbf{q},\uparrow}(1 - f_{-\mathbf{p}+\mathbf{q},\uparrow})(1 - f_{\mathbf{p},\downarrow})(1 - f_{\mathbf{k},\uparrow})}{\epsilon_{\mathbf{k}+\mathbf{q}}^{\uparrow} + \epsilon_{\mathbf{p}-\mathbf{q}}^{\downarrow} - \epsilon_{\mathbf{k}}^{\uparrow} - \epsilon_{\mathbf{p}}^{\downarrow}}$$

$$+ 2g^2 \sum_{\mathbf{k},\mathbf{p},\mathbf{q}} \frac{|\Delta_{\mathbf{p}}|^2}{(\xi_{\mathbf{p}}^{\uparrow} + \xi_{-\mathbf{p}}^{\downarrow})^2} \frac{f_{\mathbf{k}+\mathbf{q},\uparrow} f_{\mathbf{p}-\mathbf{q},\downarrow} f_{-\mathbf{p},\uparrow}(1 - f_{\mathbf{k},\uparrow})}{\epsilon_{\mathbf{k}+\mathbf{q}}^{\uparrow} + \epsilon_{\mathbf{p}-\mathbf{q}}^{\downarrow} - \epsilon_{\mathbf{k}}^{\uparrow} - \epsilon_{\mathbf{p}}^{\downarrow}}$$

$$+ 2g^2 \sum_{\mathbf{k},\mathbf{p},\mathbf{q}} \frac{|\Delta_{\mathbf{k}}|^2}{(\xi_{\mathbf{k}}^{\uparrow} + \xi_{-\mathbf{k}}^{\downarrow})^2} \frac{f_{\mathbf{k}+\mathbf{q},\uparrow} f_{\mathbf{p}-\mathbf{q},\downarrow}(1 - f_{\mathbf{p},\downarrow}) f_{-\mathbf{k},\downarrow}}{\epsilon_{\mathbf{k}+\mathbf{q}}^{\uparrow} + \epsilon_{\mathbf{p}-\mathbf{q}}^{\downarrow} - \epsilon_{\mathbf{k}}^{\uparrow} - \epsilon_{\mathbf{p}}^{\downarrow}}$$

$$+ g^2 \sum_{\mathbf{k},\mathbf{p},\mathbf{q}} \frac{\bar{\Delta}_{\mathbf{k}+\mathbf{q}}}{\xi_{\mathbf{k}+\mathbf{q}}^{\uparrow} + \xi_{-\mathbf{k}-\mathbf{q}}^{\downarrow}} \frac{\Delta_{\mathbf{p}}}{\xi_{\mathbf{p}}^{\uparrow} + \xi_{-\mathbf{p}}^{\downarrow}} \frac{(1 - f_{-\mathbf{k}-\mathbf{q},\downarrow}) f_{\mathbf{p}-\mathbf{q},\downarrow}(1 - f_{\mathbf{p},\downarrow})(1 - f_{\mathbf{k},\uparrow})}{\epsilon_{\mathbf{k}+\mathbf{q}}^{\uparrow} + \epsilon_{\mathbf{p}-\mathbf{q}}^{\downarrow} - \epsilon_{\mathbf{k}}^{\uparrow} - \epsilon_{\mathbf{p}}^{\downarrow}} \quad + \quad \text{c.c.}$$

$$+ g^2 \sum_{\mathbf{k},\mathbf{p},\mathbf{q}} \frac{\bar{\Delta}_{\mathbf{p}-\mathbf{q}}}{\xi_{\mathbf{p}-\mathbf{q}}^{\uparrow} + \xi_{-\mathbf{p}+\mathbf{q}}^{\downarrow}} \frac{\Delta_{\mathbf{k}}}{\xi_{\mathbf{k}}^{\uparrow} + \xi_{-\mathbf{k}}^{\downarrow}} \frac{f_{\mathbf{k}+\mathbf{q},\uparrow}(1 - f_{-\mathbf{p}+\mathbf{q},\uparrow})(1 - f_{\mathbf{p},\downarrow})(1 - f_{\mathbf{k},\uparrow})}{\epsilon_{\mathbf{k}+\mathbf{q}}^{\uparrow} + \epsilon_{\mathbf{p}-\mathbf{q}}^{\downarrow} - \epsilon_{\mathbf{k}}^{\uparrow} - \epsilon_{\mathbf{p}}^{\downarrow}} \quad + \quad \text{c.c.}$$

$$+ g^2 \sum_{\mathbf{k},\mathbf{p},\mathbf{q}} \frac{\bar{\Delta}_{\mathbf{k}+\mathbf{q}}}{\xi_{\mathbf{k}+\mathbf{q}}^{\uparrow} + \xi_{-\mathbf{k}-\mathbf{q}}^{\downarrow}} \frac{\Delta_{\mathbf{p}}}{\xi_{\mathbf{p}}^{\uparrow} + \xi_{-\mathbf{p}}^{\downarrow}} \frac{f_{\mathbf{k}+\mathbf{q},\uparrow} f_{\mathbf{p}-\mathbf{q},\downarrow} f_{-\mathbf{p},\uparrow}(1 - f_{\mathbf{k},\uparrow})}{\epsilon_{\mathbf{k}+\mathbf{q}}^{\uparrow} + \epsilon_{\mathbf{p}-\mathbf{q}}^{\downarrow} - \epsilon_{\mathbf{k}}^{\uparrow} - \epsilon_{\mathbf{p}}^{\downarrow}} \quad + \quad \text{c.c.}$$

$$+ g^2 \sum_{\mathbf{k},\mathbf{p},\mathbf{q}} \frac{\bar{\Delta}_{\mathbf{p}-\mathbf{q}}}{\xi_{\mathbf{p}-\mathbf{q}}^{\uparrow} + \xi_{-\mathbf{p}+\mathbf{q}}^{\downarrow}} \frac{\Delta_{\mathbf{k}}}{\xi_{\mathbf{k}}^{\uparrow} + \xi_{-\mathbf{k}}^{\downarrow}} \frac{f_{\mathbf{k}+\mathbf{q},\uparrow} f_{\mathbf{p}-\mathbf{q},\downarrow}(1 - f_{\mathbf{p},\downarrow}) f_{-\mathbf{k},\downarrow}}{\epsilon_{\mathbf{k}+\mathbf{q}}^{\uparrow} + \epsilon_{\mathbf{p}-\mathbf{q}}^{\downarrow} - \epsilon_{\mathbf{k}}^{\uparrow} - \epsilon_{\mathbf{p}}^{\downarrow}} \quad + \quad \text{c.c.}$$

$$\underbrace{\phantom{+ g^2 \sum_{\mathbf{k},\mathbf{p},\mathbf{q}}}}_{\textbf{B. pairs of } \mathcal{H}_{int} \text{ perturbed to linear order in } \Delta}$$

$$-g^2 \sum_{\mathbf{k},\mathbf{p},\mathbf{q}} \frac{\bar{\Delta}_{\mathbf{k}+\mathbf{q}}}{\xi^{\uparrow}_{\mathbf{k}+\mathbf{q}} + \xi^{\downarrow}_{-\mathbf{k}-\mathbf{q}}} \frac{\Delta_{\mathbf{p}}}{\xi^{\uparrow}_{\mathbf{p}} + \xi^{\downarrow}_{-\mathbf{p}}} \frac{(1 - f_{-\mathbf{k}-\mathbf{q},\downarrow}) f_{\mathbf{p}-\mathbf{q},\downarrow} f_{-\mathbf{p},\uparrow} (1 - f_{\mathbf{k},\uparrow})}{\epsilon^{\uparrow}_{\mathbf{k}+\mathbf{q}} + \epsilon^{\downarrow}_{\mathbf{p}-\mathbf{q}} - \epsilon^{\uparrow}_{\mathbf{k}} - \epsilon^{\downarrow}_{\mathbf{p}}} \quad + \quad \text{c.c.}$$

$$-g^2 \sum_{\mathbf{k},\mathbf{p},\mathbf{q}} \frac{\bar{\Delta}_{\mathbf{p}-\mathbf{q}}}{\xi^{\uparrow}_{\mathbf{p}-\mathbf{q}} + \xi^{\downarrow}_{-\mathbf{p}+\mathbf{q}}} \frac{\Delta_{\mathbf{k}}}{\xi^{\uparrow}_{\mathbf{k}} + \xi^{\downarrow}_{-\mathbf{k}}} \frac{f_{\mathbf{k}+\mathbf{q},\uparrow} (1 - f_{-\mathbf{p}+\mathbf{q},\uparrow})(1 - f_{\mathbf{p},\downarrow}) f_{-\mathbf{k},\downarrow}}{\epsilon^{\uparrow}_{\mathbf{k}+\mathbf{q}} + \epsilon^{\downarrow}_{\mathbf{p}-\mathbf{q}} - \epsilon^{\uparrow}_{\mathbf{k}} - \epsilon^{\downarrow}_{\mathbf{p}}} \quad + \quad \text{c.c.}$$

$$-g^2 \sum_{\mathbf{k},\mathbf{p},\mathbf{q}} \frac{\bar{\Delta}_{\mathbf{p}-\mathbf{q}}}{\xi^{\uparrow}_{\mathbf{p}-\mathbf{q}} + \xi^{\downarrow}_{-\mathbf{p}+\mathbf{q}}} \frac{\Delta_{\mathbf{k}}}{\xi^{\uparrow}_{\mathbf{k}} + \xi^{\downarrow}_{-\mathbf{k}}} \frac{f_{\mathbf{k}+\mathbf{q},\uparrow} f_{\mathbf{p}-\mathbf{q},\downarrow} (1 - f_{\mathbf{p},\downarrow})(1 - f_{\mathbf{k},\uparrow})}{\epsilon^{\uparrow}_{\mathbf{k}+\mathbf{q}} + \epsilon^{\downarrow}_{\mathbf{p}-\mathbf{q}} - \epsilon^{\uparrow}_{\mathbf{k}} - \epsilon^{\downarrow}_{\mathbf{p}}} \quad + \quad \text{c.c.}$$

$$-g^2 \sum_{\mathbf{k},\mathbf{p},\mathbf{q}} \frac{\bar{\Delta}_{\mathbf{k}+\mathbf{q}}}{\xi^{\uparrow}_{\mathbf{k}+\mathbf{q}} + \xi^{\downarrow}_{-\mathbf{k}-\mathbf{q}}} \frac{\Delta_{\mathbf{p}}}{\xi^{\uparrow}_{\mathbf{p}} + \xi^{\downarrow}_{-\mathbf{p}}} \frac{f_{\mathbf{k}+\mathbf{q},\uparrow} f_{\mathbf{p}-\mathbf{q},\downarrow} (1 - f_{\mathbf{p},\downarrow})(1 - f_{\mathbf{k},\uparrow})}{\epsilon^{\uparrow}_{\mathbf{k}+\mathbf{q}} + \epsilon^{\downarrow}_{\mathbf{p}-\mathbf{q}} - \epsilon^{\uparrow}_{\mathbf{k}} - \epsilon^{\downarrow}_{\mathbf{p}}} \quad + \quad \text{c.c.} \qquad (6.23)$$

C. pairs of the regular $\mathcal{H}_{int}$ contracted with $\mathcal{H}_{int}$ quadratic in Δ

These terms are given by all possible contractions of vertices formed from the Bogoliubov transformation of the original creation and annihilation operators. Again we draw Feynman diagrams for each of the first terms in each block of terms.
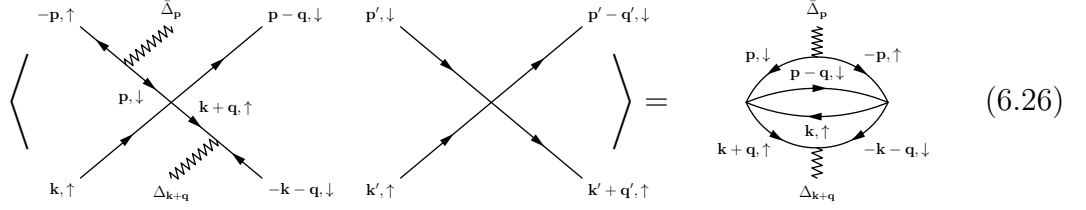
A. Regular term:

$$(6.24)$$

B. Next let us take a look at the diagrams corresponding to the first term of the contribution with both vertices linear in Δ. These terms can be contracted in two ways each. We can either form a susceptibility or self-energy like term (first and second diagram in (6.25) respectively):

$$(6.25)$$

C. Finally, we draw the diagram for the first term of the contribution from a regular vertex contracted with one quadratic in Δ. Here, there is only one possible pairing

of operators forming susceptibility terms:

$$\left\langle \quad \right\rangle = \tag{6.26}$$

We may further simplify the fluctuation corrections by shifting momentum labels and collecting terms:

$$\mathcal{F}_{\text{fluct}}(\Delta) =$$

$$2g^2 \sum_{\mathbf{k,p,q}} |\Delta_\mathbf{k}|^2 \frac{1 - f_\mathbf{k}^\uparrow - f_{-\mathbf{k}}^\downarrow}{(\xi_{\mathbf{k},\uparrow} + \xi_{-\mathbf{k},\downarrow})^2} \left[\frac{f_\mathbf{p}^\downarrow(1 - f_{\mathbf{k+q}}^\uparrow)(1 - f_{\mathbf{p-q}}^\downarrow) + (1 - f_\mathbf{p}^\downarrow)f_{\mathbf{k+q}}^\uparrow f_{\mathbf{p-q}}^\downarrow}{\epsilon_\mathbf{k}^\uparrow + \epsilon_\mathbf{p}^\downarrow - \epsilon_{\mathbf{k+q}}^\uparrow - \epsilon_{\mathbf{p-q}}^\downarrow} \right]$$

$$+ 2g^2 \sum_{\mathbf{k,p,q}} |\Delta_\mathbf{p}|^2 \frac{1 - f_\mathbf{p}^\downarrow - f_{-\mathbf{p}}^\uparrow}{(\xi_{-\mathbf{p},\uparrow} + \xi_{\mathbf{p},\downarrow})^2} \left[\frac{f_\mathbf{k}^\uparrow(1 - f_{\mathbf{k+q}}^\uparrow)(1 - f_{\mathbf{p-q}}^\downarrow) + (1 - f_\mathbf{k}^\downarrow)f_{\mathbf{k+q}}^\uparrow f_{\mathbf{p-q}}^\downarrow}{\epsilon_\mathbf{k}^\uparrow + \epsilon_\mathbf{p}^\downarrow - \epsilon_{\mathbf{k+q}}^\uparrow - \epsilon_{\mathbf{p-q}}^\downarrow} \right]$$

$$+ g^2 \sum_{\mathbf{k,p,q}} \bar{\Delta}_{\mathbf{k+q}} \frac{1 - f_{\mathbf{k+q}}^\uparrow - f_{-\mathbf{k-q}}^\downarrow}{(\xi_{\mathbf{k+q},\uparrow} + \xi_{-\mathbf{k-q},\downarrow})} \Delta_\mathbf{p} \frac{1 - f_{-\mathbf{p}}^\uparrow - f_\mathbf{p}^\downarrow}{(\xi_{-\mathbf{p},\uparrow} + \xi_{\mathbf{p},\downarrow})} \frac{f_{\mathbf{p-q}}^\downarrow(1 - f_\mathbf{k}^\uparrow)}{\epsilon_{\mathbf{k+q}}^\uparrow + \epsilon_{\mathbf{p-q}}^\downarrow - \epsilon_\mathbf{k}^\uparrow - \epsilon_\mathbf{p}^\downarrow} \quad + \text{ c.c.}$$

$$+ g^2 \sum_{\mathbf{k,p,q}} \bar{\Delta}_{\mathbf{p-q}} \frac{1 - f_{-\mathbf{p+q}}^\uparrow - f_{\mathbf{p-q}}^\downarrow}{(\xi_{-\mathbf{p+q},\uparrow} + \xi_{\mathbf{p-q},\downarrow})} \Delta_\mathbf{k} \frac{1 - f_\mathbf{k}^\uparrow - f_{-\mathbf{k}}^\downarrow}{(\xi_{\mathbf{k},\uparrow} + \xi_{-\mathbf{k},\downarrow})} \frac{f_{\mathbf{k+q}}^\uparrow(1 - f_\mathbf{p}^\downarrow)}{\epsilon_{\mathbf{k+q}}^\uparrow + \epsilon_{\mathbf{p-q}}^\downarrow - \epsilon_\mathbf{k}^\uparrow - \epsilon_\mathbf{p}^\downarrow} \quad + \text{ c.c..}$$

$$\tag{6.27}$$

After shifting momentum labels in the complex conjugate terms:

$$\mathcal{F}_{fluct}(\Delta) =$$

$$2g^2 \sum_{\mathbf{k,p,q}} |\Delta_\mathbf{k}|^2 \frac{1 - f_\mathbf{k}^\uparrow - f_{-\mathbf{k}}^\downarrow}{(\xi_{\mathbf{k},\uparrow} + \xi_{-\mathbf{k},\downarrow})^2} \left[\frac{f_\mathbf{p}^\downarrow(1 - f_{\mathbf{k+q}}^\uparrow)(1 - f_{\mathbf{p-q}}^\downarrow) + (1 - f_\mathbf{p}^\downarrow)f_{\mathbf{k+q}}^\uparrow f_{\mathbf{p-q}}^\downarrow}{\epsilon_\mathbf{k}^\uparrow + \epsilon_\mathbf{p}^\downarrow - \epsilon_{\mathbf{k+q}}^\uparrow - \epsilon_{\mathbf{p-q}}^\downarrow} \quad + \uparrow\leftrightarrow\downarrow \right]$$

$$+ g^2 \sum_{\mathbf{k,p,q}} \bar{\Delta}_{\mathbf{k+q}} \frac{1 - f_{\mathbf{k+q}}^\uparrow - f_{-\mathbf{k-q}}^\downarrow}{(\xi_{\mathbf{k+q},\uparrow} + \xi_{-\mathbf{k-q},\downarrow})} \Delta_\mathbf{p} \frac{1 - f_{-\mathbf{p}}^\uparrow - f_\mathbf{p}^\downarrow}{(\xi_{-\mathbf{p},\uparrow} + \xi_{\mathbf{p},\downarrow})} \left[\frac{f_{\mathbf{p-q}}^\downarrow - f_\mathbf{k}^\uparrow}{\epsilon_{\mathbf{k+q}}^\uparrow + \epsilon_{\mathbf{p-q}}^\downarrow - \epsilon_\mathbf{k}^\uparrow - \epsilon_\mathbf{p}^\downarrow} \quad + \uparrow\leftrightarrow\downarrow \right].$$

$$\tag{6.28}$$

Using the standard form of the antiferromagnetic susceptibility, $\chi^{\uparrow\downarrow}$, and electron

self-energy, Σ,

$$\chi_{AF}^{\uparrow\downarrow}(\mathbf{q}, \epsilon_{\mathbf{p}}^{\downarrow} - \epsilon_{\mathbf{p+q}}^{\uparrow}) = \sum_{\mathbf{k}} \frac{f_{\mathbf{k-q}}^{\downarrow} - f_{\mathbf{k}}^{\uparrow}}{\epsilon_{\mathbf{k-q}}^{\downarrow} + \epsilon_{\mathbf{p+q}}^{\uparrow} - \epsilon_{\mathbf{k}}^{\uparrow} - \epsilon_{\mathbf{p}}^{\downarrow}} \tag{6.29}$$

$$\Sigma^{\uparrow}(\mathbf{k}, \epsilon_{\mathbf{k}}) = g^2 \sum_{\mathbf{p,q}} \frac{f_{\mathbf{p}}^{\downarrow}(1 - f_{\mathbf{k+q}}^{\uparrow})(1 - f_{\mathbf{p-q}}^{\downarrow}) + (1 - f_{\mathbf{p}}^{\downarrow})f_{\mathbf{k+q}}^{\uparrow}f_{\mathbf{p-q}}^{\downarrow}}{\epsilon_{\mathbf{k}}^{\uparrow} + \epsilon_{\mathbf{p}}^{\downarrow} - \epsilon_{\mathbf{k+q}}^{\uparrow} - \epsilon_{\mathbf{p-q}}^{\downarrow}}, \tag{6.30}$$

we can rewrite Equation (6.28) as

$$
\begin{aligned}
\mathcal{F}_{fluct}(\Delta) = \\
-\sum_{\mathbf{k}} |\Delta_{\mathbf{k}}|^2 \left(\partial_{\epsilon_{\mathbf{k}}} \frac{1}{(\xi_{\mathbf{k},\uparrow} + \xi_{-\mathbf{k},\downarrow})} \right) \left(1 - f_{\mathbf{k}}^{\uparrow} - f_{-\mathbf{k}}^{\downarrow} \right) \left[\Sigma^{\uparrow}(\mathbf{k}, \epsilon_{\mathbf{k}}) + \Sigma^{\downarrow}(\mathbf{k}, \epsilon_{\mathbf{k}}) \right] \\
+ g^2 \sum_{\mathbf{p,q}} \bar{\Delta}_{\mathbf{p+q}} \frac{1 - f_{\mathbf{p+q}}^{\uparrow} - f_{-\mathbf{p-q}}^{\downarrow}}{(\xi_{\mathbf{p+q},\uparrow} + \xi_{-\mathbf{p-q},\downarrow})} \Delta_{\mathbf{p}} \frac{1 - f_{-\mathbf{p}}^{\uparrow} - f_{\mathbf{p}}^{\downarrow}}{(\xi_{-\mathbf{p},\uparrow} + \xi_{\mathbf{p},\downarrow})} \left[\chi_{AF}^{\uparrow\downarrow}(\mathbf{q}, \epsilon_{\mathbf{p}}^{\downarrow} - \epsilon_{\mathbf{p+q}}^{\uparrow}) + \uparrow\leftrightarrow\downarrow \right].
\end{aligned}
\tag{6.31}
$$

The diagrams corresponding to the spin susceptibility and electron self-energy are given by

$$\chi_{AF}^{\uparrow\downarrow}(\mathbf{q}, \epsilon_{\mathbf{p}}^{\uparrow} - \epsilon_{\mathbf{p+q}}^{\downarrow}) = \tag{6.32}$$

$$\Sigma^{\uparrow}(\mathbf{k}, \epsilon_{\mathbf{k}}) = \tag{6.33}$$

The self-energy-like term may be integrated by parts assuming a constant density of states at the Fermi energy. This allows us to rewrite this term with an energy derivative on the self-energy factor. Including the mean field contribution we may write the formal expression of the free energy of d-wave superconductivity in the

Hubbard model as

$$
\begin{aligned}
\mathcal{F}(\Delta) \;=\;& \mathcal{F}_{MF} + \mathcal{F}_{fluct} = \\
& -T\sum_{\mathbf{k},\sigma} \ln\left(e^{-\xi_{\mathbf{k},\sigma}/T} + 1\right) - \sum_{\mathbf{k}} |\Delta_{\mathbf{k}}|^2 \frac{2f_{\mathbf{k}}-1}{\xi_{\mathbf{k}}} \\
& + \sum_{\mathbf{k}} |\Delta_{\mathbf{k}}|^2 \frac{1 - f^\uparrow_{\mathbf{k}} - f^\downarrow_{-\mathbf{k}}}{(\xi_{\mathbf{k},\uparrow} + \xi_{-\mathbf{k},\downarrow})} \left[\partial_\epsilon \Sigma^\uparrow(\mathbf{k},\epsilon_{\mathbf{k}}) + \partial_\epsilon \Sigma^\downarrow(\mathbf{k},\epsilon_{\mathbf{k}})\right] \\
& + g^2 \sum_{\mathbf{p},\mathbf{q}} \bar{\Delta}_{\mathbf{p}+\mathbf{q}} \frac{1 - f^\uparrow_{\mathbf{p}+\mathbf{q}} - f^\downarrow_{-\mathbf{p}-\mathbf{q}}}{(\xi_{\mathbf{p}+\mathbf{q},\uparrow} + \xi_{-\mathbf{p}-\mathbf{q},\downarrow})} \Delta_{\mathbf{p}} \frac{1 - f^\uparrow_{-\mathbf{p}} - f^\downarrow_{\mathbf{p}}}{(\xi_{-\mathbf{p},\uparrow} + \xi_{\mathbf{p},\downarrow})} \\
& \qquad \left[\chi^{\uparrow\downarrow}_{AF}(\mathbf{q}, \epsilon^\downarrow_{\mathbf{p}} - \epsilon^\uparrow_{\mathbf{p}+\mathbf{q}}) + \chi^{\downarrow\uparrow}_{AF}(\mathbf{q}, \epsilon^\uparrow_{\mathbf{p}} - \epsilon^\downarrow_{\mathbf{p}+\mathbf{q}})\right].
\end{aligned}
\tag{6.34}
$$

6.2.3 Regularising the interaction

Exactly as for Chapters 4 and 5 the Hamiltonian, Equation (6.1), contains an unphysical, singular contribution to the free energy. The regularisation of the interaction to avoid this singularity follows the exact same steps as in Section 5.2.3 by including the first order shift into the definition of the momentum eigenstates.

6.3 *Saddle point equation for d-wave superconducting order*

We may now find the formal expression of the Eliashberg-equation. From the free energy of d-wave superconductivity - Equation (6.34) - we set $\partial_{\Delta_{\mathbf{k}}} \mathcal{F}(\Delta) = 0$ and rearrange to find the saddle point equation;

$$
\bar{\Delta}_{\mathbf{k}} \left(1 + 2\left(\partial_{\epsilon_{\mathbf{k}}} \Sigma'^\uparrow(\mathbf{k},\epsilon_{\mathbf{k}}) + \partial_{\epsilon_{\mathbf{k}}} \Sigma'^\downarrow(\mathbf{k},\epsilon_{\mathbf{k}})\right)\right)
$$

$$
=
$$

$$
g^2 \sum_{\mathbf{q}} \bar{\Delta}_{\mathbf{k}+\mathbf{q}} \frac{f^\uparrow_{\mathbf{k}+\mathbf{q}} + f^\downarrow_{-\mathbf{k}-\mathbf{q}} - 1}{\xi^\uparrow_{\mathbf{k}+\mathbf{q}} + \xi^\downarrow_{-\mathbf{k}-\mathbf{q}}} \left(\chi^{\uparrow\downarrow}(\mathbf{q}, \epsilon^\uparrow_{\mathbf{p}+\mathbf{q}} - \epsilon^\downarrow_{\mathbf{p}}) + \chi^{\downarrow\uparrow}(\mathbf{q}, \epsilon^\downarrow_{\mathbf{p}+\mathbf{q}} - \epsilon^\uparrow_{\mathbf{p}})\right).
\tag{6.35}
$$

6.4 Evaluation of the free energy of d-wave superconducting order

Having derived the formal expression for the free energy of d-wave superconductivity, we now would like to evaluate these integrals.
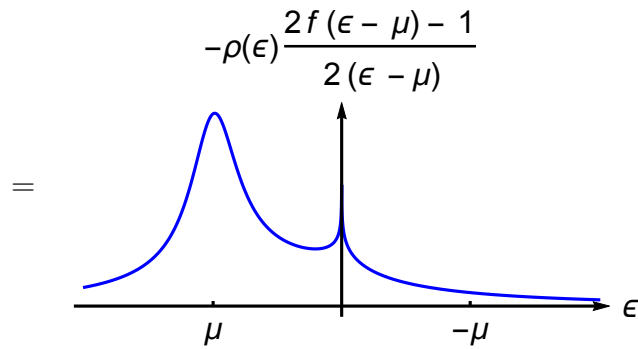
6.4.1 Overview of the calculation

The assumptions and approximations used here are very similar to those in the treatment of the bond density wave in Section 5.4.1. We are interested in the low temperature behaviour of the model close to half filling - temperature is chosen lower than the chemical potential, which in turn is smaller than the band width: $T \ll |\mu| \ll t$.

The common factors in the mean field free energy and fluctuation corrections take the form:

$$\frac{f_{\mathbf{k}}^{\uparrow} + f_{-\mathbf{k}}^{\downarrow} - 1}{\xi_{\mathbf{k}}^{\uparrow} + \xi_{-\mathbf{k}}^{\downarrow}}. \tag{6.36}$$

These terms correspond to the susceptibility to superconducting order. In the absence of antiferromagnetic order the dispersion is spin and and time reversal symmetric and we may simplify these terms to:

$$\frac{f_{\mathbf{k}}^{\uparrow} + f_{-\mathbf{k}}^{\downarrow} - 1}{\xi_{\mathbf{k}}^{\uparrow} + \xi_{-\mathbf{k}}^{\downarrow}} = \frac{2f_{\mathbf{k}} - 1}{2\xi_{\mathbf{k}}} = \frac{2f(\epsilon_{\mathbf{k}} - \mu) - 1}{2(\epsilon_{\mathbf{k}} - \mu)} \tag{6.37}$$

The susceptibility factors are dominated by peaks in the vicinity of $\epsilon = \mu$, whose

width is set by temperature. The secondary peak at $\epsilon = 0$ is sub-leading and vanishes in the limit of $T \to 0$. The height of the peak at $\epsilon = \mu$ is cut off by finite temperature. In particular, for temperatures smaller than the chemical potential, we may treat these factors as weighted delta functions.

$$\frac{f^\uparrow_\mathbf{k} + f^\downarrow_{-\mathbf{k}} - 1}{\xi^\uparrow_\mathbf{k} + \xi^\downarrow_{-\mathbf{k}}} \approx \frac{\delta(\epsilon_\mathbf{k} - \mu)}{\rho(\mu)} \int_{\mu+T}^{4t} d\epsilon \frac{-\rho(\epsilon)}{2(\epsilon - \mu)} \tag{6.38}$$

such that

$$\boxed{\frac{f^\uparrow_\mathbf{k} + f^\downarrow_{-\mathbf{k}} - 1}{\xi^\uparrow_\mathbf{k} + \xi^\downarrow_{-\mathbf{k}}} \approx \frac{1}{2}\delta(\epsilon_\mathbf{k} - \mu) \log\left(\frac{T}{|\mu|}\right)} \, , \tag{6.39}$$

where we inserted the approximate density of states $\rho(\epsilon) = \frac{-1}{2\pi^2 t} \log\left(\frac{|\epsilon|}{4t}\right)$.

Significantly, the superconducting susceptibility is equal to the susceptibility to bond density wave order in the limit of half filling. Then, both of these susceptibilities are peaked at $\mu = 0$ and diverge identically. Formally, the two susceptibilities take the form

Superconductivity:

$$\chi_{SC} = \sum_\mathbf{k} \frac{f(\epsilon_\mathbf{k} - \mu) - f(-\epsilon_\mathbf{k} + \mu)}{2\epsilon_\mathbf{k} - 2\mu} \xrightarrow{\mu \to 0} \sum_\mathbf{k} \frac{f(\epsilon_\mathbf{k}) - f(-\epsilon_\mathbf{k})}{2\epsilon_\mathbf{k}}. \tag{6.40}$$

Bond density wave:

$$\chi_{BDW} = \sum_\mathbf{k} \frac{f(\epsilon_\mathbf{k} - \mu) - f(\epsilon_{\mathbf{k}+\mathbf{Q}} - \mu)}{\epsilon_\mathbf{k} - \epsilon_{\mathbf{k}+\mathbf{Q}}} \xrightarrow[\mathbf{Q} \to (\pi,\pi)]{\mu \to 0} \sum_\mathbf{k} \frac{f(\epsilon_\mathbf{k}) - f(-\epsilon_\mathbf{k})}{2\epsilon_\mathbf{k}}, \tag{6.41}$$

where we have used that $\epsilon_{\mathbf{k}+\mathbf{Q}} = -\epsilon_\mathbf{k}$ in the limit of $\mathbf{Q} \to (\pi, \pi)$.

Additionally, this similarity between the two orders can be seen in the definitions of their pairings. Since the model is particle-hole symmetric at half filling, the order parameters of these two phases may be mapped to one another by a particle hole transformation. Thus in the limit of half filling bond density wave order and superconductivity become degenerate as noted by Metlitski and Sachdev [71].

This particle-hole symmetry is broken in the presence of a finite chemical poten-

tial. In the case of bond density wave order, the finite chemical potential cuts off the divergent susceptibility. However, for superconductivity the finite chemical potential is not able to cut off this divergence. Instead, finite temperature controls the logarithmic singularity. Thus, at low temperatures, the model is always more susceptible to forming superconductivity than bond density wave order.

For convenience we split the free energy into various parts that we calculate separately. The free energy as derived in Sections 6.1 and 6.2 separated into its parts is

$$\mathcal{F}(\Delta) = \mathcal{F}_{MF} + \underbrace{\delta\mathcal{F}_{\chi_{AF}^{\uparrow\downarrow}} + \delta\mathcal{F}_{\Sigma}}_{\mathcal{F}_{fluct}}, \tag{6.42}$$

with

$$\mathcal{F}_{MF} = -T \sum_{\mathbf{k},\sigma} \ln\left(e^{-\xi_{\mathbf{k},\sigma}/T} + 1\right) - \sum_{\mathbf{k}} |\Delta_{\mathbf{k}}|^2 \frac{2f_{\mathbf{k}} - 1}{\xi_{\mathbf{k}}} \tag{6.43}$$

$$\delta\mathcal{F}_{\chi_{AF}^{\uparrow\downarrow}} = 2g^2 \sum_{\mathbf{p},\mathbf{q}} \bar{\Delta}_{\mathbf{p}+\mathbf{q}} \frac{1 - f_{\mathbf{p}+\mathbf{q}}^{\uparrow} - f_{-\mathbf{p}-\mathbf{q}}^{\downarrow}}{(\xi_{\mathbf{p}+\mathbf{q},\uparrow} + \xi_{-\mathbf{p}-\mathbf{q},\downarrow})} \Delta_{\mathbf{p}} \frac{1 - f_{-\mathbf{p}}^{\uparrow} - f_{\mathbf{p}}^{\downarrow}}{(\xi_{-\mathbf{p},\uparrow} + \xi_{\mathbf{p},\downarrow})} \chi_{AF}^{\uparrow\downarrow}(\mathbf{q}, \epsilon_{\mathbf{p}}^{\downarrow} - \epsilon_{\mathbf{p}+\mathbf{q}}^{\uparrow}) \tag{6.44}$$

$$\delta\mathcal{F}_{\Sigma} = 2 \sum_{\mathbf{k}} |\Delta_{\mathbf{k}}|^2 \frac{1 - f_{\mathbf{k}}^{\uparrow} - f_{-\mathbf{k}}^{\downarrow}}{(\xi_{\mathbf{k},\uparrow} + \xi_{-\mathbf{k},\downarrow})} \partial_\epsilon \Sigma^{\uparrow}(\mathbf{k}, \epsilon_{\mathbf{k}}). \tag{6.45}$$

We will first analyse the mean field contributions and then the fluctuation contributions, which in turn will treated term by term.

6.4.2 Evaluation of mean field contribution

The simplest term is the mean field contribution,

$$\mathcal{F}_{MF}(\Delta) = -T \sum_{\mathbf{k},\sigma} \ln\left(e^{-\xi_{\mathbf{k},\sigma}/T} + 1\right) - \sum_{\mathbf{k}} |\Delta_{\mathbf{k}}|^2 \frac{2f_{\mathbf{k}} - 1}{\xi_{\mathbf{k}}} \tag{6.46}$$

To quadratic order, using $\Delta_{\mathbf{k}} = \Delta\theta_{\mathbf{k}}$ and $\xi_{\mathbf{k}}^{\sigma} = \sigma\sqrt{(\epsilon_{\mathbf{k}} - \mu)^2 + |\Delta_{\mathbf{k}}|^2}$, this takes the form

$$\partial_{|\Delta|^2}\mathcal{F}_{MF}(\Delta)|_{\Delta=0} = -\sum_{\mathbf{k}} |\theta_{\mathbf{k}}|^2 \frac{2f_{\mathbf{k}} - 1}{2\xi_{\mathbf{k}}} \tag{6.47}$$

This is same as the superconducting susceptibility that was evaluated previously in (6.39), such that

$$\partial_{|\Delta|^2}\mathcal{F}_{MF}(\Delta)|_{\Delta=0} = -\frac{1}{2}\langle\langle|\theta_{\mathbf{k}}|^2\rangle\rangle\rho(\mu)\log\left(\frac{T}{|\mu|}\right), \tag{6.48}$$

where $\langle|\theta_{\mathbf{k}}|^2\rangle$ denotes the angular average over the Fermi surface of the d-wave factor squared.

This Landau coefficient is positive, so we conclude, that there is no mean field drive to a second order transition to d-wave superconductivity.

6.4.3 Evaluation of fluctuation contribution

Next, we will calculate the fluctuation terms.

Evaluation of the $\delta\mathcal{F}_{\chi^{\uparrow\downarrow}}$

Let us start with the $\chi^{\uparrow\downarrow}$ term:

$$\delta\mathcal{F}_{\chi^{\uparrow\downarrow}} = 2g^2\sum_{\mathbf{p},\mathbf{q}}\bar{\Delta}_{\mathbf{p}+\mathbf{q}}\frac{1-f^{\uparrow}_{\mathbf{p}+\mathbf{q}}-f^{\downarrow}_{-\mathbf{p}-\mathbf{q}}}{(\xi_{\mathbf{p}+\mathbf{q},\uparrow}+\xi_{-\mathbf{p}-\mathbf{q},\downarrow})}\Delta_{\mathbf{p}}\frac{1-f^{\uparrow}_{-\mathbf{p}}-f^{\downarrow}_{\mathbf{p}}}{(\xi_{-\mathbf{p},\uparrow}+\xi_{\mathbf{p},\downarrow})}\chi^{\uparrow\downarrow}_{AF}(\mathbf{q},\epsilon^{\downarrow}_{\mathbf{p}}-\epsilon^{\uparrow}_{\mathbf{p}+\mathbf{q}}), \tag{6.49}$$

where the pairing function is

$$\chi^{\uparrow\downarrow}_{AF}(\mathbf{q},\epsilon^{\downarrow}_{\mathbf{p}}-\epsilon^{\uparrow}_{\mathbf{p}+\mathbf{q}}) = \sum_{\mathbf{k}}\frac{f^{\downarrow}_{\mathbf{k}-\mathbf{q}}-f^{\uparrow}_{\mathbf{k}}}{\epsilon^{\downarrow}_{\mathbf{k}-\mathbf{q}}+\epsilon^{\uparrow}_{\mathbf{p}+\mathbf{q}}-\epsilon^{\uparrow}_{\mathbf{k}}-\epsilon^{\downarrow}_{\mathbf{p}}}. \tag{6.50}$$

The presence of two superconducting susceptibility factors allows for significant simplifications:

$$\delta\mathcal{F}_{\chi^{\uparrow\downarrow}} = \frac{g^2}{2}\sum_{\mathbf{p},\mathbf{q}}\rho(\mu)^2\log^2\left(\frac{T}{|\mu|}\right)\bar{\Delta}_{\mathbf{p}+\mathbf{q}}\delta(\epsilon_{\mathbf{p}+\mathbf{q}}-\mu)\Delta_{\mathbf{p}}\delta(\epsilon_{\mathbf{p}}-\mu)\chi^{\uparrow\downarrow}_{AF}(\mathbf{q},\epsilon^{\downarrow}_{\mathbf{p}}-\epsilon^{\uparrow}_{\mathbf{p}+\mathbf{q}}).$$
$$\tag{6.51}$$

These superconducting susceptibilities are only strictly delta-functions at zero temperature, at finite temperature they are peaks of a finite width given by temperature.

We note these peaks are situated along the Fermi surface $\epsilon_\mathbf{p} = \mu$ and a Fermi surface shifted by momentum $\mathbf{q}$, that is $\epsilon_\mathbf{p+q} = \mu$. Hence, the product of susceptibilities only has non-vanishing support if $\epsilon_\mathbf{p} = \epsilon_\mathbf{p+q}$. The trivial case is $\mathbf{q} = \mathbf{0}$. However, this corresponds to a minimum in the pairing function and is therefore not the dominant contribution to superconducting pairing. Instead we may consider the case of non-zero $\mathbf{q}$, corresponding to fluctuations that nest the Fermi surface, i.e. $\mathbf{q} = (\pi, \pi)$. The pairing function then becomes:

$$\chi_{AF}^{\uparrow\downarrow}((\pi, \pi), 2\mu) = \sum_\mathbf{k} \frac{f(\epsilon_\mathbf{k} - \mu) - f(-\epsilon_\mathbf{k} - \mu)}{2\epsilon_\mathbf{k} - 2\mu} \tag{6.52}$$

For temperatures lower than the Fermi energy, this may be approximated as

$$\chi_{AF}^{\uparrow\downarrow}((\pi, \pi), 2\mu) \ = \ \int\limits_{4t}^{\mu-T} d\epsilon \frac{\rho(\epsilon)}{2\epsilon - 2\mu} \ = \ \frac{\rho(\mu)}{2} \log\left(\frac{T}{|\mu|}\right) \tag{6.53}$$

Combining the above result with the weight of the superconducting susceptibility and we arrive at:

$$\delta\mathcal{F}_{\chi^{\uparrow\downarrow}} \ = \ \frac{g^2}{4} \langle\langle|\Delta_\mathbf{p}|^2\rangle\rangle \rho(\mu)^3 \log^3\left(\frac{T}{|\mu|}\right) \tag{6.54}$$

The above analysis is only an approximation to the superconducting pairing function and product of susceptibilities. In principle the strongest spin fluctuations could be found at an incommensurate wave vector, leading to hot spots of superconducting susceptibility at particular parts of the Fermi surface. This is similar to the incommensurate antiferromagnetic pairing discussed in Chapter 2. Treatment of these incommensurate contributions to the superconducting pairing fluctuations is highly non-trivial.

Evaluation of the $\mathcal{F}_\Sigma$ term

Lastly, let us evaluate the self-energy-like term,

$$\delta\mathcal{F}_\Sigma \ = \ 2\sum_\mathbf{k} |\Delta_\mathbf{k}|^2 \frac{1 - f_\mathbf{k}^\uparrow - f_{-\mathbf{k}}^\downarrow}{(\xi_{\mathbf{k},\uparrow} + \xi_{-\mathbf{k},\downarrow})} \partial_\epsilon \Sigma^\uparrow(\mathbf{k}, \epsilon_\mathbf{k}), \tag{6.55}$$

where

$$\Sigma^{\uparrow}(\mathbf{k}, \epsilon_{\mathbf{k}}) \;\; = \;\; g^2 \sum_{\mathbf{p}, \mathbf{q}} \frac{f_{\mathbf{p}}^{\downarrow}(1 - f_{\mathbf{k}+\mathbf{q}}^{\uparrow})(1 - f_{\mathbf{p}-\mathbf{q}}^{\downarrow}) + (1 - f_{\mathbf{p}}^{\downarrow})f_{\mathbf{k}+\mathbf{q}}^{\uparrow}f_{\mathbf{p}-\mathbf{q}}^{\downarrow}}{\epsilon_{\mathbf{k}}^{\uparrow} + \epsilon_{\mathbf{p}}^{\downarrow} - \epsilon_{\mathbf{k}+\mathbf{q}}^{\uparrow} - \epsilon_{\mathbf{p}-\mathbf{q}}^{\downarrow}}. \tag{6.56}$$

Using the results of Abanov et al [41] ,

$$\Sigma(\mathbf{k}, \epsilon_{\mathbf{k}}) = \frac{3g^2 \chi(\mathbf{Q}, 0)}{4\pi\mu} \epsilon_{\mathbf{k}}, \tag{6.57}$$

where the susceptibility, $\chi(\mathbf{Q}, 0)$, takes the usual form in the limit of $\mathbf{Q} \to (\pi, \pi)$ and small temperatures. So that

$$\chi(\mathbf{Q}, 0) \;\; = \;\; \sum_{\mathbf{k}} \frac{f(\epsilon_{\mathbf{k}} - \mu) - f(\epsilon_{\mathbf{k}-\mathbf{Q}} - \mu)}{\epsilon_{\mathbf{k}} - \epsilon_{\mathbf{k}-\mathbf{Q}}} \tag{6.58}$$

$$= \;\; \sum_{\mathbf{k}} \frac{f(\epsilon_{\mathbf{k}} - \mu) - f(-\epsilon_{\mathbf{k}} - \mu)}{2\epsilon_{\mathbf{k}}} \tag{6.59}$$

$$= \;\; -\frac{1}{2}\rho(\mu) \log\left(\frac{|\mu|}{4t}\right). \tag{6.60}$$

Inserting into the expression for the self energy contribution to the free energy, Equation 6.55, we obtain

$$\delta\mathcal{F}_{\Sigma} = \frac{3g^2}{8\pi\mu}\langle\langle|\Delta_{\mathbf{k}}|^2\rangle\rangle\rho(\mu)^2 \log\left(\frac{|\mu|}{4t}\right) \log\left(\frac{T}{|\mu|}\right) \tag{6.61}$$

6.5 *Interplay of d-wave superconductivity and antiferromagnetism*

In this section we would like to extend our analysis to the behaviour of d-wave superconductivity in an antiferromagnetic background. As in the case of bond density order we derive additional terms in the Landau expansion of the free energy to order $\Delta^2 M^2$. These will give us insight to whether antiferromagnetism supports or hinders the formation of d-wave superconductivity. The antiferromagnetic order is assumed to be static and superconductivity is treated as a perturbation to this static background. Therefore we assume the superconducting gap to be much smaller than the amplitude of the background magnetic order.

6.5.1 Overview of calculation

As in the previous section we use the principle, that all physics happens around the Fermi surface. This restricts the supported momentum space and thereby simplifying the integrations.

Assuming static background order allows us to simply replace all dispersions in the expression of the d-wave superconducting free energy by the dispersion in the presence of antiferromagnetism:

$$\xi_{\mathbf{k}}^{\sigma} = \sigma\sqrt{\epsilon_{\mathbf{k}}^2 + g^2 M^2} - \mu \tag{6.62}$$

As before, we split the free energy of superconducting order into mean field and fluctuation parts and evaluate them separately. We will first analyse the mean field and then the fluctuation contribution, which we will treat term by term.

6.5.2 Expanding the mean field free energy in orders of magnetisation

The mean field free energy in the presence of d-wave superconductivity, to leading order in $\Delta_{\mathbf{k}}$, is

$$\mathcal{F}_{MF}(\Delta) = -\sum_{\mathbf{k}} |\Delta_{\mathbf{k}}|^2 \frac{f_{\mathbf{k}}^{\uparrow} + f_{-\mathbf{k}}^{\downarrow} - 1}{\xi_{\mathbf{k}}^{\uparrow} + \xi_{-\mathbf{k}}^{\downarrow}}. \tag{6.63}$$

In the presence of background, commensurate antiferromagnetic order this become

$$\mathcal{F}_{MF}(\Delta, M) = \sum_{\mathbf{k}} |\Delta_{\mathbf{k}}|^2 \frac{f(\sqrt{\epsilon_{\mathbf{k}}^2 + g^2 M^2} - \mu) + f(-\sqrt{\epsilon_{\mathbf{k}}^2 + g^2 M^2} - \mu) - 1}{2\mu}. \tag{6.64}$$

Expanding to quadratic order in magnetisation:

$$\partial_{M^2} \mathcal{F}_{MF}(\Delta, M)|_{M=0} = \sum_{\mathbf{k}} g^2 |\Delta_{\mathbf{k}}|^2 \frac{f'(\epsilon_{\mathbf{k}} - \mu)}{2\mu\epsilon_{\mathbf{k}}}. \tag{6.65}$$

Next we introduce the density of states and use the derivative of the Fermi function as a delta function to perform the integration:

$$\partial_{M^2} \mathcal{F}_{MF}(\Delta, M)|_{M=0} = -\langle\langle |\Delta_{\mathbf{k}}|^2 \rangle\rangle \frac{g^2 \rho(\mu)}{2\mu^2}. \tag{6.66}$$

6.5.3 Expanding the fluctuation corrections in orders of magnetisation

The fluctuation correction to the free energy of d-wave superconductivity only has two principal terms - the self-energy and susceptibility term. Let us start with the latter.

Expansion of the $\delta\mathcal{F}_{\chi_{AF}^{\uparrow\downarrow}}$ term in M^2

The $\delta\mathcal{F}_{\chi_{AF}^{\uparrow\downarrow}}$ term takes the form:

$$\delta\mathcal{F}_{\chi^{\uparrow\downarrow}} = 2g^2 \sum_{\mathbf{p},\mathbf{q}} \bar{\Delta}_{\mathbf{p}+\mathbf{q}} \frac{1 - f_{\mathbf{p}+\mathbf{q}}^{\uparrow} - f_{-\mathbf{p}-\mathbf{q}}^{\downarrow}}{\xi_{\mathbf{p}+\mathbf{q},\uparrow} + \xi_{-\mathbf{p}-\mathbf{q},\downarrow}} \Delta_{\mathbf{p}} \frac{1 - f_{-\mathbf{p}}^{\uparrow} - f_{\mathbf{p}}^{\downarrow}}{\xi_{-\mathbf{p},\uparrow} + \xi_{\mathbf{p},\downarrow}} \chi_{AF}^{\uparrow\downarrow}(\mathbf{q}, \epsilon_{\mathbf{p}}^{\downarrow} - \epsilon_{\mathbf{p}+\mathbf{q}}^{\uparrow}), \tag{6.67}$$

with

$$\chi_{AF}^{\uparrow\downarrow}(\mathbf{q}, \epsilon_{\mathbf{p}}^{\downarrow} - \epsilon_{\mathbf{p}+\mathbf{q}}^{\uparrow}) = \sum_{\mathbf{k}} \frac{f_{\mathbf{k}-\mathbf{q}}^{\downarrow} - f_{\mathbf{k}}^{\uparrow}}{\epsilon_{\mathbf{k}-\mathbf{q}}^{\downarrow} + \epsilon_{\mathbf{p}+\mathbf{q}}^{\uparrow} - \epsilon_{\mathbf{k}}^{\uparrow} - \epsilon_{\mathbf{p}}^{\downarrow}} \tag{6.68}$$

In the presence of commensurate antiferromagnetism the dispersion takes the form:

$$\xi_{\mathbf{k}}^{\sigma} = \epsilon_{\mathbf{k}}^{\sigma} - \mu = \sigma\sqrt{\epsilon_{\mathbf{k}}^2 + g^2 M^2} - \mu, \tag{6.69}$$

so that $\epsilon_{\mathbf{k}}^{\sigma} = -\epsilon_{\mathbf{k}}^{-\sigma}$ and the superconducting susceptibility factors become:

$$\frac{1 - f_{\mathbf{p}}^{\uparrow} - f_{-\mathbf{p}}^{\downarrow}}{\xi_{\mathbf{p}}^{\uparrow} + \xi_{-\mathbf{p}}^{\downarrow}} = \frac{1 - f_{\mathbf{p}}^{\uparrow} - f_{-\mathbf{p}}^{\downarrow}}{-2\mu}. \tag{6.70}$$

The leading contribution to the $\Delta^2 M^2$ coefficient comes from the M^2-derivatives of $\chi_{AF}^{\uparrow\downarrow}$. The M^2 derivatives on the superconducting susceptibility factors only con-

tribute a multiplicative numerical factor.

As for the previous cases, the superconducting susceptibility factors constrain the allowed energies and momentum of $\chi_{AF}^{\uparrow\downarrow}$ and lead to factors of $\rho(\mu)$. Since physics is dominated by processes at the Fermi surface, we may write

$$\frac{1 - f_{\mathbf{p}}^{\uparrow} - f_{-\mathbf{p}}^{\downarrow}}{\xi_{\mathbf{p}}^{\uparrow} + \xi_{-\mathbf{p}}^{\downarrow}} \approx \delta(\epsilon_{\mathbf{p}} \pm \mu). \tag{6.71}$$

Therefore, $\epsilon_{\mathbf{p}} = \pm\mu$ and $\epsilon_{\mathbf{p}+\mathbf{q}} = \pm\mu$, which leads to $\mathbf{q} = \mathbf{0}$ or $\mathbf{q} = (\pi, \pi)$. The dominant contribution to $\chi_{AF}^{\uparrow\downarrow}$ in the presence of antiferromagnetism arrives from $\epsilon_{\mathbf{p}} + \epsilon_{\mathbf{p}+\mathbf{q}} = 2\mu$ and $\mathbf{q} = 0$. Then

$$\delta\mathcal{F}_{\chi^{\uparrow\downarrow}} = 3g^2 \langle|\Delta_{\mathbf{p}}|^2\rangle\rho(\mu)^2 \sum_{\mathbf{k}} \frac{f(-\sqrt{\epsilon_{\mathbf{k}}^2 + g^2 M^2}) - f(\sqrt{\epsilon_{\mathbf{k}}^2 + g^2 M^2})}{\sqrt{\epsilon_{\mathbf{k}}^2 + g^2 M^2} + \mu} \tag{6.72}$$

Expanding to leading order in M and keeping only the most divergent contribution we arrive at

$$\partial_{M^2}\delta\mathcal{F}_{\chi^{\uparrow\downarrow}}|_{M=0} = -g^4\langle|\Delta_{\mathbf{p}}|^2\rangle\frac{3\rho(\mu)^2}{2}\int_{-4t}^{4t} d\epsilon\rho(\epsilon)\frac{f(\epsilon)}{\epsilon^2(\epsilon - \mu)} \tag{6.73}$$

$$= -g^4\langle|\Delta_{\mathbf{p}}|^2\rangle\frac{3\rho(\mu)^3}{2\mu^2}\log\left(\frac{T}{|\mu|}\right). \tag{6.74}$$

Expansion of the $\delta\mathcal{F}_{\Sigma}$ term in M^2

Lastly, let us evaluate the self-energy-like term,

$$\delta\mathcal{F}_{\Sigma} = 2\sum_{\mathbf{k}} |\Delta_{\mathbf{k}}|^2 \frac{1 - f_{\mathbf{k}}^{\uparrow} - f_{-\mathbf{k}}^{\downarrow}}{(\xi_{\mathbf{k},\uparrow} + \xi_{-\mathbf{k},\downarrow})}\partial_{\epsilon}\Sigma^{\uparrow}(\mathbf{k}, \epsilon_{\mathbf{k}}). \tag{6.75}$$

As for the bond density wave, Section 5.5.3, the derivative of the self energy, $\partial_{\epsilon_{\mathbf{k}}}\Sigma(\mathbf{k}, \epsilon_{\mathbf{k}})$, does not contribute to order M^2. Hence, the only contribution stems from the M^2 derivative of the superconducting susceptibility factor. We obtain:

$$\partial_{M^2}\delta\mathcal{F}_{\Sigma}|_{M=0} = \frac{3g^4\rho(\mu)^2}{8\pi\mu^3}\langle|\Delta_{\mathbf{p}}|^2\rangle\log\left(\frac{|\mu|}{4t}\right) \tag{6.76}$$

6.6   *Phase diagram*

Now we are in position to add superconductivity to the phase diagram. First we solve for the second order transition to d-wave superconducting order in the absence of antiferromagnetic order. Then, we will include terms to order $M^2|\Delta|^2$ and investigate their effect.

To locate the second order transition to superconductivity we solve

$$\partial_{|\Delta|^2}\mathcal{F}(\Delta)|_{\Delta=0} = \alpha = 0, \tag{6.77}$$

for temperature as a function of interaction strength. Where $\mathcal{F}(\Delta)$ is the sum of mean field and fluctuation contributions evaluated in Section 6.4. In particular, we collect the contribution from the mean field, Equation (6.48), pairing function, Equation (6.54) and self-energy, Equation (6.61).

The transition temperature takes the form of a BCS exponential:

$$T = |\mu| \, exp\left(-\frac{1 - g^2 \frac{3\rho(\mu)\log(\mu/4t)}{4\pi\mu}}{g^2\rho(\mu)^2}\right). \tag{6.78}$$

The resulting phase transition line is plotted in Figure 6.1.

Next, we include the effect of commensurate antiferromagnetism on the superconducting transition. Hence, we collect the relevant terms from mean field theory and fluctuations from Section 6.5. The free energy to leading order in superconducting gap and magnetisation takes the general form

$$\mathcal{F}(\Delta, M) = \left(\alpha + \beta M^2\right)\Delta^2, \tag{6.79}$$

where α and β are the contribution in the absence and presence of antiferromagnetism, respectively. In particular, β is the sum of contributions from mean field (6.66), pairing function (6.74) and self-energy (6.76) in the presence of magnetism.

α, β and M are functions of temperature T and interaction strength g. The precise dependence of M on these parameters is determined numerically from the mean field analysis in Chapter 2.
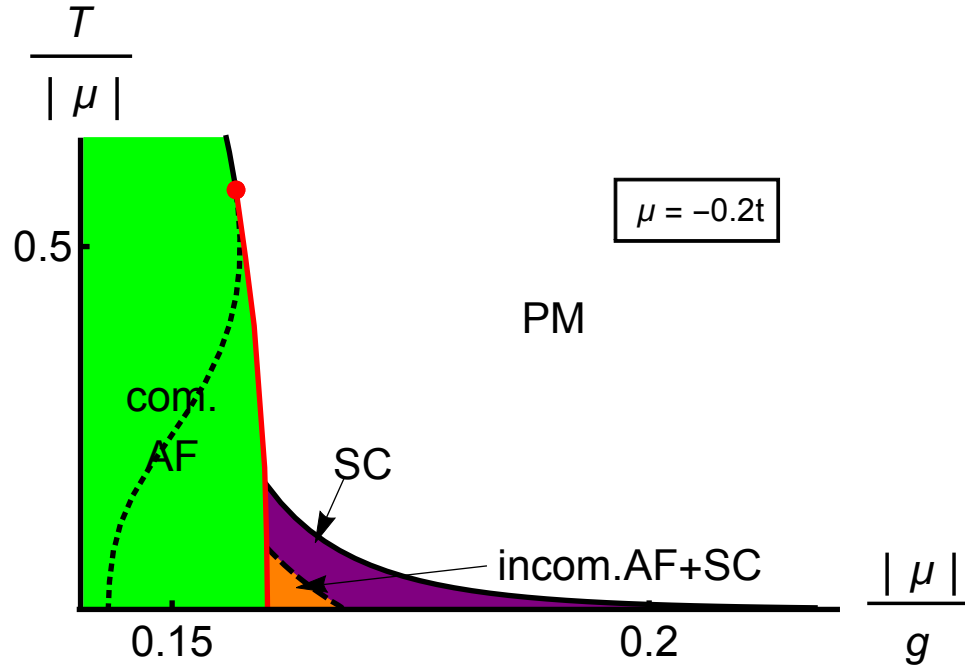
Figure 6.1: **Phase diagram of superconducting order and antiferromagnetism.** The orders in this diagram are commensurate antiferromagnetism (AF), superconductivity (SC) and the paramagnetic phase (PM). Additionally, superconductivity is shown coexisting with incommensurate antiferromagnetism in the small orange region.

Calculating the superconducting phase transition line inside the commensurate magnetic order we obtain the phase diagram in Figure 6.2.

As for the bond density wave, all transition lines were calculated consistently with the help of the logarithmic approximation to the density of states. Perturbative corrections to the first order transition line and incommensurate antiferromagnetism are beyond the scope of the present work. The first order transition to commensurate antiferromagnetism and the region of incommensurate order were shifted by hand to match the topology of the phase diagram calculated in Chapter 2. Thus there is some ambiguity in the exact position of these transition lines. Hence, the phase diagrams should be viewed as a qualitative summary of the connectivity of phases, rather than a quantitative prediction of the boundary locations for real systems.

The coupling of commensurate antiferromagnetism and superconducting order leads to phase competition. Inside the antiferromagnetic phase the superconducting transition temperature drops dramatically. In this region the Fermi surface becomes
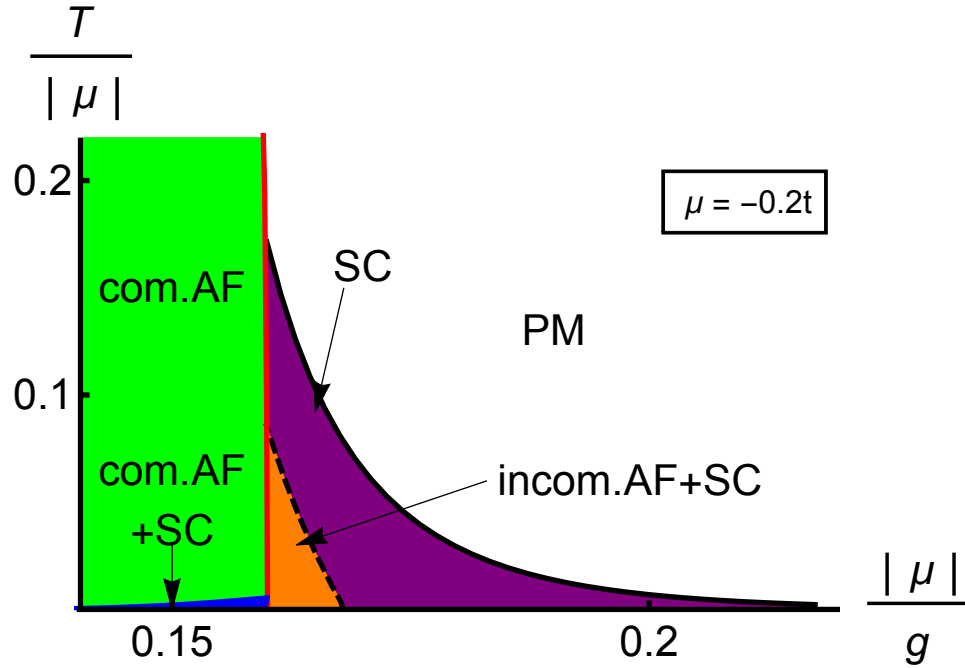
Figure 6.2: **Phase diagram of superconducting order and antiferromagnetism.** The orders in this diagram are commensurate antiferromagnetism (AF), superconductivity (SC) and the paramagnetic phase (PM). Additionally, superconductivity is shown coexisting with commensurate and incommensurate antiferromagnetism in the blue and orange region, respectively.

completely gapped by the presence of strong antiferromagnetic order. Thus, there is no phase space for fluctuations, which would drive superconductivity. Higher order terms in magnetisation probably suppress superconducting order inside the antiferromagnetic phase completely. Considering the size of the magnetisation below the tricritical point, it is likely necessary to treat magnetisation to all orders.

This phase competition between commensurate antiferromagnetism and d-wave superconductivity is consistent with experimental evidence from cuprate samples in general [72,73]. Here, in order to observe superconductivity, antiferromagnetic order has to be suppressed. This is achieved by either electron or hole doping of the Mott insulating antiferromagnetic parent compound. Other methods of destroying the antiferromagnetic order are not sufficient, since the parent compound has no free charge carriers due to its Mott insulating character.

There is some evidence for coexistence of antiferromagnetic order and d-wave superconductivity [74, 75]. However, this is not likely to be true long range phase

coexistence, but rather phase separation due to the first order magnetic transition and dirty samples leading to impurity pinning of either phase.

In contrast, the incommensurate antiferromagnetic order is very weak and does not completely gap the Fermi surface. As a consequence there remains phase space for fluctuations. Hence, we propose a coexistence of incommensurate magnetic order and d-wave superconductivity. This is in accordance with experimental evidence for incommensurate magnetic order in superconducting cuprate samples [50, 52, 56, 74, 76] as well as theoretical studies of the Hubbard model with next nearest neighbour hopping [55, 77, 78].

Finally, we would like to comment on the relevance of the present work to the physics of iron based superconductors.

At first glance the phase diagram shows some resemblance to that of iron based superconductors. Indeed, the familiar pattern of superconducting order in the vicinity of an antiferromagnetic quantum critical point is present. Additionally, there is evidence for the coexistence of commensurate, as well as incommensurate, antiferromagnetic order with superconductivity in iron based superconductors [79–83].

However, there are important differences between our work and iron based superconductors. The Fermi surface in the iron compounds consists of a small pocket in the Brillouin zone center (Γ point) and four in the corners of the Brillouin zone. Fermi surface nesting leads to striped antiferromagnetic or spin density wave order. Instead of all neighbouring spins being aligned anti-parallel, as in the Hubbard model, only neighbours along one direction are antiferromagnetically aligned, while neighbours along the other direction align ferromagnetically. The superconducting pairing symmetry is different, too. d-wave pairing, as present in the cuprates, was initially proposed for the iron-pnictides, but closer examination suggest s$\pm$ pairing is the most likely candidate. s$\pm$ is normal s-wave pairing at any one Fermi pocket, but changes sign when switching between the central and the outer Fermi surface pockets. The parent compounds are different as well. While the Hubbard model and the cuprates are Mott-insulators at zero doping, iron based superconductors are bad metals in the this limit. Finally, the Hubbard model considered here is two dimensional, motivated by negligible tunneling rates between copper-oxide planes. However, the dimensionality of electron transport is not consistent within the set of

iron based superconductors [21, 22, 73, 83].

6.7 *Variational ansatz vs Legendre transformation*

As for the d-wave bond density wave order, Section 5.7, it can be shown that a Legendre transformation is equivalent to the variational approach used in the above analysis. The proof of their equivalence follows the same principal steps, so we only highlight the differences here.

6.7.1 Variational ansatz

In case of d-wave superconducting order the variational term added and subtracted to the Hamiltonian is

$$\mathcal{H}_{var} = \sum_{\mathbf{k}} \left(\Delta_{\mathbf{k}} c^{\dagger}_{-\mathbf{k},\uparrow} c^{\dagger}_{\mathbf{k},\downarrow} + \bar{\Delta}_{\mathbf{k}} c_{\mathbf{k},\downarrow} c_{-\mathbf{k},\uparrow} \right). \tag{6.80}$$

The remainder of the variational analysis follow the same path as for the bond density wave order in Section 5.7.1.

6.7.2 Legendre transformation

Here, the only difference is the form of the field, $j_{\mathbf{k}}$, that is conjugate to the d-wave superconducting order. It is given by:

$$\mathcal{H}_{leg} = \sum_{\mathbf{k}} \left(j_{\mathbf{k}} c^{\dagger}_{-\mathbf{k},\uparrow} c^{\dagger}_{\mathbf{k},\downarrow} + \bar{j}_{\mathbf{k}} c_{\mathbf{k},\downarrow} c_{-\mathbf{k},\uparrow} \right). \tag{6.81}$$

The analysis of this Legendre transform follows the same steps as in Section 5.7.2.

6.8 *Summary*

In this chapter we analysed the behaviour of d-wave superconducting order in the Hubbard model close to half filling. The starting point was a variational mean field approach, which showed no drive to the superconducting order. We then applied the fermionic quantum order-by disorder approach to calculate contributions to the free energy from self-consistent second order perturbation theory. As expected, these quantum fluctuation support d-wave superconductive pairing in the Hubbard model. The resulting phase diagram includes an area of superconducting order outside the antiferromagnetic region. Phase competition leads to a dramatic suppression of the superconducting critical temperature beyond the antiferromagnetic first order transition. The relevance of the results in the context of experimental evidence from cuprate and pnictide superconductors was discussed.

Chapter 7

Intertwining of bond density wave and d-wave superconductivity

In this chapter we will analyse the intertwining of bond density wave and superconductivity. We calculate corrections to the free energy arising from the simultaneous presence of both orders. The two phases are treated equally, without bias towards either. In principle, such cross-terms may be calculated from mean field theory as well as fluctuations. Here, we derive the leading term in their interaction, $D^2\Delta^2$, from mean field theory. This cross term reveals whether the coexistences of bond density wave and superconductivity is favoured at this order or whether the two phases suppress each other.

7.1   *Mean field theory of bond density wave and d-wave superconductivity*

7.1.1   Hamiltonian

Consider the following Hamiltonian

$$\mathcal{H} - \mu\mathcal{N} = \underbrace{\sum_{\mathbf{k},\sigma} \xi_{\mathbf{k}} c^\dagger_{\mathbf{k},\sigma} c_{\mathbf{k},\sigma}}_{\text{kinetic}} + \underbrace{\sum_{\mathbf{k},\mathbf{p},\mathbf{q}} V_{\mathbf{q}} c^\dagger_{\mathbf{k},\uparrow} c^\dagger_{\mathbf{p},\downarrow} c_{\mathbf{p}-\mathbf{q},\downarrow} c_{\mathbf{k}+\mathbf{q},\uparrow}}_{\text{interaction}}, \qquad (7.1)$$

where $\xi_{\mathbf{k}} = \epsilon_{\mathbf{k}} - \mu$ and the kinetic, $\mathcal{H}_{kin}$, and interaction, $\mathcal{H}_{int}$, part of the Hamiltonian have been identified.

Our task is to construct the free energy of this Hamiltonian in the simultaneous presence of d-wave superconducting and d-wave bond density order.

7.1.2   The order parameter

We define the d-wave bond density order and d-wave superconducting order respectively as

$$\begin{aligned}
D_{\mathbf{k}} &= \theta_{\mathbf{k}} \sum_{\mathbf{p},\sigma} (c^\dagger_{\mathbf{p}-\frac{\mathbf{Q}}{2},\sigma} c_{\mathbf{p}+\frac{\mathbf{Q}}{2},\sigma} + c.c.) & (7.2) \\
\Delta_{\mathbf{k}} &= \theta_{\mathbf{k}} \sum_{\mathbf{k},\sigma} c^\dagger_{\mathbf{k},\sigma} c^\dagger_{-\mathbf{k},-\sigma}. & (7.3)
\end{aligned}$$

These definitions are identical to the definitions in Chapters 5 and 6 respectively.

7.1.3 Variational ansatz

We include both orders equally in the Hamiltonian by a variational ansatz. We add and subtract a term,

$$
\mathcal{H}_{var} = \tag{7.4}
$$
$$
\frac{1}{2} \sum_{\mathbf{k},\sigma} \left(g D_{\mathbf{k}} c^{\dagger}_{\mathbf{k}+\frac{\mathbf{Q}}{2},\sigma} c_{\mathbf{k}-\frac{\mathbf{Q}}{2},\sigma} + g \bar{D}_{\mathbf{k}} c^{\dagger}_{\mathbf{k}-\frac{\mathbf{Q}}{2},\sigma} c_{\mathbf{k}+\frac{\mathbf{Q}}{2},\sigma} + \sigma \Delta_{\mathbf{k}} c^{\dagger}_{-\mathbf{k},\sigma} c^{\dagger}_{\mathbf{k},-\sigma} + \sigma \bar{\Delta}_{\mathbf{k}} c_{\mathbf{k},-\sigma} c_{-\mathbf{k},\sigma} \right),
$$

to the Hamiltonian. So that,

$$
\mathcal{H} - \mu \mathcal{N} = \underbrace{\mathcal{H}_{kin} + \mathcal{H}_{var}}_{\text{diagonalise}} \underbrace{-\mathcal{H}_{var} + \mathcal{H}_{int}}_{\text{perturbation}}. \tag{7.5}
$$

The first two terms will be diagonalised and the second two terms are treated a perturbative correction. Including the positive contribution in the kinetic Hamiltonian, we may write

$$
\mathcal{H}_{kin} + \mathcal{H}_{var} = \frac{1}{4} \sum_{\mathbf{k},\sigma}
$$
$$
\begin{pmatrix} c^{\dagger}_{\mathbf{k}+\frac{\mathbf{Q}}{2},\sigma} \\ c^{\dagger}_{\mathbf{k}-\frac{\mathbf{Q}}{2},\sigma} \\ c_{-\mathbf{k}+\frac{\mathbf{Q}}{2},-\sigma} \\ c_{-\mathbf{k}-\frac{\mathbf{Q}}{2},-\sigma} \end{pmatrix}^{T}
\begin{pmatrix}
\xi_{\mathbf{k}+\frac{\mathbf{Q}}{2}} & g D_{\mathbf{k}} & 0 & \sigma \Delta_{\mathbf{k}+\frac{\mathbf{Q}}{2}} \\
g \bar{D}_{\mathbf{k}} & \xi_{\mathbf{k}-\frac{\mathbf{Q}}{2}} & \sigma \Delta_{\mathbf{k}-\frac{\mathbf{Q}}{2}} & 0 \\
0 & \sigma \bar{\Delta}_{\mathbf{k}-\frac{\mathbf{Q}}{2}} & -\xi_{-\mathbf{k}+\frac{\mathbf{Q}}{2}} & -g \bar{D}_{\mathbf{k}} \\
\sigma \bar{\Delta}_{\mathbf{k}+\frac{\mathbf{Q}}{2}} & 0 & -g D_{\mathbf{k}} & -\xi_{-\mathbf{k}-\frac{\mathbf{Q}}{2}}
\end{pmatrix}
\begin{pmatrix} c_{\mathbf{k}+\frac{\mathbf{Q}}{2},\sigma} \\ c_{\mathbf{k}-\frac{\mathbf{Q}}{2},\sigma} \\ c^{\dagger}_{-\mathbf{k}+\frac{\mathbf{Q}}{2},-\sigma} \\ c^{\dagger}_{-\mathbf{k}-\frac{\mathbf{Q}}{2},-\sigma} \end{pmatrix}
$$
$$
\tag{7.6}
$$

7.1.4 Diagonalisation

Next, we diagonalise the Hamiltonian (7.6). Note, the diagonal and off-diagonal two by two blocks encode bond density and superconductivity respectively.

We may diagonalise the bond density contributions by rotating the operators into a

new basis;

$$
\begin{pmatrix} c_{\mathbf{k}+\frac{\mathbf{Q}}{2},\sigma} \\ c_{\mathbf{k}-\frac{\mathbf{Q}}{2},\sigma} \end{pmatrix} = \begin{pmatrix} u_{D,\mathbf{k}} & -v_{D,\mathbf{k}} \\ v_{D,\mathbf{k}}^* & u_{D,\mathbf{k}}^* \end{pmatrix} \begin{pmatrix} \alpha_{\mathbf{k}+\frac{\mathbf{Q}}{2},\sigma} \\ \alpha_{\mathbf{k}-\frac{\mathbf{Q}}{2},\sigma} \end{pmatrix},
\tag{7.7}
$$

where

$$
|u_{D,\mathbf{k}}|^2 = \frac{1}{2}\left(1 + \frac{\epsilon_{\mathbf{k}+\frac{\mathbf{Q}}{2}}}{\sqrt{\epsilon_{\mathbf{k}+\frac{\mathbf{Q}}{2}}^2 + g^2|D_{\mathbf{k}}|^2}} \right)
\tag{7.8}
$$

$$
|v_{D,\mathbf{k}}|^2 = \frac{1}{2}\left(1 - \frac{\epsilon_{\mathbf{k}+\frac{\mathbf{Q}}{2}}}{\sqrt{\epsilon_{\mathbf{k}+\frac{\mathbf{Q}}{2}}^2 + g^2|D_{\mathbf{k}}|^2}} \right)
\tag{7.9}
$$

In general, this rotation also alters the structure of the superconducting contribution. However, using the bond density ordering vector, $\mathbf{Q} = (\pi, \pi)$, such that $\Delta_{\mathbf{k}+\mathbf{Q}} = -\Delta_{\mathbf{k}}$, the off-diagonal blocks are invariant under the rotation. The resultant Hamiltonian may be written as:

$$
\mathcal{H}_{kin} + \mathcal{H}_{var} = \frac{1}{4}\sum_{\mathbf{k},\sigma,\delta} \begin{pmatrix} \alpha_{\mathbf{k}+\delta\frac{\mathbf{Q}}{2},\sigma}^{\dagger} \\ \alpha_{-\mathbf{k}-\delta\frac{\mathbf{Q}}{2},-\sigma} \end{pmatrix}^T \begin{pmatrix} \xi_{\mathbf{k}}^{\delta} & \sigma\Delta_{\mathbf{k}+\delta\frac{\mathbf{Q}}{2}} \\ \sigma\bar{\Delta}_{\mathbf{k}+\delta\frac{\mathbf{Q}}{2}} & -\xi_{\mathbf{k}}^{\delta} \end{pmatrix} \begin{pmatrix} \alpha_{\mathbf{k}+\delta\frac{\mathbf{Q}}{2},\sigma} \\ \alpha_{-\mathbf{k}-\delta\frac{\mathbf{Q}}{2},-\sigma}^{\dagger} \end{pmatrix},
\tag{7.10}
$$

where

$$
\xi_{\mathbf{k}}^{\delta} = \delta\sqrt{\epsilon_{\mathbf{k}+\frac{\mathbf{Q}}{2}}^2 + g^2|D_{\mathbf{k}}|^2} - \mu,
\tag{7.11}
$$

and we have introduced a new band label δ and used the fact, that $\epsilon_{\mathbf{k}+\frac{\mathbf{Q}}{2}}^2 = \epsilon_{\mathbf{k}-\frac{\mathbf{Q}}{2}}^2$ for $\mathbf{Q} = (\pi, \pi)$.

To diagonalise the superconducting contributions we apply a Bogoliubov transformation,

$$
\begin{pmatrix} \alpha_{\mathbf{k}+\delta\frac{\mathbf{Q}}{2},\sigma} \\ \alpha_{-\mathbf{k}-\delta\frac{\mathbf{Q}}{2},-\sigma}^{\dagger} \end{pmatrix} = \begin{pmatrix} u_{\Delta,\mathbf{k}}^* & -\sigma v_{\Delta,\mathbf{k}}^* \\ \sigma v_{\Delta,\mathbf{k}} & u_{\Delta,\mathbf{k}} \end{pmatrix} \begin{pmatrix} \beta_{\mathbf{k}+\delta\frac{\mathbf{Q}}{2},\sigma} \\ \beta_{-\mathbf{k}-\delta\frac{\mathbf{Q}}{2},-\sigma}^{\dagger} \end{pmatrix},
\tag{7.12}
$$

where

$$u_{\Delta,\mathbf{k}}^2 = \frac{1}{2}\left(1 + \frac{\xi_{\mathbf{k}}^\delta}{\sqrt{(\xi_{\mathbf{k}}^\delta)^2 + |\Delta_{\mathbf{k}+\frac{\mathbf{Q}}{2}}|^2}}\right) \tag{7.13}$$

$$v_{\Delta,\mathbf{k}}^2 = \frac{1}{2}\left(1 - \frac{\xi_{\mathbf{k}}^\delta}{\sqrt{(\xi_{\mathbf{k}}^\delta)^2 + |\Delta_{\mathbf{k}+\frac{\mathbf{Q}}{2}}|^2}}\right). \tag{7.14}$$

The Hamiltonian now takes the diagonal form:

$$\mathcal{H}_{kin} + \mathcal{H}_{var} = \frac{1}{4}\sum_{\mathbf{k},\sigma,\delta}\xi_{\mathbf{k}}^{\sigma,\delta}\beta_{\mathbf{k}+\delta\frac{\mathbf{Q}}{2},\sigma}^\dagger\beta_{\mathbf{k}+\delta\frac{\mathbf{Q}}{2},\sigma}, \tag{7.15}$$

where the dispersion in the simultaneous presence of superconductivity and bond density wave is

$$\xi_{\mathbf{k}}^{\sigma,\delta} = \sigma\sqrt{(\xi_{\mathbf{k}}^\delta)^2 + |\Delta_{k+\frac{\mathbf{Q}}{2}}|^2} \tag{7.16}$$

$$= \sigma\sqrt{\left(\delta\sqrt{\epsilon_{\mathbf{k}+\frac{\mathbf{Q}}{2}}^2 + g^2|D_{\mathbf{k}}|^2} - \mu\right)^2 + |\Delta_{k+\frac{\mathbf{Q}}{2}}|^2} \tag{7.17}$$

The diagonalisation may also be expressed in one, by compounding the rotation and Bogoliubov transformation:

$$\begin{pmatrix} c_{\mathbf{k}+\frac{\mathbf{Q}}{2},\sigma} \\ c_{\mathbf{k}-\frac{\mathbf{Q}}{2},\sigma} \\ c_{-\mathbf{k}+\frac{\mathbf{Q}}{2},-\sigma}^\dagger \\ c_{-\mathbf{k}-\frac{\mathbf{Q}}{2},-\sigma}^\dagger \end{pmatrix} = \begin{pmatrix} u_{\Delta,\mathbf{k}}^*\begin{pmatrix} u_{D,\mathbf{k}} & -v_{D,\mathbf{k}} \\ v_{D,\mathbf{k}}^* & u_{D,\mathbf{k}}^* \end{pmatrix} & -\sigma v_{\Delta,\mathbf{k}}\begin{pmatrix} -v_{D,\mathbf{k}} & u_{D,\mathbf{k}} \\ u_{D,\mathbf{k}}^* & v_{D,\mathbf{k}}^* \end{pmatrix} \\ \sigma v_{\Delta,\mathbf{k}}^*\begin{pmatrix} -v_{D,\mathbf{k}}^* & u_{D,\mathbf{k}}^* \\ u_{D,\mathbf{k}} & v_{D,\mathbf{k}} \end{pmatrix} & u_{\Delta,\mathbf{k}}\begin{pmatrix} u_{D,\mathbf{k}}^* & -v_{D,\mathbf{k}}^* \\ v_{D,\mathbf{k}} & u_{D,\mathbf{k}} \end{pmatrix} \end{pmatrix}\begin{pmatrix} \beta_{\mathbf{k}+\frac{\mathbf{Q}}{2},\sigma} \\ \beta_{\mathbf{k}-\frac{\mathbf{Q}}{2},\sigma} \\ \beta_{-\mathbf{k}+\frac{\mathbf{Q}}{2},-\sigma}^\dagger \\ \beta_{-\mathbf{k}-\frac{\mathbf{Q}}{2},-\sigma}^\dagger \end{pmatrix}. \tag{7.18}$$

7.2 Free energy

Having diagonalised the Hamiltonian we now construct the free energy.

7.2.1 *Formal expression of the free energy*

Free particle contribution

The partition function is given by

$$Z = \text{Tr}\, e^{-\beta \mathcal{H}} \tag{7.19}$$

$$= \text{Tr}\, e^{-\beta(\mathcal{H}_{kin} + \mathcal{H}_{var} - \mathcal{H}_{var} + \mathcal{H}_{int})} \tag{7.20}$$

$$= \text{Tr}\, e^{-\beta(\mathcal{H}_{kin} + \mathcal{H}_{var})} \langle e^{-\beta(-\mathcal{H}_{var} + \mathcal{H}_{int})} \rangle, \tag{7.21}$$

where the thermal expectation $\langle ... \rangle$ in the second term is taken over the diagonal modes of $\mathcal{H}_{kin} + \mathcal{H}_{var}$. Using $F = -T \log Z$, we obtain the mean field contribution to the free energy

$$\mathcal{F}_{log} = -T \sum_{\mathbf{k}, \sigma, \delta} \log \left(1 + e^{-\frac{\xi_{\mathbf{k}}^{\sigma, \delta}}{T}} \right) \tag{7.22}$$

where

$$\xi_{\mathbf{k}}^{\sigma, \delta} = \sigma \sqrt{ \left(\delta \sqrt{\epsilon_{\mathbf{k}+\frac{\mathbf{Q}}{2}}^2 + g^2 |D_{\mathbf{k}}|^2} - \mu \right)^2 + |\Delta_{k+\frac{\mathbf{Q}}{2}}|^2}. \tag{7.23}$$

We may expand this mean field contribution to the free energy to quadratic order in the superconducting gap and bond density amplitude :

$$|\partial_{|D|^2} \partial_{|\Delta|^2} F_{log}(\Delta, D)|_{\Delta=0, D=0} = g^2 \sum_{\mathbf{k}} \theta_{\mathbf{k}}^4 \left\{ \frac{f'(\epsilon_{\mathbf{k}} - \mu)}{(\epsilon_{\mathbf{k}} - \mu)\epsilon_{\mathbf{k}}} - \frac{f(\epsilon_{\mathbf{k}} - \mu)}{(\epsilon_{\mathbf{k}} - \mu)^2 \epsilon_{\mathbf{k}}} \right\} \tag{7.24}$$

Variational contribution

Corrections to the logarithmic contribution to the mean field free energy are given by

$$-T \log \langle e^{-\beta(-\mathcal{H}_{var} + \mathcal{H}_{int})} \rangle \approx \langle -\mathcal{H}_{var} + \mathcal{H}_{int} \rangle. \tag{7.25}$$

Here we derive a formal expression for $\langle -\mathcal{H}_{var}\rangle^1$. As usual this term takes the same form as the free particle contribution up to multiplicative factors. This variational contribution is calculated by transforming its operators into the diagonal basis of $\mathcal{H}_{kin} + \mathcal{H}_{var}$ and keeping terms to order $D^2\Delta^2$. This produces a large number of terms given by:

$$
\begin{aligned}
\langle -\mathcal{H}_{var}\rangle = \langle -\frac{1}{2}\sum_{\mathbf{k},\sigma}\Bigg\{ & gD_{\mathbf{k}} & & \Big[\sigma v^*_{\Delta,\mathbf{k}}v^*_{D,\mathbf{k}}\beta_{-\mathbf{k}+\frac{\mathbf{Q}}{2},-\sigma}\ (-\sigma v_{\Delta,\mathbf{k}})u^*_{D,\mathbf{k}}\beta^{\dagger}_{-\mathbf{k}+\frac{\mathbf{Q}}{2},-\sigma} \\
& & & -\sigma v^*_{\Delta,\mathbf{k}}u^*_{D,\mathbf{k}}\beta_{-\mathbf{k}-\frac{\mathbf{Q}}{2},-\sigma}\ (-\sigma v_{\Delta,\mathbf{k}})v^*_{D,\mathbf{k}}\beta^{\dagger}_{-\mathbf{k}-\frac{\mathbf{Q}}{2},-\sigma} \\
& & & +u_{\Delta,\mathbf{k}}u^*_{D,\mathbf{k}}\beta^{\dagger}_{\mathbf{k}+\frac{\mathbf{Q}}{2},\sigma}\ u^*_{\Delta,\mathbf{k}}v^*_{D,\mathbf{k}}\beta_{\mathbf{k}+\frac{\mathbf{Q}}{2},\sigma} \\
& & & +\ u_{\Delta,\mathbf{k}}(-v^*_{D,\mathbf{k}})\beta^{\dagger}_{\mathbf{k}-\frac{\mathbf{Q}}{2},\sigma}\ u^*_{\Delta,\mathbf{k}}u^*_{D,\mathbf{k}}\beta_{\mathbf{k}-\frac{\mathbf{Q}}{2},\sigma}\Big] \\
& +g\bar{D}_{\mathbf{k}} & & \Big[-\sigma v^*_{\Delta,\mathbf{k}}u_{D,\mathbf{k}}\beta_{-\mathbf{k}+\frac{\mathbf{Q}}{2},-\sigma}\ \sigma v_{\Delta,\mathbf{k}}v_{D,\mathbf{k}}\beta^{\dagger}_{-\mathbf{k}+\frac{\mathbf{Q}}{2},-\sigma} \\
& & & -\sigma v^*_{\Delta,\mathbf{k}}v_{D,\mathbf{k}}\beta_{-\mathbf{k}-\frac{\mathbf{Q}}{2},-\sigma}\ (-\sigma v_{\Delta,\mathbf{k}})u_{D,\mathbf{k}}\beta^{\dagger}_{-\mathbf{k}-\frac{\mathbf{Q}}{2},-\sigma} \\
& & & +u_{\Delta,\mathbf{k}}v_{D,\mathbf{k}}\beta^{\dagger}_{\mathbf{k}+\frac{\mathbf{Q}}{2},\sigma}\ u^*_{\Delta,\mathbf{k}}u_{D,\mathbf{k}}\beta_{\mathbf{k}+\frac{\mathbf{Q}}{2},\sigma} \\
& & & +\ u_{\Delta,\mathbf{k}}u_{D,\mathbf{k}}\beta^{\dagger}_{\mathbf{k}-\frac{\mathbf{Q}}{2},\sigma}\ u^*_{\Delta,\mathbf{k}}(-v_{D,\mathbf{k}})\beta_{\mathbf{k}-\frac{\mathbf{Q}}{2},\sigma}\Big] \\
& +\sigma\Delta_{\mathbf{k}+\frac{\mathbf{Q}}{2}} & & \Big[\sigma v^*_{\Delta,\mathbf{k}}(-v^*_{D,\mathbf{k}})\beta_{-\mathbf{k}+\frac{\mathbf{Q}}{2},\sigma}\ u_{\Delta,\mathbf{k}}v_{D,\mathbf{k}}\beta^{\dagger}_{-\mathbf{k}+\frac{\mathbf{Q}}{2},\sigma} \\
& & & -\sigma v^*_{\Delta,\mathbf{k}}u^*_{D,\mathbf{k}}\beta_{-\mathbf{k}-\frac{\mathbf{Q}}{2},\sigma}\ u_{\Delta,\mathbf{k}}u_{D,\mathbf{k}}\beta^{\dagger}_{-\mathbf{k}-\frac{\mathbf{Q}}{2},\sigma} \\
& & & +u_{\Delta,\mathbf{k}}u^*_{D,\mathbf{k}}\beta^{\dagger}_{\mathbf{k}+\frac{\mathbf{Q}}{2},-\sigma}\ (-\sigma v^*_{\Delta,\mathbf{k}})u_{D,\mathbf{k}}\beta_{\mathbf{k}+\frac{\mathbf{Q}}{2},-\sigma} \\
& & & +\ u_{\Delta,\mathbf{k}}(-v^*_{D,\mathbf{k}})\beta^{\dagger}_{\mathbf{k}-\frac{\mathbf{Q}}{2},-\sigma}\ \sigma v^*_{\Delta,\mathbf{k}}v_{D,\mathbf{k}}\beta_{\mathbf{k}-\frac{\mathbf{Q}}{2},-\sigma}\Big] \\
& +\sigma\bar{\Delta}_{\mathbf{k}+\frac{\mathbf{Q}}{2}} & & \Big[u^*_{\Delta,\mathbf{k}}u_{D,\mathbf{k}}\beta_{\mathbf{k}+\frac{\mathbf{Q}}{2},-\sigma}\ (-\sigma v_{\Delta,\mathbf{k}})u^*_{D,\mathbf{k}}\beta^{\dagger}_{\mathbf{k}+\frac{\mathbf{Q}}{2},-\sigma} \\
& & & +u^*_{\Delta,\mathbf{k}}(-v_{D,\mathbf{k}})\beta_{\mathbf{k}-\frac{\mathbf{Q}}{2},-\sigma}\ (-\sigma v_{\Delta,\mathbf{k}})v^*_{D,\mathbf{k}}\beta^{\dagger}_{\mathbf{k}-\frac{\mathbf{Q}}{2},-\sigma} \\
& & & \sigma v_{\Delta,\mathbf{k}}(-v_{D,\mathbf{k}})\beta^{\dagger}_{-\mathbf{k}+\frac{\mathbf{Q}}{2},\sigma}\ u^*_{\Delta,\mathbf{k}}v^*_{D,\mathbf{k}}\beta_{-\mathbf{k}+\frac{\mathbf{Q}}{2},\sigma} \\
& & & +\ \sigma v_{\Delta,\mathbf{k}}u_{D,\mathbf{k}}\beta^{\dagger}_{-\mathbf{k}-\frac{\mathbf{Q}}{2},\sigma}\ u^*_{\Delta,\mathbf{k}}u^*_{D,\mathbf{k}}\beta_{-\mathbf{k}-\frac{\mathbf{Q}}{2},\sigma}\Big]\ \Bigg\}\rangle \quad (7.26)
\end{aligned}
$$

---

[1]The expectation over the interaction Hamiltonian would be treated in second order perturbation theory, which is beyond the scope of the current work.

Forming Fermi functions from the expectation over operators we arrive at:

$$
\langle -\mathcal{H}_{var} \rangle = -\frac{1}{2} \sum_{\mathbf{k},\sigma} \Bigg\{ \quad g D_{\mathbf{k}} v^*_{D,\mathbf{k}} u^*_{D,\mathbf{k}} \quad \Big[-|v_{\Delta,\mathbf{k}}|^2 \left(1 - f^{-\sigma}_{-\mathbf{k}+\frac{\mathbf{Q}}{2}} \right)
$$

$$
+ |v_{\Delta,\mathbf{k}}|^2 \left(1 - f^{-\sigma}_{-\mathbf{k}-\frac{\mathbf{Q}}{2}} \right)
$$

$$
+ |u_{\Delta,\mathbf{k}}|^2 f^{\sigma}_{\mathbf{k}+\frac{\mathbf{Q}}{2}}
$$

$$
- |u_{\Delta,\mathbf{k}}|^2 f^{\sigma}_{\mathbf{k}-\frac{\mathbf{Q}}{2}} \Big]
$$

$$
+ \quad g \bar{D}_{\mathbf{k}} v_{D,\mathbf{k}} u_{D,\mathbf{k}} \quad \Big[-|v_{\Delta,\mathbf{k}}|^2 \left(1 - f^{-\sigma}_{-\mathbf{k}+\frac{\mathbf{Q}}{2}} \right)
$$

$$
+ |v_{\Delta,\mathbf{k}}|^2 \left(1 - f^{-\sigma}_{-\mathbf{k}-\frac{\mathbf{Q}}{2}} \right)
$$

$$
+ |u_{\Delta,\mathbf{k}}|^2 f^{\sigma}_{\mathbf{k}+\frac{\mathbf{Q}}{2}}
$$

$$
- |u_{\Delta,\mathbf{k}}|^2 f^{\sigma}_{\mathbf{k}-\frac{\mathbf{Q}}{2}} \Big]
$$

$$
+ \quad \Delta_{\mathbf{k}+\frac{\mathbf{Q}}{2}} v^*_{\Delta,\mathbf{k}} u_{\Delta,\mathbf{k}} \quad \Big[+|u_{D,\mathbf{k}}|^2 \left(1 - f^{\sigma}_{-\mathbf{k}+\frac{\mathbf{Q}}{2}} \right)
$$

$$
- |v_{D,\mathbf{k}}|^2 \left(1 - f^{\sigma}_{-\mathbf{k}-\frac{\mathbf{Q}}{2}} \right)
$$

$$
+ |v_{D,\mathbf{k}}|^2 f^{-\sigma}_{\mathbf{k}+\frac{\mathbf{Q}}{2}}
$$

$$
- |u_{D,\mathbf{k}}|^2 f^{-\sigma}_{\mathbf{k}-\frac{\mathbf{Q}}{2}} \Big]
$$

$$
+ \quad \bar{\Delta}_{\mathbf{k}-\frac{\mathbf{Q}}{2}} v_{\Delta,\mathbf{k}} u^*_{\Delta,\mathbf{k}} \quad \Big[-|u_{D,\mathbf{k}}|^2 \left(1 - f^{-\sigma}_{\mathbf{k}+\frac{\mathbf{Q}}{2}} \right)
$$

$$
+ |v_{D,\mathbf{k}}|^2 \left(1 - f^{-\sigma}_{\mathbf{k}-\frac{\mathbf{Q}}{2}} \right)
$$

$$
- |v_{D,\mathbf{k}}|^2 f^{\sigma}_{-\mathbf{k}+\frac{\mathbf{Q}}{2}}
$$

$$
+ |u_{D,\mathbf{k}}|^2 f^{\sigma}_{-\mathbf{k}-\frac{\mathbf{Q}}{2}} \Big] \Bigg\} \tag{7.27}
$$

Using $u^2 = 1 - v^2$ and $u \in \Re$ and furthermore, the definitions of $v_{D,\mathbf{k}}$ and $v_{\Delta,\mathbf{k}}$, we collect terms to order $D^2 \Delta^2$, such that:

$$
\langle -\mathcal{H}_{var} \rangle = -g^2 \sum_{\mathbf{k}} |D_{\mathbf{k}+\frac{\mathbf{Q}}{2}}|^2 \frac{|\Delta_{\mathbf{k}}|^2}{(\epsilon_{\mathbf{k}} - \mu)^2} \frac{f_{\mathbf{k}} - f_{\mathbf{k}+\mathbf{Q}}}{\epsilon_{\mathbf{k}} - \epsilon_{\mathbf{k}+\mathbf{Q}}},
$$

$$
\tag{7.28}
$$

where we have shifted the momentum label to reduce notational burden.

7.2.2 *Evaluation of the free energy*

Having derived the formal expression for the free energy in the presence of bond density and superconducting order, we now evaluate the integrals.

We use the same approximations detailed in Section 5.4.1 - choosing small temperatures and close to half filling: $T \ll |\mu| \ll t$

The mean field free energy of the intertwined bond density wave and d-wave superconductivity takes the form:

$$\mathcal{F}_{MF}(D, \Delta) = \mathcal{F}_{log} - \langle \mathcal{H}_{var} \rangle \tag{7.29}$$

Expanding to quadratic order in D and Δ we define the relevant Landau expansion coefficient and arrive at

$$\beta_{D,\Delta} = |\partial_{|D|^2} \partial_{|\Delta|^2} \mathcal{F}_{MF}|_{D=0, \Delta=0} \tag{7.30}$$

$$= g^2 \sum_{\mathbf{k}} \theta_{\mathbf{k}}^4 \left\{ \frac{f'(\epsilon_{\mathbf{k}} - \mu)}{(\epsilon_{\mathbf{k}} - \mu)\epsilon_{\mathbf{k}}} - \frac{f(\epsilon_{\mathbf{k}} - \mu)}{(\epsilon_{\mathbf{k}} - \mu)^2 \epsilon_{\mathbf{k}}} \right\} - g^2 \sum_{\mathbf{k}} \theta_{\mathbf{k}}^4 \frac{f(\epsilon_{\mathbf{k}} - \mu) - f(-\epsilon_{\mathbf{k}} - \mu)}{2\epsilon_{\mathbf{k}}(\epsilon_{\mathbf{k}} - \mu)^2} \tag{7.31}$$

$$= g^2 \sum_{\mathbf{k}} \theta_{\mathbf{k}}^4 \left\{ \frac{f'(\epsilon_{\mathbf{k}} - \mu)}{(\epsilon_{\mathbf{k}} - \mu)\epsilon_{\mathbf{k}}} - 2\frac{f(\epsilon_{\mathbf{k}} - \mu)}{(\epsilon_{\mathbf{k}} - \mu)^2 \epsilon_{\mathbf{k}}} \right\} \tag{7.32}$$

Integrating the first term by parts whilst keeping only the most divergent contribution:

$$\beta_{D,\Delta} = -3g^2 \sum_{\mathbf{k}} \theta_{\mathbf{k}}^4 \frac{f(\epsilon_{\mathbf{k}} - \mu)}{(\epsilon_{\mathbf{k}} - \mu)^2 \epsilon_{\mathbf{k}}} \tag{7.33}$$

Here, we may introduce the density of states and use the Fermi distribution function to cut off the range of integration at $\epsilon = \mu - T$, such that

$$\beta_{D,\Delta} = 3g^2 \langle\langle \theta_{\mathbf{k}}^4 \rangle\rangle \frac{\rho(\mu - T)}{T|\mu - T|}. \tag{7.34}$$

Finally way write the leading mean field contribution to the free energy from the

interaction of bond density wave order and d-wave superconductivity as

$$\mathcal{F}_{MF}(D, \Delta) = 3g^2 \langle\langle \theta_{\mathbf{k}}^4 \rangle\rangle \frac{\rho(\mu - T)}{T|\mu - T|} D^2 \Delta^2 \tag{7.35}$$

This term is positive. Hence, the coexistence of bond density wave and d-wave superconductivity is disfavoured in mean field theory.

This is consistent with evidence from a range of underdoped cuprates [11, 84–90]. Here, charge order competes with superconductivity, too. In these materials, the superconducting dome has a dip as a function of doping. By suppressing superconductivity with an external magnetic field, a dome of charge order arises at the very doping the superconducting dome had its dip. An example phase diagram for YBCO is plotted in Figure 7.1.
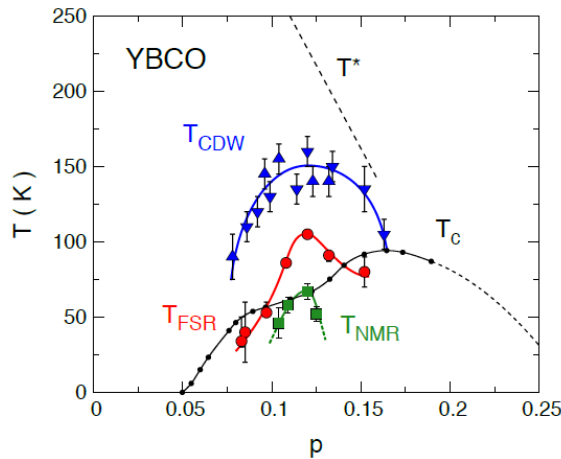

Figure 7.1: **Temperature-doping phase diagram of YBCO.** T_c denotes the superconducting transition temperature. Note the dip in the transition temperature around $p = 0.12$. In the presence of magnetic field, T_{CDW}, T_{FSR} and T_{NMR} denote the onset of charge order as seen by X-ray diffraction, Hall and NMR measurements, respectively. T^* denotes the onset of the pseudogap phase. [89]

In the next section we will explore the effect of this contribution on the phase diagram.

7.3   *Phase diagram*

In order to evaluate the free energy contribution of intertwined bond density wave and d-wave superconductivity we require knowledge of the size of the order parameters as a function of interaction strength and temperature. Then, we could utilise equation (7.35) and recursively calculate the effect of the presence of one phase on the transition temperature of the other.

In Chapters 5 and 6 we analysed the contributions to the free energy in the presence of bond density wave order and superconductivity, respectively. Their analysis was limited to quadratic order in their respective order parameter. This enabled us to derive their second order phase transition lines. However, a quadratic Landau expansion is not sufficient to determine the minimum of the free energy as a function of the order parameter. Hence, we are restricted to a qualitative analysis of the effect of phase competition of bond density and superconducting order.

The phase diagram in the presence of superconductivity and bond density wave, while neglecting their mutual interaction is plotted in Figure 7.2.
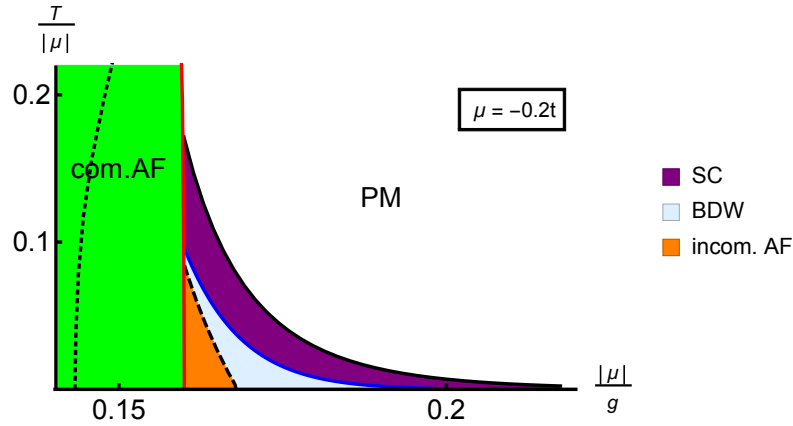

Figure 7.2: **Temperature-interaction phase diagram including both bond density wave (BDW) order and d-wave superconductivity (SC).** This diagram compares the transition temperature of superconducting (black line) and bond density wave order (blue line). The green and orange region denote commensurate and incommensurate antiferromagnetic order. This plot does not take into account phase competition between superconductivity and bond density wave and their fate inside the antiferromagnetic dome.

Figure 7.2 shows that the transition temperature of d-wave superconductivity is

higher than of bond density wave order. Thus, the superconducting phase is more stable. Further we note, that the phase competition has a strong $1/T$ divergence compared to the $\log(T)$ driving the formation of either phase. We conclude therefore, that phase competition will completely suppress bond density order, while lowering the superconducting transition temperature.

As a consequence of this phase competition, one may increase the transition temperature of either phase by suppressing the other. Applying a magnetic field will break time-reversal symmetry, suppressing d-wave superconductivity, while simultaneously reviving bond density wave order. Analogously one might suppress the charge order by application of pressure and thereby enhance the superconducting transition temperature.
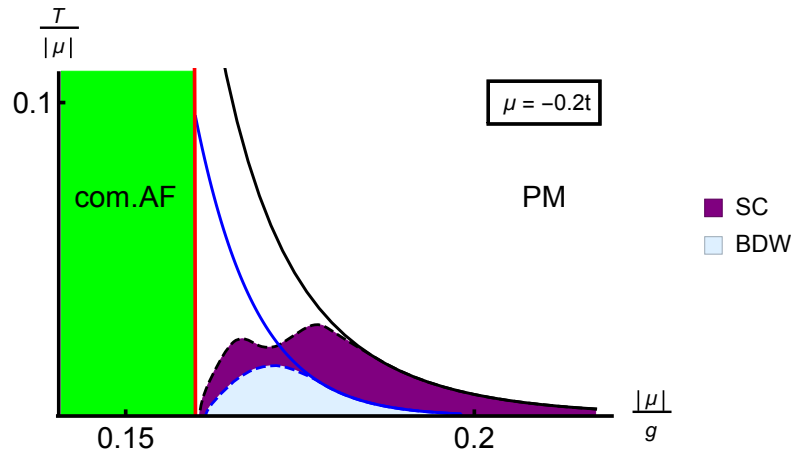

Figure 7.3: **Sketch of temperature-interaction phase diagram including both bond density wave (BDW) order and d-wave superconductivity (SC).** Compared to Figure 7.2 this plot includes a cartoon of the interaction of d-wave superconducting order (black lines) and bond density wave order (blue lines). The solid lines are identical to Figure 7.2. The dashed black and blue lines are a sketch of the possible phase transition lines to superconducting order and bond density wave order in the presence of mode-mode competition. The green region denote commensurate antiferromagnetic order. To avoid overcrowding of the diagram we did not draw the region of incommensurate antiferromagnetic order.

Figure 7.3 shows a cartoon of a possible phase diagram taking into account mode-mode coupling. Here, d-wave superconducting order is suppressed in regions of maximal bond density wave transition temperature. The region of bond density wave order sketched in Figure 7.3 would be suppressed entirely by mode-mode competition of the form obtained in Equation 7.35. It would only be visible in this form, when

superconducting order is suppressed, for instance by an external magnetic field. Figure 7.3 further displays the finding that both superconducting and bond density wave order are suppressed in the presence of commensurate antiferromagnetic order.

7.4   *Summary*

In this chapter we analysed the interaction of d-wave bond density and d-wave superconducting order. We found that within a mean field approach the two phases compete strongly. The effect on the overall phase diagram was discussed. The result is in qualitative agreement with recent experimental evidence of competition between charge order and superconductivity in YBCO [11, 84–90].

Part IV

Nematic quantum critical point

Chapter 8

Fluctuation-induced instabilities of the spin-triplet nematic

8.1 Introduction

The main focus of this thesis is the extension of the fermionic order-by-disorder formalism to antiferromagnetic order and thus developing a phase diagram for the Hubbard model. Amongst its features we found bond density wave order, which is favoured by a combination of fluctuations and the enhanced density of states in the vicinity of the Fermi energy originating from the van-Hove singularity. Bond density wave order has been the subject of intense study recently [25, 71, 91–94]. In systems away from an antiferromagnetic critical point, we can consider an alternative mechanism of forming bond density waves. Ferromagnetic order may be thought of as the zero wave wavevector limit of spin density wave orders. Similarity we can take the zero wave vector limit of a d-wave bond density wave order. The resultant phase is a d-wave spin-triplet nematic order.

In this chapter we show, that a model with spin triplet nematic order harbours a fluctuation induced instability towards d-density order near the nematic quantum critical point. Further, we investigate the intertwining of the nematic with p-wave superconducting order. The physics of this is a direct translation of earlier work on ferromagnetism [29, 30].

This work was carried out in close collaboration with Dr. Chris Pedder, Dr. Frank Krüger and Prof. Andrew G. Green. I have mainly been involved in the addition of superconductivity to the model and will emphasise this aspect here. This chapter is the basis of the following publication:

G. Hannappel, C. J. Pedder, F. Krüger, and A. G. Green, "Electronic spin-triplet nematic with a twist," *Arxiv ID: 1601.05414*, submitted to Physical Review B.

Before diving into the detail of the analysis of the d-wave spin-triplet nematic order and the associated p-wave superconductivity, we will consider a slightly simpler model of ferromagnetic order. Here we explain the principle steps of the calculation without distraction from the messy detail of the nematic order. Having laid these foundations we continue by introducing the model for nematic order and calculate its free energy including corrections from self-consistent second order perturbation theory. Finally, we consider the possibility of p-wave superconducting order and how the presence of nematic order affects the superconducting transition temperature.

8.2 Fluctuation corrections to the ferromagnet

In this section we will summarise the main results of [30]. In this work Pedder et.al. employed the fermionic order-by-disorder approach to the itinerant ferromagnet near the quantum critical point in two and three dimensions. The starting point of their work is a Hamiltonian consisting of a free electron dispersion with a repulsive contact interaction. In this isotropic model it is possible to evaluate the leading corrections to the free energy at all orders. This leads to a non-analytic correction to the free energy below the tricritical point due to quantum fluctuations.

The free energy is a functional of the mean field dispersion. In case of the itinerant ferromagnet it takes the form

$$\epsilon_{\pm}(\boldsymbol{k}) = \frac{k^2}{2} \pm gM. \tag{8.1}$$

The mean field free energy then takes the familiar form

$$\mathcal{F}_{MF} = gM^2 - T \sum_{\mathbf{k},\sigma} \log\left(e^{\frac{\epsilon_{\mathbf{k}}^{\sigma}-\mu}{T}} + 1\right). \tag{8.2}$$

Expanding to sixth order in magnetisation one obtains

$$\mathcal{F}_{MF} = (g + \beta_2)M^2 + \beta_4 M^4 + \beta_6 M^6, \tag{8.3}$$

where the mean field Landau coefficients are

$$\beta_{2n} = \frac{g^{2n}}{n(2n-1)!} \sum_{\mathbf{k}} f^{(2n-1)}(k^2). \tag{8.4}$$

The fluctuation correction to the free energy of the itinerant ferromagnet in terms of particle-hole densities of states takes the form derived in Equation (3.17) :

$$\delta\mathcal{F}(M) = 2g^2 \sum_{\substack{\sigma,\mathbf{q} \\ \epsilon_1,\epsilon_2}} \frac{\Delta\rho^{\sigma}(\mathbf{q},\epsilon_1)\tilde{\rho}^{-\sigma}(-\mathbf{q},\epsilon_2)}{\epsilon_1 + \epsilon_2} \tag{8.5}$$

After expansion in orders of magnetisation one may identify the most divergent term at any order. Summation over these leading terms to all orders in magnetisation leads to a logarithmic correction to the free energy. All other contributions are sub-leading. They do not change the overall physics but merely renormalise the phase boundaries.

The leading fluctuation correction to the free energy of the itinerant ferromagnet then takes the form

$$\delta\mathcal{F}(M) = -2\lambda(1 + \log 2)M^2 + \lambda M^4 \log\left(\frac{4g^2 M^2 + T^2}{4\mu^2}\right), \tag{8.6}$$

where we defined $\lambda = 4g^6 v_F^3/(3\mu^2)$ with Fermi velocity $v_F = k_F/2\pi^2$ and chemical potential $\mu = k_F^2/2$.

One may expand the analysis of the ferromagnet by considering the possibility of a spiral magnetic order parameter:

$$\mathbf{M_Q}(\mathbf{r}) = \mathbf{M}\left(\hat{\mathbf{n}}_{\mathbf{x}}\cos(\mathbf{Q}\cdot\mathbf{r}) + \hat{\mathbf{n}}_{\mathbf{y}}\sin(\mathbf{Q}\cdot\mathbf{r})\right), \tag{8.7}$$

with $\mathbf{Q} = Q\hat{\mathbf{n}}_z$ and $\hat{\mathbf{n}}_i$ being the unit vector directed along i. This describes magnetic moments rotating in the x-y-plane as a function of position along the z-direction. The mean field dispersion now takes the form

$$\epsilon_{\mathbf{k}}^{\pm} = \frac{k^2}{2} \pm \sqrt{(\mathbf{k} \cdot \mathbf{Q})^2 + (gM)^2}. \tag{8.8}$$

M and Q enter the dispersion in a similar manner. Since the free energy is a functional of the mean field dispersion, contributions at any order in Q are proportional contributions to the same order in M. In addition, the Landau coefficients are strongly peaked at the Fermi surface, such that the evaluation of factors of the form $\mathbf{k}.\mathbf{Q}$ reduces to angular averages at the Fermi energy. Thus, the proportionality factors are a combination of combinatoric factors and angular averages over powers of $\zeta_k^2 = (\mathbf{k} \cdot \mathbf{Q})^2 / k_F^2 Q^2$.

For instance the ratio of the $Q^2 M^2$ and M^4 coefficients is $2\langle \zeta_k^2 \rangle$. Hence, the M^4 and $Q^2 M^2$ coefficients turn negative simultaneously and thus the first order transition to the homogeneous ferromagnet is preempted by a second order transition to the spiral order. (Recall, the condition for a first order transition requires the fourth order coefficient to grow sufficiently negative to overcome positive higher order terms, while a second order transition occurs for any negative quadratic coefficient.)

The phase diagram of ferromagnetism in this model including the possibility for spatial modulation is plotted in Figure 8.1.

8.3 Fluctuation corrected spin-triplet nematic

In this section we will introduce the spin-triplet nematic order and derive its free energy. The calculation closely follows the analysis of ferromagnetic order in Section 8.2.

8.3.1 Spin-triplet nematic order

We consider a model consistent of free electrons in three dimensions interacting via a short-ranged quadrupole density-density interaction which drives nematic order
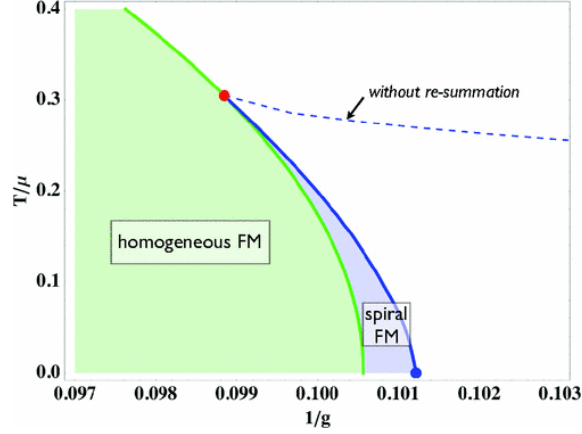
Figure 8.1: **Phase diagram of ferromagnetism as a function of inverse electron repulsion** $1/g$ **and temperature** T/μ **by Pedder *et al* [30].** The second order transition to homogeneous ferromagnetism (FM) at high temperatures turns first order at the tricritical point (red). This first order transition is preempted by formation of the spiral phase (blue region).

in mean-field [95]. Since we are interested in the nematic instability of the system, we neglect the Coulomb-like s-wave density-density interaction, which is present in a real system. The Hamiltonian takes the form

$$\mathcal{H} = \sum_{\mathbf{r}} \left\{ \sum_{\sigma=\uparrow,\downarrow} c_\sigma^\dagger(\boldsymbol{r}) \left[\epsilon_0(-i\nabla) - \mu \right] c_\sigma^\dagger(\boldsymbol{r}) + \sum_{\mathbf{r},\mathbf{r}'} V(\mathbf{r} - \mathbf{r}') \left[\hat{\boldsymbol{Q}}_\uparrow(\mathbf{r}) \hat{\boldsymbol{Q}}_\downarrow(\mathbf{r}') \right] \right\}, \quad (8.9)$$

where we have defined the quadrupole density operators

$$\hat{Q}_\sigma^{ij}(\boldsymbol{r}) = -c_\sigma^\dagger(\boldsymbol{r}) \left(3\partial_i\partial_j - \nabla^2\delta_{ij} \right) c_\sigma(\boldsymbol{r}). \quad (8.10)$$

The indices $i, j = x, y, z$ and $\sigma = \uparrow, \downarrow$ run over real space and electron spin, respectively. The operators $\hat{\boldsymbol{Q}}_\sigma$ in the Hamiltonian (8.9) are three-dimensional matrices and $V(\mathbf{r} - \mathbf{r}')$ describes some interaction in the nematic channel - this may have a variety of origins as discussed in [95]. We include it as a phenomenological interaction driving the formation of spin-triplet nematic order. By analogy with the conventional decoupling of the Coulomb repulsion into charge and spin contributions, $\hat{n}_\uparrow\hat{n}_\downarrow = \hat{\rho}^2 - \hat{\boldsymbol{S}}^2$, we decouple the quadrupole density-density interaction into singlet and triplet parts and Fourier transform to momentum space,

$$\mathcal{H}_{\text{int}} = \sum_{\mathbf{k}} \sum_{\alpha=1}^{5} V(\mathbf{k}) \left\{ \hat{R}_\alpha^s(\mathbf{k}) \hat{R}_\alpha^s(-\mathbf{k}) - \hat{\boldsymbol{R}}_\alpha^t(\mathbf{k}) \hat{\boldsymbol{R}}_\alpha^t(-\mathbf{k}) \right\}, \quad (8.11)$$

where

$$\hat{R}^s_\alpha(\mathbf{k}) = \frac{1}{2}\Psi^\dagger(\mathbf{k})\zeta(\mathbf{k})\Phi_\alpha(\mathbf{k})\Psi(\mathbf{k}), \tag{8.12}$$

$$\hat{\boldsymbol{R}}^t_\alpha(\mathbf{k}) = \frac{1}{2}\Psi^\dagger(\mathbf{k})\boldsymbol{\sigma}\zeta(\mathbf{k})\Phi_\alpha(\mathbf{k})\Psi(\mathbf{k}) \tag{8.13}$$

are the quadrupolar density operators in spin singlet (s) and triplet (t) channel, respectively.

For brevity, we have adopted the standard spinor notation, $\Psi = (c_\uparrow, c_\downarrow)^T$, while $\boldsymbol{\sigma} = (\sigma^x, \sigma^y, \sigma^z)^T$ denotes a vector of Pauli matrices and $\hat{\boldsymbol{R}}^t_\alpha(\mathbf{k})$ is a three-dimensional vector in spin space. The index α labels the five independent d-orbital channels ($\ell = 2$). Using the standard basis, the orbital form factors are given by $\Phi_1(\boldsymbol{k}) = k_x^2 - k_y^2$, $\Phi_2(\boldsymbol{k}) = (2k_z^2 - k_x^2 - k_y^2)/\sqrt{3}$, $\Phi_3(\boldsymbol{k}) = 2k_x k_y$, $\Phi_4(\boldsymbol{k}) = 2k_x k_z$, and $\Phi_5(\boldsymbol{k}) = 2k_y k_z$. We include a factor $\zeta_\mathbf{k}$ into the definition of the nematic form factor. This serves to compensate for neglecting the effects of the lattice and a finite range Coulomb repulsion. Without this extra factor large nematic order parameters lead to pathologies such as a divergent electron density.

The Hamiltonian (8.9) is symmetric under rotation of spins. Hence, without loss of generality, we choose z as the spin quantisation axis and choose $\Phi_1(\boldsymbol{k}) = k_x^2 - k_y^2$ as the orientation of the nematic distortion. Then we can identify the mean field order parameter

$$\eta = \langle \hat{R}^{t,z}_1 \rangle \tag{8.14}$$

The mean field dispersion takes the familiar form of ferromagnetism with additional angular dependence:

$$\epsilon_\pm(\boldsymbol{k}) = k^2 \mp \eta V(\mathbf{k})\zeta(\mathbf{k})\Phi_1(\boldsymbol{k}). \tag{8.15}$$

This corresponds to a d-wave distortion of the Fermi surface that is anti-symmetric under the exchange of spin labels. The dispersion, (8.15), is like the dispersion in the presence of ferromagnetism, (8.1), with the addition of an orbital factor. The effect on the shape of the Fermi surface is plotted in Figure 8.2.

At this point, it is worth noting the crucial role $V(\mathbf{k})\zeta(\mathbf{k})$ plays in Equation (8.15).
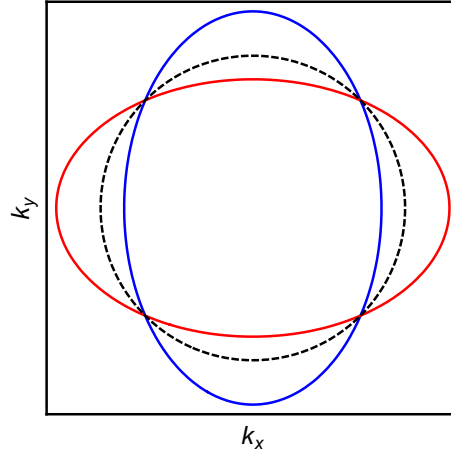
Figure 8.2: **Cross section of the Fermi surface in the presence of nematic order.** The blue and red contours are the Fermi surfaces of the two bands in the presence of nematic order. The black, dashed contour is the isotropic Fermi surface in the absence of the nematic distortion. The nematic Fermi surface is not distorted along the spin quantisation axis, $\mathbf{z}$.

If it was a constant, the electron density would diverge as $V\zeta\eta \to 1$, which is clearly unphysical. In the calculations that follow, the dispersion appears in integrands that are strongly peaked at the Fermi energy. $V(\mathbf{k})\zeta(\mathbf{k})\Phi_1(\boldsymbol{k})$, on the other hand, varies slowly in the vicinity of the Fermi surface. Thus we may approximate these factors by evaluating them at the Fermi surface and thus neglect the their radial dependence. The mean field dispersion may now be written as

$$\epsilon_{\pm}(\boldsymbol{k}) = k^2 \mp g\eta\Phi_1(\hat{\boldsymbol{k}}), \tag{8.16}$$

where $g = V(0)$ is the effective interaction and η has been rescaled accordingly.

Just as for the ferromagnet we may allow for spatial modulation of the nematic order. We consider a helical spin triplet nematic order of the form

$$\boldsymbol{\eta}(\boldsymbol{r}) = \eta\left[\cos(\boldsymbol{q}\cdot\boldsymbol{r})\boldsymbol{n}_1^x + \sin(\boldsymbol{q}\cdot\boldsymbol{r})\boldsymbol{n}_1^y\right], \tag{8.17}$$

where $\boldsymbol{n}_1^x$ and $\boldsymbol{n}_1^y$ denote unit vectors in spin-orbital space with orbital component $\Phi_1(\hat{\mathbf{k}})$.

This leads to a mean field dispersion with a form very similar to the modulated

ferromagnet:

$$\epsilon_{\pm}(\boldsymbol{k}) = k^2 \mp \sqrt{(\boldsymbol{k} \cdot \boldsymbol{q})^2 + \eta^2 \Phi_1(\hat{\boldsymbol{k}})^2}. \tag{8.18}$$

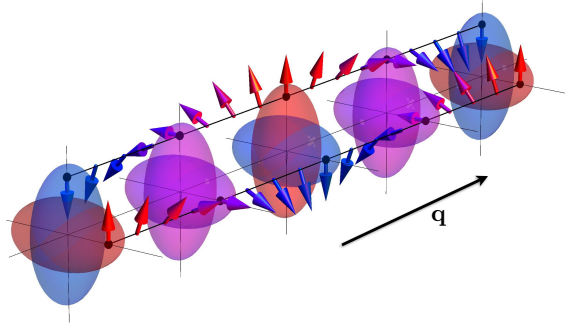A sketch of the spiraling nematic is displayed in Figure 8.3.

Figure 8.3: **Sketch of spin-triplet nematic order with helical modulation.** The colours represent the projection of spins onto the z-axis. This sketch assumes the length-scale of the helical modulation, $1/q$ to be much smaller than the lattice constant. This permits us to consider the local Fermi surface of a given lattice subspace.

8.3.2   Free energy of the spin-triplet nematic

In the previous section we introduced nematic order. Here we will derive the mean field free energy and corrections due to fluctuations. We find that a modulated nematic is formed in a similar manner to modulated ferromagnetism.

Mean field free energy

From Equation (8.15) we conclude, that the Landau expansion in powers of η will take the same functional form as the Landau expansion of the free energy of the ferromagnet, with the addition of angular factors. In particular, the mean field free energy takes the form

$$\mathcal{F}_{MF} = g\eta^2 - T \sum_{\mathbf{k},\sigma} \log\left(\exp\left(\frac{\epsilon_{\mathbf{k}}^{\sigma} - \mu}{T}\right) + 1\right). \tag{8.19}$$

We expand to sixth order in the nematic order parameter

$$\mathcal{F}_{MF} = (g + \beta_2)\eta^2 + \beta_4\eta^4 + \beta_6\eta^6, \tag{8.20}$$

where the expansion coefficients are

$$\beta^{2n} = \frac{g^{2n}}{n(2n-1)!} \sum_{\mathbf{k}} \Phi(\hat{\mathbf{k}})^{2n} f^{(2n-1)}(k^2). \tag{8.21}$$

This expression is similar to the itinerant ferromagnet, Equation (8.4), with the addition of the nematic symmetry factors. The derivatives of Fermi functions are strongly peaked around the Fermi surface and are only a function of the radial momentum component. We use this to factorise the integrand, with the result

$$\beta^{2n} = g^{2n} \frac{\langle\langle \Phi(\hat{\mathbf{k}})^{2n} \rangle\rangle}{n(2n-1)!} \sum_{k} f^{(2n-1)}(k^2), \tag{8.22}$$

where $\langle\langle \Phi_{\mathbf{k}}^{2n} \rangle\rangle$ is the angular average over powers of the d-wave symmetry factors.

For the spatially modulated nematic, the analysis follows similar lines. Inserting this dispersion in the presence of spatial modulation (8.18) into the expression for the mean field free energy (8.19) and expanding in powers of η and $\boldsymbol{q}$ we obtain

$$F_{\mathrm{mf}}(\eta, \boldsymbol{q}) = F_{\mathrm{mf}}^{(0)}(\eta) + \left(2\alpha_4 \langle\langle \Phi_1^2(\hat{\mathbf{k}})(\hat{\mathbf{k}}.\hat{\mathbf{q}})^2 \rangle\rangle\eta^2 + 3\alpha_6 \langle\langle \Phi_1^4(\hat{\mathbf{k}})(\hat{\mathbf{k}}.\hat{\mathbf{q}})^2 \rangle\rangle\eta^4\right) q^2$$
$$+ 3\alpha_6 \langle\langle \Phi_1^2(\hat{\mathbf{k}})(\hat{\mathbf{k}}.\hat{\mathbf{q}})^4 \rangle\rangle\eta^2 q^4, \tag{8.23}$$

where $F_{\mathrm{mf}}^{(0)}(\eta)$ denotes the mean-field free energy of the homogeneous spin-triplet nematic (8.20). Since the angular averages and the coefficients α_4 and α_6 are always positive, spatial modulations of the spin-triplet nematic order lead to an increase of the mean field free energy and are therefore not favored at mean-field.

Fluctuation corrected free energy

The analysis of the fluctuation correction to the mean field free energy follows Section 3.2.3 closely. There is one difference. The interaction considered here is not a contact interaction, but has a finite range in real space and thus its Fourier trans-

form has some momentum dependence. Even though for completeness we will track this momentum dependence, we eventually approximate its value at the Fermi surface. We start by decoupling the quadrupole interaction (8.11) using a Hubbard-Stratonovich transformation in both spin and charge channels. Self-consistency is ensured by including the static nematic order parameter into the definition of the propagator;

$$G_\sigma(\boldsymbol{k}, \omega) = \frac{1}{-i\omega + k^2 - \sigma g \eta \Phi_1(\hat{\mathbf{k}}) - \mu}. \tag{8.24}$$

Next, we perform the usual Gaussian integration over fermions. As in Section 3.2.3 we now expand to quadratic order in the finite frequency fluctuations and subsequently integrate over them. The fluctuation contribution to the free energy then takes the form

$$F_{\text{fl}} = -\frac{T}{2} \sum_{\substack{\mathbf{q}, \omega \\ \alpha, \beta}} V(\mathbf{q})^2 \left\{ \Pi_{++}^{\alpha\beta}(\mathbf{q}, \omega) \Pi_{--}^{\alpha\beta}(\mathbf{q}, \omega) + \mathbf{\Pi}_{+-}^{\alpha\beta}(\mathbf{q}, \omega) \mathbf{\Pi}_{-+}^{\alpha\beta}(\mathbf{q}, \omega) \right\}, \tag{8.25}$$

where we have defined

$$\Pi_{\sigma,\sigma'}^{\alpha\beta}(\boldsymbol{q}, \tilde{\omega}) = \sum_\omega \int_{\boldsymbol{k}} G_\sigma(\boldsymbol{k}, \omega) G_{\sigma'}(\boldsymbol{k} + \boldsymbol{q}, \omega + \tilde{\omega}) \Phi_\alpha(\hat{\boldsymbol{k}}) \Phi_\beta(\hat{\boldsymbol{k}}). \tag{8.26}$$

Finally, we integrate over the bosonic Matsubara frequencies, ω, and obtain

$$F_{\text{fl}} = \frac{1}{2} \sum_{\substack{\boldsymbol{k}_1, \boldsymbol{k}_2 \\ \boldsymbol{k}_3, \boldsymbol{k}_4}} \delta(\boldsymbol{k}_1 + \boldsymbol{k}_2 - \boldsymbol{k}_3 - \boldsymbol{k}_4) V(\mathbf{k}_1 - \mathbf{k}_2)^2 \Omega(\boldsymbol{k}_1, \dots, \boldsymbol{k}_4) \frac{f(\epsilon_{\boldsymbol{k}_1}^+) f(\epsilon_{\boldsymbol{k}_2}^-) [f(\epsilon_{\boldsymbol{k}_3}^+) + f(\epsilon_{\boldsymbol{k}_4}^-)]}{\epsilon_{\boldsymbol{k}_1}^+ + \epsilon_{\boldsymbol{k}_2}^- - \epsilon_{\boldsymbol{k}_3}^+ - \epsilon_{\boldsymbol{k}_4}^-}. \tag{8.27}$$

The fluctuation correction in (8.27) is identical to the expression derived in Chapter 3 up to the additional factor

$$\Omega(\boldsymbol{k}_1, \dots, \boldsymbol{k}_4) = \sum_{\alpha\beta} \Phi_\alpha(\hat{\boldsymbol{k}}_1) \Phi_\beta(\hat{\boldsymbol{k}}_2) \Phi_\alpha(\hat{\boldsymbol{k}}_3) \Phi_\beta(\hat{\boldsymbol{k}}_4). \tag{8.28}$$

This factor may be approximated by realising that the main contribution to the fluctuation correction comes from pairs anti-parallel momenta close to the Fermi

wave-vector. Then, $V(\mathbf{k}_1 - \mathbf{k}_2) = V(2k_F)$ and

$$\Omega(\boldsymbol{k}_1, \ldots, \boldsymbol{k}_4) \approx \left(\sum_\alpha \Phi_\alpha^2(\hat{\boldsymbol{k}}) \right)^2 = \frac{16}{9}. \tag{8.29}$$

After this approximation the fluctuation corrections take the same form as for the ferromagnet, with magnetisation M replaced by the product of nematic form factor and order parameter: $\Phi_1(\boldsymbol{k})\eta$.

The second order perturbative corrections to the Landau coefficients are integrals of derivatives of Fermi functions, which are strongly peaked at the Fermi surface. Thus, we may approximate the additional symmetry factors by their angular averages and otherwise equate terms of order η^n to their corresponding terms in the ferromagnet of order M^n. Thus we modify (8.6) to obtain the fluctuation correction for the nematic:

$$\mathcal{F}_{\text{fl}}(\eta) = \frac{16}{9} \left\langle\!\!\left\langle -2\lambda(1 + \log 2)\Phi_1(\hat{\boldsymbol{k}})^2 \eta^2 + \lambda\Phi_1(\hat{\boldsymbol{k}})^4 \eta^4 \log\left(\frac{4g^2 \Phi_1(\hat{\boldsymbol{k}})^2 \eta^2 + T^2}{4\mu^2}\right)\right\rangle\!\!\right\rangle, \tag{8.30}$$

where we have defined $\lambda = 4g^6 v_F^3/(3\mu^2)$, with Fermi velocity $v_F = k_F/2\pi^2$ and chemical potential $\mu = k_F^2/2$. As for the ferromagnet this fluctuation term is the result of an infinite sum of leading corrections to all orders in the order parameter.

Calculating the angular average, we arrive at

$$\begin{aligned}
F_{\text{fl}}(\eta) = \frac{16}{9}\lambda\Big(& -2(1 + 2\ln 2)\langle\langle\Phi_1(\hat{\mathbf{k}})^2\rangle\rangle\eta^2 \\
& + \eta^4\left[\langle\langle\Phi_1(\hat{\mathbf{k}})^4\rangle\rangle\left(2 + \ln\frac{T^2}{\mu^2}\right) + \Omega_0\left(\frac{\kappa^2\eta^2}{T^2}\right)\right]\Big),
\end{aligned} \tag{8.31}$$

with

$$\Omega_0(x) = \sum_{k=1}^{\infty} \frac{(-1)^{k-1}}{k}\langle\langle\Phi_1(\hat{\mathbf{k}})^{2(k+2)}\rangle\rangle x^k. \tag{8.32}$$

The function $\Omega_0(x)$ is a special hypergeometric function that is positive definite for $x \geq 0$ and vanishes linearly as $x \searrow 0$.

The resulting contributions are, therefore, at least of order η^6. As for the ferromagnet, fluctuations give rise to a $\log(T)$ contribution to the η^4 coefficient, causing the transition to become first-order at sufficiently low temperatures.

In case of the modulated spin-triplet nematic we have to take into account additional angular averages compared to the ferromagnet. We obtain

$$
F_{\text{fl}}(\eta, \boldsymbol{q}) = F_{\text{fl}}^{(0)}(\eta) + \lambda\,\Omega_4^{\hat{\boldsymbol{q}}}\left(\frac{\kappa^2\eta^2}{T^2}\right) q^4
$$
$$
+ \lambda\left[2\langle\langle\Phi_1^2(\hat{\mathbf{k}})(\hat{\mathbf{k}}.\hat{\mathbf{q}})^2\rangle\rangle\left(2 + \ln\frac{T^2}{\mu^2}\right) + \Omega_2^{\hat{\boldsymbol{q}}}\left(\frac{\kappa^2\eta^2}{T^2}\right)\right]\eta^2 q^2, \qquad (8.33)
$$

where the functions

$$
\Omega_2^{\hat{\boldsymbol{q}}}(x) = \sum_{k=1}^{\infty} \frac{(-1)^{k-1}}{k}\binom{k+2}{1}\langle\langle\Phi_1^{2(2k+1)}(\hat{\mathbf{k}})(\hat{\mathbf{k}}.\hat{\mathbf{q}})^2\rangle\rangle x^k
$$
$$
\Omega_4^{\hat{\boldsymbol{q}}}(x) = \sum_{k=1}^{\infty} \frac{(-1)^{k-1}}{k}\binom{k+2}{2}\langle\langle\Phi_1^{2k}(\hat{\mathbf{k}})(\hat{\mathbf{k}}.\hat{\mathbf{q}})^4\rangle\rangle x^k \qquad (8.34)
$$

are positive definite for $x > 0$ and vanish linearly as $x \searrow 0$.

This shows, that the $\eta^2 q^2$ and η^4 terms behave similarly to one another. In particular, particle-hole fluctuations give rise to the same $\log(T)$ divergence and the two coefficients are simply proportional to each other independent of temperature. Hence, wherever we might suspect a first order transition to the homogeneous nematic, we find instead a transition to the modulated state. The direction of the modulation, $\boldsymbol{q}$, is a function of the values of the angular averages and the functions defined in Equation (8.34).

In summary, the nematic phase and its spatially modulated version behave very similarly to the ferromagnet. The phase diagram takes the same general form, with the nematic phase taking a larger fraction of the phase space. As in the case of the ferromagnet, fluctuations lead to spatial modulation of the order.

8.4 Superconductivity in the critical spin triplet nematic

Earlier work on itinerant ferromagnetism demonstrated that p-wave superconductivity is driven by fluctuations and intertwines with spiraling ferromagnetic order [29]. Given the similarities to the spin-triplet nematic order presented in Section 8.3, we expect p-wave superconducting order to behave similarly in the vicinity of a nematic quantum critical point.

In this section we analyse the free energy of p-wave superconductivity and its intertwining with the spin-triplet nematic. First, we will outline the formalism within a model of ferromagnetism and then apply it to the nematic itself.

8.4.1 Superconductivity in fermionic order-by-disorder

We include superconducting order exactly as in the antiferromagnet, Chapter 6, and closely follow the treatment of superconductivity in the ferromagnet by Conduit *et al* [29].

In the presence of ferromagnetic order, the Fermi momenta of spin up and down electrons are different. Hence, pairing between opposite spins at their respective Fermi surfaces carries non-zero total momentum, which exponentially suppresses this type of pairing. We can choose instead to pair spin up electrons only. This is analogous to the A1 phase in superfluid Helium 3. Here the spin-half Helium atoms form spin-triplet Cooper pairs with finite angular momentum as a result of spin fluctuations [96]. In the absence of an external magnetic field their mixture is homogeneous and the average over the spin projections is zero. However, in the presence of an external magnetic field Cooper pairs with $S_z = +1$ gain energy relative to states with $S_z = 0$ or $S_z = -1$. This new polarised state is the A1 phase and is a magnetic superfluid order. Similarly we pair electrons of the same spin. This allows for pairing with zero total momentum, even in the presence of an external magnetic field, but necessitates a pairing function with odd angular momentum to preserve the antisymmetry of the wavefunction under exchange of fermions. In standard s-wave superconductors, this anti-symmetry is provided by the spin-label.

We include superconductivity in the model by adding and subtracting a variational term to the Hamiltonian

$$\mathcal{H}_{var} = \sum_{\mathbf{k}} \left(\Delta_{\mathbf{k}} c^{\dagger}_{-\mathbf{k},\uparrow} c^{\dagger}_{\mathbf{k},\uparrow} + c.c. \right), \tag{8.35}$$

where the superconducting order parameter contains a p-wave symmetry factor

$$\Delta_{\mathbf{k}} = \Delta \theta_{\mathbf{k}} = \Delta \frac{k_z}{|\mathbf{k}|}. \tag{8.36}$$

Since we are only pairing spin up electrons, the presence of superconducting order only changes the mean field dispersion of one of the bands. In case of ferromagnetism we obtain

$$\xi^{\uparrow}_{\mathbf{k}} = \pm(\sqrt{(\epsilon_{\mathbf{k}} - \mu)^2 + 4|\Delta_{\mathbf{k}}|^2} + gM) \tag{8.37}$$

$$\xi^{\downarrow}_{\mathbf{k}} = \epsilon_{\mathbf{k}} - \mu - gM. \tag{8.38}$$

The mean field free energy takes its usual form

$$\mathcal{F}_{MF} = -T \sum_{\mathbf{k},\sigma} \log \left(e^{-\xi^{\sigma}_{\mathbf{k}}/T} + 1 \right) + \sum_{\mathbf{k}} |\Delta_{\mathbf{k}}|^2 \frac{2f_{\mathbf{k}} - 1}{(\epsilon_{\mathbf{k}} - \mu)}. \tag{8.39}$$

The diagonalisation in the presence of superconducting order modifies the interaction vertex, leading to additional terms in the fluctuation corrections. Keeping only the leading contribution in the superconducting order parameter, we obtain

$$\mathcal{F}(\Delta) = g^2 \underbrace{\sum_{\mathbf{k},\mathbf{q}} \bar{\Delta}_{\mathbf{k}+\mathbf{q}} \frac{2f^{\uparrow}_{\mathbf{k}+\mathbf{q}} + 1}{2\xi^{\uparrow}_{\mathbf{k}+\mathbf{q}}} \Delta_{\mathbf{k}} \frac{2f^{\uparrow}_{\mathbf{k}} + 1}{2\xi^{\uparrow}_{\mathbf{k}}} \mathcal{R}e\chi^{\downarrow\downarrow}(\mathbf{q}, \epsilon^{\uparrow}_{\mathbf{k}+\mathbf{q}} - \epsilon^{\uparrow}_{\mathbf{k}})}_{\delta\mathcal{F}_{\chi}}$$

$$- \underbrace{\sum_{\mathbf{k}} |\Delta_{\mathbf{k}}|^2 \frac{2f^{\uparrow}_{\mathbf{k}} + 1}{2\xi^{\uparrow}_{\mathbf{k}}} \left[1 - \partial_{\epsilon_{\mathbf{k}}} \Sigma^{\uparrow}(\mathbf{k}, \epsilon_{\mathbf{k}}) \right]}_{\delta\mathcal{F}_{\Sigma}}. \tag{8.40}$$

In the case of ferromagnetism mode-mode coupling leads to an enhancement of the superconducting transition temperature. In the absence of spin-orbit coupling, the orientations of the p-wave orbital and the magnetic order are independent. For the spiral ferromagnet the spin of the superconducting order rotates with the ferromag-

netic alignment, while the orbital order is unaffected. Spin orbit coupling would lead to a pinning of the superconducting orbital order to the magnetic order.

The resultant phase diagram is plotted in Figure 8.4. Note the enhancement of the superconducting transition temperature upon entering the ferromagnetic phase space region.
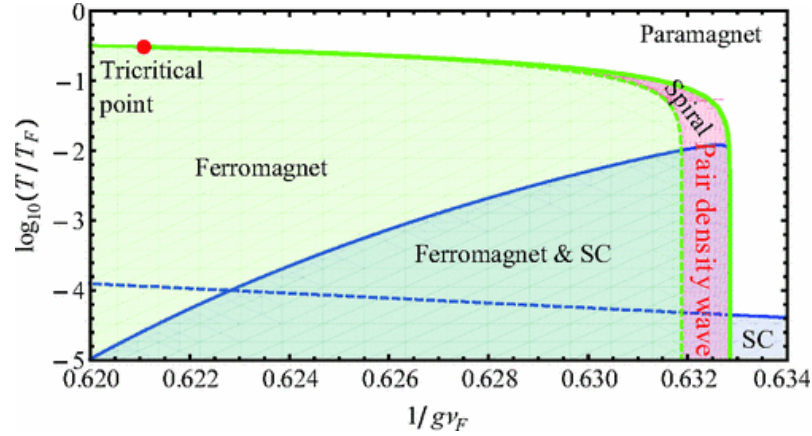

Figure 8.4: **Phase diagram of ferromagnetism and p-wave superconductivity(SC) as a function of inverse electron repulsion $1/g$ and temperature T/μ by Conduit et al [29].** This phase diagram extends Figure 8.1. In addition to ferromagnet and helimagnet, we allow for p-wave superconductivity. The dotted blue line denotes the superconducting transition in the absence of ferromagnetic order. In the presence of ferromagnetism mode-mode coupling leads to an enhancement of the superconducting transition temperature (blue line). Furthermore, the coexistence of spiral ferromagnet and superconductivity leads to the formation of an unusual type of p-wave superconducting order, whose spin quantisation axis rotates in space (in red).

The nematic order, unlike ferromagnetic order, breaks the rotational symmetry in momentum space. We expect that p-wave superconductivity in the presence of d-wave nematic order prefers particular relative orientations of their two orbital symmetry factors, $\Phi_{\mathbf{k}}$ and $\theta_{\mathbf{k}}$. Unless pinned by spin-orbit coupling the spin quantisation axis is along an independent direction, which may in principle rotate in the helical spin-triplet nematic order.

In the following section we will analyse the intertwining of spin triplet nematic and superconductivity in detail.

8.4.2 Free energy of superconductivity in the critical spin triple nematic

In Chapter 6 we treated superconductivity as a small perturbation to the static background of antiferromagnetic order. We evaluated the free energy of the intertwined superconducting and antiferromagnetic order by calculating the superconducting free energy as a functional of the mean field dispersion in the presence of antiferromagnetism. Similarly, here we analyse the intertwining of spin-triplet nematic order with p-wave superconductivity by calculating the free energy of the superconductor as a functional of the nematic mean field dispersion.

The contributions to the free energy of superconducting order all share common factors of the susceptibility to superconducting order. Close to zero temperature these factors are strongly peaked at the Fermi surface. Thus, they are approximated as weighted delta functions of the form:

$$\frac{2f_{\mathbf{k}}^{\uparrow} - 1}{2\xi_{\mathbf{k}}^{\uparrow}} \approx \log\left(\frac{2\mu e^C}{\pi T}\right) \delta(\epsilon_{\mathbf{k}}^{\uparrow} - \mu) \tag{8.41}$$

where $C \approx 0.577$ is the Euler constant. This allows us to write the free energy of superconducting order, Equation (8.40), as

$$\mathcal{F}(\Delta) = g^2 |\Delta|^2 \log^2\left(\frac{2\mu e^C}{\pi T}\right) \underbrace{\frac{16}{9} \sum_{\mathbf{k},\mathbf{q}} \theta_{\mathbf{k+q}} \delta(\epsilon_{\mathbf{k+q}}^{\uparrow} - \mu) \theta_{\mathbf{k}} \delta(\epsilon_{\mathbf{k}}^{\uparrow} - \mu) \mathcal{R}e\chi^{\downarrow\downarrow}(\mathbf{q}, \epsilon_{\mathbf{k+q}}^{\uparrow} - \epsilon_{\mathbf{k}}^{\uparrow})}_{\langle\langle \mathcal{R}e\chi^{\downarrow\downarrow} \rangle\rangle}$$

$$- |\Delta|^2 \log\left(\frac{2\mu e^C}{\pi T}\right) \underbrace{\sum_{\mathbf{k}} \theta_{\mathbf{k}}^2 \delta(\epsilon_{\mathbf{k}}^{\uparrow} - \mu) \left[1 - \partial_{\epsilon_{\mathbf{k}}} \Sigma^{\uparrow}(\mathbf{k}, \epsilon_{\mathbf{k}})\right]}_{\langle\langle 1 - \partial_\epsilon \Sigma \rangle\rangle}, \tag{8.42}$$

where we included the normalisation factor $\frac{16}{9}$ of the quadrupole interaction as defined in Equation (8.29). From equation (8.42) we obtain the superconducting transition temperature in the familiar form of Fay and Appel [97];

$$T = \frac{2\mu e^C}{\pi} \exp\left(\frac{\langle\langle 1 - \partial_\epsilon \Sigma \rangle\rangle}{g^2 \langle\langle \mathcal{R}e\chi^{\downarrow\downarrow} \rangle\rangle}\right). \tag{8.43}$$

We will split the analysis of the free energy of intertwined superconductivity and

nematic order into the the self energy and pairing function contributions as identified in Equation (8.42). Our task is to expand these terms to quadratic order in the nematic order parameter to reveal the effects of such a phase in favouring or disfavouring superconductivity.

$\delta\mathcal{F}_\chi$ contribution to the intertwining of superconductivity and nematic order

The pairing function contribution identified in Equation (8.42) is

$$\langle\langle\mathcal{R}e\chi^{\downarrow\downarrow}\rangle\rangle = \frac{16}{9}\sum_{\mathbf{k},\mathbf{q}}\theta_{\mathbf{k}+\mathbf{q}}\delta(\epsilon^\uparrow_{\mathbf{k}+\mathbf{q}}-\mu)\theta_\mathbf{k}\delta(\epsilon^\uparrow_\mathbf{k}-\mu)\mathcal{R}e\chi^{\downarrow\downarrow}(\mathbf{q},\epsilon^\uparrow_{\mathbf{k}+\mathbf{q}}-\epsilon^\uparrow_\mathbf{k}) \qquad (8.44)$$

The product of the two delta functions restricts the pairing function to its zero frequency component, $\epsilon^\uparrow_{\mathbf{k}+\mathbf{q}} - \epsilon^\uparrow_\mathbf{k} = 0$. Thus we neglect the frequency dependence of the pairing function, an approach also used in the calculation of antiferromagnetic fluctuations supporting d-wave bond density wave order and d-wave superconductivity in Chapters 5 and 6. A complementary approximation scheme by Roussev and Millis [98] neglects the momentum dependence and instead analyses the full frequency dependence.

The pairing function itself is given by

$$\mathcal{R}e\,\chi^{\downarrow\downarrow}(\mathbf{q},\omega) = \sum_\mathbf{p}\frac{n^\downarrow_\mathbf{p} - n^\downarrow_{\mathbf{p}+\mathbf{q}}}{\epsilon^\downarrow_{\mathbf{p}+\mathbf{q}} - \epsilon^\downarrow_\mathbf{p} - \omega}, \qquad (8.45)$$

With the dispersion in the presence of nematic order, $\epsilon^\pm_\mathbf{k} = k^2 \mp g\eta\Phi(\hat{\mathbf{k}})$, the evaluation of this and the self-energy contribution to the free energy is difficult. However, there is a neat trick in the limit of small η that allows us to make progress. If we assume a radially dependent nematic order parameter with a dispersion of the form:

$$\epsilon^\pm_\mathbf{k} = k^2 \mp g\eta\Phi(\mathbf{k}), \qquad (8.46)$$

then, the we can write the pairing function in the presence of finite nematic order in terms of its $\eta = 0$ form by applying a suitable transformation of its momentum argument. The algebraic detail is messy and ultimately the integrals are evaluated

numerically (the details of this may be found in appendix, Section 8.6). Here we just give the result:

$$\langle\langle \mathcal{R}e\chi^{\downarrow\downarrow} \rangle\rangle = -\frac{16}{9(2\pi)^6} \left\{0.026 + 0.084g\eta + g^2\eta^2(0.057 - 0.113\log(T))\right\} \qquad (8.47)$$

The sign and size of the linear η term is a function of the relative orientation of nematic and superconducting symmetry factor. The quadratic η term is independent of the relative orientation. Thus, the linear η term determines the preferred alignment of nematic and superconducting order. Equation (8.47) assumes the most favoured relative orientation - assuming a $d_{x^2-y^2}$ nematic order, the p-wave superconductivity aligns along the x-direction (See Figure 8.5). A p_y orientation of the superconducting order has the opposite sign and is the most disfavoured orientation by mode-mode coupling to linear order in η, while the p_z orbital does not contribute at this order.
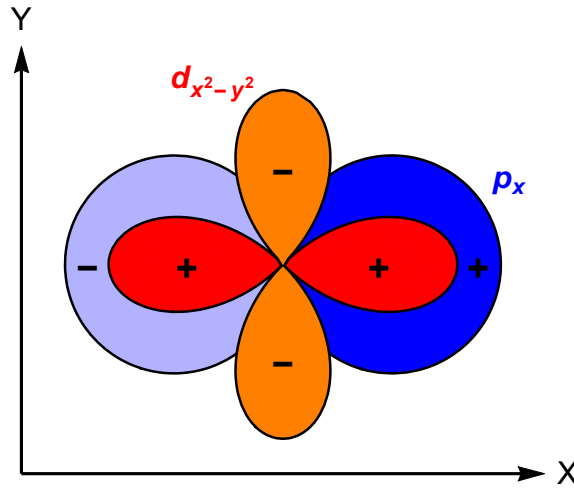

Figure 8.5: **Plot of relative orientation of symmetry factors of the d-wave spin-triplet nematic and p-wave superconductivity.** The $d_{x^2-y^2}$ form factor is displayed in red and orange, while the p_x form factor is coloured in blue and light blue.

$\delta\mathcal{F}_\Sigma$ contribution to the intertwining of superconductivity and nematic order

In this section we would like to evaluate the self energy contribution to the fluctuation corrections. Particularly, we aim to find the expansion coefficients up to

$\eta^2\Delta^2$.

We start off, by splitting the self energy into two parts:

$$\partial_{\epsilon_{\mathbf{k}}}\Sigma(\mathbf{k},\epsilon_{\mathbf{k}}) = g^2\partial_{\epsilon_{\mathbf{k}}}\sum_{\mathbf{p},\mathbf{q}}\frac{f^{\downarrow}_{\mathbf{p}-\mathbf{q}}f^{\uparrow}_{\mathbf{k}-\mathbf{q}}}{\epsilon^{\uparrow}_{\mathbf{k}}+\epsilon^{\downarrow}_{\mathbf{p}-\mathbf{q}}-\epsilon^{\uparrow}_{\mathbf{k}-\mathbf{q}}-\epsilon^{\downarrow}_{\mathbf{p}}} + g^2\partial_{\epsilon_{\mathbf{k}}}\sum_{\mathbf{p},\mathbf{q}}\frac{f^{\downarrow}_{\mathbf{p}}\left(f^{\downarrow}_{\mathbf{p}-\mathbf{q}}-f^{\uparrow}_{\mathbf{k}-\mathbf{q}}\right)}{\epsilon^{\uparrow}_{\mathbf{k}}+\epsilon^{\downarrow}_{\mathbf{p}-\mathbf{q}}-\epsilon^{\uparrow}_{\mathbf{k}-\mathbf{q}}-\epsilon^{\downarrow}_{\mathbf{p}}} \quad (8.48)$$

Now we change the differentiation in the two terms to $\epsilon^{\uparrow}_{\mathbf{k}-\mathbf{q}}$ and $\epsilon^{\downarrow}_{\mathbf{p}}$, respectively, integrate by parts and linearise at the Fermi surface to obtain

$$\partial_{\epsilon_{\mathbf{k}}}\Sigma(\mathbf{k},\epsilon_{\mathbf{k}}) = -\frac{g^2}{2}\sum_{\mathbf{q}}\partial_{\epsilon}f^{\uparrow}_{\mathbf{q}}\,\chi^{\downarrow\downarrow}(\mathbf{k}-\mathbf{q},\epsilon^{\downarrow}_{\mathbf{k}}-\epsilon^{\uparrow}_{\mathbf{q}}) - g^2\sum_{\mathbf{p}}\partial_{\epsilon}f^{\downarrow}_{\mathbf{p}}\,\chi^{\uparrow\downarrow}(\mathbf{k}-\mathbf{p},\epsilon^{\uparrow}_{\mathbf{k}}-\epsilon^{\downarrow}_{\mathbf{p}}) \quad (8.49)$$

Treating the derivatives of Fermi functions as delta functions in the zero temperature limit we may write the self energy contribution to the free energy as

$$\delta\mathcal{F}_{\Sigma} = \frac{g^2}{2}\log\left(\frac{2\mu e^C}{\pi T}\right)\sum_{\mathbf{k},\mathbf{p}}|\Delta_{\mathbf{k}}|^2\delta(\epsilon^{\uparrow}_{\mathbf{k}}-\mu)\delta(\epsilon^{\uparrow}_{\mathbf{p}}-\mu)\chi^{\downarrow\downarrow}(\mathbf{k}-\mathbf{p},\epsilon^{\uparrow}_{\mathbf{k}}-\epsilon^{\uparrow}_{\mathbf{p}})$$

$$+ g^2\log\left(\frac{2\mu e^C}{\pi T}\right)\sum_{\mathbf{k},\mathbf{p}}|\Delta_{\mathbf{k}}|^2\delta(\epsilon^{\uparrow}_{\mathbf{k}}-\mu)\delta(\epsilon^{\downarrow}_{\mathbf{p}}-\mu)\chi^{\uparrow\downarrow}(\mathbf{k}-\mathbf{p},\epsilon^{\uparrow}_{\mathbf{k}}-\epsilon^{\downarrow}_{\mathbf{p}}) \quad (8.50)$$

The analysis of these terms follows a very similar path to the evaluation of the pairing function contribution. The details may be found in the appendix to this chapter, Section 8.6. The resulting correction to the free energy to order $\Delta^2\eta^2$ is given by:

$$\mathcal{F}_{\Sigma} = -g^2|\Delta|^2\frac{16}{9(2\pi)^6}\log\left(\frac{2\mu e^C}{\pi T}\right)\left\{0.398+0.199g\eta+(0.976+0.060\log(T))\,g^2\eta^2\right\}$$

$$(8.51)$$

The complete fluctuation contribution to the free energy of superconductivity in the presence of nematic order to quadratic order is given by the sum of the pairing function (8.47) and self-energy term (8.51).

We are now in a position to plot the superconducting transition line in the vicinity of the continuous nematic transition.

The approximations used in the analysis of p-wave superconductivity in the pres-

ence of nematic order assumed small values of η. In fact, the radially dependent nematic order used to compute the superconducting free energy harbours an unphysical divergence of the electron density as $g\eta \to 1$. This singularity would lead to a divergence of fluctuation corrections inside the nematic phase and thus renders our analysis of superconducting order invalid for large value of the nematic order parameter.

Further into the nematically ordered region the nematic order parameter does indeed become sufficiently large to render the expansion in η invalid. However, from the analysis of p-wave superconductivity in the ferromagnet we know that the superconducting transition temperature should decrease deep inside the ferromagnetic phase. This is a result of the vanishing number of down-spin electrons as the magnetisation approaches saturation, with $gM \to 1$. This could be analysed by an expansion around the saturated state. In case of nematic order this kind of expansion is non-trivial due to the singular behaviour at $g\eta = 1$. Moreover, in contrast to the ferromagnet, both Fermi surfaces survive even for larger values of nematicity. Thus, the phase space for fluctuations that support superconductivity in the spin-triple nematic is finite for all values of the nematic order parameter.

The divergent electron density may also be viewed as a result of the idealised single-band free electron dispersion. The inclusion of lattice effects would add higher order momentum contributions and serve as a cut-off. So far we only considered the quadrupole component of the interaction. Coulomb-like s-wave density-density repulsion would strongly suppress a divergence of the electron density, too.

In order to plot the superconducting phase transition line inside the nematic we first require the nematicity as a function of temperature and interaction strength. Inserting these into the free energy of the superconducting phase in the presence of nematic order we determine the line along which the quadratic Δ coefficient turns negative. As discussed earlier, our approximations are only valid in areas, where the nematicity takes small or moderate values. Thus, we terminate the superconducting transition line before entering regions of large nematicity. Here, we draw a dotted line to suggest the behaviour of the superconducting transition temperature for large value of the nematic order parameter, where our approximations are no longer applicable. The phase diagram is plotted in Figure 8.6.
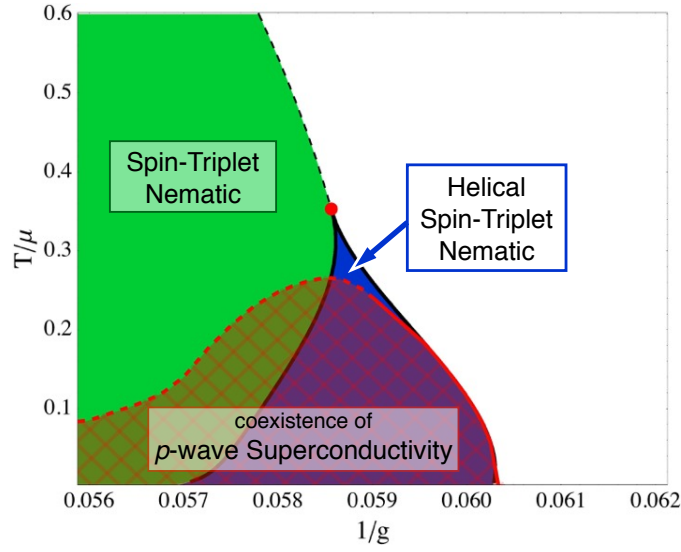
Figure 8.6: **Phase diagram of the spin-triplet nematic as a function of in-verse electron repulsion** $1/g$ **and temperature** T/μ**.** Above the tricritical point (red) the transition from the isotropic Fermi liquid to the homogeneous spin-triple nematic (green region) is continuous. At lower temperatures fluctuations drive the transition first order and support the formation of spatially modulated spin-triplet nematic order (blue region). The transition between homogeneous and helical nematic order is continuous. The transition temperature to p-wave superconductivity (solid red line) is very low outside the nematic area. In the presence of weak to moderate nematic order the superconducting transition temperature is enhanced dramatically (shaded region). In regions of strong nematic order superconducting order is expected to be suppressed, though calculations in this regions are beyond the scope of the present work (dashed red line).

8.5 Conclusion

In this chapter we started by summarising the work of Pedder *et al* [30] and Conduit *et al* [29] on itinerant homogeneous and spiral ferromagnetism and the addition of p-wave superconductivity in the quantum order-by-disorder approach. Next, we explained how this work may be extended by considering spin-triplet nematic order similarly to ferromagnetism with the addition of angular factors. Finally, we considered how p-wave superconductivity may intertwine with the nematic order.

Similarly to the itinerant ferromagnet, nematic order develops a first order transition and a spatially modulated phase at sufficiently low temperatures. This is analogous to the spontaneous formation of bond density wave order due to fluctuations in

the vicinity of an antiferromagnetic quantum critical point. In the latter case these fluctuations are enhanced by the closeness of the Fermi energy to saddle points in the dispersion and the associated van-Hove singularity in the density of states. Further, we show that weak to moderately strong nematic order supports the formation of a novel coexistence of p-wave superconductivity with a spin-triplet nematic phase. The interaction between the two orders leads to an interlocking of their respective orbital symmetries. Conversely, when nematicity approaches saturation, superconducting order is suppressed due to a lack of phase space for the supporting fluctuations.

8.6 Appendix to the spin-triplet nematic

$\delta\mathcal{F}_\chi$ contribution to the intertwining of superconductivity and nematic order

The pairing function contribution identified in Equation (8.42) in the presence of nematic order with radial dependence is give by

$$\langle\langle\mathcal{R}e\chi^{\downarrow\downarrow}\rangle\rangle = \frac{16}{9}\sum_{\mathbf{k},\mathbf{q}}\theta_{\mathbf{k}+\mathbf{q}}\delta(\epsilon^\uparrow_{\mathbf{k}+\mathbf{q}}-\mu)\theta_{\mathbf{k}}\delta(\epsilon^\uparrow_{\mathbf{k}}-\mu)\mathcal{R}e\chi^{\downarrow\downarrow}(\mathbf{q},\epsilon^\uparrow_{\mathbf{k}+\mathbf{q}}-\epsilon^\uparrow_{\mathbf{k}}) \tag{8.52}$$

The product of the two delta functions restricts the pairing function to its zero frequency component, $\epsilon^\uparrow_{\mathbf{k}+\mathbf{q}}-\epsilon^\uparrow_{\mathbf{k}}=0$. The pairing function itself is given by

$$\mathcal{R}e\,\chi^{\downarrow\downarrow}(\mathbf{q},\omega) = \sum_{\mathbf{p}}\frac{n^\downarrow_{\mathbf{p}}-n^\downarrow_{\mathbf{p}+\mathbf{q}}}{\epsilon^\downarrow_{\mathbf{p}+\mathbf{q}}-\epsilon^\downarrow_{\mathbf{p}}-\omega}, \tag{8.53}$$

Transforming to an elliptic coordinate system given by

$$\tilde{\mathbf{p}} = \left(\sqrt{1-g\eta}\,p_x,\sqrt{1+g\eta}\,p_y,p_z\right) \tag{8.54}$$

the dispersion in the presence of nematic order may be written in the isotropic form

$$\epsilon^\downarrow_{\mathbf{p}} = \epsilon_{\mathbf{p}} - g\eta\Phi_1(\mathbf{p}) = \epsilon_{\tilde{\mathbf{p}}} = \tilde{\mathbf{p}}^2 \tag{8.55}$$

Inserting this into the pairing function in the presence of nematic order we find

$$\mathcal{R}e\,\chi^{\downarrow\downarrow}(\mathbf{q},\omega) = \frac{1}{\sqrt{1-(g\eta)^2}}\mathcal{R}e\chi_0(\tilde{\mathbf{q}},\omega), \tag{8.56}$$

where χ_0 is the pairing function in the absence of nematic order:

$$\mathcal{R}e\,\chi^{\downarrow\downarrow}_0(\mathbf{q},\omega) = \frac{1}{64\pi^2q^3}\left[4\mu\epsilon_{\mathbf{q}}-(\epsilon_{\mathbf{q}}-\omega)^2\right]\ln\left|\frac{\epsilon_{\mathbf{q}}+qv_F-\omega}{\epsilon_{\mathbf{q}}-qv_F-\omega}\right| - \frac{k_F}{16\pi^2}\left[1+\frac{\omega}{\epsilon_{\mathbf{q}}}\right]$$
$$+\quad \omega\to-\omega. \tag{8.57}$$

Its zero frequency limit is given by:

$$\chi_0(q,0) \quad = \quad \frac{\epsilon_{\mathbf{q}} - 4\mu}{32\pi^2 q} \log\left|\frac{\epsilon_{\mathbf{q}} + qv_F}{\epsilon_{\mathbf{q}} - qv_F}\right| - \frac{k_F}{8\pi^2} \tag{8.58}$$

Note that $\chi_0(q,\omega)$ is only a function of the modulus of $\mathbf{q}$.

The fluctuation correction to the free energy due to the pairing function now takes the form:

$$\delta\mathcal{F}_\chi = g^2 \frac{16}{9} \log^2\left(\frac{2\mu e^C}{\pi T}\right) \sum_{\mathbf{k},\mathbf{q}} \bar{\Delta}_{\mathbf{q}}\delta(\epsilon_{\mathbf{q}}^\uparrow - \mu)\Delta_{\mathbf{k}}\delta(\epsilon_{\mathbf{k}}^\uparrow - \mu)\frac{\chi_0(|\tilde{\mathbf{k}} - \tilde{\mathbf{q}}|,0)}{\sqrt{1 - (g\eta)^2}}. \tag{8.59}$$

Here, the delta functions are dependent on the nematic order parameter, which prevents straight forward integration over their argument. To integrate over the delta functions, we first transform both momenta into elliptical coordinates. Then, we may perform the integration over the radial component of both momenta and obtain

$$\delta\mathcal{F}_\chi = -\frac{|\Delta|^2 g^2}{(1 - (g\eta)^2)^{3/2}} \log^2\left(\frac{2\mu e^C}{\pi T}\right) \frac{4}{9} \sum_{\Omega_{\mathbf{p}},\Omega_{\mathbf{k}}} \tilde{\theta}_{\mathbf{p}}\tilde{\theta}_{\mathbf{k}}$$
$$\times \ \chi_0\left(\sqrt{\frac{1 + g\eta}{1 - g\eta}(\hat{k}_x - \hat{p}_x)^2 + \frac{1 - g\eta}{1 + g\eta}(\hat{k}_y - \hat{p}_y)^2 + (\hat{k}_z - \hat{p}_z)^2}, 0\right), \tag{8.60}$$

where $\hat{k}_i$ denote the unit Cartesian vector components and the remaining integrals are over the angular directions of the two momenta. The superconducting symmetry factors, $\theta_{\mathbf{k}}$, are now functions of the nematic order parameter. In particular, assuming a p_x orbital the superconducting form factors are

$$\Delta_{\mathbf{k}} = \Delta\theta_{\mathbf{k}} = \Delta\frac{k_x}{|\mathbf{k}|} \to \Delta\frac{\tilde{k}_x}{\sqrt{1 - g\eta}\sqrt{\frac{\tilde{k}_x^2}{1-g\eta} + \frac{\tilde{k}_x^2}{1+g\eta} + \tilde{k}_z^2}} = \Delta\tilde{\theta}_{\tilde{\mathbf{k}}}, \tag{8.61}$$

where

$$\tilde{\mathbf{k}} \quad = \quad \left(\sqrt{1 - g\eta}\,k_x, \sqrt{1 + g\eta}\,k_y, k_z\right). \tag{8.62}$$

Finally, we expand in powers of the nematic order parameter. The resulting expansion coefficients are messy. Even though they may be calculated analytically the

result is no more revealing than numerical integration over the remaining angular momentum components.

As mentioned in the main text, the linear η contribution is a function of the relative orientation of superconducting and nematic orbital symmetries. The expression below assumes the most favoured relative orientation, for a nematic $d_{x^2-y^2}$ the superconducting orders forms p_x orbitals.

It turns out, that the $\Delta^2\eta^2$ term harbours a zero temperature singularity, due the logarithmic divergence of the pairing functions at two Fermi momenta. Treating the delta functions as derivatives of Fermi functions cuts off this divergence by shifting their peaks from μ to $\mu - T$. Allowing for this the superconducting fluctuation correction to the free energy due to the pairing function is

$$\delta\mathcal{F}_\chi = -g^2|\Delta|^2 \frac{16}{9(2\pi)^6} \log^2\left(\frac{2\mu e^C}{\pi T}\right) \left\{0.026 + 0.084g\eta + g^2\eta^2(0.057 - 0.113\log(T))\right\}$$

(8.63)

$\delta\mathcal{F}_\Sigma$ contribution to the intertwining of superconductivity and nematic order

In the main text we already split the self-energy contribution into two pairing-function-like terms:

$$\delta\mathcal{F}_\Sigma = \frac{g^2}{2} \log\left(\frac{2\mu e^C}{\pi T}\right) \sum_{\mathbf{k},\mathbf{p}} |\Delta_\mathbf{k}|^2 \delta(\epsilon_\mathbf{k}^\uparrow - \mu)\delta(\epsilon_\mathbf{p}^\uparrow - \mu)\chi^{\downarrow\downarrow}(\mathbf{k} - \mathbf{p}, \epsilon_\mathbf{k}^\uparrow - \epsilon_\mathbf{p}^\uparrow)$$

$$+ g^2 \log\left(\frac{2\mu e^C}{\pi T}\right) \sum_{\mathbf{k},\mathbf{p}} |\Delta_\mathbf{k}|^2 \delta(\epsilon_\mathbf{k}^\uparrow - \mu)\delta(\epsilon_\mathbf{p}^\downarrow - \mu)\chi^{\uparrow\downarrow}(\mathbf{k} - \mathbf{p}, \epsilon_\mathbf{k}^\uparrow - \epsilon_\mathbf{p}^\downarrow) \qquad (8.64)$$

The first term in Equation (8.64) exactly follows the analysis of the pairing function earlier. The result is

$$\frac{g^2}{2} \log\left(\frac{2\mu e^C}{\pi T}\right) \sum_{\mathbf{k},\mathbf{p}} |\Delta_{\mathbf{k}}|^2 \delta(\epsilon_{\mathbf{k}}^\uparrow - \mu)\delta(\epsilon_{\mathbf{p}}^\uparrow - \mu)\chi^{\downarrow\downarrow}(\mathbf{k}-\mathbf{p}, \epsilon_{\mathbf{k}}^\uparrow - \epsilon_{\mathbf{p}}^\uparrow)$$

$$=$$

$$- g^2|\Delta|^2 \frac{16}{9(2\pi)^6} \log\left(\frac{2\mu e^C}{\pi T}\right)\left\{0.132 + 0.056g\eta + (0.418 + 0.060\log(T))g^2\eta^2\right\}.$$

(8.65)

Exactly as for the pairing function contribution the linear η term is a function of the relative orientation of nematic and superconducting order. Additionally, the quadratic η term harbours the same $\log T$ singularity.

The second term in Equation (8.50) requires a bit more work and can not be evaluated using the same transformation to elliptical coordinates. Instead we expand $\chi^{\uparrow\downarrow}$ explicitly to quadratic order in η. The expansion is given by

$$\chi^{\uparrow\downarrow}(q,0) = \chi_0(q,0) + g^2\eta^2 \left\{\frac{k_f(4k_f^2 + q^2)}{2^6\pi^2 q^2} - \frac{(4k_f^2 - q^2)^2}{2^8\pi^2 q^3}\log\left|\frac{2k_f + q}{2k_f - q}\right|\right\}$$

(8.66)

Next, we follow the analysis of the pairing function with one slight difference. The dispersion appearing in the delta functions come with opposite spin labels. Hence, in the respective elliptical transforms of the two momenta, $\mathbf{k}$ and $\mathbf{q}$, η changes its sign.

After numerical integration over the angular momentum components we obtain:

$$g^2 \log\left(\frac{2\mu e^C}{\pi T}\right) \sum_{\mathbf{k},\mathbf{p}} |\Delta_{\mathbf{k}}|^2 \delta(\epsilon_{\mathbf{k}}^\uparrow - \mu)\delta(\epsilon_{\mathbf{p}}^\downarrow - \mu)\chi^{\uparrow\downarrow}(\mathbf{k}-\mathbf{p}, \epsilon_{\mathbf{k}}^\uparrow - \epsilon_{\mathbf{p}}^\downarrow)$$

$$=$$

$$- g^2|\Delta|^2 \frac{16}{9(2\pi)^6} \log\left(\frac{2\mu e^C}{\pi T}\right)\left\{0.265 + 0.144g\eta + 0.558g^2\eta^2\right\}$$

(8.67)

Combining (8.65) and (8.67) we find:

$$\mathcal{F}_\Sigma = -g^2|\Delta|^2 \frac{16}{9(2\pi)^6} \log\left(\frac{2\mu e^C}{\pi T}\right)\left\{0.398 + 0.199g\eta + (0.976 + 0.060\log(T))\,g^2\eta^2\right\}$$

(8.68)

Part V

Conclusion

Chapter 9

Conclusion

9.1 Summary

The main aim of this thesis was to apply the fermionic order by disorder approach
to a model of itinerant antiferromagnetism in two spatial dimensions. This was
motivated by earlier success of the formalism in models of itinerant ferromagnetism
in two and three spatial dimensions [27–31] and the great lack of understanding of
the formation of high temperature superconductivity and other exotic orders in the
vicinity of antiferromagnetic quantum critical points. We started by analysing the
free energy of the most fundamental model of itinerant antiferromagnetism within
a Ginzburg-Landau expansion. Already at this point, the phase diagram turned
out to be surprisingly complex: The main actor is a commensurate antiferromag-
netic order, whose phase transition line is driven discontinuous at low temperature.
Far below the tricritical point however, the commensurate phase is preempted by
the formation of incommensurate antiferromagnetism. The latter is a natural con-
sequence of nesting effects and may be viewed analogously to the formation of a
Larkin-Ovchinnikov-Fulde-Ferrell (LOFF) state. We continued by including d-wave
superconductivity and d-wave bond density wave order. Both phases are driven
by magnetic fluctuations in the vicinity of the antiferromagnetic quantum criti-
cal point, but are suppressed inside the antiferromagnetic region itself. Finally,
we demonstrated competition between d-wave superconductivity and bond density
wave order and discussed its effect on the phase diagram.

In Chapter 8 we considered an alternative approach to formation of bond density wave order in systems with ferromagnetic instead of antiferromagnetic fluctuations. Here fluctuations self-consistently stabilise d-wave spin-triple nematic order, which is the zero wave vector limit of the commensurate d-wave bond density order considered in Chapter 5. We found, that this model harbours a fundamental instability towards the formation of a helical distortion of the nematic order similar to spiraling ferromagnetic order analysed by Conduit *et* al [29]. Similarly, these ferromagnetic fluctuations act as pairing glue for p-wave superconducting order and dramatically enhance the superconducting transition temperature in the presence of d-wave spin-triplet nematic order for a particular relative orientation of the p-wave orbital.

9.2 Quantum order by disorder vs alternative theoretical approaches

Fermionic quantum order by disorder is formally equivalent to self-consistent second order perturbation theory. However, in contrast to naive perturbation theory it automatically re-sums an infinite series of Feynman diagrams. It therefore presents an alternative and in many cases easier route through the calculation. Moreover, fermionic quantum order by disorder provides an additional physical interpretation of the physics of quantum criticality. It paints an intuitive picture of low-energy particle-hole excitations. The spectrum of these is highly dependent on the characteristics of the Fermi surface. Thus, particular orders, which change the shape of the Fermi surface, may be stabilised by a self-consistent change in the spectrum of fluctuations. This additional point of view may illuminate phenomena opaque to alternative approaches.

In conventional treatments of quantum criticality non-analytic corrections to the Hertz-Millis action lead to spatial modulation and first order transitions, while the exchange of magnetic fluctuations acts as pairing glue for the formation of novel phases such as high temperature superconductivity. Both of these effects are reproduced by a self-consistent treatment of the fluctuation spectrum [97,99]. Here, spatially modulated phases and first order transitions are an effect of the self-consistent perturbative treatment of the interaction vertex, while novel orders, such as super-

conductivity, change the interaction vertex and thereby the spectrum of fluctuations, which in turn drive the formation of order.

9.3   Comparison with experiment

Fermionic quantum order by disorder is a very young approach. Nevertheless, in case of itinerant ferromagnetism it already reproduces a range of experimental phenomena [27–31]. Moreover, nematic order can be treated by a straightforward extension of the ferromagnetic work [100]. In this thesis we applied the order by disorder formalism to a model for antiferromagnetic order for the first time. The main outcomes reformulate and consolidate results obtained otherwise. As such it presents an alternative path to conclusions drawn in the alternative spin-fermion or hot-spots model [23, 41, 43, 71, 92, 93, 101, 102]. This work demonstrates that the main characteristics of the cuprate phase diagram are not reliant on the existence of hot-spots. A complete model of cuprate physics remains an enigma. Quantitative predictions and the unification of the large and small doping limit further elude the theoretical community.

9.4   *Outstanding issues and future extensions of current research*

There exist three major directions in which the current work may be extended. Firstly one may consider additional features within the model presented. Secondly one may extend the analysis of the model. Finally one may extend the model itself.

The treatment of commensurate antiferromagnetic and bond density wave order took advantage of the system's symmetry under translation by a commensurate wave vector. This allowed for the analytic treatment of most expressions. However, the mean field analysis of the antiferromagnet demonstrated the model's fundamental susceptibility to incommensurate order. Incommensurate order breaks the exploited symmetry of the system. Thus, their treatment is highly non-trivial. To our best knowledge there is very little known about the fate of incommensurate an-

tiferromagnetic and other orders within the present Hubbard model beyond a mean field treatment. Experimental evidence from the incommensurate spin glass phase and incommensurate charge order in the cuprates [11, 86, 103] suggests, that this direction for future work may indeed be highly fruitful.

Moreover, we may extend the current work by considering any of the multitudes of orders suggested in the literature, for example intertwined order such as pair density waves [93, 104], or charge order with different ordering symmetries and wave vectors, such as stripe [92] and checkerboard phases [43, 101].

The second path of extending the presented work is an extension of the method of analysis. The calculations of perturbative corrections to the free energy were consistently performed at zero frequency. We assumed that the fluctuations corrections are dominated by the static component. However, this neglects the possible effects of finite frequency fluctuations and in particular Landau damping. Vekter and Chubukov show that low frequency, finite wave-vector, overdamped fluctuations give rise to non-Fermi liquid contributions to the electron self-energy inside the anti-ferromagnetically ordered region. In ferromagnetic systems these contribution lead to non-analytic corrections, which drive the transition first order [105–108]. In an antiferromagnetic system finite frequency fluctuation contributions to the Ginzburg Landau functional are not non-analytic. They do however change the electron propagation. The latter effect can be measured experimentally in a change of the temperature dependence of electronic specific heat and resistivity as expected for a non-Landau liquid [69]. Such effects are in principle accounted for by the quantum order-by-disorder approach. However, to simplify the calculations, these effects have been neglected in the present work. Explanations for non-Landau liquid behaviour in the cuprates remain a challenging research objective. In particular the strange metal region above the superconducting dome is presenting a hard to solve mystery.

The final direction of extending the current work is the extension of the model itself. The most obvious choice would be the inclusion of higher order hopping terms beyond nearest neighbours. This results in a Fermi surface more similar to that present in the cuprates. Hence, it allows for a clearer comparison with experimental work. Moreover, the presence of hot-spots on this Fermi surface allows for linearisation of the dispersion at the Fermi surface. This in turn may simplify the treatment of incommensurate phases and support the formation of orders, whose

wave vectors connect pairs of hot-spots. However, we note that at present it is not clear if all orders in the cuprates are related to inter hot-spot vectors [109]. Indeed, there is evidence for contributions to charge order perpendicular to the copper-oxide planes [104, 110]. Finally, we like to mention the possibility of fluctuating instead of static order, whose analysis presents further challenges to the theoretical community [111].

Bibliography

[1] Bardeen, J., Cooper, L. N., and Schrieffer, J. R. *Physical Review* **108**(5), 1175–1204 (1957).

[2] Bardeen, J., Cooper, L., and Schrieffer, J. *Physical Review* **106**(1), 162–164 (1957).

[3] W. L. McMillan. *Physical Review* **167**(2) (1968).

[4] Bednorz, J. G. and Muller, K. A. *Zeitschrift für Physik B: Condensed Matter* **64**, 189–193 (1986).

[5] Wu, M. K., Ashburn, J. R., Torng, C. J., Hor, P. H., Meng, R. L., Gao, L., Huang, Z. J., Wang, Y. Q., and Chu, C. W. *Physical Review Letters* **58**(9), 908–910 (1987).

[6] Schilling, A., Cantoni, M., Guo, J. D., and Ott, H. R. *Nature* **363**(6424), 56–58 (1993).

[7] Barisic, N., Chan, M. K., Li, Y., Yu, G., Zhao, X., Dressel, M., Smontara, A., and Greven, M. *Proceedings of the National Academy of Sciences of the United States of America* **110**(30), 12235–40 (2013).

[8] Anderson, P. W. *Science* **235**(1), 1–3 (1987).

[9] Mott, N. F. *Reviews of Modern Physics* **40**(4), 677–683 (1968).

[10] Loram, J. W., Mirza, K. A., Cooper, J. R., and Liang, W. Y. *Physical Review Letters* **71**(11), 1740–1743 (1993).

[11] Comin, R., Frano, A., Yee, M. M., Yoshida, Y., Eisaki, H., Schierle, E., Weschke, E., Sutarto, R., He, F., Soumyanarayanan, A., He, Y., Tacon, M. L., Elfimov, I. S., Hoffman, J. E., Sawatzky, G. a., Keimer, B., and Damascelli, A. *Science* **343**(January), 390–392 (2014).

[12] Comin, R., Sutarto, R., He, F., da Silva Neto, E. H., Chauviere, L., Fraño, A., Liang, R., Hardy, W., Bonn, D. A., Yoshida, Y., Eisaki, H., Achkar, A. J., Hawthorn, D. G., Keimer, B., Sawatzky, G., and Damascelli, A. *Nature Materials* **14**(8), 796–800 (2015).

[13] Chou, F. C., Belk, N. R., Kastner, M. A., Birgeneau, R. J., and Aharony, A. *Physical Review Letters* **75**(11), 2204–2207 (1995).

[14] Galanakis, D., Khatami, E., Mikelsons, K., Macridin, A., Moreno, J., Browne, D. a., and Jarrell, M. *Philosophical transactions. Series A, Mathematical, physical, and engineering sciences* **369**(1941), 1670–1686 (2011).

[15] Coleman, P. and Schofield, A. J. *Nature* **433**(7023), 226–9 (2005).

[16] Custers, J., Gegenwart, P., Wilhelm, H., Neumaier, K., Tokiwa, Y., Trovarelli, O., Geibel, C., Steglich, F., Pépin, C., and Coleman, P. *Nature* **424**(6948), 524–527 (2003).

[17] Hertz, J. A. *Physical Review B* **14**(3), 1165–1184 (1976).

[18] Millis, A. J. *Physical Review B* **48**(10), 7183–7196 (1993).

[19] Löhneysen, H. V., Pietrus, T., Portisch, G., Schlager, H. G., Schröder, a., Sieck, M., and Trappmann, T. *Physical Review Letters* **72**(20), 3262–3265 (1994).

[20] Schroder, A., Aeppli, G., Coldea, R., Adams, M., Stockert, O., Lohneysen, H. v., Bucher, E., Ramazashvili, R., and Coleman, P. *Nature* **407**(6802), 351–355 (2000).

[21] Chubukov, A. V., Efremov, D. V., and Eremin, I. *Physical Review B* **78**(13), 1–10 (2008).

[22] Mazin, I. I., Singh, D. J., Johannes, M. D., and Du, M. H. *Physical Review Letters* **101**(5), 1–4 (2008).

[23] Abanov, A. and Chubukov, A. *Physical Review Letters* **84**(24), 5608–11 (2000).

[24] Abanov, A. and Chubukov, A. *Physical Review Letters* **93**(25), 1–4 (2004).

[25] Metlitski, M. A. and Sachdev, S. *Physical Review B* **82**(7), 75128 (2010).

[26] Villain, J., Bidaux, R., Carton, J.-P., and Conte, R. *Journal de Physique* **41**(11), 1263–1272 (1980).

[27] Karahasanovic, U., Krüger, F., and Green, A. G. *Physical Review B* **85**(16) (2012).

[28] Krüger, F., Karahasanovic, U., and Green, A. G. *Physical Review Letters* **108**(6), 1–5 (2012).

[29] Conduit, G. J., Pedder, C. J., and Green, A. G. *Physical Review B* **87**(12), 121112 (2013).

[30] Pedder, C. J., Krüger, F., and Green, A. G. *Physical Review B* **88**(16), 17–19 (2013).

[31] Krüger, F., Pedder, C. J., and Green, A. G. *Physical Review Letters* **113**(14), 147001 (2014).

[32] Anderson, P. W. *Physical Review* **115**(1), 2–13 (1959).

[33] Hubbard, J. *Proceedings of the Royal Society of London A: Mathematical, Physical and Engineering Sciences* **276**(1365), 238–257 (1963).

[34] Kanamori, J. *Progress of Theoretical Physics* **30**(3), 275–289 (1963).

[35] Gutzwiller, M. C. *Physical Review* **134**(4A), 3–6 (1964).

[36] Van Hove, L. *Physical Review* **89**(6), 1189–1193 (1953).

[37] Berridge, A. M. *Itinerant metamagnetism and magnetic inhomogeneity: a magnetic analogue of the superconducting Fulde-Ferrell-Larkin-Ovchinnikov phase in $Sr_3Ru_2O_7$*. Phd thesis, University of St Andrews, (2009).

[38] Landau, L. and Ginzburg, V. *JETP* **20**, 1064 (1950).

[39] Gor'kov, L. *JETP* **36**(9), 1364–1367 (1959).

[40] Rice, T. *Physical Review B* **2**(9), 3619–3630 (1970).

[41] Abanov, A., Chubukov, A. V., and Schmalian, J. *Advances in Physics* **52**(3), 119–218 (2003).

[42] Sachdev, S., Metlitski, M. A., and Punk, M. *Journal of Physics: Condensed Matter* **24**(29), 294205 (2012).

[43] Meier, H., Pépin, C., Einenkel, M., and Efetov, K. B. *Physical Review B* **89**(19), 195115 (2014).

[44] Fulde, P. and Ferrell, R. A. *Physical Review* **135**(3A) (1964).

[45] Larkin, A. and Ovchinnikov, Y. N. *Sov. Phys. JETP* **20**(762) (1965).

[46] Casalbuoni, R. and Nardulli, G. *Reviews of Modern Physics* **76**(January) (2004).

[47] Monthoux, P. and Lonzarich, G. *Physical Review B* **71**(5) (2005).

[48] Monthoux, P., Pines, D., and Lonzarich, G. G. *Nature* **450**(7173), 1177–1183 (2007).

[49] Yamada, K., Lee, C. H., Kurahashi, K., Wada, J., Wakimoto, S., Ueki, S., Kimura, H., Endoh, Y., Shirane, G., Birgeneau, R. J., Greven, M., Kastner, M. a., and Kim, Y. J. *Physical Review B* **57**(10), 6165–6172 (1998).

[50] Fujita, M., Yamada, K., Hiraka, H., Gehring, P. M., Lee, S. H., Wakimoto, S., and Shirane, G. *Physical Review B* **65**(6), 1–7 (2002).

[51] Drachuck, G., Razzoli, E., Bazalitski, G., Kanigel, A., Niedermayer, C., Shi, M., and Keren, A. *Nature Communications* **5**, 3390 feb (2014).

[52] Haug, D., Hinkov, V., Sidis, Y., Bourges, P., Christensen, N. B., Ivanov, A., Keller, T., Lin, C. T., and Keimer, B. *New Journal of Physics* **12**(10), 105006 (2010).

[53] Schulz, H. J. *Physical Review Letters* **64**(12), 1445–1448 (1990).

[54] Frésard, R., Dzierzawa, M., and Wölfle, P. *Europhysics Letters* **15**(3), 325–330 (1991).

[55] Yamase, H., Eberlein, A., and Metzner, W. *Arxiv preprint arXiv:1507.00560* (2015).

[56] Cheong, S.-W., Aeppli, G., Mason, T. E., Mook, H. A., Hayden, S. M., Canfield, P. C., Fisk, Z., Clausen, K. N., and Martinez, J. L. *Physical Review Letters* **67**(13), 1791 (1991).

[57] Mason, T. E., Aeppli, G., and Mook, H. A. *Physical Review Letters* **68**(9), 1414–1417 (1992).

[58] Mook, H. A., Dai, P., Hayden, S. M., Aeppli, G., Perring, T. G., and Doan, F. *Nature* **395**(6702), 580–582 (1998).

[59] Mook, H. A. and Doan, F. *Nature* **401**(6749), 145–148 (1999).

[60] Coleman, S. and Weinberg, E. *Physical Review D* **7**(6), 1888–1910 (1973).

[61] Chandra, P., Coleman, P., and Larkin, A. I. *Physical Review Letters* **64**(1), 88–91 (1990).

[62] Chubukov, A. *Physical Review Letters* **69**(5), 832–835 (1992).

[63] Feiner, L. F., Oles, A. M., and Zaanen, J. *Journal of Physics: Condensed Matter* **10**(32), L555–L561 (1998).

[64] Zaanen, J. *Physical Review Letters* **84**(4), 753–756 (2000).

[65] Neumayr, A. and Metzner, W. *Physical Review B* **67**(3), 035112 (2003).

[66] Conduit, G. J., Green, A. G., and Simons, B. D. *Physical Review Letters* **103**(20), 1–4 (2009).

[67] Chubukov, A. V. and Maslov, D. L. *Physical Review Letters* **103**(21), 216401 nov (2009).

[68] Belitz, D. and Vojta, T. *Reviews of Modern Physics* **77**(2), 579–632 (2005).

[69] Vekhter, I. and Chubukov, A. *Physical Review Letters* **93**(1), 016405 (2004).

[70] Zwierlein, M. W., Schirotzek, A., Schunck, C. H., and Ketterle, W. *Science* **311**(5760), 492–496 (2006).

[71] Metlitski, M. A. and Sachdev, S. *New Journal of Physics* **12**(10), 105007 (2010).

[72] Shen, K. M. and Davis, J. C. S. *Materials Today* **11**(9), 14–21 (2008).

[73] Mazin, I. I. *Nature* **464**(7286), 183–186 (2010).

[74] Miller, R. I., Kiefl, R. F., Brewer, J. H., Callaghan, F. D., Sonier, J. E., Liang, R., Bonn, D. A., and Hardy, W. *Physical Review B* **73**(14), 144509 (2006).

[75] Motoyama, E. M., Yu, G., Vishik, I. M., Vajk, O. P., Mang, P. K., and Greven, M. *Nature* **445**(7124), 186–189 (2007).

[76] Yoshizawa, H., Mitsuda, S., Kitazawa, H., and Katsumata, K. *Journal of the Physical Society of Japan* **57**(11), 4 (1988).

[77] Reiss, J., Rohe, D., and Metzner, W. *Physical Review B* **75**(7), 75110 (2007).

[78] Rowe, W., Eremin, I., Rømer, a. T., Andersen, B. M., and Hirschfeld, P. J. *New Journal of Physics* **17**(2), 023022 (2015).

[79] Chu, J. H., Analytis, J. G., Kucharczyk, C., and Fisher, I. R. *Physical Review B* **79**(1), 1–6 (2009).

[80] Ishida, K., Nakai, Y., and Hosono, H. *Journal of the Physical Society of Japan* **78**(6), 1–20 (2009).

[81] Bonville, P., Rullier-Albenque, F., Colson, D., and Forget, A. *Europhysics Letters* **67008**, 7 (2010).

[82] Pratt, D. K., Kim, M. G., Kreyssig, A., Lee, Y. B., Tucker, G. S., Thaler, A., Tian, W., Zarestky, J. L., Bud'Ko, S. L., Canfield, P. C., Harmon, B. N., Goldman, A. I., and McQueeney, R. J. *Physical Review Letters* **106**(25), 1–4 (2011).

[83] Kordyuk, A. A. *Low Temperature Physics* **38**(9) (2012).

[84] Tranquada, J. M., Sternlieb, B. J., Axe, J. D., Nakamura, Y., and Uchida, S. *Nature* **375**(6532), 561–563 (1995).

[85] Wu, T., Mayaffre, H., Krämer, S., Horvatić, M., Berthier, C., Hardy, W. N., Liang, R., Bonn, D. A., and Julien, M.-H. *Nature* **477**(7363), 191–194 (2011).

[86] Chang, J., Blackburn, E., Holmes, a. T., Christensen, N. B., Larsen, J., Mesot, J., Liang, R., Bonn, D. a., Hardy, W. N., Watenphul, A., Zimmermann, M. V., Forgan, E. M., and Hayden, S. M. *Nature Physics* **8**(12), 871–876 (2012).

[87] Croft, T. P., Lester, C., Senn, M. S., Bombardi, A., and Hayden, S. M. *Physical Review B* **89**(22), 224513 (2014).

[88] Cyr-Choinière, O., Grissonnanche, G., Badoux, S., Day, J., Bonn, D. A., Hardy, W. N., Liang, R., Doiron-Leyraud, N., and Taillefer, L. *Physical Review B* **92**(22), 224502 (2015).

[89] Cyr-Choinière, O., LeBoeuf, D., Badoux, S., Dufour-Beauséjour, S., Bonn, D. a., Hardy, W. N., Liang, R., Doiron-Leyraud, N., and Taillefer, L. *arXiv preprint arXiv:1503.02033* (2015).

[90] Hamidian, M. H., Edkins, S. D., Fujita, K., Kostin, A., Mackenzie, A. P., Eisaki, H., Uchida, S., Lawler, M. J., Kim, E. A., Sachdev, S., and Davis, J. C. S. *arXiv preprint arXiv:1508.00620* (2015).

[91] Sachdev, S. and Vojta, M. *Physica B: Condensed Matter* **280**(1-4), 333–340 (2000).

[92] Wang, Y. and Chubukov, A. *Physical Review B* **90**(3), 35149 (2014).

[93] Efetov, K. B., Meier, H., and Pépin, C. *Nature Physics* **9**(7), 442–446 (2013).

[94] Wang, Y., Agterberg, D. F., and Chubukov, A. *Physical Review Letters* **114**(19), 197001 (2015).

[95] Oganesyan, V., Kivelson, S. A., and Fradkin, E. *Physical Review B* **64**(19), 195109 (2001).

[96] Anderson, P. and Morel, P. *Physica* **26**(5), S137–S142 (1960).

[97] Fay, D. and Appel, J. *Physical Review B* **22**(7), 3173–3182 (1980).

[98] Roussev, R. and Millis, A. J. *Physical Review B* **63**(14), 140504 (2001).

[99] Monthoux, P. and Lonzarich, G. G. *Physical Review B* **59**(22), 14598–14605 (1999).

[100] Hannappel, G., Pedder, C. J., Krüger, F., and Green, A. G. *arXiv preprint arXiv: 1601.05414* , 1–11 (2016).

[101] Pépin, C., de Carvalho, V. S., Kloss, T., and Montiel, X. *Physical Review B* **90**(19), 195207 (2014).

[102] Freire, H., de Carvalho, V. S., and Pépin, C. *Physical Review B* **92**(4), 045132 (2015).

[103] Ghiringhelli, G., Le Tacon, M., Minola, M., Blanco-Canosa, S., Mazzoli, C., Brookes, N. B., De Luca, G. M., Frano, A., Hawthorn, D. G., He, F., Loew, T., Sala, M. M., Peets, D. C., Salluzzo, M., Schierle, E., Sutarto, R., Sawatzky, G. A., Weschke, E., Keimer, B., and Braicovich, L. *Science* **337**(6096), 821–825 (2012).

[104] Gerber, S., Jang, H., Nojiri, H., Matsuzawa, S., Yasumura, H., Bonn, D. a., Liang, R., Hardy, W. N., Islam, Z., Mehta, A., Song, S., Sikorski, M., Stefanescu, D., Feng, Y., Kivelson, S. A., Devereaux, T. P., Shen, Z. X., Kao, C. C., Lee, W. S., Zhu, D., and Lee, J. S. *Le Journal de Physique Colloques* **49**(C8) (2015).

[105] Belitz, D., Kirkpatrick, T. R., and Vojta, T. *Phys. Rev. B* **55**(15), 9452–9462 (1997).

[106] Belitz, D., Kirkpatrick, T. R., and Vojta, T. *Phys. Rev. Lett.* **82**(23), 4707–4710 (1999).

[107] Rech, J., Pépin, C., and Chubukov, A. V. *Phys. Rev. B* **74**(19), 195126 (2006).

[108] Efremov, D. V., Betouras, J. J., and Chubukov, A. *Physical Review B* **77**(22), 220401 jun (2008).

[109] Kivelson, S. A. *Magnetism, Bad Metals and Superconductivity: Iron Pnictides and Beyond, Santa Barbara Oct 2014, http://online.kitp.ucsb.edu/online/ironic14/kivelson, last accessed: 24.01.2016* .

[110] Forgan, E. M., Blackburn, E., Holmes, A. T., Briffa, A. K. R., Chang, J., Bouchenoire, L., Brown, S. D., Liang, R., Bonn, D., Hardy, W. N., Chris-

tensen, N. B., Zimmermann, M. V., Hücker, M., and Hayden, S. M. *Nature Communications* **6**, 10064 dec (2015).

[111] Torchinsky, D. H., Mahmood, F., Bollinger, A. T., Božović, I., and Gedik, N. *Nature Materials* **12**(5), 387–391 (2013).